

The University of Nottingham

UNITED KINGDOM · CHINA · MALAYSIA

Facile synthesis of novel activated carbons for the post-combustion capture of CO_2

Xin Liu

Thesis submitted to the University of Nottingham for the degree of Doctor of Philosophy

July 2017

Abstract

The world faces unprecedented challenges in mitigating climate change and reducing CO_2 emissions from fossil fuel utilisation has been clearly taken as one of the major climate change mitigation strategies. Among the carbon capture technologies, solid adsorbent looping technology (SALT) using activated carbon is considered to be one of the most promising methods due to the extensive sources raw materials, low price, high specific surface area and low energy requirement for regeneration. Synthesis of activated carbons with high adsorption capacity and CO_2/N_2 selectivity for post combustion capture (at a low CO_2 partial pressure and high temperature) is the focus of current research on carbons. This project aims to utilize abundant and easy access materials such as biomass or polymers as precursors and alkaline metal based compounds as activating agents to prepare novel activated carbons with exceptional CO_2 adsorption performance to meet the requirement of post combustion CO_2 capture in power plants.

Two kinds of precursors, biomass (rice husk) and polymer (polyisocyanurate foam), were employed to prepare effective activated carbons for post-combustion CO_2 capture. A novel cost-effective methodology able to achieve the carbonization, chemical activation and simultaneous surface functionalization essentially in a one-step process were developed.

The work on carbons derived from rice husk (RH) showed that the synthesised bio-carbons exhibit exceedingly high ultra-microporosity, accounting for up to 95% of total porosity. With a modest surface area of 1035 m^2/g and a total pore volume of 0.43 cm^3/g, the best performing RH carbon showed a record high and fully reversible CO_2 uptake capacity of 2.0 mmol/g at 25 ^oC and a CO_2 partial pressure of 0.15 bar, which was the highest uptake ever reported for bio-carbons. Furthermore, it was attempted to tablet precursors with different compacting pressures before activation in order to further improve the adsorption performance. The results showed that the compacted rice husk-derived carbons exhibited much higher ultra-microporosity, especially volume of pores smaller than 0.42 nm and a large amount of mesopores. This has led to exceedingly high CO_2 uptake, up to 6.80

and 4.50 mmol/g at 0 and 25 ℃ respectively and 1 bar and 1.90 mmol/g at 25 ℃ and a CO_2 partial pressure of 0.15 bar, which was much higher than samples prepared at 700 ℃ without compaction. Meanwhile, the compacted samples showed much higher initial slope (IS) CO_2/N_2 selectivity up to 170 at 25 ℃ while the selectivity of the sample prepared at 700℃ without compaction was only 56.

Polymer-derived carbons also showed exceedingly high levels of ultra-microporosity and unique surface chemistry for CO_2 adsorption. The resulting ultra-microporous carbon foam achieved a record-high CO_2 uptake of 2.12 mmol/g at 25 ℃ and 0.15 bar as well as a record-high CO_2/N_2 selectivity of 200, which is among the highest ever reported for porous carbon materials and most MOFs. In addition, the adsorption performance of samples at flue gas conditions (0.15 bar CO_2 and 40-50 ℃) were also studied. The samples showed record-high CO_2 uptake of about 2 mmol/g at flue gas condition (40-50℃ and 0.15 bar CO_2), which was higher than any carbon materials from more sophisticated and cost-prohibitive methodologies, most zeolites and MOFs. The polymer-derived carbons investigated here exhibited fast adsorption kinetics and excellent stability and regenerability under simulated flue gas condition.

Further studies in this project showed that the excellent performance of carbons from different precursors can be attributed to ultra-microporosity and favourable surface chemistry achieved by the facil one-step synthesis. The CO_2 adsorption capacity is associated with the pore volume of pores smaller than a specific size, which varied with the temperature and partial pressure. The ultra-micropore volumes of pores smaller than 0.44 nm and 0.40 nm is responsible for the CO_2 adsorption at 0.15 bar 25 ℃ and 50 ℃ respectively. In addition to ultra-micropores, this work showed that surface potassium groups on surface identified by EDX and XPS could significantly improve the CO_2 adsorption performance, especially at low partial pressures. As for RH carbons, up to 50% of the total CO_2 uptake was attributable to the unique surface chemistry, which appears to be dominated by the enhanced formation of extra-framework potassium cations, owing to the presence of zeolitic structures incorporated within the carbon matrices. The work on polymer derived carbons showed that there was a linear relationship existing between CO_2

adsorption capacity and surface potassium content, while no direct relationship between nitrogen containing groups and CO_2 adsorption capacity was observed. Meanwhile, the high heat of adsorption and IS selectivity also indicated the strong surface affinity to CO_2. Overall, the prepared potassium doped carbons possess great potential as adsorbents for post combustion CO_2 capture.

Acknowledgements

I would like to express my gratitude to my supervisors, Dr. Cheng-Gong Sun, Prof. Colin Snape and Prof. Hao Liu for their precious support, advice, guidance, encouragement and invaluable input to my PhD research. I hope one day I can be as good a lecturer and a researcher just like them.

Special thanks for Dr. Cheng-Gong Sun, he is not only my supervisor but also my enlightened tutor. He has been very patient in many discussions on my experimental work. I appreciate his persistence in the fundamental understanding of scientific problems and his attitude of digging into the root of the problem.

I would like to thank Dr. Michael Fay for assistance of the TEM, Dr. Emily Smith for assistance of the XPS work, Professor Xinyong Chen and Dr. Guping He for teaching me to use AFM, Elisabeth Steer and Nicola Weston and David Clift for the assistance of SEM, Nigel Neate for the assistance of XRD and Dr Jackie Deans for the assistance of XRF.

I also wish to express my appreciation to the laboratory technician, Adrian Quinn and technical manager, Mick Winfield for their technical support and assistance with everyday lab issues.

I would like to thank my colleagues Dr. Jingjing Liu and Dr. Lee Stevens for the helpful discussion in sample characterization and preparation. Many thanks go to my colleagues Yuan Sun, Hetian Chi, Dr. Mohd Hafiz Abu Hassan, Dr. Farooq Sher, Dr. Wenbin Zhang, Dr. Hui Deng, Kaixuan Zhou, Shaobo Wang, Christopher Bridge, Gary Newbolt for their help in the past three years. I really enjoy all the group activities with everyone. I will keep all the cheerful time in heart.

I would like to further thank my friends outside the university, Xujiang Wang, Long Zhou and Mengze Zhang, for their moral support and encouragement since my arrival in the UK.

I would like to thank the graduate school of the University of Nottingham and the China Scholarship Council (CSC) for their scholarship to offer me a chance to study for a doctorate.

Finally, I am especially grateful to my parents and my girlfriend. They are and will be always the source of the motivity for my achievement.

Content

Abstract I
Acknowledgements IV
Content VI
List of Figures IX
List of Tables XIV
Chapter 1 Introduction 1
Chapter 2 Literature Review 6
2.1 CO_2 capture technologies 6
2.1.1 Pre-combustion technologies 6
2.1.2 Oxy-fuel combustion technology 7
2.1.3 Post combustion technologies 8
2.2 Activated carbon adsorbents 13
2.2.1 Mechanisms of various activating agents 16
2.2.2 The influencing factors during activation process 22
2.2.3 The change of heteroatom during activation 26
2.2.4 The performance of activated carbon on CO_2 absorption 34
2.3 Aims and objectives 45
Chapter 3 Methodologies 46
3.1 General sample preparation 46
3.2 Characterization of samples 47
3.2.1 Textural properties 47
3.2.2 Morphology 54
3.2.3 Composition analysis 54
3.2.4 Surface chemistry 55
3.3 CO_2 adsorption 56
3.3.1 CO_2 adsorption isotherms 56
3.3.2 CO_2 adsorption kinetics 58
3.3.3 Thermogravimetric analysis 60
3.3.4 Heat of adsorption 61
3.4 Repeatability and reproductivity 61

3.4.1 Repeatability of measurements 62
3.4.2 Reproductivity of samples 63
Chapter 4 Renewable feedstocks derived carbons with favorable surface chemistry for CO_2 capture 64
4.1 Introduction 64
4.2 Experimental procedure 65
4.3 Results and Discussion 65
4.3.1 XRD and XRF characterisation 65
4.3.2 Textural properties of RH-derived carbons 68
4.3.3 The role of RH inherently contained silicon in ultra-microporosity development 76
4.3.4 CO_2 adsorption properties of RH carbons 78
4.3.5 The role of surface textual and chemical properties on CO_2 adsorption 83
4.3.6 Heat of CO_2 adsorption of RH carbons 90
4.4 Conclusions 92
Chapter 5 Mechanochemical method to boost the CO_2 adsorption capacity and selectivity of bio-carbons 94
5.1 Introduction 94
5.2 Experimental procedure 94
5.3 Results and discussion 95
5.3.1 Textual properties 95
5.3.2 CO_2 adsorption performance 100
5.4 Conclusions 108
Chapter 6 Ultra-microporous carbon foams for exceptional CO_2 adsorption and separation from flue gas 109
6.1 Introduction 109
6.2 Experiments 109
6.3 Results and Discussion 110
6.3.1 Textual properties 110
6.3.2 Chemical components of the prepared samples 115
6.3.3 CO_2 capture at low partial pressure 120
6.4 Conclusions 133

Chapter 7 Ultra-microporous K doped carbons with exceedingly high adsorption capacity at flue gas conditions 135
7.1 Introduction 135
7.2 Experimental Procedure 135
7.3 Results and discussions 136
7.3.1 Textual properties 136
7.3.2 Chemical properties 142
7.3.3 CO_2 adsorption performance 144
7.4 Conclusions 158
Chapter 8 Conclusions and future work 159
8.1 General discussion 159
8.1.1 Textural properties of samples from different precursors and pretreatment method 159
8.1.2 CO_2 adsorption performance 161
8.2 Conclusions 165
Chapter 9 Future work 168
9.1 The role of potassium intercalated in carbon 168
9.2 Study on CO_2/N_2 selectivity 168
9.3 The effect of moisture 169
9.4 Others 169
References 171

List of Figures

Figure 1.1 Energy consumption and CO_2 emission till 2035 (Energy Outlook 2035) 2

Figure 2.1 CO_2 Capture Technologies 6

Figure 2.2 Framework structures of selected MOFs: (a) HKUST-1, Green, gray, and red spheres represent Cu, C, and O atoms, respectively; H atoms are omitted for clarity (Chui et al., 1999). (b) MOF-74-Mg, C atoms are shown in gray, O atoms in red, 6-coordinate Mg atoms and terminal ligands in pink, and 5-coordinate Mg atoms in blue. H atoms and terminal ligands on the fragment at top right are omitted for clarity. (Britt et al., 2009) 12

Figure 2.3 Surface oxygen containing groups on carbon and their decomposition by TPD reproduced from reference (Shen et al., 2008) 27

Figure 2.4 Possible N-containing groups existing in activated carbon (Jeon et al., 2014) 28

Figure 2.5 The sorption potential between adsorbate and micropores (slit pores) (Zhang et al., 2013) 35

Figure 3.1 Classification of N_2 sorption isotherms (Kumar et al., 2016) 48

Figure 4.1 XRD patterns of RH carbons samples from different activation conditions: (a) samples prepared with different KOH/RH ratio at 600 ºC; samples prepared with KOH/RH=1 at different temperatures 67

Figure 4.2 N_2 adsorption isotherms obtained at -196 ºC for RH-derived carbons from different chemical activation protocols: (a) samples prepared with KOH/RH=1 at different temperatures; (b) samples prepared with different KOH/RH ratio at 600 ºC; (c) samples prepared with K_2CO_3/RH=1 at different temperatures; (b) samples prepared with different K_2CO_3/RH ratio at 700 ºC. 70

Figure 4.3 NLDFT pore size distributions for RH samples from KOH activation with different KOH/RH mass ratios at 600 ℃ 72

Figure 4.4 Effect of activation temperatures and KOH/RH mass ratios on ultra-microporosity of KOH-activated RH carbons: (a) effect of KOH/RH weight ratio; (b) effect of temperature 73

Figure 4.5 SEM images of raw RH (a) and its derived carbons from KOH and K_2CO_3 activation (HC-600-1 (b-c); KC-700-1((d-e))) and TEM images of sample HC6001 (f)-(g)..... 75

Figure 4.6 Schematic diagram for the silicon-containing RH framework and the pore-creating reactions of silicon with activating agents (*a*) and the relationship between the ultra-micropore volume and the residual silicon content of the carbons (*b*)..... 78

Figure 4.7 CO_2 adsorption profiles at 0 and 25 ℃ for RH carbons from the one-step carbonization-activation with KOH under different conditions. a: CO_2 adsorption isotherms at 0 ℃; b: CO_2 adsorption isotherms at 25 ℃ (c), adsorption isotherms at 0ºC for carbons from different carbonization/activation temperatures..... 81

Figure 4.8 CO_2 adsorption profiles at 0 °C for the RH carbons from the carbonization-activation scheme with K_2CO_3 as the activating agent under different conditions 81

Figure 4.9 (a) the isothermal adsorption curve of selected RH carbons; (b) the cyclic adsorption/desorption performance of the best-performing HC-600-2 sample: both under simulated flue gas conditions of 15% CO_2 and 85% N_2 at 25 ℃ for adsorption and 120 ℃ for desorption in N_2 83

Figure 4.10 Relationship between CO_2 uptake and ultra-micropore volume of RH carbons: (a) 0 ℃, 0.15 bar CO_2; (b) 0℃, 1 bar; (c) 25℃, 0.15 bar CO_2; (d) the change of coefficient of determination R^2 with the increase of pore size..... 86

Figure 4.11 (a) SEM-EDX element mapping showing the spatial distribution of potassium in HC-600-2; (b)-(f) XPS spectra of the major heteroatoms identified in HC-600-2 90

Figure 4.12 (a) Specific heat of CO_2 adsorption measured by TG-DSC (flue gases: 15% CO_2 + 85% N_2; adsorption temperature: 25℃); (b) the relationship between K content and adsorption heat. 92

Figure 5.1 N_2 adsorption isotherms obtained at -196 °C: (a) sample prepared with different compaction load; (b)samples with additives and sample without compaction. 95

Figure 5.2 PSDs of all prepared samples by NLDFT method 97

Figure 5.3 SEM images of selected samples: (a) (b) sample R; (c) (d) sample R2T 99

Figure 5.4 CO_2 adsorption profiles: (a) CO_2 adsorption at 0 °C; (b) CO_2 adsorption at 25 ℃; (c) CO_2 and N_2 isotherms of selected samples at 25 ℃ 101

Figure 5.5 Relationship between CO_2 uptake at 0.15 bar and 25 ℃ and ultra-micropore volume of all samples prepared in this chapter 103

Figure 5.6 Isosteric heat of CO_2 adsorption on different samples calculated from the adsorption isotherms at 0 and 25 °C 104

Figure 5.7 CO_2/N_2 adsorption selectivity at 298 K based initial slope method: (a) sample without compaction (b) sample R2T; (c) Sample R10T; (d) sample R2T_PEI 107

Figure 6.1 N_2 isotherms at -196 ℃ of carbon foam samples prepared at different KOH to foam weight ratio and temperatures. 110

Figure 6.2 NLDFT pore size distributions for FC samples: (a) PSDs of samples prepared at 600 °C; (b) PSDs of samples prepared at 700 °C (c) cumulative pore volume vs pore size of all samples (continued) 113

Figure 6.3 SEM Images of FC7001 (a, c) and of FC7003 (b, d) 115

Figure 6.4 (a) C1s and (b) N1s and spectra for FC6001; (c) the amount of nitrogen containing groups in samples; (d) relative proportion of different nitrogen containing groups in samples 117

Figure 6.5 K-maps of samples: (a) FC6003 and (b) FC7001 119

Figure 6.6 CO_2 isotherms of all samples: (a) CO_2 isotherms at 0 ℃;(b) CO_2 and N_2 isotherms of selected samples at 25 ℃ 121

Figure 6.7 The relationship between CO_2 adsorption capacity at 25 ℃ and 0.15 bar and different parameters: (a)-(d) micropore volume of pores smaller than certain pore size and heteroatom content (e) nitrogen content; (f) potassium content 126

Figure 6.8 (a) Isosteric heat of CO_2 adsorption on FC samples calculated from the adsorption isotherms at 0 and 25 °C; (b) isosteric heat of CO_2 adsorption on different porous materials from references: amine tethered carbon & porous carbon (Lu et al., 2012); NaX (Bae et al., 2013); MIL-101 (Xiang et al., 2012). 128

Figure 6.9 the relationship between initial Q_{st} and potassium and nitrogen content 129

Figure 6.10 CO_2/N_2 adsorption selectivity at 298 K based on initial slope method: (a) FC6003; (b)FC6001; (c) FC7001; (d) the relationship between CO_2/N_2 selectivity calculated by IS and IAST method and fraction of ultra-micropore volume (<0.5 nm) 132

Figure 6.11 CO_2 adsorption curve and cyclic performance of selected samples (flue gases: 15% CO_2 + 85% N_2; adsorption temperature: 25℃; desorption temperature: 120℃) 133

Figure 7.1 N_2 adsorption isotherms obtained at -196 °C: (a) samples prepared with 2 tons compaction load at different temperatures; (b) samples prepared with different compaction load at 700 °C 137

Figure 7.2 NLDFT pore size distributions for the samples prepared at 700 ℃ with different compaction loads 139

Figure 7.3 SEM images of sample P71_2T (a)-(b) 140

Figure 7.4 TEM images of sample P71_2T (a)-(b) 141

Figure 7.5 XPS spectra of prepared samples (a) C1s of sample P71_2T (b) N1s of sample P61_2T 142

Figure 7.6 Elemental mapping of sample P71_2T: (a) potassium; (b) oxygen; (c) carbon; (d) mapping area 144

Figure 7.7 CO_2 adsorption profiles: (a) adsorption isotherms at 0 ºC; (b) adsorption isotherms at 25ºC 145

Figure 7.8 CO_2 adsorption profiles: the change of CO_2 adsorption capacity with the increase of temperature in simulated flue gas condition (15% CO_2 + 85% N_2): (a) samples prepared with different compaction load at 700 ℃ and selected samples (P71 and P71_5T) for further 48 h washing using soxhlet extraction; (b) samples prepared at 600 and 800 ℃ and carbon beads 147

Figure 7.9 Adsorption curves of CO_2: (a) kinetics curves and fitting results of sample P71 at different temperatures; (b) kinetics curves and fitting results of different samples at 40 ℃; (c) cyclic performance of selected samples at different adsorption temperatures (flue gases: 15% CO_2 + 85% N_2; adsorption temperature: 40 ℃; desorption temperature: 120 ℃). 150

Figure 7.10 Relationship between CO_2 uptake and different factors: (a) the volume of pores smaller than 0.4nm, (b) nitrogen content, (c) potassium 155

Figure 7.11 Heat of adsorption of P samples: (a)-(b) heat of adsorption of all samples; (c) the relationship between heat of adsorption and potassium and pore structures 157

Figure 8.1 Relationship between CO_2 uptake and ultra-micropore volume of carbons at 25 ℃, 0.15 bar CO_2: (a) rice husk derived samples without pre-compaction (b) rice husk derived samples with pre-compaction (c) PIR derived carbons without compaction 162

List of Tables

Table 2.1 Typical compositions of flue gas 11

Table 2.2 Source of precursors 15

Table 2.3 The comparison between NaOH and KOH 19

Table 2.4 Basic parameter of different activating agents 23

Table 2.5 the performance of different activating agents for different precursors 31

Table 2.6 CO_2 adsorption capacity of activated carbon materials at 25 ℃ and 0.15 bar 40

Table 2.7 CO_2 adsorption capacities of samples reported at 0.15 bar and 40-50 ℃ 44

Table 3.1 Textural properties of sample FC6003 (repeated 3 times) 62

Table 3.2 Adsorption capacities of selected samples at 0.15 bar and 25 °C tested by TGA for 3 times 62

Table 3.3 Textural properties of sample HC-600-2 63

Table 3.4 Adsorption capacities of selected samples at 0.15 bar and 25 °C tested by TGA 63

Table 4.1 Chemical analysis by XRF of RH carbons 68

Table 4.2 Specific surface areas, pore structure parameters of the bio-carbons ... 71

Table 5.1 Specific surface areas, pore structures of prepared samples 97

Table 5.2 Selectivity of samples at 25 °C 102

Table 6.1 Specific surface areas, pore structure parameters of polymer based activated carbons 111

Table 6.2 CO_2 adsorption capacity and selectivity of selected samples at low CO_2 partial pressure 122

Table 7.1 Specific surface areas and pore structures of polymer derived carbons 138

Table 7.2 CO_2/N_2 selectivity of selected samples at 25 °Ccalculated with the IS method 146

Table 7.3 Pseudo second order kinetics model parameters of CO_2 adsorption for the selected samples 152

Table 8.1 Textural properties and CO_2 adsorption capacities of selected samples derived from rice husk and polymer..... 160

Chapter 1 Introduction

The sharply rising anthropogenic CO_2 emissions largely as a result of sustained consumption of fossil fuels over the past decades have been considered as the main origin of climate change and global warming (Mondal et al., 2012; IEA, 2015). Various scenarios show that for a likelihood of limiting the rise in global temperature to 2ºC above pre-industrial levels, global greenhouse gas emissions would have to be reduced by 40 ~ 70% relative to 2010 by 2050, and to near-zero by 2100, with ambitious mitigation even requiring the removal of greenhouse gases from the atmosphere in order to avoid dangerous climate change (IPCC 2014). Currently, different approaches including improving energy efficiency, deploying renewable energy sources such as sunlight, wind, bioenergy and CO_2 capture and storage have been considered to reduce CO_2 emission.

The BP Energy Outlook 2035 (Petroleum, 2014) predicts that fossil fuels such as coal, natural gas and oil are still the main power source in the next 20 years despite the development of hydro power, nuclear energy, renewable energy and others. By the year 2035, anthropogenic CO_2 emission will reach 40 billion tones, which amounts to an increase by approximately 224% since 1965. Over 50% of the total CO_2 emission is from large stationary emission sources like coal-fired power plants, chemical and petrochemical industries, iron and steel industries, and cement industries (Yang et al., 2008; Sumida et al., 2011; Olivier et al., 2016). Considering the current status of energy demand and renewable energy technologies, fossil fuels will continue to be the main sources of energy in the foreseeable future. Thus, carbon capture and storage (CCS) is widely regarded as the most efficient strategy in the short term (IPCC, 2014).

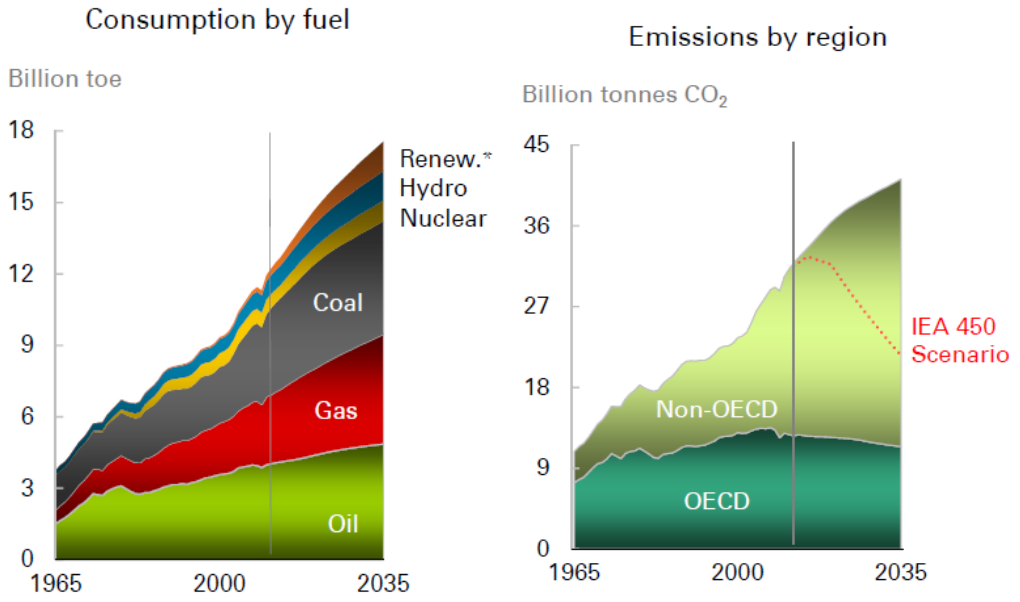


Figure 1.1 Energy consumption and CO_2 emission till 2035 (Energy Outlook 2035)

Lots of CCS technologies including pre-combustion technologies, oxy-fuel combustion technology and post combustion technologies have been developed in recent years, each of which has unique advantages and disadvantages (Rahman et al., 2017; Schoedel et al., 2016). However, for existing power plants, neither pre-combustion technologies nor oxy-fuel combustion technology are suitable. The major issue of pre-combustion technologies is the total capital cost of new facilities and retrofit cost of existing plants (Olajire et al., 2010; Theo et al., 2016), while oxy-fuel combustion technology has problem like high energy consumption from the air separation unit (Burdyny et al., 2010). In comparison, post combustion technologies are one of the most promising options to cut through CO_2 emission from existing power plants.

Of all post combustion technologies, amine scrubbing has been extensively studied to date and is commonly used in oil refineries and natural gas processing plants (Rochelle et al., 2009). However, the main drawback is the high energy consumption especially in the regeneration process. According to statistics by IPCC, removal of 90% CO_2 from flue gas streams produced by different kinds of power plant will reduce the power generation efficiency by 11-40% (IPCC 2014). In return, more fuel is needed to generate same amount of electricity as a power plant without

CCS, subsequently producing new CO_2 and reducing the efficiency of the process. In addition, it also suffers from corrosion problems and degradation of amines during regeneration process (MacDowell et al., 2010). Therefore, there is an urgent need to develop alternative sorption materials with high CO_2 capture efficiencies.

To circumvent these problems, solid adsorbent looping technology (SALT) is considered to be one of the most promising technologies being researched and developed in recent years (Sun et al., 2015). Several classes of CO_2 sorbents have been investigated for this purpose including solid amine adsorbents, metal-organic frameworks (MOFs), zeolites, zeolitic imidazolate frameworks (ZIFs), porous carbon materials (El-Kaderiet al., 2009; D'Alessandro, et al., 2010; Bae et al., 2011; Zhang et al., 2014a). However, the development of solid adsorbents is still at the research stage and there are various limitations for many solid adsorbents developed so far that hinder their commercialization progress. Although solid amine-functionalized CO_2 adsorbents have smaller heat capacities compared to aqueous amine solution, they still suffer from thermal and oxidative degradation as well as high energy required for breaking the C-N bound formed between CO_2 and amine functionality (Wang et al., 2014). Zeolites that have high CO_2 uptake (zeolite CaA ~3.7mmol/g at 40 °C and 0.15 bar) and high CO_2 selectivity are probably the most promising adsorbents for flue gas CO_2 capture (Bae et al., 2013). However, they have the major drawback in low tolerance to water vapor that is always present in the flue gas steam with their CO_2 adsorption capacity tending to steadily decline unless the flue gas is extensively dried (Brandani et al., 2004; Li et al., 2008). Meanwhile, due to the strong interactions produced by extra framework alkali cations the CO_2 desorption temperature is relative high, being at about 135 °C (Konduru et al., 2007; Sumida et al., 2011). Metal-organic frameworks (MOFs) that are constructed from metal ions and various organic spacers with high surface area as well as controlled surface affinity to CO_2 are another type of attractive porous material for CO_2 capture. MOFs are usually seen as CO_2 storage materials rather than capture materials. Most of MOFs show super high adsorption capacities at high pressures resulting from the high surface areas (Furukawa et al., 2010) while low adsorption capacities at typical flue gas conditions (<1.6 mmol/g at 0.15bar and 25 °C) with the exception of only a few types of MOFs like MOF-74, HKUST

possessing high CO_2 uptakes (Mason et al., 2011; Aprea et al., 2010). However, adsorption capacity is not the major problem for MOFs and similar to zeolites, the key issue for MOFs is the effect of moisture. Moisture will not only reduce the adsorption capacity and selectivity of MOFs but also cause severe degradation of MOF structures (Samanta et al., 2011).

Activated carbons have been widely studied as CO_2 adsorbents due to their flexibility in surface properties, excellent thermal and chemical stability (Plaza et al., 2014; Morris et al., 2008). Most importantly, unlike MOFs and zeolites, the carbons do not surfer from decomposition or reduced capacity under humid condition due to their hydrophobic nature (Samanta et al., 2011). However, the homogeneous surface of carbon has no adsorption sites like cations in zeolites or MOFs. Therefore, the adsorption of CO_2 only relied on the weak interaction force, Von der Waals force. The weak interaction between CO_2 and carbon results in low regeneration energy as well as the low adsorption capacity at low partial pressure. So key issue for carbon materials is how to increase their CO_2 adsorption capacity at low partial pressure and flue gas conditions.

This PhD project aims to take advantage of the precursor's chemistry, activating agents and preparation methods to control the pore size and surface chemistry of activated carbons so as to boost the adsorption capacity of carbons at low partial pressure and high temperature. Two abundant and easily accessible but distinct materials (rice husk and polyisocyanurate based material) were selected as the precursor to prepare activated carbon base adsorbents by chemical activation using alkaline metal based compounds as activating agents. Among them, rice husk is a kind of nitrogen-free agricultural waste with low energy density on a volumetric basis, which is produced at a scale of 140 million tonnes a year worldwide (Kalderis et al., 2008). Meanwhile, it possesses very high silica content in molecular level, which could be considered as naturally molecular template that would be beneficial for the development of porosity. As for PIR based materials, a kind of nitrogen-rice materials, they have been widely used as thermal insulation in buildings, which was normally prepared in foam-like structure.

This PhD project developed a facile approach that essentially integrated the carbonization and simultaneous activation into a single one-step process, which was verified as an effective method to prepare activated carbons with favorable surface chemistry for CO_2 capture. The results showed that the prepared samples showed record-high CO_2 adsorption capacity at low partial pressure and high temperature, which was higher than any carbon materials and most MOFs and zeolites. It was found that both surface chemistry and pore structure play important roles on CO_2 adsorption. The CO_2 adsorption capacity is associated with the pore volume of pores smaller than a specific size, which varied with the temperature and partial pressure. The ultra-micropore volumes of pores smaller than 0.44 nm and 0.40 nm is responsible for the CO_2 adsorption at 0.15 bar 25 °C and 50 °C respectively. In addition to ultra-micropores, it should be highlighted that surface potassium intercalation made big contribution to CO_2 adsorption especially at low partial pressure and high temperature.

Chapter 2 Literature Review

2.1 CO_2 capture technologies

CO_2 is produced by the combustion of diverse types of carbon fuel which also directly affects the choice of CO_2 capture process. Associated with different combustion processes, a variety of CO_2 capture technologies are under evaluation, including chemical absorption techniques, adsorption and membrane methods, which can simply fall into several categories depending upon different plant configurations: pre-combustion capture, oxy-fuel combustion capture and post combustion capture (see Figure 2.1).

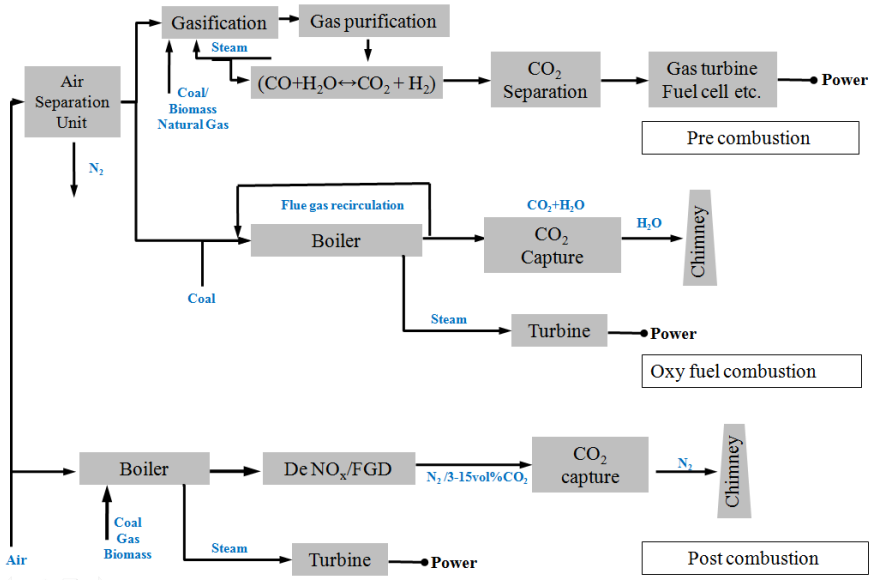


Figure 2.1 CO_2 Capture Technologies

2.1.1 Pre-combustion technologies

In the pre-combustion capture process (Figure 2.1), fuel such as biomass, coal and natural gas is pretreated using a gasifier before utilisation to produce syngas (CO and H_2). As shown in Equation 2.1 and 2.2, the syngas then forms more H_2 via water-gas shift reaction with steam while converting CO to CO_2 (Olajire et al., 2010; Leung et al., 2014; Jansen et al., 2015). Then the high concentration of CO_2 (>20%)

in the H_2/CO_2 fuel gas (total pressure 2.5 to 5 Mpa) (Kim et al., 2011) is removed via separation process, which results in nearly carbon and pollutant free fuel.

Gasification:

$$\text{Coal/Biomass} \rightarrow CO + H_2 \quad (2.1)$$

$$\text{Natural gas } (CH_4) + H_2O \rightarrow CO + H_2 \quad (2.2)$$

Water-gas shift reaction:

$$CO + H_2O \rightarrow CO_2 + H_2 \quad (2.3)$$

Pre-combustion capture could bring several advantages: (1) the transformation process of carbon fuel to carbonless fuel, hydrogen, also removals of pollutants like SO_x and NO_x before combustion; (2) hydrogen could be used as fuel for many systems, such as gas boiler, gas turbine, and fuel cell; (3) the high partial pressure of CO_2 brings benefits for CO_2 separation and various CO_2 capture technologies can be employed in this process (Olajire et al., 2010; Theo et al., 2016). It has been estimated that the energy consumption of a power plant equipped with a pre-combustion system is only half compared to that with a post-combustion system. Hence, the pre-combustion technology is expected to be applied to the Integrated Gasification Combined Cycle (IGCC) power plant using coal as fuel. However, there are still some challenges on commercialization of the pre-combustion CO_2 capture system. The major issue is that total capital costs of the generating facility and retrofit cost of existing plants are very high (Olajire et al., 2010; Theo et al., 2016). Additionally, the efficiency of the IGCC power plant with a pre-combustion capture system will decrease by 7-8% (Wall, 2007).

2.1.2 Oxy-fuel combustion technology

In the oxy-fuel combustion process, fuel is combusted in oxygen-rich gas or even pure oxygen instead of air, resulting in high CO_2 concentrations, normally over 80%, as well as reduction in thermal NO_x. If pure oxygen is used, the main components in flue gas stream are CO_2, water, SO_x and particulates. After removal of SO_x and particulates by a conventional electrostatic precipitator (ESP) and flue gas

desulphurization methods, the remaining gases contain 80%-98% CO_2 depending on the fuel used and can be directly compressed for storage. Many papers have discussed the application of the oxy-fuel combustion technology (Stanger et al., 2015; Toftegaard et al., 2010; Carrasco-Maldonado et al., 2016; [a] Chen et al., 2012).

The main drawback of oxy-fuel combustion is that large amounts of oxygen are needed for combustion process, which can only be produced by energy intensive air separation via a physical separation process, which results in the boost of capital cost and energy consumption (Burdyny et al., 2010).

2.1.3 Post combustion technologies

In the post combustion capture process, CO_2 is directly captured from the flue gas after desulfurization processes. The composition of a typical post-combustion flue gas is shown in Table 2.1. Flue gas from coal-fired power plants contains CO_2 (12-15%), N_2 (73~77%) and H_2O (5-7%) at about 40-50 °C (D'Alessandro et al., 2010; Sumida et al., 2011). Therefore, sorbents with high CO_2 adsorption capacities, CO_2/N_2 selectivity and stability under flow gas condition are crucial. Among many technologies, amine scrubbing using 20-30 wt% aqueous amine solution has been extensively studied to date for post combustion CO_2 capture and is commonly used in oil refineries and natural gas processing plants (Rochelle et al., 2009). The fundamental reaction of this process is (Dutcher et al., 2015):

Using MEA as absorbent:

$$2C_2H_4OHNH_2 + CO_2 \rightarrow RNHCOO^- + RNH_3^+ \quad (2.4)$$

Using TEA as absorbent:

$$(C_2H_4OH)_3N + CO_2 + H_2O \rightarrow (C_2H_4OH)_3NH^+ + HCO_3^- \quad (2.5)$$

The flue gas is bubbled through the solvent in a packed absorber column, and CO_2 molecules react with amine functionalities to form C-N bonds, a strong chemical bond. As shown in the equations, MEA will react with CO_2 to form carbamate $RNHCOO^-$ while bicarbonate is formed in the reaction between TEA and CO_2.

Because of the strong chemical bond between CO_2 and amine, the CO_2-rich solvent was regenerated at 100-200 °C in a regenerator and then the solvent is cooled down to 40-65 °C and recycled into the adsorption column. However, the amine scrubbing technology suffers from many problems: high energy intensity due to a high regeneration energy requirement to break C-N bond, severe thermal and oxidative degradation of the amine, corrosion issues and degradation of the amine by NO_x and SO_x impurities (Spigarelli et al., 2013; MacDowell et al., 2010). Thus, the cost-effective processes for CO_2 capture from the flue gas streams of coal-based power plants are essential to cut off the CO_2 emission.

Table 2.1 Typical compositions of flue gas

Composition	Content	Condition	
CO_2	~15%	temperature	40-50°C
N_2	70-75%	pressure	1bar
H_2O	5-7%		
O_2	3-4%		

Compared to aqueous absorption, the heat capacity of solid sorbent is lower than that of an aqueous solvent. Solid absorbents have received increasing attention in recent years, which has stimulated the development of several classes of materials including zeolites, MOFs, carbons and amine-containing porous materials. However, in their present development stage, these approaches are still not ready for implementation on coal-based power plants. The successful adsorbents must meet important criteria to be both economical and operational for CO_2 capture from flue gas. The criteria are as follows:

1) **High adsorption capacity** The adsorption capacity of adsorbents determines the capital cost of capture system. The high adsorption capacity of CO_2 reduces the quantity of adsorbent required as well as the size of equipment. In order to be competitive to amine scrubbing, the capacity should reach 3-4 mmol/g (Samanta et al., 2011).

2) **The heat of adsorption** The heat or enthalpy of adsorption is an important parameter to indicate the energy required for regeneration and the surface affinity

of an adsorbent toward CO_2. Ideally, a suitable adsorbent for CO_2 capture should have a moderate heat of adsorption to facilitate high CO_2 uptakes at reasonable flue gas temperatures without energy-intensive flue gas deep cooling. This is because too high a heat of adsorption can lead to increased energy requirement for CO_2 desorption or sorbent regeneration whilst if the heat of adsorption of a sorbent is too low (Himeno et al., 2005; Sethia et al., 2015; Zhang et al., 2013), the sorbent will give rise to unacceptably low CO_2 uptakes at typical flue gas temperatures and CO_2 partial pressures.

3) **CO_2/N_2 selectivity** To be a good candidate of sorbent for CO_2 capture from flue gases, the sorbent must have high CO_2/N_2 selectivity, which has direct impact on CO_2 purity separated. However, the purity of CO_2 will affect the transportation and sequestration of CO_2 and therefore, has influence on the cost of CO_2 storage.

4) **Chemical and thermal stability** In flue gas, impurities like SOx, NOx and moisture also exist, which will reduce the CO_2 adsorption capacity of adsorbents and may cause irreversible change of sorbent's structure.

2.1.3.1 Amine modified adsorbents

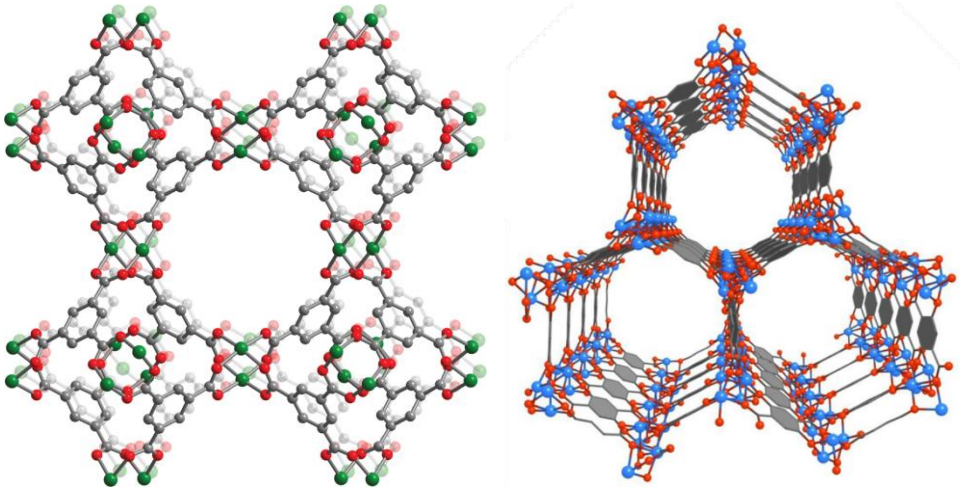
A wide variety of materials such as carbon-based material, mesoporous silica, molecular sieves, silica, meso-porous silicon or mesoporous foam (MCF) have been used as substrates to load basic groups containing materials especially amines like PEI, TEPA, DEA so as to chemisorb CO_2 from flue gas (Li et al., 2010a; Sanz-Pérez et al., 2016; Gadipelli et al., 2015). Because of the low heat capacities of solid supports, the regeneration heat of amine modified adsorbents is lower than that of aqueous amine solution. Amines, substrates and moisture all have significant influence on the CO_2 absorption capacity of absorbents (Heydari-Gorji et al., 2011; Sayari et al., 2011; Bollini et al., 2012). The CO_2 capacities of those chemical absorbents mainly depend on the characteristics of basic groups contained within the materials, rather than porosity and textural structure of substrate. The presence of water changes the reaction between amine and CO_2, via the formation of ammonium carbonate species under anhydrous conditions and, in addition, via transformation to ammonium bicarbonate and carbonate species (Sayari et al.,

2011). Because of the formation of a C-N chemical bond between the CO_2 and amine, amine adsorbents always showed high CO_2/N_2 selectivity. However, despite a reduction in heat of capacity of the solid-functionlised CO_2 adsorbents, they still suffer from thermal and oxidative degradation as well as a relatively high energy required to break the C-N bond that is formed between CO_2 and amine functionality, compared to physical sorbents (Zhao et al., 2013; Wang et al., 2014).

2.1.3.2 Zeolites

Zeolites that are composed of Si/Al frameworks with negative charge and exchangeable cations like Na^+, K^+, Ca^{2+}, Mg^{2+} within the pore structure have been widely studied, especially for flue gas streams (Bae et al., 2013; Wang et al., 2014). Because of their crystalline structure, zeolites have uniform pore sizes between 0.5 nm and 1.2 nm depending on the exchangeable cations (Chester et al., 2009). For instance, the pore diameter of a typical zeolite NaA was 0.4 nm while the pore diameter increased to 0.5 nm when Na^+ was exchanged by Ca^{2+} (Xu et al., 2009). The existence of cations in pores can create strong electric field that have strong interaction with gases possessing a high dipole or quadrupole, like CO_2 (Coriani et al., 2000; Samanta et al., 2011). The CO_2 is adsorbed around the extra framework ions and forms carbonate specials associated with bi-coordination as the amount of CO_2 increased (Wang et al., 2011). Due to their strong affinity to CO_2, zeolites have shown great potential for separation of CO_2 from gas streams. For example, zeolites like MgA and CaA have been shown to possess promising adsorption capacities and CO_2/N_2 selectivity at 298 K and 0.15 bar (2.4 mmol/g and 4.0 mmol/g, 54 and 45 respectively) (Bae et al., 2013). However, the main drawback of zeolites is their low tolerance to the water vapor which exists in flue gas steams. Their CO_2 adsorption capacity steadily decline with the increase of adsorption-desorption cycles unless the flue gas was extensively dried (Brandani et al., 2004; Li et al., 2008). Furthermore, due to the strong interactions produced by extra framework alkali cations the CO_2 desorption temperature is relative high about 135 °C (Konduru et al., 2007; Sumida et al., 2011).

2.1.3.3 MOFs



(a) (b)

Figure 2.2 Framework structures of selected MOFs: (a) HKUST-1, Green, gray, and red spheres represent Cu, C, and O atoms, respectively; H atoms are omitted for clarity (Chui et al., 1999). (b) MOF-74-Mg, C atoms are shown in gray, O atoms in red, 6-coordinate Mg atoms and terminal ligands in pink, and 5-coordinate Mg atoms in blue. H atoms and terminal ligands on the fragment at top right are omitted for clarity.（Britt et al., 2009）

MOFs are constructed by coordinate bonds between metal ions or small metal-containing clusters and organic linkers. A variety of organic spacers has made it possible to control pore size, pore shape and surface chemistry for different types of CO_2 capture. Therefore, MOFs performed well both at high pressure and low partial pressure. For instance, MOF-210 with a high BET surface area of 6240 m^2/g holds the record for CO_2 storage capacity about 74.2 wt% at 298 K and 50 bar, which is much higher than any conventional material (Furukawa et al., 2010). As for low partial pressure CO_2 capture, strong surface affinity rather than surface area and pore volume determines the adsorption capacity, and structure bearing exposed metal cation sites on the surface of MOFs have shown strong affinity towards CO_2 similar to zeolite (Zheng et al., 2014). HKUST-1 and MOF-74-Mg, affording open Cu^{2+} and Mg^{2+} on their surface showed high CO_2 adsorption capacities of 20.6 wt% and 11.6 wt%, respectively at room temperature and 0.15 bar (Mason et al., 2011; Aprea et al., 2010). However, the key issue for MOFs is the effect of moisture,

which will not only reduce the adsorption and selectivity of MOFs because of the competition between CO_2 and H_2O for the adsorption sites but also cause severe degradation of the MOF structure (Liu et al., 2010; Samanta et al., 2011). So, developing new MOFs with high adsorption capacity at low partial pressure and stability has become a focus, and MOFs modified by amine groups or carboxyl groups have been considered as a potential method (Choi et al., 2012; Yeon et la., 2015). Recently, efforts have been made to improve the water stability of MOFs via surface modification, but the modifications affected their adsorption performance. For example, the adsorption capacity of Ni-MOF-74 reduced from 3.2 mmol/g to 1.9 mmol/g at 0.15 bar and 25 °C after surface modification by pyridine molecules (Bae et al., 2014a). Similarly, the adsorption capacity of Mg-MOF-74 decreased from 4.3 mmol/g to 3.0 mmol/g at 0.15 bar and 40 °C after N, N'-Dimethylethylenediamine modification (McDonald et al., 2012), and the average heat of adsorption reached 61kJ/mol, indicating that a high energy is needed to regenerate adsorbents. Meanwhile, adsorption of modified Mg-MOF-74 was slowed down, and the adsorption capacity reached 83% of the equilibrium capacity at 0.15 bar and 313 K after exposure to 15% CO_2 for 15 min.

2.2 Activated carbon adsorbents

As discussed in the former section, porous materials satisfy the requirements of the CO_2 capture process (dynamics, operation, etc.) because of their unique advantages such as greater capacity, ease of handling compared to other techniques (Shafeeyan et al., 2010). Among them, activated carbons are gaining increasing attention as CO_2 adsorbents because of their unique advantages like easy availability, flexibility in surface properties, and excellent thermal and chemical stability (Plaza et al., 2014; Morris et al., 2008). Most importantly, the carbons do not suffer from decomposition or reduced capacity under humid condition due to their hydrophobic nature (Hong et al., 2016).

Activated carbon in a broad sense makes up of a wide range of amorphous carbonaceous materials that possess high porosity and surface area, which are obtained from thermal treatment of a variety of carbon materials under different

conditions. A variety of raw materials or precursors have been studied, which can be divided into 4 categories: coal based materials, biomass, waste materials produced from industrial process and synthesized materials (details in Table 2.2). As can be seen from Table 2.2, biomass and synthesized materials are the most-studied precursors for preparing activated carbons for CO_2 adsorption. Biomass is renewable organic materials derived from plants and animals, which is generally composed of lignin, hemicellulose, cellulose, proteins, lipids, sugars, starches and inorganic compounds (Zhang et al., 2010). In biomass, those compounds are strongly intermeshed and are chemically bonded by either non-covalent forces or covalent linkage (Saidur et al. 2011). Of all, cellulose, hemicellulose and lignin are the main components in biomass. Based on the results of elemental analysis, a typical biomass contains about 50 wt% carbon, 42 wt% oxygen 5 wt% hydrogen (Zhang et al., 2010). Unlike biomass, the chemical composition and components of synthesized materials derived from different monomers show great difference from each other. Unique advantage of synthesized materials is that they have the ability to design and control the surface chemistry (Bae et al., 2014).

Table 2.2 Source of precursors

Precursors	
biomass	glucose, maize stalks, fir woods, pistachio, corncob, rice straw, wood, cellulose, lignin, coffee fruit, cherry stones, xylan, sugarcane bagasse, rice husk, coconut shells, walnut shells, mango pits, tobacco stems, coffee bean husks, cherry stones, olive pits, sawdust
coal	coal-based cokes, coal tar pitches, anthracite, bituminous coal, lignite
synthesized materials	Acetylene based nanotubes, Polystyrene-based cation exchangeable resin, poly (vinylidene chloride)-based carbon, saran-derived carbons, phenol–formaldehyde resins, N-carbon monoliths, honeycomb-monoliths, acrylic resin, N-doped oxidized resorcinol formaldehyde, polyaniline
waste	decanted oil vacuum residue, sewage sludge, green petroleum coke，waste newspaper

Basically, the preparation of active carbon normally involves two steps: carbonisation/oxidation of the raw materials at a certain temperature in an inert atmosphere and the activation of the obtained carbonized materials, including physical and chemical activation approaches that could create new pores or remove the blockage in pores and further develop the pore structure (Bansal et al., 2005). The physical activation process usually carried out at higher temperatures 800-900 °C in the presence of oxidizing gases like CO_2 or steam (Bouchelta et al., 2008; Teng et al., 1998; Ioannidou et al., 2007). The purpose of the chemical activation is to mix activating agents like H_3PO_4, KOH and zinc chloride with carbonaceous materials, which is followed by activation at 400-900 °C in an insert atmosphere (Rufford et al., 2014; Wang et al., 2012; Ioannidou et al., 2007). Compared to the physical activation, chemical activation presents unique advantages such as lower activation temperature, higher surface area and controlled micropore size distribution (Lillo-Ródenas et al., 2007), higher yields and short activation time

(Lillo-Ródenas et al., 2003). Industrially, it is common to produce activated carbon from physical activation. However, the prepared samples with high surface areas and pore volumes usually showed low CO_2 adsorption capacities especially at low partial pressure (Dreisbach et al., 1999; Sevilla et al., 2013). Despite the disadvantages of chemical activation, such as corrosiveness and necessary washing process to remove activating agent, it has been proved to be an efficient method to prepare activated carbons with suitable textural properties and surface chemistry for CO_2 adsorption. In this chapter, a review about chemical activation mechanisms and CO_2 adsorption on activated carbons will be carried out.

2.2.1 Mechanisms of various activating agents

Many reactants have been tested as activating agents, which can be divided into three types: alkaline medium (KOH/NaOH), metal chloride ($FeCl_3$, $ZnCl_2$, $CaCl_2$) and carbonate (K_2CO_3, Na_2CO_3, Li_2CO_3, and Cs_2CO_3). The mechanism of each type of activating agents, influencing factor and their performance on porosity development are summarized in this section and the carbons prepared using different activating agents were listed in Table 2.5.

2.2.2.1 Alkaline hydroxide/ carbonate

Activation using alkaline hydroxides like NaOH and KOH is a widely-used method to generate rich porosity in carbon materials. However, the activation mechanism has not been well understood due to the complexity of process (Raymundo-Pinero et al., 2005). In general review, chemical activation by alkaline hydroxides is two-step process: dehydration reactions between carbon and MOH and reactions at higher temperature including the formation of metallic M by reduction of the ions and the oxidation of carbon.

KOH Chemical activation using KOH was first proposed by Wennerberg and O'Grady in 1978 (Wennerberg & O'Grady, 1978). After that, many research groups have studied it, the global reaction (Reaction 1) was proposed by Linares-Solano and co-workers using anthracite as a precursor (Lozano-Castello et al., 2001). Combining experimental results from temperature-programmed reaction (TPR)

experiments, XRD, FTIR, and theoretical calculation, the reaction shown in Reaction 2.6 was proposed, and the main products during activation process were shown to be H_2, H_2O, CO, CO_2, M_2CO_3.

$$6MOH + 2C \rightarrow 2M + 3H_2 + 2M_2CO_3 \quad (2.6)$$

The global reaction consists of several simultaneous/consecutive reactions that can be divided into two groups via reaction temperature: the reactions between carbon and KOH below 700 °C and the reactions related to K_2CO_3 at temperatures higher than 700 °C.

When the temperature was lower than 700 °C, the reactions between carbon and KOH (Reaction 2.7 – 2.10) were shown to be based on the petroleum activation using KOH by Otowa and co-workers (Otowa et al., 1993). During this process, KOH first dehydrated to produce K_2O and water which are then consumed by carbon via a two-step reaction to form CO_2, CO and H_2. After that, K_2CO_3 is produced by the reaction between K_2O and CO_2.

$$2KOH \rightarrow K_2O + H_2O \quad (2.7)$$

$$C + H_2O \rightarrow CO + H_2 \quad (2.8)$$

$$CO + H_2O \rightarrow CO_2 + H_2 \quad (2.9)$$

$$CO_2 + K_2O \rightarrow K_2CO_3 \quad (2.10)$$

When the temperature is higher than 700 °C, the as-formed products would further react with carbon. K_2CO_3 firstly decomposes to K_2O and CO_2 (Reaction 2.11). Then CO_2 is reduced by carbon to produce CO at high temperatures (Reaction 2.12). Metallic K forms via reaction between C and metal compounds K_2O (Reaction 2.13). Potassium metal formed in this stage further intercalates into the carbon lattice so as to expand the carbon lattices. In addition to the mechanism above, Yong bin Ji et al. showed that potassium carbonate would directly react with carbon to form metallic K and CO (Reaction 2.14) rather than by the pathway shown in Reaction 2.11-2.12, by analyzing the XRD data from experiments, but it was only possible for ungraphitizable materials (Ji et al., 2007).

$$K_2CO_3 \rightarrow K_2O + CO_2 \quad (2.11)$$

$$CO_2 + C \rightarrow 2CO \quad (2.12)$$

$$C + K_2O \rightarrow 2K + CO \quad (2.13)$$

$$K_2CO_3 + 2C \rightarrow 2K + 3CO \quad (2.14)$$

At the same time, surface species (such as alkalides, -OK) also form from the oxygen of the alkali salt (Reaction 2.15) (Marsh et al., 1984; Shen & Xue, 2003). The formation of M_2O is beneficial to form well-dispersed metal oxide clusters during the rearrangement of materials like coal and lignocellulosic materials at initial stage, which is useful for the development of porosity (Addoun et al., 2002).

$$C + K_2O \rightarrow K + C\text{-}O\text{-}K \quad (2.15)$$

After activation, the potassium compounds are washed out using water or acid, while the expanded lattice cannot return to the original state. Thus, the carbon lattice remains apart causing porosity and yielding high surface area carbon (Marsh et al., 1984).

NaOH Compared to KOH, the mechanism of NaOH activation is similar. The activation process such as the formation of carbonate proceeds at temperatures below 700 °C, decomposition of the carbonate to produce CO and CO_2 at higher temperatures (normally >800 °C) and the formation of metallic Na is observed. In addition to carbonate formation reactions, Tseng studied the NaOH activation process of char and proposed the following reversible reactions between Na and C that are possible during NaOH activation process (Reaction 2.16-2.17) (Tseng, 2007):

$$4NaOH + C \leftrightarrow 4Na + 2H_2O + CO_2 \quad (2.16)$$

$$2Na \rightarrow Na_2O \rightarrow NaOH \quad (2.17)$$

NaOH reacts with carbon to produce Na, H_2O and CO_2, where the Na produced is oxidised to Na_2O and subsequently hydrated back to NaOH. Surface species (such

as alkalides, -ONa) at the edges of the graphene planes are also formed in NaOH activation (Yamashita & Ouchi, 1982; Freitas et al., 2007).

$$C + Na_2O \rightarrow Na + C\text{-}O\text{-}Na \quad (2.18)$$

There are differences between KOH and NaOH activation:

1) Metallic K forms during KOH activation is intercalated between the graphene layers of the carbon crystalline, which is predominant to activate ordered graphitic carbon materials. However, there is hardly any evidence for the intercalation of Na, and Na was only efficient in the activation of low structural-ordered materials. Raymundo-Pinero and co-workers found the same phenomenon when they activated multiwalled nanotubes using the same mixing methods (Raymundo-Pinero et al., 2005; Choi & Ryoo, 2007).

2) The starting temperature of KOH is lower than that of NaOH. Lillo-Ródenas studied the NaOH and KOH chemical activation of coal samples via TPD experiments (lignite, subbituminous coal and anthracite) (Lillo-Ródenas et al., 2004). As shown in Table 2.3, the starting temperature of activation is lower for KOH, confirming that KOH is a more reactive agent, which is mainly attributable to the higher reactivity of KOH than NaOH.

Table 2.3 The comparison between NaOH and KOH

Precursor	Starting temperature (℃) (NaOH)	Starting temperature (℃) (KOH)	ref
Lignite	250	225	Lillo-Ródenas et al., 2004
subbituminous coal	375	325	
anthracite	570	400	

Although alkali metal hydroxides like KOH and NaOH are effective activating agents to produce carbon materials possessing high surface areas and porosities, the disadvantages such as there corrosiveness and hazardous natures also need to be considered. While, alkaline metal carbonates that are environmental friendly and

mild could be an alternative choice to activate carbon materials. Carbonate is similar to intermediate product in the activation process by alkaline metal hydroxides, and the reaction mechanism is similar to the reaction of MOH at high temperature (Reaction 2.14). However, there are slight differences among various carbonates.

2.2.1.2 Alkaline carbonate

$Na_2CO_3/K_2CO_3/Cs_2CO_3$ For Na_2CO_3, K_2CO_3 and Cs_2CO_3, the global activation reaction is shown in Reaction 2.19. Metallic Na/K/Cs and CO are formed due to the reaction between carbonate and C, which were proposed by different research groups (Addoun et al., 2002, Fox & White, 1931; McKee, 1983).

$$2C + M_2CO_3 \rightarrow 2M + 3CO \quad (2.19)$$

$$M_2CO_3 \leftrightarrow M_2O + CO_2 \quad (2.20)$$

$$M_2O + C \rightarrow 2M + CO \quad (2.21)$$

The global reaction can be separated into several simultaneous/consecutive reactions during the activation process like the decomposition of K_2CO_3 and formation of metal. Fox and White showed that the thermal dissociation of Na_2CO_3 happens during the activation process (Reaction 2.20) (Fox & White, 1931). The formed Na_2O further reacts with C as well (Yamashita & Ouchi, 1982). Addoun et al. studied the Cs_2CO_3 activation of a low rank coal by mass spectrometry and showed that Reaction 2.20 and Reaction 2.21 occurs during activation (Addoun et al., 2002).

However, the reaction with Li_2CO_3 followed a different route as shown in reaction 2.22, which was mainly attributed to the relatively higher stability of Li_2O compared to other alkali metal oxides, and therefore it remained during activation (McKee, 1983).

$$Li_2CO_3 + C \rightarrow Li_2O + 2CO \quad (2.22)$$

From a synthetic standpoint, the activation mechanism of various carbonates is similar; the only difference is the size of the cation of the activating agent. The experimental results showed that the radius of cation has a significant effect on porosity and specific surface area of precursors. Okada, K et al. (2003) examined the performance of various activating agents Li_2CO_3, Na_2CO_3, K_2CO_3, Rb_2CO_3 and Cs_2CO_3 on the same materials at 1073 K for 2 h and at the mass ratio of 1. An increase of pore volume and surface area was observed with the increase of the radii of cation (Li < Na < K <<Rb< Cs), which agreed with the study of Addoun et al. (2002). In addition to the radius of the cation of the activating agent, the thermal stability of the alkali metal carbonate in the presence of carbon material was also found to have a profound influence on the activation process. As shown in Reaction 2.20-2.21, the lower the thermal stability of the activating agent, the greater the effect of activation on the evolution of porosity and surface area.

2.2.1.3 Metal chlorides

In addition to alkaline metal compounds, zinc chloride is also an extensively used activating agent. Zinc chloride is a Lewis acid; it is able to interact with nonbonding electrons of oxygen atoms in precursors to form Zn-O complexes. Because of this, it is often used to activate oxygen rich precursors like biomass materials and low-rank coal (Rufford et al., 2014).

Zinc chloride acting as a dehydrogenating agent has been generally recognized (Caturla et al., 1991, Rodriguez-Reinoso et al., 1992 and Ibarra et al., 1991), which has been reported by several research groups. Caturla et al. suggested that the existence of zinc chloride promotes the dehydrogenation and aromatization of raw materials like cellulose that increas the formation of pores. Ibarra et al. reported that zinc chloride promotes the dehydrogenation reaction, which makes the materials react quickly below 400 °C. A systematic investigation of the effect of $ZnCl_2$/elutrilithe ratios, activation temperatures, and activation time on the properties of the adsorbents was carried out by Hu et al. (Hu & Vansant et al., 1995), and they pointed out that the ability of $ZnCl_2$ to activate (generate porosity) carbon precursors is based on its dehydrating function.

A detailed mechanism of $ZnCl_2$ activation given by the study of different raw materials like wood and coals is as follows (Rufford et al., 2014). During thermal treatment, the impregnated zinc chloride protonates different oxygen containing groups on carbon materials. After that, various reactions occur. The main reactions are dehydration of –OH groups to promote double bond formation, hydrolysis of glycosidic linkages in polysaccharides, and degradation of sugar monomers.

$ZnCl_2$ acts as an activating agent as well as a template for the creation of microporosity. After removal of activating agent on washing process, the matrix generated by the activating agents' removal leaves behind a considerable number of pore. During the process of activation, the elimination of hydrogen and oxygen is in the form of water, rather than volatile with the presence of $ZnCl_2$, so a higher yield of active carbon is obtained.

2.2.2 The influencing factors during activation process

During the activation process, the development of porosity and surface area depends on not only the real reaction by various activation agents but also the activation parameters (i.e. activation temperature, operating parameters, etc.) (Wang et al 2012).

2.2.2.1 Activation temperature

Activation temperature is an important parameter during activation, which can ensure the reaction between activating agents and precursors occurs successfully. As for alkaline metal hydroxides, alkaline metal compounds work effectively in two temperature ranges, including dehydration at lower temperatures and the decomposition of carbonates and formation of surface species (such as alkalides, -OM) at temperature higher than 700°C (Reaction 2.11-2.13) which are very important for the development of porosity and surface area. It is similar to metal carbonates. Normally, the activation temperature is in the temperature range from 700 to 800 °C in order to ensure the fully development of porosity and surface area. Detailed activation temperatures in various papers are illustrated in Table 2.4. The severe thermal treatment causes the breakdown of cross-links in the carbon matrix,

leading to the collapse and widening of pores and the decrease of porosity (Hsu & Teng, 2000), which is not beneficial for adsorption of gases like CO_2.

Table 2.4 Basic parameter of different activating agents

Agents	Activation temperature (°C)
KOH	700-900
NaOH	700-800
K_2CO_3	800
Na_2CO_3	760
Li_2CO_3	800-900
Cs_2CO_3	800-900
$ZnCl_2$	500-700
$FeCl_3$	280

For metal chloride like $FeCl_3$ and $ZnCl_2$, the optimized activating temperature chosen depends on not only the reaction, but also the melting point and boiling point. This is mainly caused by the difference of the reactivity mechanism. $FeCl_3$ and $ZnCl_2$ act as activating agents as well as templates for the creation of microporosity. The boiling point of $FeCl_3$ and $ZnCl_2$ is 315 °C and 732 °C respectively. If the temperature is too high, some metal chlorides evaporate and cannot become the template, which will influence the surface area and porosity of the final product. Therefore, the optimized activation temperature for $ZnCl_2$ is around 600 °C, while for $FeCl_3$ it is 280 °C. Unlike carbonates and hydroxides; the proportion of micropores is stable with the increase of activation temperature (Hsu & Teng, 2000).

Jun'ichi Hayashi et al. (2000) did a comprehensive study on the influence of activation temperature on the activation of lignin using various activating agents such as $ZnCl_2$ and some alkali metal compounds such as KOH, NaOH, K_2CO_3 and Na_2CO_3. The surface area of the product was found to be at a maximum value at a temperature of 800 °C for alkali metal compound activation, and at the temperature of 600 °C with $ZnCl_2$. The surface area and porosity were higher than $ZnCl_2$.

2.2.2.2 Operating parameters

In addition to the characteristics of the activating agents themselves, operating parameters such as the weight ratio between activating agents and precursors, the methods of mixing of the activating agent, and the flow of gas during the activation are also key factors which decide the porosity and textual structure of the active carbon.

Impregnation ratio The impregnation ratio, defined as the weight ratio between activating agent and precursor, possesses a similar variation trend as activation temperature. As mentioned above, the increase of activation temperature results in the degeneration of micropores and the formation of mesopores. Taking KOH activation as an example, by increasing the KOH:C weight ratio, the amount of metallic potassium penetrated into the carbon matrix increases (Wang et al., 2009 and Romanos et al., 2012). Consequently, the carbon matrix will be enlarged more and the porosity will increase under their experimental condition. However, the increase of impregnation ratio is not always good to the development of porosity and textual structure; micropores are widened to become big pores by excessive amount of activating agents. Tseng studied the effect of the KOH/char ratio using corncob-derived active carbon (Tseng & Tseng, 2005), the results showed that the surface area and pore volume grow with the increase of impregnation ratio, from 309 to 2595 m^2/g and from 0.2 to 1.43cm^3/g. However, the micropore volume decreases when the impregnation ratio beyond 3. The conclusion is in accordance with the study by Wu et al., using porous carbons from PAN-based peroxidised cloth. The results are similar to other activating agents like $ZnCl_2$, carbonate (Wu et al., 2004).

Duration time Duration time is defined as the duration of activation at a certain temperature. With the increase of activation time, the pore volume and surface area increase (Zhang et al., 2013). However, the volume and surface area of the micropores decreased dramatically if the activation time was too long, which was attributed to the collapse and widening of pores and the decrease of porosity (Tsai et al., 1998), The optimum activation time for various precursors is different, for

PCs (Wu et al., 2004) it is about 30 min, while the time reported for anthracite in literature is about 2 h (Ahmadpour et al., 1997 and Lozano-Castello et al. 2001).

Atmosphere It is important to state that nitrogen, a cheap and inert gas, is the gas most commonly used in chemical activation. The nitrogen flow is important and beneficial to the development of porosity even to a greater extent than the activating agent to coal ratio (Lozano-Castello et al., 2001 and Lillo-Ródenas et al., 2001). High flow accelerates the removal of the gases produced during activation process which would promote the reactions so as to create more micropres. For KOH activation, it will also increase the evaporation of potassium metal that is produced by reaction between carbon and activating agents like KOH/carbonate during activation process, which in return increases the development of porosity. The activation in various atmospheres N_2, CO_2 and steam was also studied by Lillo-Ródenas and co-workers (2003), and it was found that other gases has little effect on the development of porosity, while CO_2 have negative effect on activation at relatively low temperatures, under 800°C.

2.2.2.3 The effect of precursors

In addition to activation temperature and operational parameters, precursors also played an important role in the porosity development. As aforementioned, the main components of biomass were cellulose, hemicellulose and lignin. It was studied by Gergova et al (1994) the porous structure of activated carbons from agricultural wastes were closely related to the original textural properties of raw materials. Higher pore volume of activated carbon derived from lignin than that of carbon derived from cellulose. The results obtained by Reed and Williams (2004) also showed that the precursor with high lignin content had higher carbon yield as well as microporous surface area, which was also approved by Daud and Ali (2004) by using coconut shell and palm shell. They suggested that the surface area and porosity of sample with higher lignin content were higher. In addition, it was found by Jagtoyen and Derbyshire (1998) that the performance of lignin and cellulose was different. Carbons derived from lignin via chemical activation possessed mostly micropores while carbons derived from cellulose were more likely a mixture of pores with wide pore size range.

In addition to the organic components in carbons, inorganic component like silicon could also help the development of porosity. The typical agricultural material was rice husk, a kind of materials that rich in silicon. It was found that the molecular level silicon could be considered as natural template which was beneficial to the development of porosity (Wang et al., 2012; Liu et al., 2017).

Moreover, there are also other influencing factors like pre-oxidation and pre-carbonization, more information can be found from reference (Wang J et al., 2012 and Teng & Wang, 2000).

2.2.3 The change of heteroatom during activation

In addition to carbon, there are also heteroatoms like O, N forming surface functional groups that exist in the starting materials (Moreno-Castilla et al., 2000, Gómez-Serrano et al., 1999, Snoeyink et al., 1967, El-Sayed et al., 2004), on surface or at the edge. During chemical activation, some of the heteroatoms are removed in the form of gas while others transform from heat-liable forms into relatively stable groups at high temperature up to 900 °C. The resulting heteroatom containing groups on surface are significantly affected by the surface chemistry of the activated carbon surface (László et al., 2001) as well as the CO_2 adsorption on carbon, especially at low CO_2 partial pressures (Yin et al., 2013; Drage et al., 2007; Pevida et al., 2008; Plaza et al 2009). Therefore, understanding the reaction of heteroatom containing groups during the activation or preparation processes is useful to produce high performance solid adsorbents. Among the surface complexes in carbons, surface oxygen groups and nitrogen groups are of vital importance.

2.2.3.1 Oxygen containing groups

The oxygen containing groups are mainly divided into two categories, acidic groups and basic groups. Typical acidic groups are arboxyl, carbonyl, phenol, lactone, and carboxylic anhydride (Park et al., 2002). The groups corresponding to chromene, pyrone, and quinone belong to the basic groups (Puri et al., 1970).

The effect of the chemical activation or thermal treatment on the chemical nature of the carbon surface has been studied by many researchers. Oxygen containing

groups will decompose to CO_2 or transform to more stable groups during activation. Reviews about the change of oxygen containing groups can be found in reference (Shafeeyan et al., 2010). Figure 2.3 illustrates surface oxygen containing groups on carbon and their decomposition by temperature-programmed desorption (TPD). High temperature treatment >700 °C like KOH activation under an inert atmosphere (N_2, helium) was able to remove most of the acidic oxygen containing groups such as carboxyl, lactone, phenol etc. Others like carbonyl, anhydride, ether and quinine on a carbon surface can be decomposed at 800-1000 °C. The existence of an activating agent also influenced the reaction of oxygen containing group. Soo-Jin Park et al. found that a large number of functional groups were formed with the increasing KOH-to-polystyrene-based cation exchangeable resin (PSI) ratio when PSI was activated at 700 °C (Park et al., 2002).

The decomposition of O containing groups is beneficial to increase the basicity of the carbon surface (Otake et al., 1993, Darmstadt et al., 2003). The main reason is that acid oxygen containing group such as carboxyl, lactone, phenol can decompose at relatively low temperature ranging from 100 to 700 °C. Weak acid groups and basic groups decompose at high temperature (800-1000 °C), which is shown in the figure. Therefore, the large amount of CO_2 releasing groups are removed, the CO releasing groups remain in the carbon (see Figure 2.3).

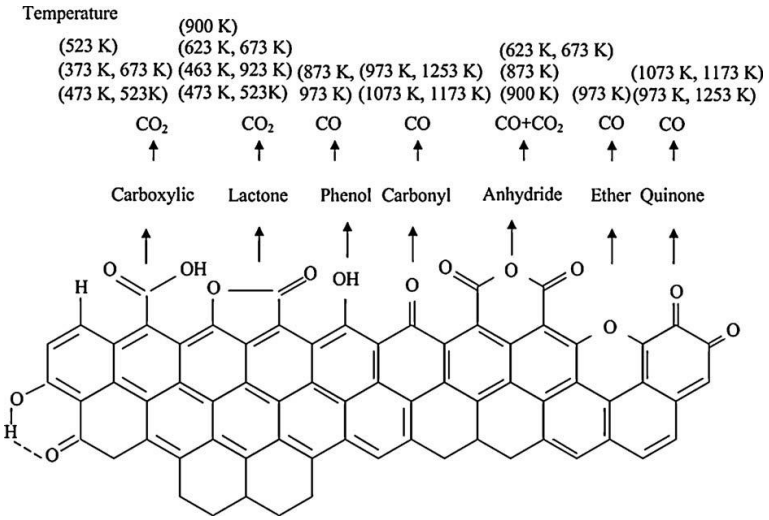


Figure 2.3 Surface oxygen containing groups on carbon and their decomposition by TPD reproduced from reference (Shen et al., 2008)

2.2.3.2 Nitrogen containing groups

Possible structures of nitrogen containing groups in the active carbon shown in Figure 2.4 include amide (–CO-NH_2), imide (-N=), pyridinic N, pyrrolic N and quaternary N, pyridine-N-oxide species (Zhang et al., 2013).

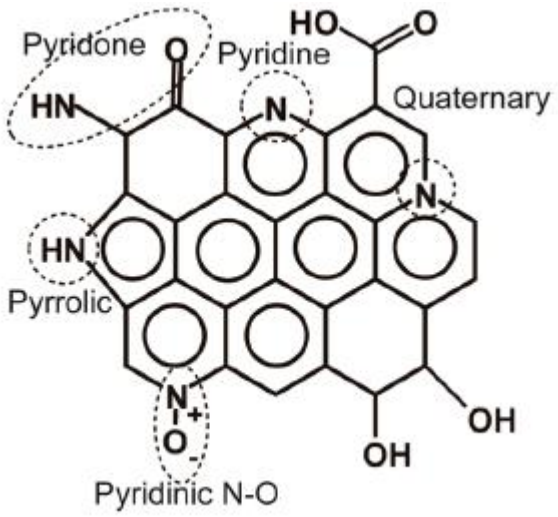


Figure 2.4 Possible N-containing groups existing in activated carbon (Jeon et al., 2014)

All the nitrogen functionalities are basic, which can increase the basicity of the carbon surface. This can enhance the interaction between surface and acidic molecular like CO_2 so as to increase its adsorption capacity. The source of nitrogen in activated carbon derives from the starting materials or ammonization after activation. Due to the limited improvement on nitrogen content and the introduction of additional complexity of the time-consuming synthetic step (Plaza et al., 2010; Zhang et al., 2016 and 2016a), using nitrogen-rich precursor to prepare nitrogen-doped activated carbon were commonly used. Therefore, many nitrogen containing precursors like polyaniline, polypyrrole, melamine based microporous organic polymers, lysine based porous carbon (Hao et al., 2013), acrylonitrile (Lu et al., 2002), melamine (Hulicova et al., 2005) and cyanamide (Goettmann et al., 2006), Porous carbon nitride (CN) spheres (Li et al., 2010), ethylenediamine based porous carbon (Lv et al., 2012), bean dreg (Xing et al., 2012) have been used to produce porous carbon or polymer. The nitrogen groups in theses precursors are not thermally stable, and therefore the nitrogen content will decrease with the increase

of temperature during activation, which is removed or form new functional group. Therefore, it is very important to find the stability of various N-containing groups during activation.

(1) **Thermal treatment without chemical activating agents:** The reaction in an inert nitrogen atmosphere is mainly decided by the thermostability of various nitrogen containing groups during carbonization. Quaternary nitrogen and pyridinic-N-oxides are more likely to be formed after thermal treatment without activating agents at high temperatures (Hao et al., 2010, Sun et al., 2014, Sevilla et al., 2011, Tian et al., 2008 and Wang et al., 2008). Hao et al (2010) found that a greater amount of amide and pyrrolic nitrogen are observed at lower pyrolysis temperatures of 400 and 500 °C during carbonization of lysine based precursors, which is in accordance with Nilantha P. Wickramaratne et al. (2014) who used ethylenediamine based carbon spheres (pyridine-type nitrogen, pyrrolic- and/or pyridone-type nitrogen) as the precursor. With the increase of temperature, amine and pyrrolic nitrogen species become unstable and transform into quaternary nitrogen and pyridine-N-oxide species over 700 °C. It was also found that the amount of pyridine-type nitrogen was higher than that of pyrrolic- and pyridone-type nitrogen analyzed by XPS before activation while new nitrogen containing group quaternary nitrogen and pyridinic-N-oxides formed after thermal treatment (Wickramaratne et al., 2014) .

(2) **Thermal treatment with activating agents:** Compared to carbonization, pyridonic-N groups are more likely to be formed in the presence of chemical activating agents during activation that create an oxidising atmosphere (Sevilla et al., 2011). It was also shown that no quaternary-N species existed in the porous carbon obtained by chemical activation unlike for carbonisation process (Lezanska et al., 2009).

The change of nitrogen groups in precursor during KOH activation was studied by Sun et al. using aminated polyvinyl chloride as precursor (Sun et al., 2014). The nitrogen containing groups such as pyridinic N, pyrrolic and pyridone N, quaternary nitrogen and pyridine-N-oxide significantly chang during KOH activation. Pyridinic N and quaternary nitrogen disappear or transform into pyrrolic and

pyridone N, which is the main form in carbon (Laszlo et al., 2001a, Pels et al., 1995). Meanwhile, the total amount of nitrogen decreases with the increase of impregnation ratio KOH/AC, which also means that the existence of activating agents like KOH accelerate the change of nitrogen containing groups in precursors compared to reference (Wickramaratne et al., 2014 and Hao et al., 2010).

Sevilla et al. (2011) found that pyrrolic nitrogen in polypyrrole transformed into pyridinic nitrogen and N-oxides of pyridine-N (Pels et al., 1995 and Shrestha et al., 2010) during activation. The proportion of pyridinic-N decreases from 16% to 11% as the activation temperature increases from 600 to 700 °C. After KOH activation at 700 °C, only pyridonic-N and a small fraction of pyridinic-N groups are observed in the active carbon as the temperature further increased to 800 °C, both the pyridinic-N and pyridonic-N groups are gradually removed, pyridinic-N is much easier to be eliminated. Quaternary-N is the most stable N containing groups in pyrolysis condition (Tian et al., 2008).

Zhao et al. (2012) obtained the porous carbon using tri-continuous mesoporous silica IBN-9 as a hard template and p-diaminobenzene as the single nitrogen-containing precursor containing pyridine nitrogen and the Ph-NH_2 group. After KOH activation at 600 °C, the total amount of nitrogen and Ph-NH_2 decreases as most of the nitrogen species is transformed into pyridine nitrogen.

Table 2.5 the performance of different activating agents for different precursors

Precursors	S_{BET} (m^2/g)	V_{micro} (cm^3/g)	V_t (cm^3/g)	D_r (nm)	Ref.
KOH activation					
coal tar pitches	2600-3600	0.8-1.03	2.56-3.18	2.89 - 4.05	Shao et al., 2011
anthracite	2326	0.62	1.05		Lillo-Ródenas et al., 2004
acetylene based nanotube	1670				Raymundo-Pinero et al., 2005
vacuum residue	3100	1.45	1.57		Wahby et al., 2010
decanted oil	2595	1.16	1.16		Wahby et al., 2010
mesoporous carbons	2700	1.00	1.70	0.84	Choi et al., 2007
cork powder waste	1336		0.56	0.66	Cardoso et al, 2008
active carbon	3190	1.09	1.69	2.5	Wang et al.,2009
glucose	1283	0.61	0.44		Li et al., 2011
maize stalks	1523	0.624	0.76	0.99	El-Hendawy 2009
fir woods	1064	0.51	0.61	2.3	Wu, et al., 2005
pistachio	1096	0.55	0.61	2.2	Wu, et al., 2005
polystyrene-based cation exchangeable resin	1947	0.83	1.28	2.6	Park et al., 2002
Graphite (C-O)	2590	0.86	2.0		Fu et al., 2011
poly(vinylidene chloride)-based carbon	2151	0.85	0.90		Cai et al., 2014
saran-derived carbons	2200	0.96	1.01		Dziura et al., 2014
corncob	2596	1.11	1.43	2.2	Tseng et al., 2005
rice straw	1917	0.73	0.94	1.03	Basta et al., 2009
anthracite	3380		1.5		Gorka et al., 2008

Precursors	S_{BET} (m^2/g)	V_{micro} (cm^3/g)	V_t (cm^3/g)	D_r (nm)	Ref.
wood	733	0.143	0.359		Hsu et al., 2000
cellulose	678	0.284	0.333		Hsu et al., 2000
lignin	514	0.214	0.246		Hsu et al., 2000
xylan	926	0.395	0.443		Hsu et al., 2000
activated carbon, Norit® SX2 POCH-Poland	2800	1.03			Lota et al., 2008
phenol–formaldehyde resins	1840	0.84	0.96	2.1	Teng et al., 2000a
commercial active carbon	1464	0.59	1.36		Jin et al., 2010
synthesized carbon using Pluronic F127	1685	0.47	1.25		Jin et al., 2010
NaOH activation					
anthracite	1630				Lillo-Ródenaset al., 2004
acetylene based nanotube	562	0.22	0.41		Raymundo-Pinero et al., 2005
rice husk	2841	0.849	1.692	2.38	Song et al., 2012
K_2CO_3 activation					
pistachio shell	1800	0.78	0.80		Hayashi et al.,2002
Na_2CO_3 activation					
spanish anthracite	45		0.02		Lillo-Ródenas et al., 2004
waste newspaper	790		0.78		Okada et al., 2003
Li_2CO_3 activation					
waste newspaper	680		0.53		Okada et al., 2003
Cs_2CO_3 activation					
waste newspaper	1310		0.80		Okada et al., 2003

Precursors	S_{BET} (m^2/g)	V_{micro} (cm^3/g)	V_t (cm^3/g)	D_r (nm)	Ref.
$ZnCl_2$ activation					
N-carbon monoliths	537	0.218	0.258		Hao et al., 2010
honeycomb-monoliths	924	0.37	0.38		Vargas et al., 2012
cherry stones	1971	0.74	1.15		Anson et al., 2004
$FeCl_3$ activation					
coffee fruit	965	0.40	0.51	0.63	Oliveira et al.,2009
$CaCl_2$ activation					
honeycomb-monoliths	1469	0.60	0.64		Vargas et al., 2012

Note: S_{BET}: specific surface area calculated by BET method; V_{micro}: micropore volume; V_t :total pore volume; D_r : average pore size.

2.2.4 The performance of activated carbon on CO_2 absorption

The adsorption behaviour of CO_2 on active carbon derived from different precursors under various temperatures and pressures has been widely studied. The results show that ACs that possess high surface area and abundant microporosity exhibit a high capacity for CO_2 under very high pressures, up to 20 bars, and low temperature 0 °C (Shao et al., 2011, Cai et al., 2014, Meng et al., 2012, Mishra et al., 2011; Hao et al., 2011). However, CO_2 uptake decreases dramatically with an increase of temperature and decrease of CO_2 partial pressure. It still fails to meet flue gas-simulated conditions. Typical flue gas from post-combustion effluents like power plant contains 3-15 % CO_2 and more than 70% nitrogen at a pressure of approximately 1 bar and high temperatures of up to 75 °C (Balsamo et al., 2014), which mean that much stronger force is needed in order to avoid CO_2 escaping from the pore structure (Zhang et al., 2013). The chemical properties of the carbon surface and characteristics of porosity (Song et al., 2012) are key factors to enhance CO_2 on active carbon. In this chapter, both of them will be discussed in detail.

2.2.4.1 The role of porosity on CO_2 adsorption

Adsorption potential in pores Gas adsorption in pores depends on the potential energy resulting from the interaction between a gas molecule and the whole pore structure, which is significantly affected by the pore shape and pore width (Lowell et al., 2012). For activated carbon, the adsorption potential of pores is from the van der Waals potential created by different pore walls. The interaction between slit pores and gas molecule in different kinds of pores are different (Lowell et al., 2012). The adsorption in macropores is similar to the adsorption on a surface because of the large pore width, so the adsorption potential is determined by interactions between gas molecules and surface. Adsorption potential in mesopores shows two shallow minima that are much stronger than the center of the pore, indicating that not only the adsorbate-pore wall interaction but also adsorbate-adsorbate intermolecular attraction dominates the adsorption potential. It is also the main reason for the existence of capillary condensation in mesopores. In micropores, for

different kinds of adsorbate molecule, the interaction potential in micropores is different.

Evertett and Powl (1976) calculated the interaction force between adsorbent and adsorbate in slit micropores. Figure 2.5 illustrates the distribution of sorption potential along with the vertical section of parallel pore walls (Zhang et al., 2013). The slit width is the distance between two adjacent graphite layers, d is half of the slit width and r_0 is the molecular radius of the adsorbate. It can be found that two energies minimum peak existed when the slit width is larger (Figure 2.5a). With the decrease of slit width, the energy minima merged to one peak at the center of the pore and the absolute value of interaction potential increases, indicating the adsorbate strongly interacts with adsorbate molecule. When d/r_0 is 1.0, the interaction potential reaches a maximum. The change from one peak to two minima peaks of interaction potential can be considered as the critical stage, because the interaction potential sharply decreased as the slit width decreases further.

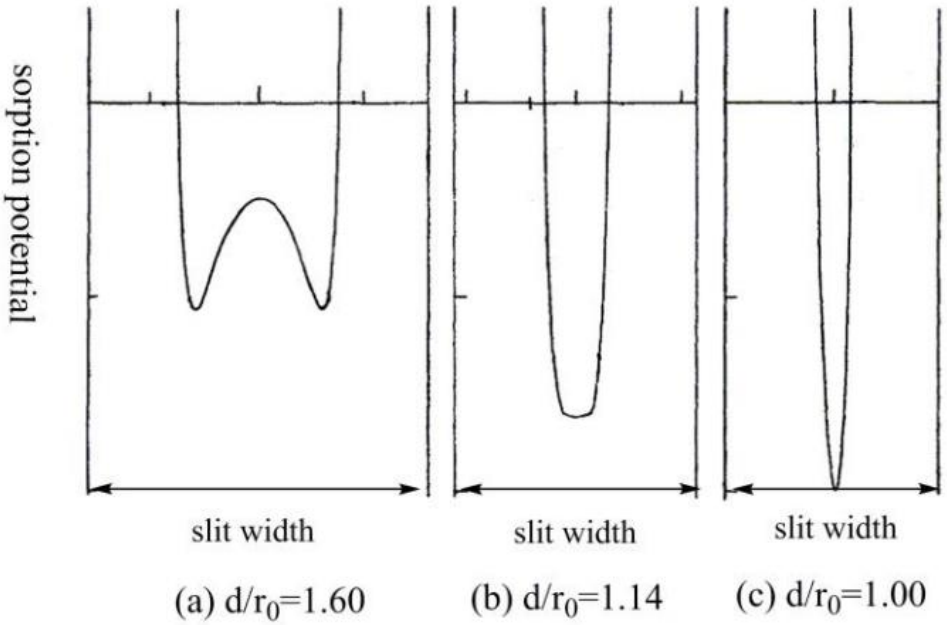


Figure 2.5 The sorption potential between adsorbate and micropores (slit pores) (Zhang et al., 2013)

CO_2 adsorption in micropores CO_2 adsorption in micropores can be divided into two stages: at low partial pressure, micropore filling dominates the process, CO_2

molecules fill the entire pore space and the adsorbate is in a liquid-like phase (Zhang et al., 2013); at higher pressures, the relative contribution of the solid-adsorbate interaction potential decreases and multilayer adsorption occurs, resulting in a reduced isotherm slope (Mishra et al., 2011). As studied, activated carbon showed high adsorption capacity at high CO_2 pressure. However, due to the weak interaction force created by Van der Waals force, adsorption on activated carbons is very sensitive to CO_2 partial pressure and temperature. The adsorption capacity was dramatically decreased with the increasing adsorption temperature or decreasing CO_2 partial pressure. Therefore, the low adsorption capacity of porous carbons at low partial pressures or high temperatures has become the major drawback that has limited their practical applications (Lee et al., 2015; Samanta et al., 2011).

As mentioned above, the van der Waals force decreases with the increase of pore diameter, and the critical slit width where the energy minimum changes from one peak to two peaks for CO_2 is 0.76 nm (0.54 nm as pore width) (Everett et al., 1976; Zhang et al., 2013). So, preparation of activated carbons with an ultra-micropore (0.70 nm) domain structure become the best choice in order to meet the requirement of post combustion CO_2 capture, and recent work has gradually shifted toward ultramicropores. (Wahby et al., 2012, Lee et al., 2013, Sun et al., 2013, Wickramaratne et al., 2013a, Wickramaratne et al., 2013b, Yin et al., 2013, Wickramaratne et al., 2014, de Souza et al., 2013 and Presser et al., 2011).

It has been established that the ultra-microporosity plays an important role in gas adsorption (Shafeeyan et al., 2010). Ultramicropores (<0.7 nm) are the preferred place for CO_2 adsorption, which fills pores to a high degree rather than multilayer or monolayer adsorption. As shown above, smaller pores possess stronger interaction between CO_2 and the carbon surface, indicating that smaller pores are more effective for CO_2 capture at high temperature or low pressure (Zhang et al., 2013). Recently, much effort has focused on this area. In particular, based on a large number of experiments, Yin et al. (2013) found that the surface area is not the determining factor for CO_2 adsorption, where ultra-micropores are more important. Similarly, Zhang et al. (2013) produced microporous carbon materials with extremely small pore size by employing polyaniline as a carbon precursor and

concluded that the capture capacity of the carbon adsorbents may strongly depend on the fine pore size distributions rather than on the specific surface area or total pore volume. Wei et al. (2012) used microporous activated carbon prepared from bamboo to investigat the role of narrow pores, the results indicate that there is a good linear relationship between volume of micropores in the range of 0.33–0.82 nm and CO_2 adsorption at 273 K and 1 bar, and micropores of about 0.55 nm diameter produced the major contribution. Moreover, Zhang et al. (2013a) further verified that the CO_2 adsorption capacity is associated with the pore volume of pores smaller than a specific pore size, which varied with temperature and CO_2 partial pressure. The critical pore size 0.8 nm, 0.7 nm and 0.54nm determined for CO_2 adsorption at 273K 1bar, 298K 1bar and 298K 0.15bar respectively. It indicates the minimal required interaction force to bind CO_2 molecules increases as the partial pressure decreases and temperature increases. On the other hand, CO_2 diffusion in microspores is the limiting step of the adsorption process (Balsamo et al., 2013 and Wahby et al., 2010), and although mesopores or macrospores have no contribution to adsorption capacity, they are still play an important role on the enhancement of the CO_2 adsorption rate.

The synthesis of the specific adsorbents containing ultra-micropores for CO_2 adsorption is the key point. Carbonizing synthesized materials with designable porosity (Liu L et al 2012, Lu et al., 2004, Pevida et al., 2008, Hao et al., 2010) and chemically activating precursor like biomass (Zhao et al., 2010; Coromina et al., 2016), polymers (Ludwinowicz et al., 2015) are the main approaches to prepare microporous carbons. In comparison, chemical activation has unique advantages, like adaptability, inexpensive and controlled micropore size distribution and is widely used and recognized. Potassium hydroxide has been proved to be the best activating agents to prepare specific ultra-microporous adsorbents. Many papers have reported that activated carbons with high CO_2 adsorption capacity were prepared by KOH activation (see Table 2.6). By now, Jujun grass (Coromina et al., 2016), coconut shell (Yang et al., 2015) and bamboo (Wei et al., 2012) present CO_2 capacities of 1.3-1.6 mmol/g at 298 K, 0.15 bar while CO_2 adsorption capacities of most commercial carbons are usually below 5 wt% (ca. 1 mmol/g) at 0.15 bar CO_2

and 25 °C despite their very high surface areas and pore volumes (Himeno et al., 2005; Hao et al., 2011).

2.2.4.2 CO_2 adsorption on surface modified activated carbon

However, the ultra-microporosity cannot be developed without limit. Another effective way to improve the CO_2 adsorption capacity at low partial pressure is to enhance the surface affinity to CO_2 via surface modification by heteroatoms including nitrogen, oxygen and metals, which have been studied by many papers (see Table 2.6).

Oxygen containing groups Based on the widely-accepted acid-based interaction mechanism for CO_2 adsorption, the presence of oxygen containing groups most of which are acidic on carbon surface, would have negative influence on CO_2 adsorption. However, Xing et al. (2014) used carbide-derived carbons with different oxygen content prepared from HNO_3 oxidation to adsorb CO_2. The results indicated that the oxidation process led to an increase in CO_2 adsorption capacity of the porous carbons and the CO_2 adsorption capacity of the CDCs had a linear correlation with their surface oxygen content, which was similar to the results obtained by using oxidized phenolic resin carbon as CO_2 adsorbent (Plaza et al. 2013). Moreover, Xing et al. (2014) also investigated the possible strengthening mechanism of O containing groups by quantum chemistry and found that H bonding formed between O containing groups and CO_2 molecules that can enhance the CO_2 capacity of samples. No more reports in this area have been published; further study needs to be carried out in order to thoroughly understand the mechanism.

Nitrogen containing groups The introduction of N containing groups into carbon materials has been widely studied because these groups increase the basicity and charge delocalization of the carbon surface which can enhance selective CO_2 adsorption (Shen et al., 2013; Sivadas et al., 2016; Xing et al., 2012; Wang et al., 2011). Two strategies have been employed: utilization of nitrogen-rich precursors and post ammonification of porous carbon at high temperatures. The post treatment method is not commonly used due to the limited improvement on CO_2 uptake and the introduction of additional complex and time-consuming synthetic steps

involving the use of corrosive reagents (Plaza et al., 2010; Zhang et al., 2016 and 2016a). Therefore, using nitrogen rich precursors like acrylonitrile, benzimidazole, polypyrrole, polyurethane and biomass like bean dreg is more attractive. As shown in Table 2.6, overall, activated carbons prepared from materials with nitrogen containing groups possessed higher CO_2 adsorption capacities than that from nitrogen-free precursors like some biomass and polymers. There are some detailed studies claiming that nitrogen functionalities could improve the CO_2 uptake and heat of adsorption (Sánchez-Sánchez et al., 2014; Sevilla et al., 2011; Fan et al., 2013; Xing et al., 2012). Sánchez-Sánchez et al. (2014) studied the effect of nitrogen containing groups on CO_2 adsorption using polyamide. The influence of different nitrogen functional groups like pyridinic, pyrrolic and quaternary N was investigated in this paper. The rank of importance of different groups were reported as pyrrolic > pyridinic > quaternary N. In Sevilla's paper, they believe that the nitrogen forms pyridonic-N structures which is the main form of nitrogen in carbon, may be beneficial for CO_2 capture (Sevilla et al. 2011). The reason was that the p orbital in its –OH group in pyridone nitrogen group produce a p-p conjugation effect with its p-π bond in pyridine nitrogen, which endows the nitrogen located in the ortho-position of –OH with stronger electron atmosphere consequently enhances its Lewis basicity. Therefore, the CO_2 uptake of porous carbon increased (Fan et al., 2013). Otherwise, Xing et al. (2012) pointed out that hydrogen-bonding between N-H and O accounted for the superior CO_2 uptake of the activated carbon based on experimental results and quantum study.

However, some papers also reported that there is no direct relation between the CO_2 adsorption capacity and the total amount of N (Zhang et al., 2012; Sun et al., 2013). Similarly, it can be observed from Table 2.6 that the uptake of porous carbon materials with a high nitrogen content of 28 wt% is 1.36 mmol/g at 25 °Cand 0.15bar, which was lower than that of RF resin derived samples with 4.32 wt% N content (1.80 mmol/g) and even well-designed N-free porous carbon materials (1.6 mmol/g). Adeniran et al. (2016) studied the CO_2 adsorption performance of N-doped and N-free carbon materials with identical or closely matched pore size and the results showed that the presence of N has no beneficial effect on the adsorption of CO_2, which was consistent with some other papers (Sun et al., 2013; [a]Sevilla

et al., 2013; Zhang et al., 2013). Simulation results from Kumar et al. (2015) also point out that N doping can only marginally improve the single component adsorption of CO_2. In other words, the effect of nitrogen on CO_2 capture is still debatable and more research is needed.

Table 2.6 CO_2 adsorption capacity of activated carbon materials at 25 °C and 0.15 bar

Samples	Surface area (m^2/g)	N Content (wt%)	CO_2 uptake (mmol/g)[a]	Ref.
Potassium hydrogen phthalate derived carbon	932	0	1.60	Adeniran et al.,2014
Jujun grass derived carbon	1512	0	1.50	Coromina et al., 2016
Phenolic resin spheres (C-K-5)	1160	0	1.50	Ludwinowicz et al., 2015
Granular Bamboo-Derived Activated Carbon	1846	0	1.30	Wei et al., 2012
Phenolic resin spheres (CS-8)	669	0	1.30	Wickramaratne et al., 2013b
Sawdust derived carbon	1390	0	1.20	sevilla et al., 2011a
Lignocellulosic feedstock derived carbon	1322	0	1.20	Parshetti et al., 2015
Waste coffee ground derived carbons	1624	0	1.20	Travis et al., 2015
Carboxylic phenolic resins	897	0	1.10	Zhou et al., 2016
Nitrogen-rich porous polymer	993	28	1.36	Chen et al., 2012
Melamine–formaldehyde (MF) resins	336	27.2	1.50	Pevida et al., 2008
1,3-bis(cynomethyl imidazolium) chloride	1317	22.3	1.70	Sethia et al., 2015
om-ph-MR	256	18.16	0.80	Lee et al., 2015
Benzimidazole	830	17.6	2.03	Ashourirad et al., 2016

Samples	Surface area (m^2/g)	N Content (wt%)	CO_2 uptake (mmol/g)[a]	Ref.
N-doped mesoporous carbons	537	13.1	1.20	Wei et al., 2013
p-diaminobenzene derived carbon	614	10.5	1.81	Zhao et al., 2012
N-Doped Polypyrrole-Based Porous Carbons	1700	10.14	0.92	Sevilla et al., 2011
Sucrose and urea based carbon	936	8.9	1.55	Sivadas et al., 2016
Benzimidazole-Linked Polymer based carbon	1630	7.88	2.10	Ashourirad et al., 2015
Ammonia modified biomass carbon	2511	7.21	1.59	Zhang et al., 2016
Nanostructured templated carbon	2559	7	1.48	Wang et al., 2011
Nitrogen-doped coconut shell-based carbon	879	6.16	1.50	Yang et al., 2015
N-doped carbon nanotube	979	5.9	1.00	Wei et al., 2013
Polypyrrole derived carbon	941	5.8	1.70	To et al., 2016
Polybenzoxazine derived carbon	1255	5.25	1.77	Wan et al., 2015
Polypyrrole functionalized graphene sheets	1360	4.8	1.50	Chandra et al., 2012
N-doped carbons	3360	4.7	1.00	Xia te al., 2011
Nitrogen-doped porous carbon	1376	4.6	1.50	Kou et al., 2016
Chitosan derived microporous carbon	1381	4.59	1.10	Fan et al., 2013
Chitosan-derived activated carbons	1355	3.23	1.58	Fujiki et al., 2016
N-doped porous carbons	1979	4.32	1.80	Ma et al., 2013
Poplar anthers derived carbon	1473	3.81	1.42	Song et al., 2013
Meta-aminophenol–formaldehyde resin	272	3.8	1.67	Zhou et al., 2015
N-enriched carbon monoliths	1740	3.38	1.51	Ma et al., 2014

Samples	Surface area (m^2/g)	N Content (wt%)	CO_2 uptake (mmol/g)[a]	Ref.
Biomass derived carbon	1636	3	1.20	Alabadi et al., 2015
Nitrogen-Doped Porous Carbon Monolith	467	1.92	1.27	Hao et al., 2010
Popcorn-Derived Porous Carbon	867	1.62	1.21	Liang et al., 2016
Nitrogen-containing carbon spheres	642	1.60	1.48	Liu et al., 2012
Bean dreg derived carbon	1060	0.28	1.40	Xing et al., 2012
Coconut shell derived carbon	832	0.20	1.40	Yang et al., 2015
ZIF-8 derived carbon	950	--	1.40	Gadipelli et al., 2012
Porous carbon monolith	670	-	1.10	Hao et al., 2011

2.2.4.3 Metal-doping carbon materials

The introduction of nitrogen improves the carbon surface and enhances the interaction between CO_2 and the carbon surface so as to increase the CO_2 uptake. In addition, metallic additives in carbon materials also draw attention. Metal doping of carbon materials has been widely used in the catalyst industry. The presence of metallic species on the carbon surface or inserted into the carbon layers can also significantly enhance CO_2 uptake. Normally, metallic additives in the form of metal oxides act as the electron donor in active carbon, which can improve the basicity of the surface.

Several research groups have shown that potassium intercalation in the form of surface potassium oxides groups achieved via an innovative chemical activation protocol can be a powerful method to boost CO_2 uptake, especially at low CO_2 partial pressure (Liu et al., 2015; Zhao et al., 2012). Liu (2015) reported that the potassium intercalation gives rise to more than double the CO_2 uptakes for nitrogen-free phenolic resin derived carbons. The results suggested that the greatly enhanced surface affinity for CO_2 is closely linked to the solid state electrostatic effects created by the extra framework cations due to alkali intercalation, a phenomenon

that is usually only observed for zeolite and MOF adsorbent materials (Wu et al., 2010; Bae et al., 2013). Potassium intercalation can potentially serve as an effective approach for remarkably enhanced CO_2 capture performance of carbon-based adsorbents at low partial pressure that can be produced from a wider range of feedstocks.

Transition metals The experiments using transition metal like nickel (Jang et al., 2012), cooper (Kim et al., 2010), zirconium and zinc (Somy et al. 2009) as metallic additives showed that the existence of metal oxide can enhance CO_2 capacity of active carbon, while pure metal or metal oxides like Fe_2O_3 had no effect. The improvement of the adsorptive properties of activated carbons using metallic species, such as NiO and Cu_2O, has been recently reported, even though the pore volume and surface area decreased after decoration (Kim et al., 2010 and Somy et al. 2009). The reason might be that the existence of metal oxide NiO and Cu_2O serving as electron donors enhance the adsorption of carbon dioxide due to the acid–base properties. The CO_2 uptake of activated carbon impregnated with Cr_2O increases about 20% in comparison to raw activated carbon, while it can be further enhanced by co-impregnation of Zn^{2+}compared to independent impregnation.

2.2.4.4 CO_2 adsorption at flue gas condition

Flue gas from a typical coal-fired power plant contains 12-15% CO_2 at about 40-50 °C and it will be commercially and technically unrealistic to further cool the flue gas to room temperature in order to cater for carbon based materials. Although many studies have tried to improve the performance of activated carbon, most of them just reported the adsorption capacity up to 25 °C and quite few reported its performance at 40-50 °C. When the adsorption temperature increased from 25 °C to real flue gas conditions, the adsorption capacity sharply decreased about 40-50%. For instance, the uptake of benzimidasol derived carbon declined from 2.03 mmol/g at 25 °C to 1.0 mmol/g at 50 °C (Ashourirad et al., 2016). The adsorption capacity of most reported samples is only 0.5 mmol/g-1.0 mmol/g at 40-50 °C and 15% CO_2 in nitrogen (Table 2.7). It seems that surface nitrogen containing groups are not the key factor that determine the adsorption. Benzonimidazole based samples (17.6wt%), N-doped carbon (5.8wt%), chitosan derived carbon (3.38wt%)

achieved similar uptakes 1 mmol/g at 50 °C and 0.15 bar (Table 2.7). However, higher interaction forces between CO_2 and carbon were needed as temperatures increase to 50 °C. Ashourirad et al. (2016) found that pores with diameters smaller than 0.4 nm are the most efficient in capturing CO_2 at 50 °C, 0.15 bar that was around 0.5 nm at 25 °C. Controlling the synthesis of samples with narrow micropore domain structures of 0.4 nm is almost impossible. Surface modifications incorporated with surface containing groups might be a potential way.

Table 2.7 CO_2 adsorption capacities of samples reported at 0.15 bar and 40-50 °C

sample	T (°C)	Capacity (mmol/g)	Reference
Benzimidazole	50	1.0	Ashourirad et al., 2016
Polypyrrole	50	1.0	To et al., 2016
om-ph-MR	50	0.45	Lee et al., 2016
CP-600-2	50	0.5	Sevilla et al., 2011
AC2-635	50	0.65	Fan et al., 2013
SA-2N-P	45	1.0	Ma et al., 2014
AS-700-2	50	0.5	Sevilla et al., 2011a
C-K-5	50	0.7	Ludwinowicz et al., 2015
HT150–800	50	0.75	Parshetti et al., 2015

Nowadays, CCS from large stationary emission sources like coal-fired power plants is widely regarded as the most efficient strategy to reduce anthropogenic greenhouse gas emission in the short term. However, as reviewed, there is no technology perfectly meeting the requirements of low concentration CO_2 capture from flue gas. Although CO_2 adsorption using activated carbon-based CO_2 adsorbents is considered to be one of the most promising technologies due to their unique advantages compared to chemical absorption process, the barriers of physical adsorption process at low partial pressure still need to be overcome. It is also the key to commercialize the SALT technology based on activated carbon.

2.3 Aims and objectives

The proposed PhD project aims to utilise abundant and easily accessible materials such as biomass or polymers as precursors, with alkaline metal based compounds as activating agents, to prepare novel activated carbons using alkaline metal based compounds as activating agents with exceptional CO_2 adsorption performance to meet the requirement of post combustion CO_2 capture in power plant. The specific objectives include:

1) To explore various precursors including polymer and renewable feedstocks to prepare novel CO_2 adsorbents with high adsorption capacity and high CO_2/N_2 selectivity at 0.15 bar CO_2.

2) To identify the role of textural structure and surface chemistry on CO_2 adsorption capacity at different temperatures and pressures and to establish the fundamentals that govern the performance of CO_2 adsorption on porous carbons.

3) To develop new approaches to boost the CO_2 adsorption of carbon materials especially at low partial pressures.

Chapter 3 Methodologies

3.1 General sample preparation

Two kind of easy accessible precursors rice husk (biomass) and polyisocyanurate (PIR) based material (polymer) were used to prepare the CO_2 adsorbents in this project. KOH and K_2CO_3 have been intensively investigated as activating agents to prepare carbon materials especially microporous carbon materials. In addition, our former research (Liu et al., 2015) and researches from other research group (Zhao et al., 2012) found that potassium intercalation during KOH activation process was beneficial to the adsorption of CO_2. So in this project, potassium compounds KOH and K_2CO_3 were chosen as the activating agents. The experimental parameters like mixing procedure, activation time, atmosphere and temperature were designed referring to the references (Liu et al., 2015; Lozano-Castello et al., 2001; Zhang et al., 2013; Tseng & Tseng, 2005).

The general activation procedure was as follows: The as-prepared sample mixed with activating agents like KOH and K_2CO_3 was heated up in a purpose-designed carbonization/activation furnace to the desired temperature at a heating rate of 5 °C/min in a nitrogen flow of 1 L/min and was maintained at this temperature for 1 h before it was cooled down to ambient conditions. To yield the final bio-carbon products, the mixture was removed from the activation furnace and washed with excessive quantities of de-ionized water until neutral.

In order to improve the performance of adsorbents, pre-treatment methods like oxidation and compaction were also employed. The procedure was as follows:
1) ***Pre-oxidation***: Pre-oxidation of carbon precursors in air is a fundamental stage in the preparation of activated carbon, with great influence on the primary pore structure and chemical property of activated carbon (Sebbahi et al., 2014). In this study, oxidation was employed to pre-treat the biomass and polymer precursors. The generally procedure was as follows: a certain amount of the sample was put in a horizontal tube furnace under flowing compressed air (50 mL/min). The temperature was then increased from ambient to the desired temperature at a heating

rate of 0.5 °C/min and was kept there for 6 hours after which it was cooled to room temperature. The sample was collected and stored for further treatment.

2) ***Pre-compaction:*** the oxidized sample was mixed with 30 ml of KOH solution with a pre-selected AC/KOH mass ratio for 24 h. These samples were then dried at 105 °C and ground into powder for pellet pressing. A 13-mm diameter evaluable pellet die with 10 tons of maximum load were employed to compress the samples into 1.5 mm thick pellets.

3.2 Characterization of samples

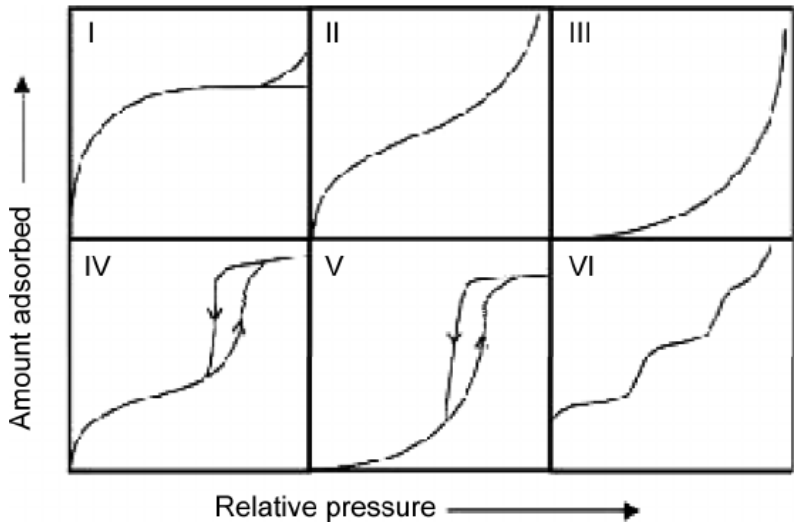
3.2.1 Textural properties

Gas adsorption techniques have been widely used to measure the textural properties of adsorbents. This method of analysis is based on the reversible physisorption of gas molecules on a solid surface to obtain the equilibrium adsorption capacity of gas as a function of pressure, and then with the help of theoretical models, the related physical quantities such as surface area, pore volume and pore size distribution can be calculated. Low temperature nitrogen adsorption method is currently the the most widely used and understood method. In this study, the micromeritics ASAP2020 system was employed to characterize the textural properties of prepared samples. This method will be discussed in detail in this section.

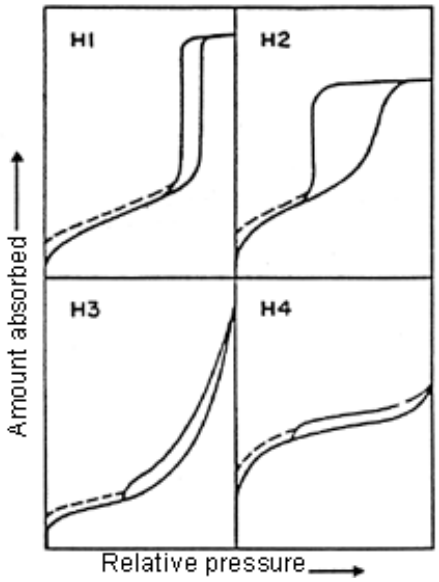
3.2.1.1 Classification of N_2 sorption isotherms

According to the IUPAC (International Union of Pure and Applied Chemistry), pores in solid materials can be divided into 3 types: micropores (smaller than 2 nm), mesopores (2-50 nm) and macropores (>50 nm) (Sing et al., 1982). Adsorption properties in the different pore types also vary. In micropores, the strong adsorption potential derived from the interaction between the N_2 molecule and surface caused by London Forces. Adsorption in micropores can be explained well by ‘micropore filling mechanism (Brown et al., 2000). Mesopores have a significant influence on the transport process of gas from the gas phase to micropores and capillary

condensation will happen at relative high pressures (P/P_0>0.4). As for macropores, they are just considered as the transportation paths. This is because of the different pore structures existing among materials. The adsorption isotherms obtained from different materials showed different shapes. Thousands of adsorption isotherms have been categorized into 6 classes (I to VI) by Brunauer, Deming, Teller and Sing, as shown in Figure 3.1a (Brunauer et al., 1940; Gregg et al., 1983).



(a)



(b)

Figure 3.1 Classification of N_2 sorption isotherms (Kumar et al., 2016)

Type-I isotherms are normally observed in porous carbon materials and zeolites that have a micropore domain structure as well as high surface area. It can be seen from

the Figure 3.1 that a sharp uptake occurs at low relative pressure typically <0.1, followed by a horizontal plateau at high relative pressures. However, when the pressure almost reaches saturated vapour pressure, adsorption isotherm quickly increases (dotted line) because of adsorption in macropores created by the gap between particles such as the N_2 adsorption on non-porous metal oxide.

Type II isotherms exhibit multiple-layer gas adsorption on non-porous materials falling into this category. When the relative pressure is increased to about 0.3, the first adsorbed layer is almost completed. With the further increase of relative pressure, a second layer adsorption begins and in theory infinite layer adsorption could happen at saturated vapor pressure.

Type III isotherms only happens when the interaction between adsorbent and adsorbate is much weaker than the intermolecular force of adsorbate. At low partial pressures, the adsorbate molecule is only adsorbed around the active site on the surface, which will become the preferential place for more molecules as pressure increased. Unlike type-II isotherms, some sites on the surface have already reached multilayer adsorption while single layer adsorption on other sites is still taking place.

Porous materials with mesopores and macropores exhibit type IV isotherm behaviour. At relative high partial pressures (P/P0>0.4), hysteresis loop started to emerge, which is associated with the filling and emptying of mesopores due to the capillary condensation. Based on the shape of hysteresis loops, de Boer divided into four classes (H1-H4) as shown in Figure 3.1. Type H1 is due to open-at-both-ends cylindrical pores; type-H2 is due to slit pores; type-H3 is because of open-at-both-ends wedge-shaped pores; type-H4 is because of inkpot-like pores (Everett et al., 1958).

Type V isotherms are like type-III isotherm. Type V isotherms also exhibit weak adsorbent-adsorbate interaction force. At high relative pressure, type V isotherms also show hysteresis loop, which is associated with mesopores.

Type VI isotherms are also called step-wise isotherms and is associated with layer-by-layer adsorption on a highly uniform surface, for example, the adsorption of krypton on clean metal surface.

3.2.1.2 Assessment of surface area

Many adsorption methods like Langmuir adsorption theory, Brunauer-Emmett-Teller (BET) adsorption model have been used to calculate the surface area of materials (Brunauer etla., 1938). Unlike Langmuir, which could only describe Type I isotherm, the BET model which extends to multilayer adsorption isotherms is widely used to calculate the specific surface area of materials, based on the assumptions as follows:

1) Gas molecules are physically adsorbed on materials in multilayers and no intermolecular radial interaction exists.

2) There was no interaction between each adsorption layer.

3) The Langmuir model can be applied to each layer and the heat of adsorption of each layer is equal to the heat of liquefaction except the first layer.

When the pressure was lower than the saturated pressure. 1, 2, 3, ……, i adsorbate molecules were adsorbed on the surface and the surface area fraction of i^{th} molecule was labelled as Θ_i. Therefore, the total adsorption capacity of each layer can be calculated as follows:

$$\mathrm{n} = n_m \sum_{i=0}^{\infty} i\theta_i \tag{3.1}$$

As for the i^{th} layer, if the percentage of occupied surface area was Θ_i, the percentage of uncovered area was Θ_{i-1}, $\Theta_i + \Theta_{i-1}$ was equal to 1. According to Langmuir model, the adsorption rate of adsorbate molecules to form the i^{th} adsorption layer was the same as the desorption rate of adsorbate molecules of i^{th} adsorption layer:

$$\mathrm{a}_i \mathrm{P}\theta_{i-1} = a_i'\theta_i \exp(\frac{-E_i}{RT}) \tag{3.2}$$

Where E_i was the heat of adsorption of the i^{th} layer. In order to simplify the calculation, when i >1, E_i was equal to heat of condensation (E_l) and all layers had the same value:

$$E_2 = E_3 = \cdots\cdots = Ei = E_l \tag{3.3}$$

$$\frac{a_2'}{a_2} = \cdots = \frac{a_i'}{a_i} \tag{3.4}$$

Based on Equation 3.1-3.4, the adsorption capacity n can be obtained:

$$\mathrm{n} = n_m \frac{C\sum_{i=0}^{\infty} ix^i}{1+\sum_{i=0}^{\infty} ix^i} \tag{3.5}$$

Where,

$$\mathrm{x} = \frac{P}{g}\exp\left(\frac{-E_l}{RT}\right) \tag{3.6}$$

$$\mathrm{C} = \frac{a_1 g}{a_1'}\exp\left(\frac{E_1-E_l}{RT}\right) \tag{3.7}$$

So, Equation 3.5 can be converted into:

$$\frac{n}{n_m} = \frac{Cx}{(1-x)(1-x+Cx)} \tag{3.8}$$

As for Equation 3.6, when $P=P_0$, x=1. So Equation 3.8 can be converted into:

$$\frac{P/P_0}{V(1-P/P_0)} = \frac{1}{V_m C} + \frac{C-1}{V_m C}\cdot\frac{P}{P_0} \tag{3.9}$$

Where, V_m is the volume of gas needed for single layer coverage on surface, V is the adsorption capacity at pressure P. V_m could be calculated based on the equation above. So the total surface area of the sample could be calculated as follows:

$$\mathrm{S} = \frac{V_m}{V_{mol}}\cdot L \cdot A_m \tag{3.10}$$

Therefore, the specific surface area of porous materials is

$$S_g = \frac{V_m \cdot L \cdot A_m}{22400m} = \frac{4.36V_m}{m} \quad (3.11)$$

Where, V_{mol} is the volume of 1 mole nitrogen under standard condition (mL), L is Avogadro's number, A_m is the equivalent cross-sectional area (m^2/g), and m is the mass of adsorbate (g).

3.2.1.3 Assessment of micropore volume and total pore volume

The t-plot method transforms the adsorption isotherm (capacity N vs relative pressure P/P_0) into a t-plot curve, where the adsorption N is replotted against the multilayer thickness as a function of relative pressure P/P_0 (Lippens et al., 1965). Based on the BET method, the adsorption layer could be calculated as follows:

$$\mathrm{N} = \frac{V}{V_m} = \frac{C \cdot P/P_0}{(1-P/P_0)[1+(C-1)P/P_0} \quad (3.12)$$

If C is a constant,

$$N = f_C\,(P/P_0) \quad (3.13)$$

If the thickness of single layer is t_m, the total thickness could be $t = t_m\, f_C\,(P/P_0)$. If the porous material contains micropores, the t-plot curve was a polyline that possess an initial linear region with a high slope related to the adsorption in micropores, followed by a linear multilayer section with low slope. As for microporous materials, the adsorption capacity of nitrogen (V) obtained by the extension of linear multilayer section to y-axis result from micropores, so the microporosity could be calculated:

$$V_{mico} = 0.001546V \quad (3.14)$$

The pores are fully filled by adsorbate at relative pressure of 1 with the adsorption capacity of M_p and density of adsorbate in liquid (d), which has been proved by Gurvisch Law that all adsorbate adsorbed in pores at saturate pressure was in the form of a liquid. So, the total pore volume could be calculated: $V = M_p/d$

3.2.1.4 Pore size distribution

Macroscopic thermodynamic methods were limited by their suitability for the whole range of pore size distributions and accuracy. For instance, Dubinin–Radushkevich (DR) or Horvath-Kawazoe (HK) models were only suitable for micropore distributions, while Barrett-Joyner-Halenda (BJH) model could be only used for mesopores. In comparison, density functional theory (DFT) supplies a more rigorous analysis since it is based on the fundamental principles of statistical mechanics. However, the difficulty is to build up the right description of the fluid-fluid interaction. So, non-local density functional theory (NLDFT) that describes the behavior of fluid in pores from a molecular level as well as correlating the properties of adsorbate with their adsorption behavior in pores with different pore size were employed. The NLDFT method can generate a series of simulated isotherms, which can be correlated with experimental isotherms by Generalised Adsorption Isotherm (GAI) equation, allowing for calculations of pore size distributions. (Smith et al., 1994).

$$\mathrm{N}(P/P_0) = \int_{r_{min}}^{r_{max}} \rho(P/P_0, r) f(r) dr \qquad (3.15)$$

Where, r_{max} and r_{min} are the minimum and maximum pore width, respectively, $\rho(P/P_0,r)$ is the density of nitrogen in pores with pore width r at relative pressure P/P_0. f(r) is the pore size distribution function. The PSD can be obtained by solving the GAI equation. In the ASAP 2020 system, the SAIEUS (Solution of Adsorption Integral Equation Using Splines) program was used to calculate the pore size distribution (PSD) of these materials from adsorption isotherms using an NLDFT model based on the following critical elements. A Kernel was used to describe the adsorption isotherms as a function of the pore size and pressure; a regularization method using non-negativity constraints combined with optimally minimizing the second derivative of the calculated distribution via the L-curve method were also employed.

In addition, the NLDFT method was also applied to CO_2 adsorption isotherm at 0 °C so the PSDs of ultra-micropores could be obtained. This because N_2 molecules do not

diffuse easily into ultra-micorpores. Therefore, the whole range of PSDs was combination of N_2 isotherms at -196 °C along with CO_2 isotherms at 0 °C.

3.2.2 Morphology

Scanning electron microscopy (SEM) is a kind of electron microscope that scans the surface with a focused beam of electrons to produce a variety of signals containing information about morphology of the structure. In SEM, an electron beam with an energy between 0.2 keV to 40 keV, is emitted from an electron gun fitted with a tungsten filament cathode and focused on a spherical area (diameter 0.4-5nm). Secondary electrons and backscattered electrons released due to the interaction between accelerated electrons and sample surface are commonly used for imaging samples but reveal different information. Secondary electrons can effectively show the morphology of samples while backscattered electrons determine the contrast between areas with different chemical compositions. SEM can generate high quality images of a sample with the magnification ranging from 20X to 30000X. The incident high energy beam excites an electron in inner shell and the hole left will then be filled by the electron from outer shell. The movement of electron emits energy in the form of X-ray, which differs depending on the atoms. Based on the calculations of the X-ray signals, using Energy-Dispersive X-Ray Spectroscopy (EDS), the composition of samples can be analysed qualitatively or semi-quantitatively.

Transmission electron microscope (TEM) was also used to characterize the structure of activated carbons. In typical TEM, a high-energy beam of electrons is focused into a small, thin, coherent beam by using a condenser lens to shine through the thin sample, part of which will be transmitted depending upon its thickness and electron transparency. The objective lens converts the transmitted portion into an image on phosphor screen or charge coupled device (CCD) camera.

3.2.3 Composition analysis

After activation, there are a certain amount of potassium and/or silica left in the carbon lattice, so X-ray fluorescence spectroscopy (XRF) was used to measure the

content of those elements and X-ray diffraction (XRD) was employed to show the microcrystalline structure for the activated carbons.

The fundamental principles of XRF are similar to other instruments like the aforementioned EDS, which depends on the interaction between electron beams and X-ray with sample. XRF is suitable for the measurement of major elements (Si, Ti, Al, Fe, Mn, Mg, Ca, Na, K, P) and trace elements like Ba, Ce, Co, Cr, Cu, Ga, La, Nb, Ni, Rb, Sc, Sr, Rh, U, V, Y, Zr, Zn in the abundance >1 ppm. The procedure is as follows: The X-ray beam produced by a Rh target excites the sample, in return, the excited sample emits X-ray along a spectrum of wavelengths characteristic of the types of atoms present in the sample, which is measured by detectors, such as flow counter or scintillation detector. The intensity of the energy measured is proportional to the abundance of the element in the sample.

XRD is based on constructive interference of monochromatic X-rays produced a cathode ray tube and a crystalline sample. The constructive interference can only be generated if the conditions of the Bragg's Law ($n\lambda=2d \sin\theta$) is met. This law correlates the wavelength of electromagnetic radiation to the diffraction angle and the lattice spacing in a crystalline sample. By scanning the sample through a range of all the diffracted X-rays the d-spacing can be determined. Because different crystalline materials have unique d-spacings, their structure can be identified by comparing the d-spacing with standard reference patterns.

3.2.4 Surface chemistry

X-ray photoelectron spectroscopy (XPS) has been widely used to characterize the surface chemistry of materials including their elemental composition, chemical state and the electronic state of the elements present (Van der Heide et al., 2011). A beam of X-rays focused on the surface of the material results in atomic absorption of the X-ray photon which ejects an electron. The kinetic energy of the electron relates to the photon energy and binding energy of electron. The number of electrons that escape from the surface are measured by XPS under ultrahigh vacuum conditions. Because the energy of X-rays is known, so the binding energy could be calculated by the following equation:

$$B.E. = h\upsilon - K.E. - \phi_{spec} \quad (3.16)$$

Where, *B.E.* is binding energy, hυ is the energy of the X-rays used, K.E. is the kinetic energy of electron and ϕ_{spec} is the work function of the analyzer. The surface chemistry of material can be deduced by the photoelectron spectrum (the number of electrons detected vs binding energy). The binding energy can be used to identify the chemical elements on surface while the proportion of the peaks area can be used to calculate the composition. The same atom in different functional groups showed different binding energies, so the peak of some elements like nitrogen could be de-convoluted into several sub-peaks.

In this study, the X-ray photoelectron spectroscopy measurements were performed using a Kratos AXIS Ultra DLD instrument. Samples were mounted on the standard Kratos sample bar using double sided tape, (sellotape brand) these were inserted into the airlock and pumped down to ~ 3 x 10^{-7} Torr overnight before being transferred into the instrument analysis chamber. The analysis chamber pressure during the measurements was lower than 5 x 10^{-9} Torr.

Wide energy range survey scans were collected using pass energy 80eV in hybrid slot lens mode with a step size of 0.5 eV. High resolution data on the elemental photoelectron peaks was collected at pass energy 20 eV over energy ranges suitable for each peak, with a collection time of 5 minutes and step sizes of 0.1 eV. The charge neutraliser filament was used to prevent sample charging over the irradiated area. The X-ray source was a mono-chromated Al k alpha emission, run at 10mA and 12kV (120W). The data was recorded using Kratos VISIONII software and exported into vms format for data processing with CASAXPS (Version 2.3.17)

3.3 CO_2 adsorption

3.3.1 CO_2 adsorption isotherms

CO_2 adsorption isotherms of samples at 0 °C and 25 °C at varying relative pressures were also measured using volumetric analysis (Micromeritics ASAP 2420).

Modelling of adsorption isotherms

Langmuir model

The Langmuir model describe the relationship between the surface coverage of the adsorbed gas and the gas pressure above the surface at a fixed temperature based on the assumption as follows (Masel et al., 1996):

1) the adsorption sites on the surface are fixed, all of which have the same shape and size; 2) only one gaseous molecule can be adsorbed by each site and the heat released is constant during the process; 3) dynamic equilibrium between the gas phase and the gas adsorbed will be established.

Based on those consumptions, the adsorption process can be treated as a chemical reaction between adsorbate molecule A and empty site on the surface B and the reaction produces an adsorbed complex AB with an associated equilibrium constant K_a for adsorption and K_d for desorption.

The reaction between gas and surface is shown in equation:

$$\mathrm{A(g)} + \mathrm{B(s)} \frac{K_a}{K_d} \mathrm{AB} \tag{3.17}$$

The equilibrium constant K is calculated based on the concentration of the reactant and product

$$\mathrm{K} = \frac{K_a}{K_d} = \frac{[AB]}{[A][B]} \tag{3.18}$$

If the surface coverage θ (θ_{max} =1) and pressure are introduced, the equation is changed to

$$\theta = \frac{KP}{1+KP} \tag{3.19}$$

In the Langmuir model, the adsorption on surface is a monolayer, so the coverage can be calculated by the gas adsorbed at pressure P (q) and equilibrium adsorption capacity q_m, so the Langmuir equation is

$$\frac{\mathrm{q}}{q_m} = \frac{KP}{1+KP} \tag{3.20}$$

Dual-Site Langmuir model

The Langmuir model assumes that all adsorption sites on the surface are the same or the surface is homogeneous. Therefore, it is not suitable for heterogeneous surfaces, such as heteroatom doped carbon surfaces. Considering the heterogeneity of the prepared samples caused by surface modification, the dual-site Langmuir model is a better model to fit CO_2 adsorption isotherms. On heterogeneous surfaces, the adsorption energy of each site varies with the surface chemistry and structure. Therefore, the gas will be adsorbed on the most favorable sites followed by less favorable sites. In a simplified case, only two kinds of sites exist on the surface and both of them can be modelled by the Langmuir equation (Koresh et al., 1983; Mason et al., 2011). The dual-site Langmuir model is defined as:

$$\mathrm{q}=\mathrm{q_a}+\mathrm{q_b}=\frac{\mathrm{q_{max}b_A P}}{1+\mathrm{b_A P}}+\frac{\mathrm{q_{max}b_B P}}{1+\mathrm{b_B P}} \tag{3.21}$$

Where the subscripts A and B represent two different adsorption sites. q is the molar loading of adsorbate, and b is the adsorption equilibrium constants. The Dual-site Langmuir equation has been widely used in CO_2 adsorption on porous materials like activated carbon and MOFs.

3.3.2 CO_2 adsorption kinetics

In addition to adsorption capacity, the adsorption kinetics are also a key factor to evaluate the performance of adsorbents. From kinetic analysis, information such as adsorption rate and the residence time required will be obtained. This information is helpful for adsorbent design and operation. Many theoretical models have been developed to describe different kinds of adsorption processes. Among them, pseudo-first order, pseudo-second order and the double-exponential model have widely used to describe the adsorption process of solid adsorbents.

1 pseudo-first order

If the concentration of one reactant is in a constant excess during the reaction, so the reaction rate only depends on one of the two reactants. Lagergren's first-order rate equation is believed to be the earliest model used to describe adsorption rate based on adsorption capacity and the equation is as follows (Qiu et al., 2009):

$$\frac{dq_t}{dt} = k_1(q_e - q_t) \tag{3.22}$$

Where q_e and q_t represents the equilibrium adsorption capacity and adsorption capacity at time t respectively, and k_1 is the first-order rate constant. After the equation above is integrated with the boundary conditions q=0 at t=0 and q=q_t at t=t, the equation could be converted to

$$\ln\left(\frac{q_e}{q_e - q_t}\right) = k_1 t \tag{3.23}$$

And after rearrangement,

$$q_t = q_e(1 - e^{-k_1 t}) \tag{3.24}$$

2 pseudo-second order

In this model, the chemical reaction plays a key role in the rate-controlling step, the rate controlling step is chemical adsorption. The pseudo-second order model is expressed by the following equation (Qiu et al., 2009):

$$\frac{dq_t}{dt} = k_2(q_e - q_t)^2 \tag{3.25}$$

Where K_2 is the pseudo-second order rate constant. By integrating with the boundary conditions, the equation takes the following form:

$$\frac{1}{(q_e - q_t)} = \frac{1}{q_e} + k_2 t \tag{3.26}$$

Which can be rearranged to

$$q_t = \frac{t}{\frac{1}{k_2 q_e^2} + \frac{t}{q_e}} \quad (3.27)$$

3 double-exponential model

In some adsorption processs, the whole process can be divided into two steps: a fast phase involving adsorbate surface diffusion, followed by a slow phase controlled by the intraparticle diffusion, which is typically observed in CO_2 adsorption on PEI/silica and lead or copper adsorption onto activated carbon. The equation is as follows (Kondo et al., 2012):

$$M_t/M_e = A_s\,(1\text{-}exp\,(-k_s\,t)) + A_d\,(1\text{-}exp\,(-k_d\,t)) \quad (3.28)$$

Where M_t and M_e represent the adsorption capacity at time t and equilibrium adsorption capacity respectively. A_s and A_d are defined as the relative contribution of surface and diffusion barriers, respectively, which control the overall adsorption process, $A_s + A_d = 1$. k_s and k_d are the corresponding surface and intraparticle diffusion rate constants, respectively.

3.3.3 Thermogravimetric analysis

Thermogravimetric analyzer (Q500, TA instruments) has been also employed to examine the CO_2 adsorption characteristics of the samples. Thermogravimetric analysis is a thermal analysis method that measures the change in physical and chemical properties of materials with increasing temperature or isothermally with increasing time in a specified atmosphere. The operating temperature for the Q-500 ranges from ambient to 1000 °C, and has a temperature accuracy of ±1 °C and isothermal temperature precision of ±0.1 °C.

The procedure is as follows: the sample (around 20 mg) was first dried at 120°C in N_2 for 30 min before it was cooled down to 25 °C for CO_2 adsorption. The gas flow is then switched from N_2 to the simulated flue gas (15% CO_2 in N_2) at the same flow rate of 100 ml/min. Once the adsorption reached equilibrium at a given

temperature, the sample was then heated up to 120 °C and held at this temperature until complete desorption. Cyclic adsorption and desorption tests (up to 50 cycles) were also conducted by TGA Q500 to study the stability and regenerability of the samples.

3.3.4 Heat of adsorption

Thermogravimetry coupled with differential scanning calorimetry (TG-DSC) is an ideal technique to evaluate the CO_2 adsorption performance on porous materials. Differential scanning calorimetry (DSC) is a thermal analytical technique that can qualitatively measure the amount of energy adsorbed or released by a sample in the heating/cooling process or an adsorption process such as CO_2 adsorption on carbons. The results obtained is a curve of heat flux versus time or temperature, the enthalpy can be calculated by integrating the peak. The TG signal can also provide the amount of CO_2 adsorbed. Based on this data, the heat of adsorption or desorption per mole of CO_2 can be calculated.

In addition, the heat of adsorption can also be calculated by the integral adsorption heat values from the isosteric heat of adsorption. The equation is as follows:

$$Q_{int} = \frac{1}{n}\int_0^n Q_{st}\,dn \tag{3.29}$$

Where, n is the equilibrium CO_2 adsorption capacity, Q_{st} is the isosteric heat of adsorption, which can be calculated by the Clausius-Clapeyron equation by using adsorption data at different temperatures:

$$Q_{st} = R\left[\frac{\partial \ln P}{\partial \ln (1/T)}\right]_q \tag{3.30}$$

R is the ideal gas constant and q is the CO_2 adsorption capacity at pressure P and temperature T. The slope of the line between lnP and ln(1/T) is Q_{st}.

3.4 Repeatability and reproductivity

Repeatability and reproductivity of prepared samples are very important parameters to show the reliability of the measurement methods and the preparation methods.

Considering the limited time on facilities, only selected samples for selected facilities were repeated for the purpose of error analysis.

3.4.1 Repeatability of measurements

Repeatability describes the difference between the measured value and the real value, including systematic and random errors. In this thesis, several instruments were employed to characterize the adsorbents. Before use, all the instruments were calibrated following the standard procedure to avoid systematic errors. The textural properties and CO_2 adsorption performance of selected samples were repeated for three times. For example, the textural properties of sample FC6003 was tested three times. The maximum and minimum difference of BET surface area was only 50 m^2/g and total pore volume, micropore volume and ultra-micropore volume were gave a different of 0.004, 0.013, 0.013 cm^3/g, respectively. As for adsorption performance, sample HC-600-1, HC-600-0.3 and KC-700-1 listed in Table 3.2 were tested for three times, which only gave a difference 0.047, 0.009 and 0.042, respectively. It means that the measurement of samples was stable and reliable.

Table 3.1 Textural properties of sample FC6003 (repeated 3 times)

Test NO.	S_{BET} (m^2/g)	V_{total} (cm^3/g)	V_{micro} (cm^3/g)	$V_{micro<1nm}$ (cm^3/g)
1	770	0.334	0.273	0.256
2	737	0.331	0.253	0.230
3	720	0.325	0.246	0.239
	742±24	0.330±0.004	0.257±0.013	0.242±0.013

Table 3.2 Adsorption capacities of selected samples at 0.15 bar and 25 °C tested by TGA for 3 times

Sample	CO_2 adsorption capacity at 0.15 bar and 25 °C (mmol/g)			Mean
	1	2	3	
HC-600-1	1.61	1.66	1.56	1.61±0.047
HC-600-0.3	1.42	1.40	1.41	1.41±0.009
KC-700-1	1.73	1.82	1.78	1.78±0.042

3.4.2 Reproductivity of samples

In addition to repeatability, the reproductivity of samples prepared in this thesis were also evaluated. Two batches of the rice husk derived carbon HC-600-2 were prepared, it can be found from Table 3.3 that the textural properties of both samples were almost the same. The difference of surface area was only 12 m^2/g, the micropore volume were same. In addition, three batches of PIR derived carbons P61_2T and P81_2T were prepared and the adsorption capacity of sample from different batch was listed in Table 3.4, which gave a difference 0.05 and 0.09, respectively. Hence, it can say that the preparation method was reliable.

Table 3.3 Textural properties of sample HC-600-2

Sample	S_{BET} (m^2/g)	V_{total} (cm^3/g)	V_{micro} (cm^3/g)	$V_{micro<1nm}$ (cm^3/g)
Batch1	1025	0.43	0.39	0.30
Batch 2	1037	0.44	0.39	0.33

Table 3.4 Adsorption capacities of selected samples at 0.15 bar tested by TGA

Sample	Adsorption temperature	Batch 1	Batch 2	Batch 3	
P61_2T	25 °C	2.10	2.01	2.00	2.04±0.05
P81_2T	40 °C	2.22	2.10	2.30	2.21±0.09

Chapter 4 Renewable feedstocks derived carbons with favorable surface chemistry for CO_2 capture

4.1 Introduction

A variety of sources like biomass, coal, waste from consumption residue/industry or synthesized polymers were used to prepare activated carbon. Among them, biomass that are easy handling, diverse and renewable have increasingly become a preferred feedstock for activated carbon production (Foo et al., 2012; Yahya et al., 2015; Kan et al., 2015). In this chapter, the use of alkali intercalation via chemical activation has been further developed as a novel methodology to produce highly functional carbon-based CO_2 adsorbents using low-cost agricultural wastes, with a particular focus on the agricultural waste of rice husk, which is produced at a scale of 140 million tonnes a year worldwide (Kalderis et al., 2008). Owing to its very low energy density on a volumetric dry basis (Chen et al., 2011), RH is usually considered as waste that is often dumped on landfills or destroyed in agricultural burning, although rice husk has been considered as a valuable alternative source for silica production due to its high silica content. In recent years, there have been some investigations into the use of rice husk to produce activated carbon materials for variable general applications, and chemical activation typically with alkali hydroxides or carbonates as being the activating agents has almost exclusively been used typically following a three-step process, namely carbonisation and activation followed by the removal of minerals by leaching (Gao et al., 2015;Yeletsky et al., 2009; Zhang et al., 2014). However, to the best of our knowledge, no investigation has ever been carried out to use rice husk to prepare alkali-intercalated ultra-microporous materials for CO_2 adsorption by making the effective use of rice husk contained silicon as a natural template for deriving ultra-microporosity and by controlling the chemical activation to achieve alkali intercalation for further enhanced CO_2 uptake.

4.2 Experimental procedure

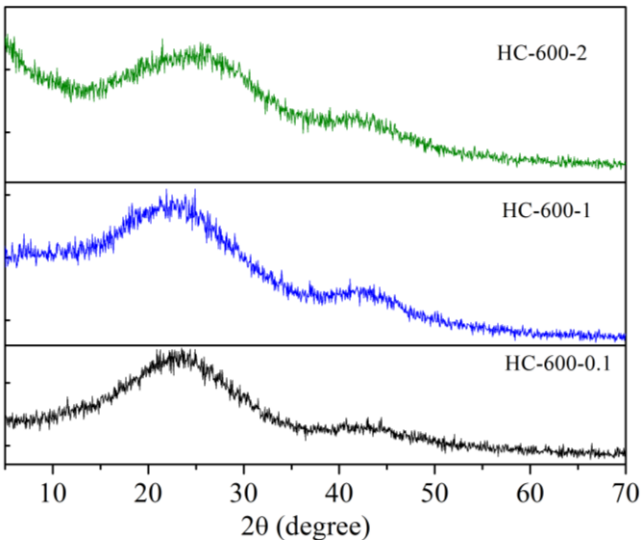
A batch of raw rice husk (RH) was sourced from China and used for the preparation of activated carbon samples. The raw RH sample was first dried, crashed and sieved into the particles in the range of 1.0-0.5mm. On a weight basis, the RH sample has an ash content of 11.54% and contains 40.4% carbon, 5.70% hydrogen, 0.64% nitrogen, and 41.72% oxygen. An innovative chemical activation protocol, which can effectively facilitate the potassium intercalation during the activation process, was used to prepare the RH activated carbon samples. 3g of as-prepared raw RH sample was first physically mixed with activating agents at different mass ratios. The mixture was then heated up in a purpose-designed carbonization/activation furnace to different pre-set final temperatures at a heating rate of 5 °C/min in a nitrogen flow of 1 L/min. Once the target temperature was reached, the sample mixture was maintained at this temperature for 1h before it was cooled down in N_2 to ambient conditions. To yield the final bio-carbon products, the mixture was removed from the activation furnace and washed till neutral with excessive quantities of de-ionized water (typically three times with 200 mL water). It was found that at the KOH/RH ratio of 1.0, the carbon yield ranged from 25% wt% at 600 ºC, 20 wt% at 700 ºC to 15 wt% at 800 ºC. For activation with K_2CO_3, the yield is slightly higher by an average of 2 wt% than for KOH activation under the same conditions. For the convenience of subsequent discussion, the carbons obtained from KOH and K_2CO_3 activation under different conditions are labelled as HC-X-Y and KC-X-Y respectively, where X represents the activation temperature and Y stands for the KOH / RH or K_2CO_3/RH mass ratios. The heat of adsorption in this chapter was measured by ATG-DSC instrument (Setaram SENSYS evo).

4.3 Results and Discussion

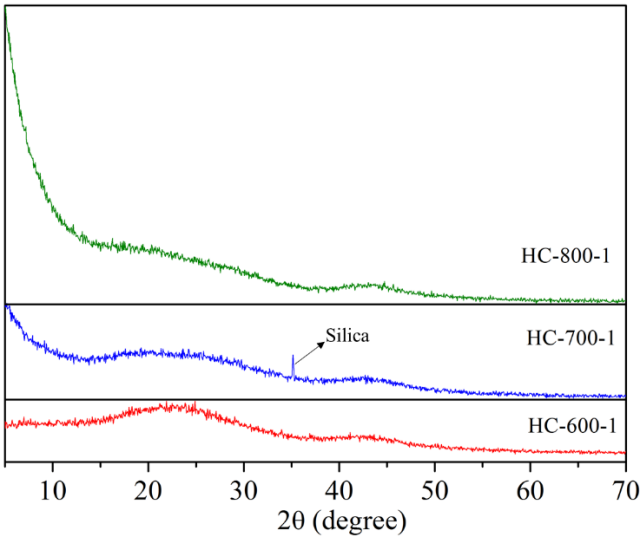
4.3.1 XRD and XRF characterisation

Fig. 4.1 shows the XRD pattern of the microcrystalline structure for the activated RH carbon samples obtained with different activation conditions. The broad and diffused peaks of the XRD profile demonstrate the disordered, amorphous

structures of the carbons. Two broad characteristic peaks were observed, one centred at around 25°, which corresponds to the (002) set of planes usually used to assess the pseudo graphic interlayer spacing and another at around 43°, corresponding to the microcrystalline lateral dimensions of (100) planes, respectively (Li et al., 2012; Wang et al., 2009). It seems that at the activation temperature of 600 °C, increasing the KOH/RH mass ratio from 0.1 to 2 inflicted insignificant structural alterations in general, despite the minor broadening observed for the (002) peak and the slightly increased 100 peak corresponding to the lateral dimension of graphitic crystallites. However, the effect of the activation temperature was found to be significantly greater. It was found that when the activation temperature increased from 600 to 800 ºC at a given KOH/RH mass ratio, the (002) peak became increasingly broader and weaker or even disappeared whilst the (100) peak remained relatively constant. This suggests that the enhanced activation at higher activation temperatures led to the collapse of interlayer structures and hence made the carbon microcrystalline structures more single-layered (Meng et al., 2014), giving rise to larger surface areas of the carbon as shown in next section. Similar relationship between the disappearance of (002) peak and surface area of carbons was also obtained by Yang et al (2002).



(a)



(b)

Figure 4.1 XRD patterns of RH carbons samples from different activation conditions: (a) samples prepared with different KOH/RH ratio at 600 °C; samples prepared with KOH/RH=1 at different temperatures

Table 4.1 shows the results of XRF analysis of the residual silica and potassium present in the RH carbon samples. As expected, the silicon content of the carbon decreased sharply with increasing KOH or K_2CO_3 to RH mass ratio used in the activation process, with most of the RH carbons prepared with high KOH or K_2CO_3 mass ratios (>1) having silicon contents below 2wt%. The residual silicon may occur either as unreacted silica or trapped silicates that are hard to be removed. Interestingly, the amount of potassium surviving the same excessive post-activation washing process was found to be disproportionately larger for all the carbon samples, varying from 5 to 12 wt% which was about 3~16 times the content of silica for different samples. This sharp contrast is a strong suggestion of the different transformational pathways of the potassium present in the activating agents and the natural silica in the rice husks, and it is believed that a significant proportion of the potassium is intercalated deep into the carbon framework formed in the activation process and is hard to be removed with the excessive washing process. Compared to our previous results reported for phenolic resin beads (Liu et al., 2015), the occurrence of potassium intercalation appears to be significantly more pronounced during the chemical activation of RH carbons, being indicative of the prominent role of the RH-contained inherent silica.

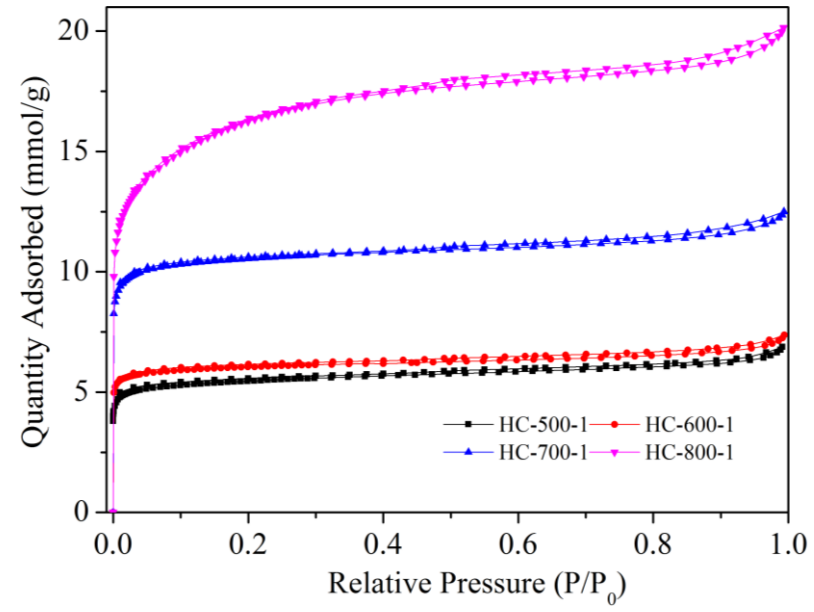
Table 4.1 Chemical analysis by XRF of RH carbons

Sample	K, wt%	Si, wt%	Sample	K, wt%	Si, wt%
Raw	0.74	17.51	KC-600-1	13.49	5.46
HC-600-0.1	10.82	9.65	KC-700-0.1	8.47	8.86
HC-600-0.5	12.12	4.56	KC-700-1	12.35	2.44
HC-600-1	9.63	2.42	KC-700-2	4.78	1.84
HC-600-2	6.75	1.41	KC-700-3	6.74	1.75
HC-600-3	11.28	1.86	KC-800-1	7.43	1.42
HC-700-1	9.85	1.29			
HC-700-2	6.15	0.89			
HC-800-1	5.36	1.30			

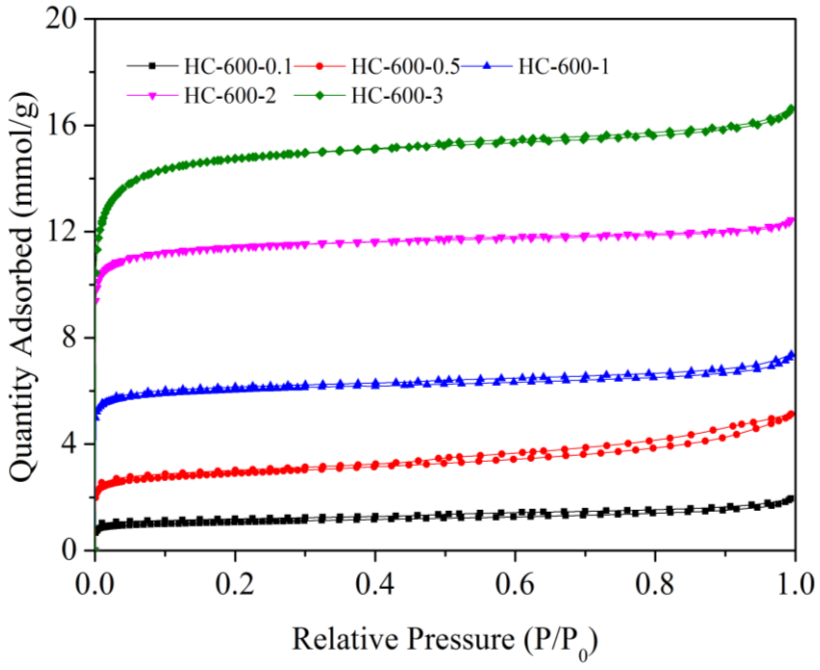
4.3.2 Textural properties of RH-derived carbons

Figure 4.2 shows the N_2 adsorption isotherms of the carbon samples prepared from the protocol of KOH activation under relatively mild conditions with the activation temperatures varying from 600 to 800 °C and RH/KOH mass ratios from as low as 0.5 to a maximum of 3. It can be seen that the adsorption isotherms of all RH-derived carbons were highly characterized by the large sharp uptake observed at low relative pressures typically < 0.1 followed by virtually horizontal plateaus at high relative pressures, this indicating the extraordinary microporosity of the RH carbons. Hysteresis at high relative pressures, which is indicative of the presence of mesoporosity, was only observed for two samples prepared from using either very low RH/KOH mass ratios or higher activation temperatures (HC-600-0.5 and HC-800-1). Compared to KOH-activated RH carbons, however, most of the K_2CO_3−activated carbons showed type IV isotherms with sloped plateaus at low relative pressures followed by variable significant amounts of hysteresis at higher relative pressures, being indicative of the wider pore size distributions ranging from micro to mesoporous structures in the K_2CO_3-activated carbons. The hysteresis in the isotherms of K_2CO_3-activated carbons was similar to that in type H4 isotherm, which means that the mesopores were narrow slit-like pores (Sing, 1985). This kind

of pores were always found in materials with internal voids of irregular shape and broad size distribution (Sing, 1985).

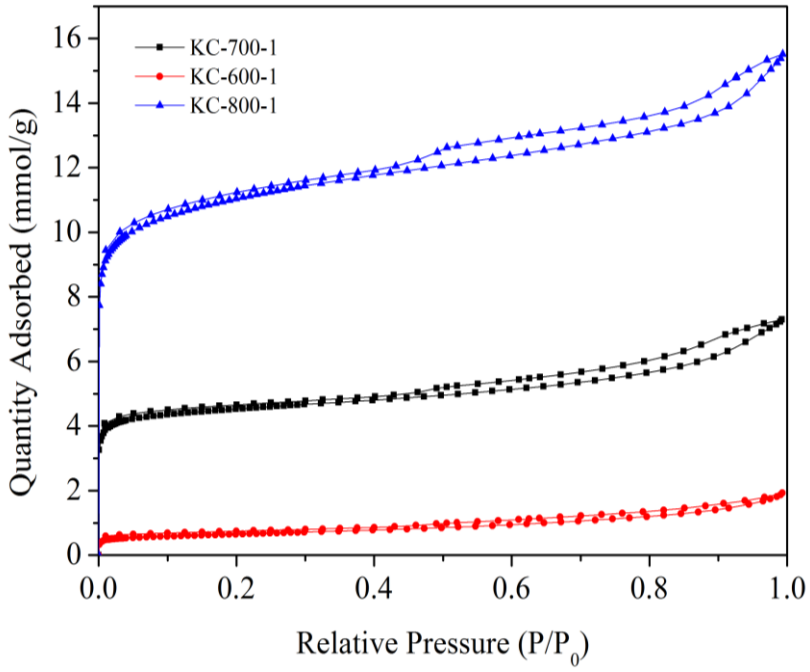


(a)

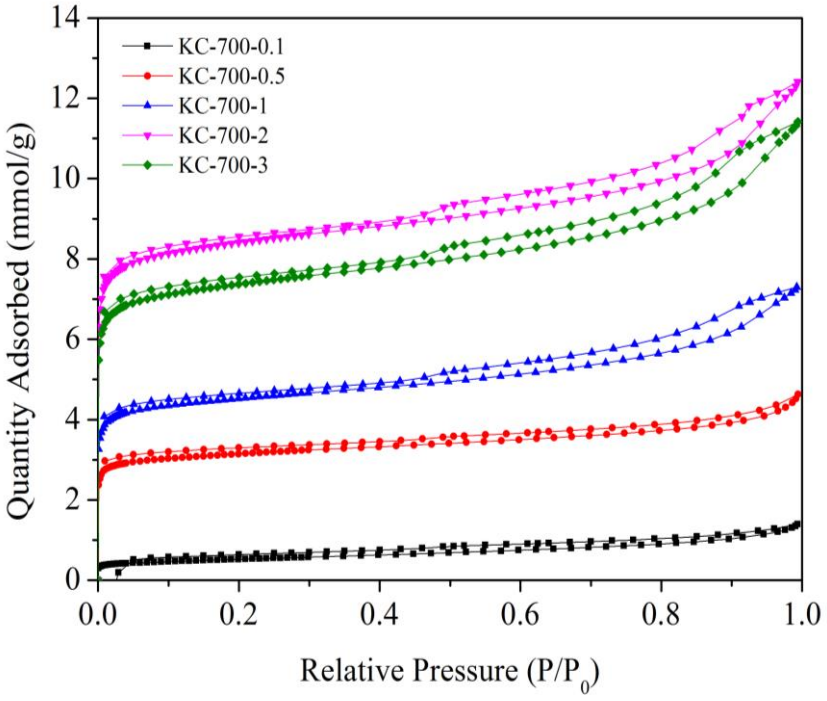


(b)

Figure 4.2 N_2 adsorption isotherms obtained at -196 ºC for RH-derived carbons from different chemical activation protocols: (a) samples prepared with KOH/RH=1 at different temperatures; (b) samples prepared with different KOH/RH ratio at 600 ºC; (c) samples prepared with K_2CO_3/RH=1 at different temperatures; (b) samples prepared with different K_2CO_3/RH ratio at 700 ºC



(c)



(d)

Figure 4.2 N_2 adsorption isotherms obtained at -196 °C for RH-derived carbons from different chemical activation protocols: (a) samples prepared with KOH/RH=1 at different temperatures; (b) samples prepared with different KOH/RH ratio at 600 °C; (c) samples prepared with K_2CO_3/RH=1 at different temperatures; (b) samples prepared with different K_2CO_3/RH ratio at 700 °C

Table 4.2 summarizes the surface textural parameters obtained from the BET measurements. It can be seen that the total pore volume and BET surface area increased from 0.061 to 0.64 cm^3/g and 89 to 1343 m^2/g, respectively when KOH/RH mass ratio increased from 0.1 to 3 and the activation temperature from 600 to 800 °C. It is clear that the RH-derived carbons from the protocol of KOH activation are extremely microporous, with the microporosity accounting for up to 95% of the total porosity. More importantly, the microporosity of the RH carbons, as shown in Fig. 4.3, was found to consist mostly of ultra-micropores with pore diameters centred on 0.36 and 0.55 nm, which represents 84% of total microporosity for the carbon sample prepared at 600 °C with a KOH/RH mass ratio of 1. Such well-defined ultra-microporosity with extremely narrow pore size distributions obtained for the RH carbons can usually only be achieved with some special metal organic frameworks (MOFs) built from a single small ligand (Nandi et al., 2015) and the carbons derived from carefully selected costly precursors and using cumbersome methodologies (Sethia et al., 2015).

Table 4.2 Specific surface areas, pore structure parameters of the bio-carbons

Sample	S_{BET} (m^2/g)	V_{total} (cm^3/g)	V_{micro} (cm^3/g)	$V_{micro<1nm}$ (cm^3/g)	$V_{micro<1nm}/V_{micro}$	V_{micro}/V_{total}
KOH−activated carbon						
HC-600-0.1	89	0.061	0.029	0.018	62%	48%
HC-600-0.5	249	0.16	0.083	0.057	69%	52 %
HC-600-1	536	0.24	0.19	0.16	84%	79 %
HC-600-2	1025	0.43	0.39	0.30	81%	95 %
HC-600-3	1303	0.52	0.47	0.34	72%	90 %
HC-700-1	976	0.39	0.33	0.26	79%	85 %
HC-700-2	1197	0.47	0.43	0.33	77%	91 %
HC-800-1	1343	0.64	0.49	0.30	61%	77 %

Sample	S_{BET} (m^2/g)	V_{total} (cm^3/g)	V_{micro} (cm^3/g)	$V_{micro<1nm}$ (cm^3/g)	$V_{micro<1nm}/V_{micro}$	V_{micro}/V_{total}
K_2CO_3−activated carbon						
KC-700-0.1	42	0.044	0.012	0.006	50%	27 %
KC-700-0.5	274	0.15	0.10	0.072	72%	67 %
KC-700-1	395	0.24	0.14	0.094	67%	58 %
KC-700-2	640	0.38	0.23	0.17	74%	61 %
KC-700-3	741	0.39	0.25	0.19	76%	64 %
KC-800-1	944	0.60	0.37	0.24	65%	62%

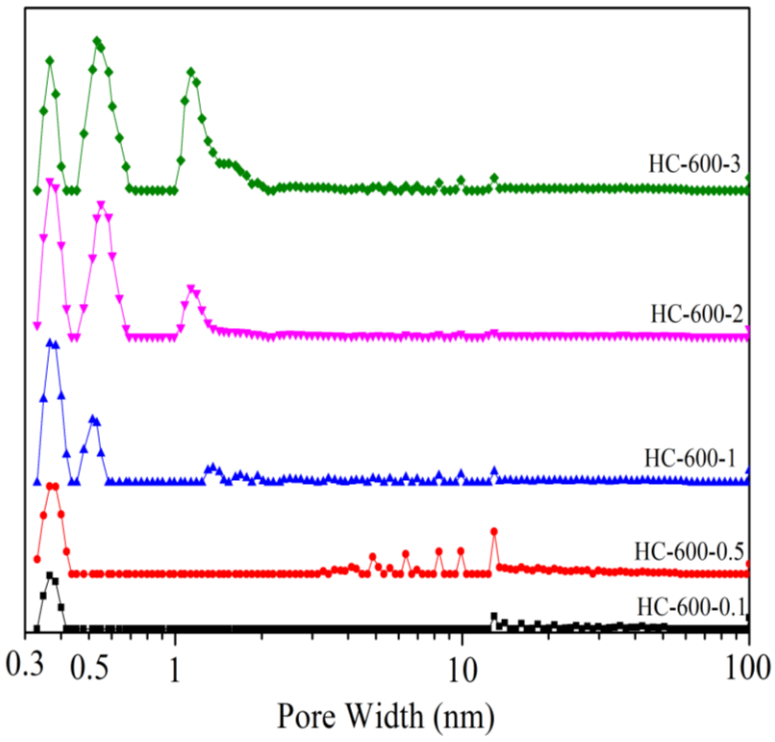
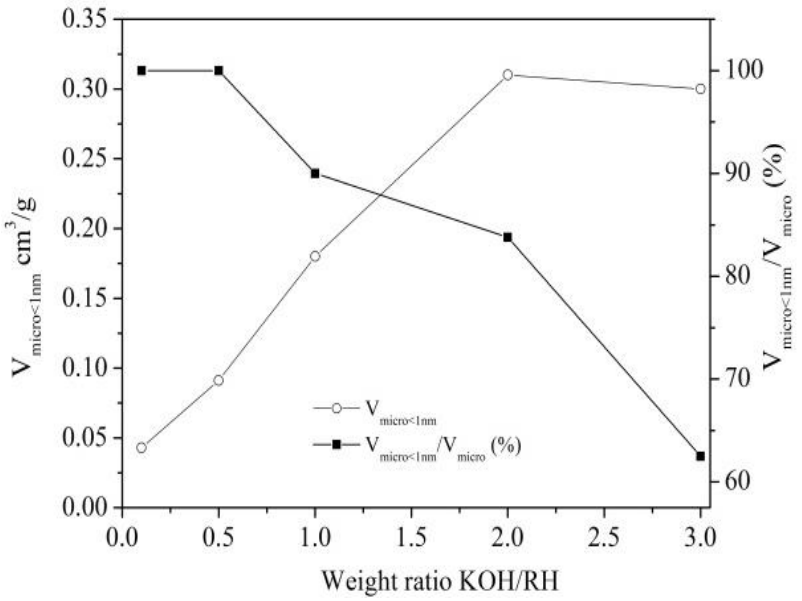


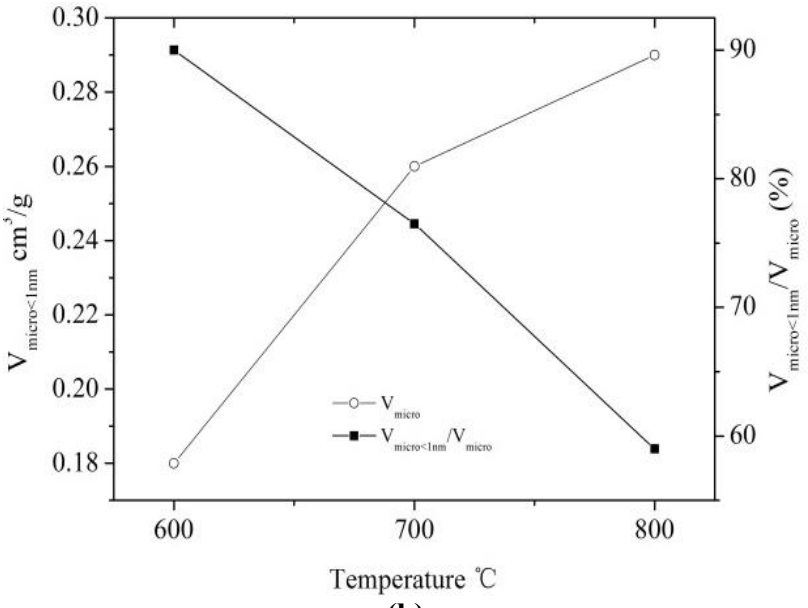
Figure 4.3 NLDFT pore size distributions for RH samples from KOH activation with different KOH/RH mass ratios at 600 °C

Figure 4.4 shows the effect of activation temperature and KOH/RH mass ratio on the development of ultra-microporosity. It can be seen that the volume of ultra-micropores increased both with the activation temperature and KOH/RH mass ratio, indicating an enhanced activation effect. However, at a given KOH/RH mass ratio, the ultra-micropore volume as a fraction of the total micropore volume decreased with activation temperature whereas at a given activation temperature, the

percentage of ultra-microporosity was found to decrease with an increase in KOH/RH ratio up to 3.0. The decrease in the relative ultra-microporosity with increasing severity of activation conditions was believed to be associated with the formation of increasingly larger micropores with a broader size distribution, with mesoporosity starting to emerge when the activation temperature was higher than 700ºC (sample HC-700-1) as shown in Fig. 4.2



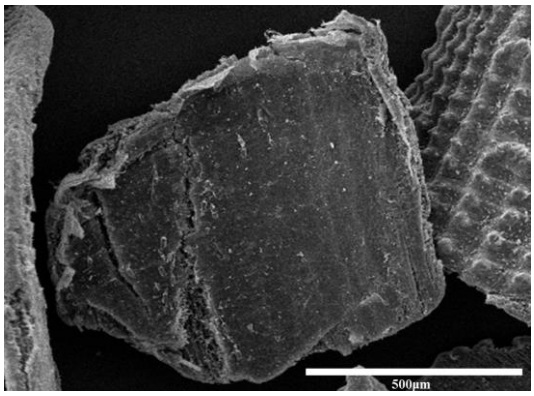
(a)



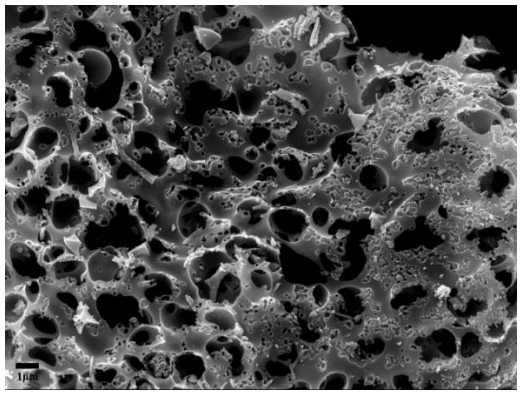
(b)

Figure 4.4 Effect of activation temperatures and KOH/RH mass ratios on ultra-microporosity of KOH-activated RH carbons: (a) effect of KOH/RH weight ratio; (b) effect of temperature

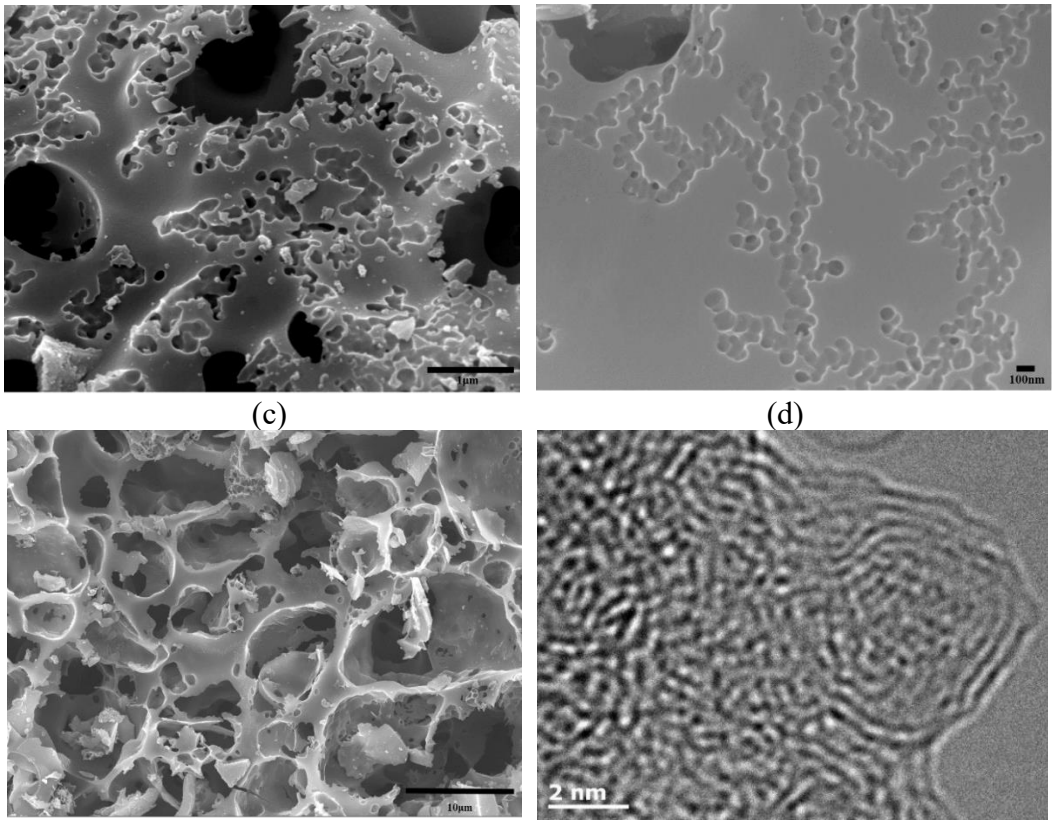
Compared to the KOH activation, the results shown in Table 4.2 and Fig. 4.2 show that the RH carbons from the one-step K_2CO_3 activation, which can be considered as part of KOH activation but can only take place at higher temperatures, were found to be significantly less microporous owing to the formation of mesoporosity that appears to become more pronounced with increasing activation temperatures. The highest surface area was obtained at only 944 m^2/g for the sample prepared at the highest K_2CO_3 activation temperature (800°C) investigated. However, it is noteworthy that despite the smaller ultra-micropore volumes, the relative ultra-microporosities of the K_2CO_3-activated RH carbons were overall comparable to those of the carbons from the one-step KOH activation under similar conditions, suggesting that the RH carbons obtained with K_2CO_3 activation essentially exhibit a distinct bimodal pore structure consisting mainly of two groups of porous structures, namely the mesopores and the ultra-micropores below 1 nm in diameter. However, as K_2CO_3 activation appears to favour the formation of mesoporosity at a cost of microporosity, it can be reasonably envisaged that the RH carbons obtained with K_2CO_3 activation will become increasingly mesoporous with increasing activation temperatures and/or K_2CO_3/RH mass ratios, eventually leading to the formation of mesoporous RH carbons (Sethia et al., 2015).



(a)

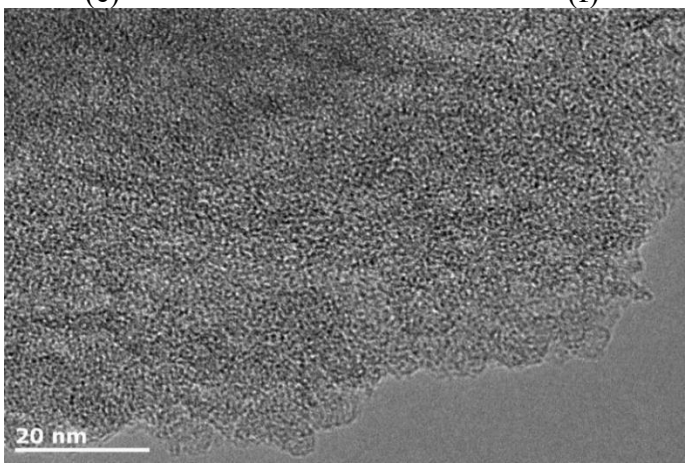


(b)



(c) (d)

(e) (f)



(g)

Figure 4.5 SEM images of raw RH (a) and its derived carbons from KOH and K_2CO_3 activation (HC-600-1 (b-c); KC-700-1((d-e))) and TEM images of sample HC6001 (f)-(g)

Figure 4.5 illustrates the SEM images of the raw RH and its derived carbon samples from KOH and K_2CO_3 activations. It can be seen that despite the lower activation temperature used, the carbon sample from the KOH activation shows a much more developed porous structure than the K_2CO_3-activated carbons, being consistent with the above results obtained. In order to further understand the microporous structure

of HC-600-1, transmission electron microscopic (TEM) imaging analysis were also performed. As shown in Figure 4.5(f, g), slit-like ultra-micropores can be clearly seen in the TEM images and the ultra-microporosity distributed across the porous network skeleton.

4.3.3 The role of RH inherently contained silicon in ultra-microporosity development

The formation of well-defined ultra-microporosity at such exceptionally high levels, which has never been observed for any other carbon materials prepared with similar methodologies (Yahya et al., 2015), is highly suggestive of other reactive element(s) involved during the activation. RH is well known for its uniquely high contents of silica (15–23 wt%) present in an inherent structural framework at molecular levels and some of the silicon species are even chemically bonded to the functional groups of the carbonaceous rice husk (Lanning, 1963; Freitas et al., 2007). During chemical activation, these inherently present silicon species within the framework of rice hulls can play a prominent in-situ template role in the development of the exceptionally high levels of ultra-microporosity observed for the RH carbons.

Previous investigations have revealed that KOH activation of carbonaceous materials for activated carbon production involves the following major chemical reactions (4.1) to (4.8) (Marsh et al., 1984; Otowa et al., 1993) whereas K_2CO_3 activation only involves the reactions (4.5) to (4.8) and requires higher temperatures to achieve high levels of activations (Addoun et al., 2002; Mckee et al., 1983). The significance of individual reactions and hence the porous structures of resultant activated carbons are determined by both the activation temperature and the amount of KOH used. In general, activation efficiency increases with increasing KOH/carbon ratio and activation temperature in particular, due to the enhanced chemical reactions and associated pore creating and widening effect. It is noteworthy that the pore widening effect accelerates significantly with increasing activation temperatures, because of the higher kinetic energy possessed by the melt of K_2CO_3, K_2O and the vapour of metallic potassium at higher temperatures.

$$2KOH \rightarrow K_2O + H_2O \quad (4.1)$$

$$C + H_2O \rightarrow CO + H_2 \quad (4.2)$$

$$CO + H_2O \rightarrow CO_2 + H_2 \quad (4.3)$$

$$CO_2 + K_2O \rightarrow K_2CO_3 \quad (4.4)$$

$$K_2CO_3 \rightarrow K_2O + CO_2 \quad (4.5)$$

$$CO_2 + C \rightarrow 2CO \quad (4.6)$$

$$C + K_2O \rightarrow C\text{-}O\text{-}K + K \quad (4.7)$$

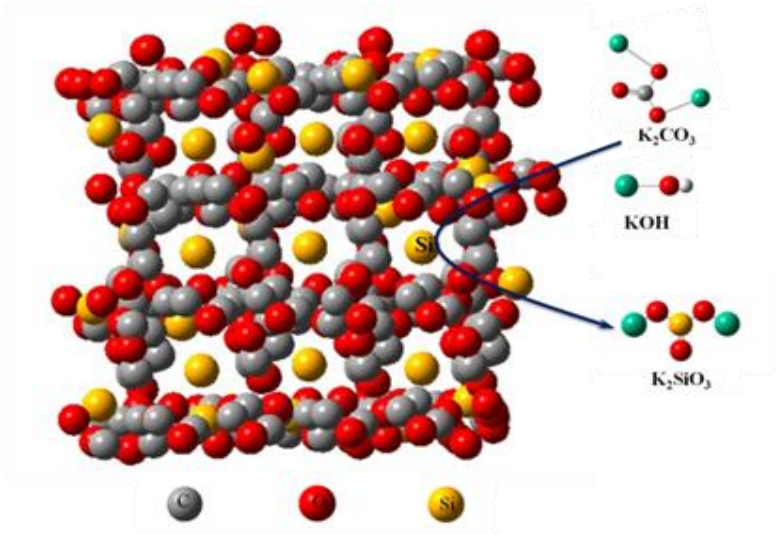
$$C + K_2O \rightarrow 2K + CO \quad (4.8)$$

In general, the results obtained for the RH carbons agree well with previous findings. However, compared to other biomass feedstocks free of silica, the following additional pore-creating reactions (4.9~4.11) between the activating agents and RH-contained silica also take place with varying significance, which provide additional activation as the water-soluble silicates formed can easily be removed to free the porosity during the washing process. The results present in Table 1 confirm the removal of silicon as a result of the additional reactions during the chemical activation process.

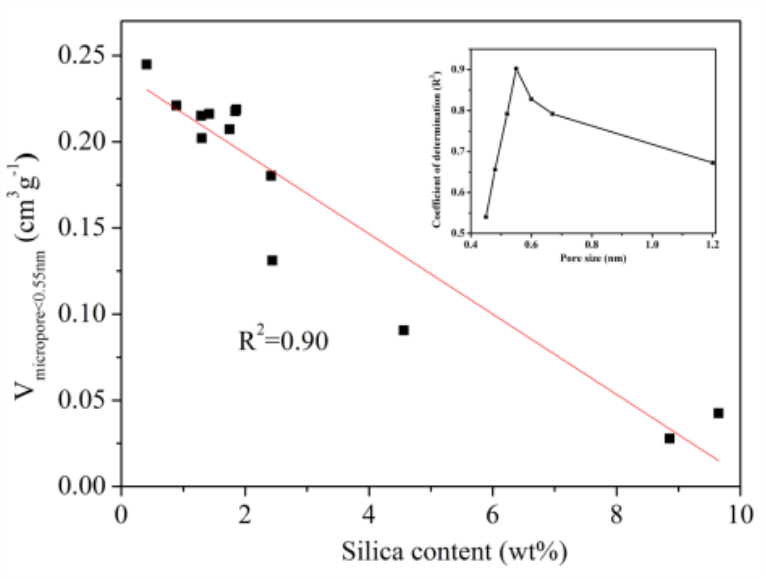
$$K_2O + SiO_2 \rightarrow K_2SiO_3 \quad (4.9)$$

$$2K_2O + SiO_2 \rightarrow K_4SiO_4 \quad (4.10)$$

$$K_2CO_3 + SiO_2 \rightarrow K_2SiO_3 + CO_2 \quad (4.11)$$



(a)



(b)

Figure 4.6 Schematic diagram for the silicon-containing RH framework and the pore-creating reactions of silicon with activating agents (*a*) and the relationship between the ultra-micropore volume and the residual silicon content of the carbons (*b*)

These additional reactions were believed to be the main factors responsible for the extraordinary ultra-microporous structures observed for the RH carbons, given the inherent nano-scale distribution of the natural templating silica within the matrix of rice husk (wang et al., 2012a). It is also reasonable to assume that the formation of silicates may also help retain the resultant ultra-microporosity by weakening the pore widening effect of further carbon reactions with the activating agents. Indeed, a linear relationship as shown in Fig. 4.6(b) was observed between the volume of ultra-micropores (<0.55nm) and the residual silicon contents of the RH carbons (Table 4.2), showing that the micropore (<0.55nm) volume increases with the increasing removal of residual silicon in the form of potassium silicates.

4.3.4 CO_2 adsorption properties of RH carbons

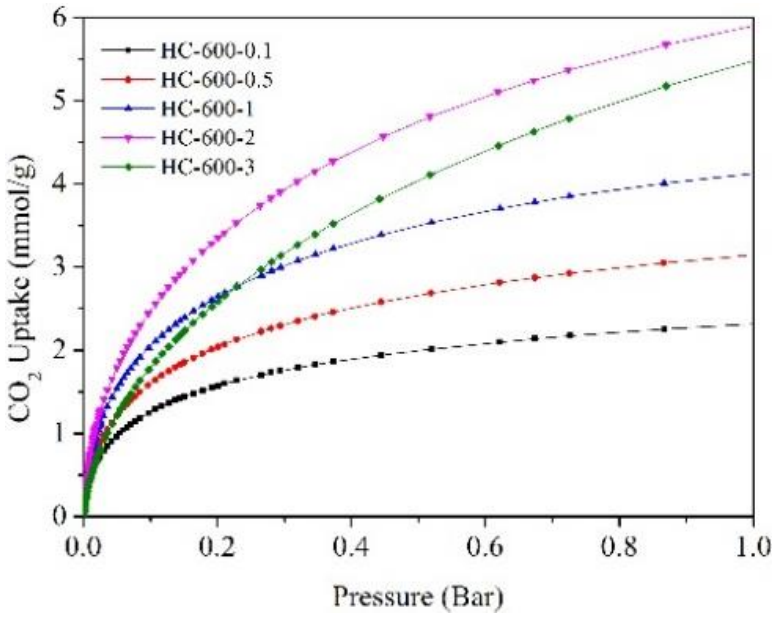
4.3.4.1 Static adsorption measurement

Fig. 4.7 shows the adsorption isotherms at 0 and 25 °C for the RH carbons prepared from the one-step carbonization−activation with KOH under different conditions. Clearly, the CO_2 uptake of the RH carbons was affected substantially by both the activation temperature and the amount of activating agent used. At the given

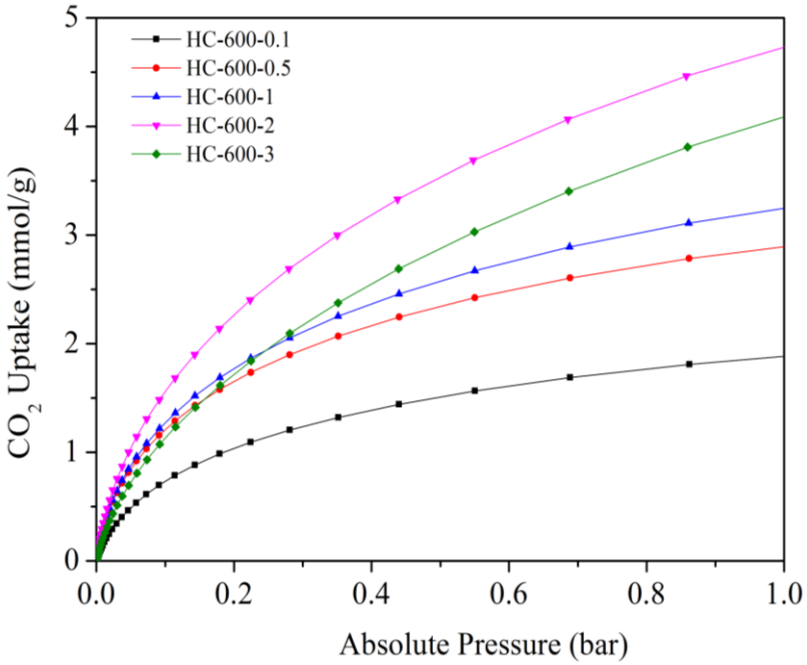
activation temperature of 600 °C, the results shown in Fig. 4.7(a, b) indicate that on increasing the KOH/RH mass ratio from 0.1 to 2, the CO_2 adsorption capacity increased sharply from 2.35 and 1.88 mmol/g to 4.75 and 5.91 mmol/g at 0 and 25 °C and 1 bar CO_2 respectively, being consistent with the increased activation efficiency and removal of RH-contained silica as shown in Table 2. However, a further increase in KOH/RH ratio from 2:1 to 3:1 resulted in a significant decrease in CO_2 uptake from 4.75 to 4.1mmol/g at 25ºC and 1 bar, despite the continuous increase in the porosity but clearly at a cost of ultra-microposity as a result of enhanced pore widening effect (Table 4.2). A similar trend was also observed for the effect of carbonisation and activation temperature (Fig. 4.7c) on CO_2 uptake, with the carbons prepared at 600 and 700 °C showing the best adsorption performance in general. Of all the KOH-activated samples, the RH carbon (HC-600-2) prepared at 600 °C with a KOH/RH ratio of 2:1 exhibited the highest adsorption capacities of 5.91 and 4.75 mmol/g at 1 bar, and 2.96 and 2.0mmol/g at 0.15 bar CO_2 at the adsorption temperatures of 0 °C and 25 °C, respectively. A comparison with other materials (Table 2.6) shows that the extraordinary CO_2 uptakes of the RH carbons of this study at low CO_2 partial pressures represent the one of the highest capacities ever reported for any carbon materials which are usually prepared from cost-prohibitive precursors and sophisticated methodologies, and exceed the performance of most MOF materials for post-combustion CO_2 capture. Compared to KOH activation, however, the carbons obtained from the integrated carbonisation and K_2CO_3 activation process appear to be generally less effective in adsorbing CO_2 (Fig. 4.8), with the sample prepared at 800 °C (KC-800-1) showing the highest CO_2 uptakes of 2.3 and 4.8 mmol/g at 0 °C and CO_2 partial pressures of 0.15 and 1 bar CO_2, respectively.

For both KOH and K_2CO_3 activations, the adsorption isotherms also show that samples prepared in relatively mild conditions often showed higher CO_2 uptake capacities at low CO_2 partial pressures up to 0.2 bar but exhibited lower capacities in the higher pressure region, compared to the samples prepared in less mild activation conditions (e.g. HC-600-1 *vs* HC-600-3; HC-600-1 *vs* HC-700-2 and HC-800-1; and KC-700-1 vs KC-800-1), highlighting the differential effect of the

surface textural and chemical properties on CO_2 uptake and related adsorption mechanisms at different partial pressures.

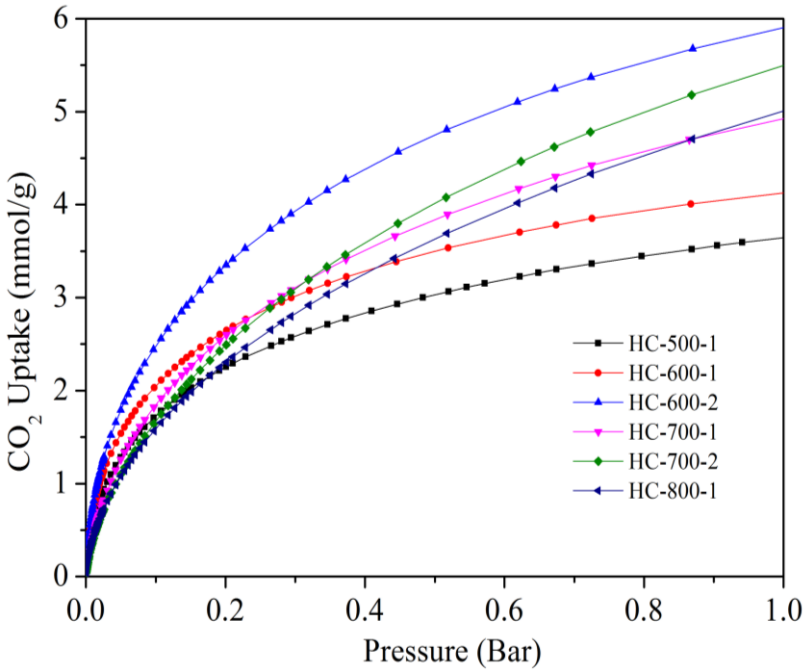


(a)



(b)

Figure 4.7 CO_2 adsorption profiles at 0 and 25 ℃ for RH carbons from the one-step carbonization-activation with KOH under different conditions. a: CO_2 adsorption isotherms at 0 ℃; b: CO_2 adsorption isotherms at 25 ℃ (c), adsorption isotherms at 0°C for carbons from different carbonization/activation temperatures (continued)



(c)

Figure 4.7 CO_2 adsorption profiles at 0 and 25 ℃ for RH carbons from the one-step carbonization-activation with KOH under different conditions. a: CO_2 adsorption isotherms at 0 ℃; b: CO_2 adsorption isotherms at 25 ℃ (c), adsorption isotherms at 0°C for carbons from different carbonization/activation temperatures.

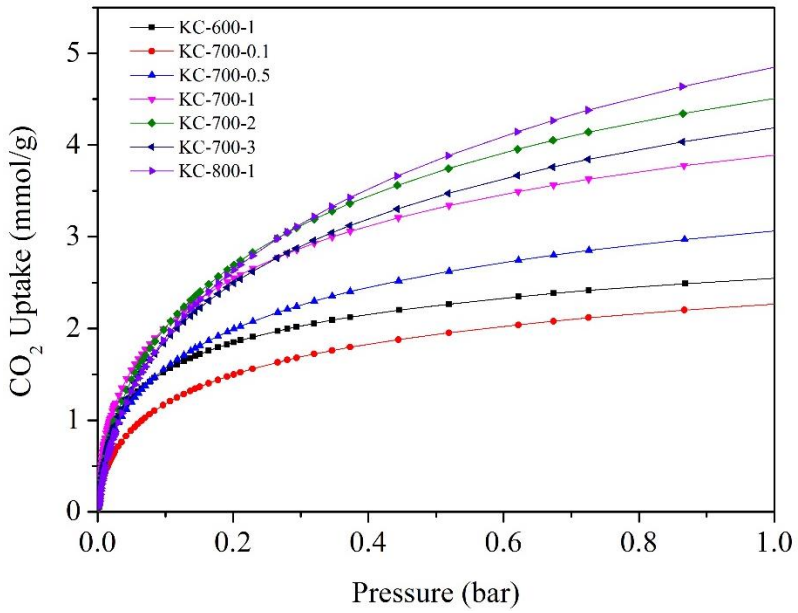
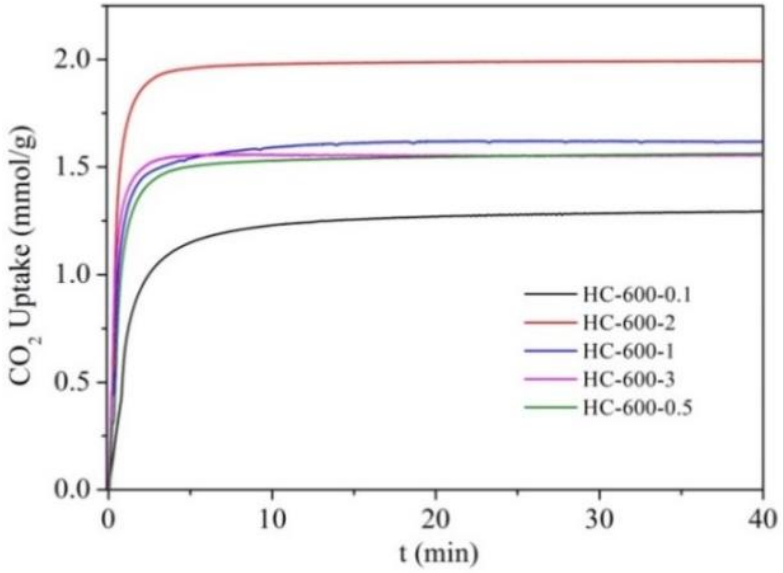


Figure 4.8 CO_2 adsorption profiles at 0 °C for the RH carbons from the carbonization-activation scheme with K_2CO_3 as the activating agent under different conditions

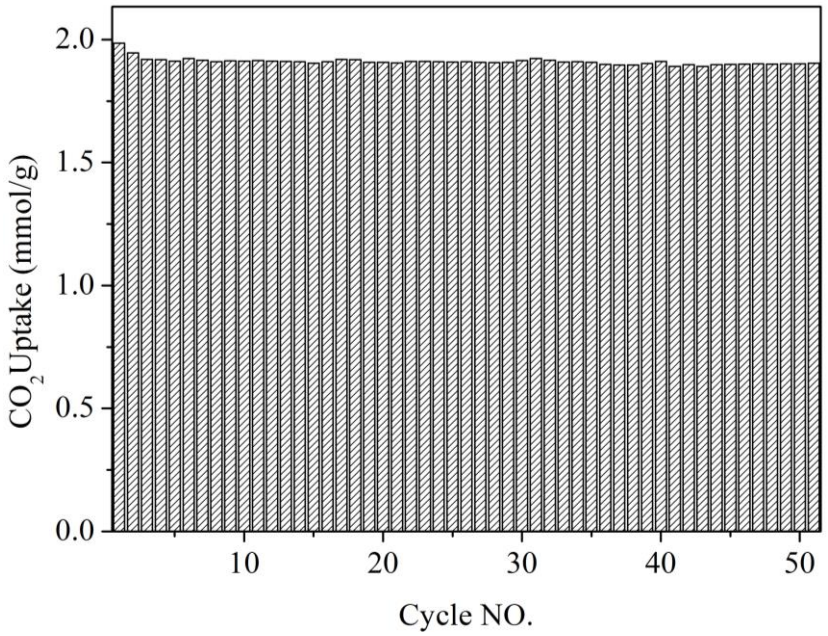
4.3.4.2 Dynamic adsorption and cyclic adsorption/desorption measurement

Fig. 4.9 shows the adsorption characteristics and the cyclic adsorption/desorption performance for selected samples, obtained from TGA at 25 °C and 0.15 bar CO_2 (N_2 balance). As shown in Fig. 4.9a, all the RH carbon samples demonstrate fast CO_2 uptake in the simulated flue gas stream under the dynamic TGA conditions, with their achieved equilibrium adsorption capacities being essentially identical to those obtained under the static BET measurement conditions (Fig. 4.7b). A remarkable equilibrium uptake capacity of 2.0mmol/g was obtained with the best-performing HC-600-2 sample and 90% of the equilibrium capacity was achieved in less than 2 minutes (Fig. 4.9a), while its stable and excellent reversible adsorption performance was demonstrated by the cyclic life-time performance test results (Fig. 4.9b). It is also worth mentioning that the least activated HC-600-0.1 sample, which has a surface area of only 89 m^2/g and a micropore volume of 0.029 cm^3/g, still achieved an impressive adsorption capacity of 1.3 mmol/g, and this may indicate the extraordinary role of the potentially unique surface chemistry of the RH carbons that has rarely been seen for any other carbon materials. The above results highlight the high adsorption capacity and desirable fast adsorption kinetics of the rice husk derived carbons of this study.



(a)

Figure 4.9 (a) the isothermal adsorption curve of selected RH carbons; (b) the cyclic adsorption/desorption performance of the best-performing HC-600-2 sample: both under simulated flue gas conditions of 15% CO_2 and 85% N_2 at 25 °C for adsorption and 120 °C for desorption in N_2 (continued)



(b)

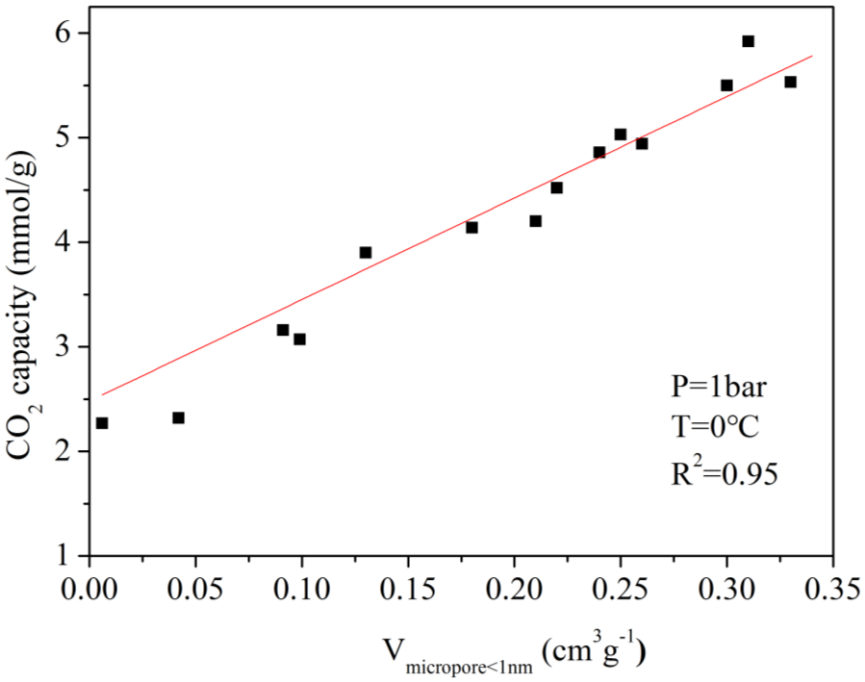
Figure 4.9 (a) the isothermal adsorption curve of selected RH carbons; (b) the cyclic adsorption/desorption performance of the best-performing HC-600-2 sample: both under simulated flue gas conditions of 15% CO_2 and 85% N_2 at 25 °C for adsorption and 120 °C for desorption in N_2

4.3.5 The role of surface textual and chemical properties on CO_2 adsorption

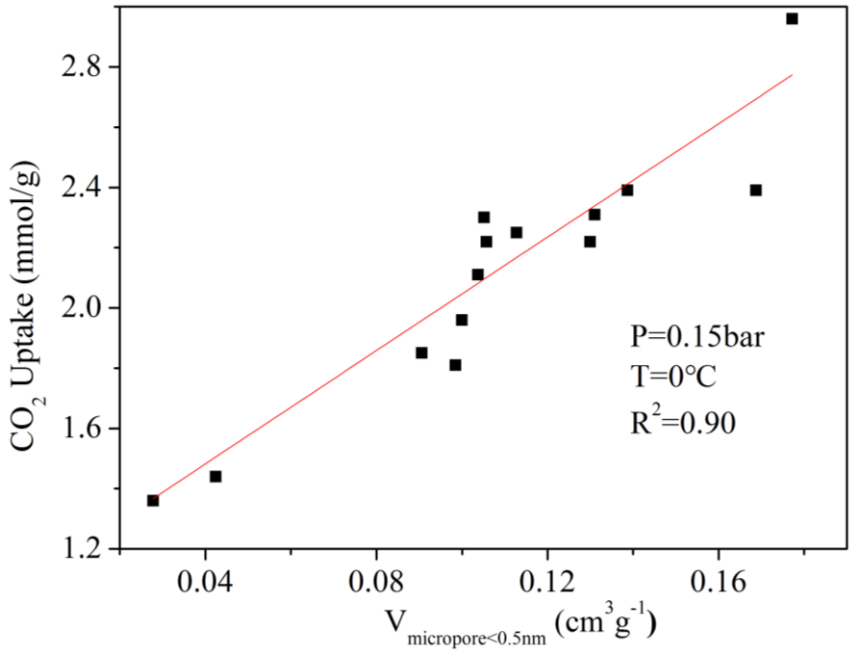
The CO_2 uptake performance of the RH carbons prepared in different carbonisation and activation conditions appears to have no direct links with the general surface textural properties as shown in Table 4.2 and Fig. 4.2. For instance, the sample HC-800-1, which had the largest surface area of 1343 m^2/g with a total volume of 0.64 cm^3/g (Table 4.2), had the lowest CO_2 uptakes of only 1.96mmol/g at 0°C and 0.15 bar CO_2, while the sample HC-600-2 with a considerably lower surface area of 1025 m^2/g and total pore volume of 0.43 cm^3/g had the remarkably higher capacity of 2.96mmol/g and the sample HC-500-1, which had the smallest surface area of only 470 m^2/g and total pore volume of 0.22 cm^3/g, had the capacity of 2.05mmol/gat 0 °C and 0.15 bar CO_2.These results strongly suggest the unique pore size distributions of the samples can be more relevant to the CO_2 uptake capacities.

Further examinations as shown in Fig. 4.10indicate that the CO_2 capture capacity of the RH carbons at the different adsorption temperatures and CO_2 partial pressures

investigated is indeed only directly proportional to the volume of micropores smaller than 1 nm. Therefore, carbonisation and activation conditions leading to widened porous structures at a cost of fine microporosity (Table 4.2) will result in a decrease in CO_2 uptake despite the induced further increase in surface area or total pore volume. At a CO_2 partial pressure of 0.15 bar, the CO_2 uptake capacity at 0 °C was found to be almost linear with the volume of micropores smaller than 0.5 nm, with a high correlation coefficient (R^2) of 0.90 (Fig. 10a). Similar linear relationships were also obtained at other adsorption temperatures and pressures, while the unique pore size giving rise to the best correlation increased to 0.60 nm at 0 °C and 1 bar (Fig. 10b, $R^2 = 0.98$) but decreased significantly to 0.44 nm when adsorption took place at 25 °C and 0.15 bar CO_2 (Fig. 9c, $R^2 = 0.92$), respectively. It was also found that the coefficient of determination (R^2) decreased sharply even with a slight increase in the pore sizes identified (Fig. 10d). It is well known that smaller micropores have higher adsorption potentials as a result of the superposition of the stronger van der Waals force produced by the adjacent walls of smaller micropores. While the above results further confirm the vital role of ultra-microporosity (< 1nm) on the CO_2 uptake, they are also highly suggestive of the existence of a critical pore size distribution that essentially determines the overall CO_2 uptake performance at specific adsorption temperatures and pressures, with the critical pore size decreasing with increasing adsorption temperature and/or decreasing CO_2 partial pressure.



(a)



(b)

Figure 4.10 Relationship between CO_2 uptake and ultra-micropore volume of RH carbons: (a) 0 °C, 0.15 bar CO_2; (b) 0°C, 1 bar; (c) 25°C, 0.15 bar CO_2; (d) the change of coefficient of determination R^2 with the increase of pore size (continued)

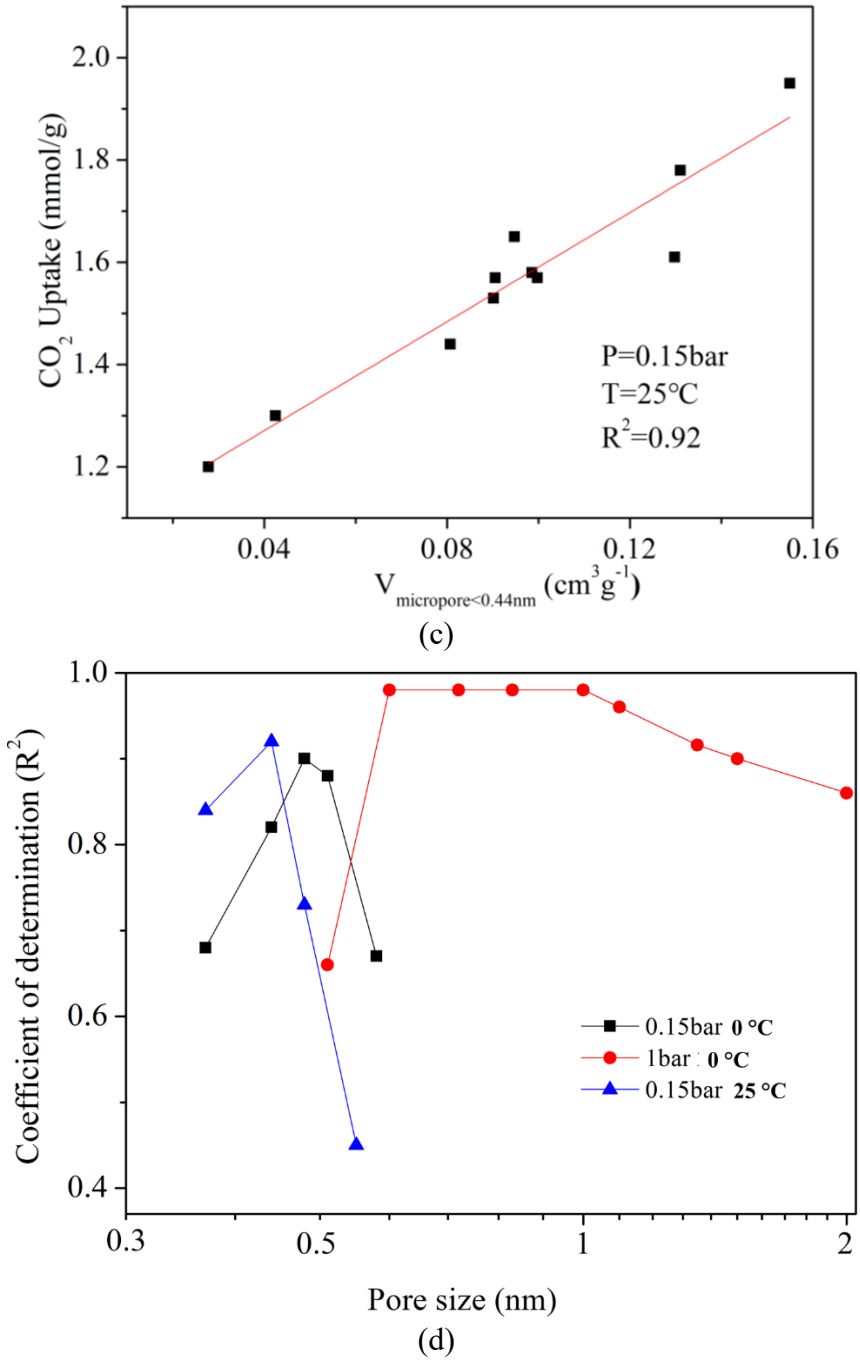


Figure 4.10 Relationship between CO_2 uptake and ultra-micropore volume of RH carbons: (a) 0 °C, 0.15 bar CO_2; (b) 0°C, 1 bar; (c) 25°C, 0.15 bar CO_2; (d) the change of coefficient of determination R^2 with the increase of pore size

At 0.15 bar CO_2, the value of intercept derived from linear extrapolation, which characterises the relative significance of surface chemical properties in CO_2 adsorption, was obtained as 1.11mmol/g at 0°C and 1.00mmol/gat 25 °C. For sample HC-600-2, this represents 37% and 50% of its CO_2 uptake capacity at 0°C and 25 °C and a CO_2 pressure of 0.15 bar, respectively. At 0 °C and 1 bar CO_2, the

intercept increased to 1.89 mmol/g, accounting for 32% of the adsorption capacity of HC-600-2. Clearly, the relative role of surface chemistry in CO_2 adsorption is even more significant for all other samples where the CO_2 uptake is lower due to smaller ultra-microporosity. The use of surface modification via various methodologies as a means to boost the adsorption capacity of carbon materials has been the focus of many investigations over recent years, but with limited improvements being achieved as shown in Table 2.6. The remarkable relative contribution of surface chemistry as characterized by the large intercept obtained for the RH carbons has never been observed in previous investigations where the intercept of similar relationships was found to be near zero while the conclusions on the role of surface chemistry were often ambiguous or contradictory (Zhang et al., 2013; Meng et al., 2014; Presser et al., 2011; Wickramaratne et al., 2013a).

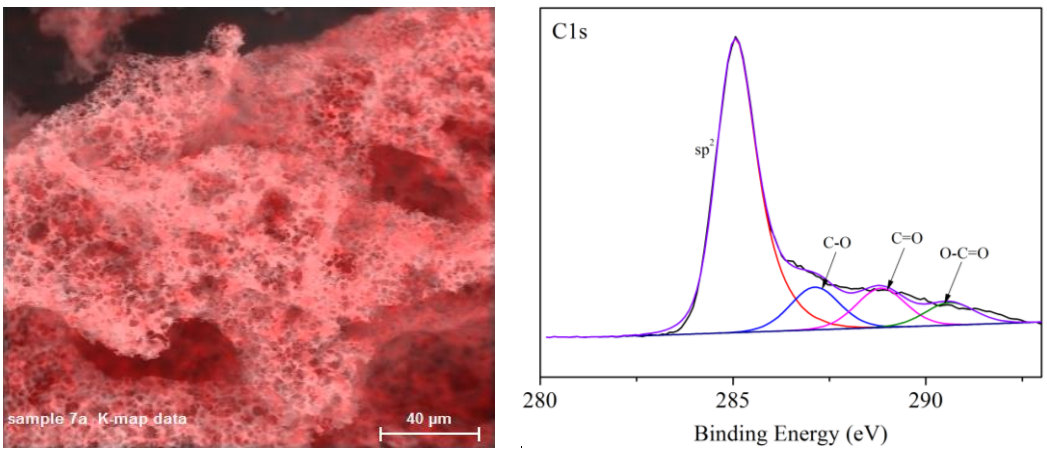
As the RH carbon is virtually nitrogen-free, it is believed that the excess adsorption capacity of the RH carbons was linked with the presence of extra framework metal (K^+) cations that were formed as a result of potassium intercalation achieved during the KOH activation or K_2CO_3 activation (Liu et al., 2015). It has been well known that extra-framework cations usually present in zeolitic materials can form strong local electric fields that can polarize adsorbate molecules and hence provide either additional active adsorption sites and/or enhance the interaction of the adsorbate with the adsorption surface, with the magnitude of the effect determined by both the charge density of the extra-framework ions and the electric quadrupole of adsorbate (Liu et al., 2015; Zhao et al., 2012; Pirngruber et al., 2010). CO_2 has a very large electrical quadrupole moment, which is over three times higher than that of N_2 ($-1.43\pm0.06 \times 10^{-39}$ Cm^2 *vs* $-4.65\pm0.08\times10^{-40}Cm^2$) (Raab et al., 1998), implying that CO_2 molecules can be preferentially polarised in an electrostatic field. Therefore, the large excess CO_2 adsorption capacity of the RH carbons, which could not possibly be accounted for by their surface textural properties, could be presumably owing to the strong preferential CO_2 polarisation by the extra-frame work K^+ ions present in the framework of the RH carbons. It has been well established that CO_2 polarisation in zeolitic materials gives rise to the formation of various adsorption complexes, which range from bridged and unbridged complexes with single and dual exposed ions to bent carbonate-like species, the latter also

involving the participation of both the exposed ions and a lattice oxygen (Pirngruber et al., 2010; Martin-Calvo et al., 2014). The great excess adsorption capacity or the large y-axis intercepts observed for the RH carbons (Fig. 4.10) are clearly attributable to the similar adsorption complexes formed via the similar adsorption mechanisms. It appears that the presence of extra-framework K^+ ions particularly benefit the CO_2 adsorption at high adsorption temperatures or low partial pressures, with its contribution to the overall CO_2 uptake increased from ca. 37% to 50% when adsorption temperature increased from 0 °C to 25 °C at 0.15 bar and from 32% to 37% when CO_2 pressure decreased from 1 to 0.15 bar at 0 °C.

Presumably, the formation of extra framework cations ($K^{+\delta}$) is particularly associated with the potassium intercalated into the carbon network structures during activation, with the degree of potassium intercalation and hence the density of the extra-framework ions determined by the activation conditions and resultant textural properties of the carbons (Liu et al., 2015). The above results suggest that the formation of extra-framework ions was considerably enhanced in the RH carbons, potentially due to their exceedingly high ultra-microporosity that may expectedly either increase potassium intercalation or stabilise the derived extra-framework ions.

The SEM-EDX element mapping obtained for the sample HC-600-2 (Fig. 4.11a) reveals the extensive uniform spatial distribution of the intercalated potassium species at microscopic scales, which is indicative of its high surface polarity, while the characterizations by XPS (Fig. 4.11b) demonstrates the presence of potassium, silicon, aluminium and calcium at varying quantities in different forms of entities. The K2p spectrum for the potassium in the sample HC-600-2 exhibited two peaks at 293.2 and 296.0 eV with an intensity ratio of 2:1 and a difference in binding energy of 2.8 ev, which are characteristic of the spin-orbit-split doublet ($K2p_{3/2}$ and $K2p_{1/2}$) of surface potassium cations and oxides (Li et al., 2001; Moulder et al., 1992) rather than carbonate species, which usually have their $K2p_{3/2}$ peak at 292.2 eV (Shchukarev et al., 2004). Given the significantly enhanced and fully reversible CO_2 adsorption, this suggests the formation of strongly bound potassium surface complexes presumably in the form of $O^{-\delta}$–$K^{+\delta}$and/or extra-framework $K^{+\delta}$ cations. The residual silicon compounds, which survived the excessive post-activation

washing, have a Si2p spectrum comprising two peaks at the binding energies of 102.6ev and 103.8ev, which is indicative of the existence of X-type zeolitic structures (Barr, 1983) and SiO_2 (Miller et al., 1985), respectively. The XPS characterization also indicates the presence of trace quantities of alumina, which had an Al2p peak at 74.6 eV that indicates the presence of X and/or Y-type zeolites (Barr, 1983), and calcium species showing two Ca2p peaks at 351.2 and 347.7eV, which are suggestive of the existence of $CaCO_3$ (Stipp et al., 1991) and A-type zeolitic entities (Pirngruber et al., 2010), respectively. XRF analysis conducted for sample HC-600-2 show that sample contained 0.15 wt% Al, 0.57 wt% Ca in addition to K and Si, confirming the existence of trace quantities of Al and Ca bearing species. Given the unique distribution of silicon compounds in rice husk at molecular levels, the above results reveals that part of the rice husk-contained silicon was transformed to different forms of zeolitic entities incorporated into the carbon networks, which essentially transformed the RH carbons to a type of zeolite-carbon nanocomposite materials, whereas the alkali-metal zeolites are well known for the abundance of extra-framework cations responsible for their usually strong surface affinity to CO_2 (Pirngruber et al., 2010).



(a) (b)

Figure 4.11 (a) SEM-EDX element mapping showing the spatial distribution of potassium in HC-600-2; (b)-(f) XPS spectra of the major heteroatoms identified in HC-600-2 (continued)

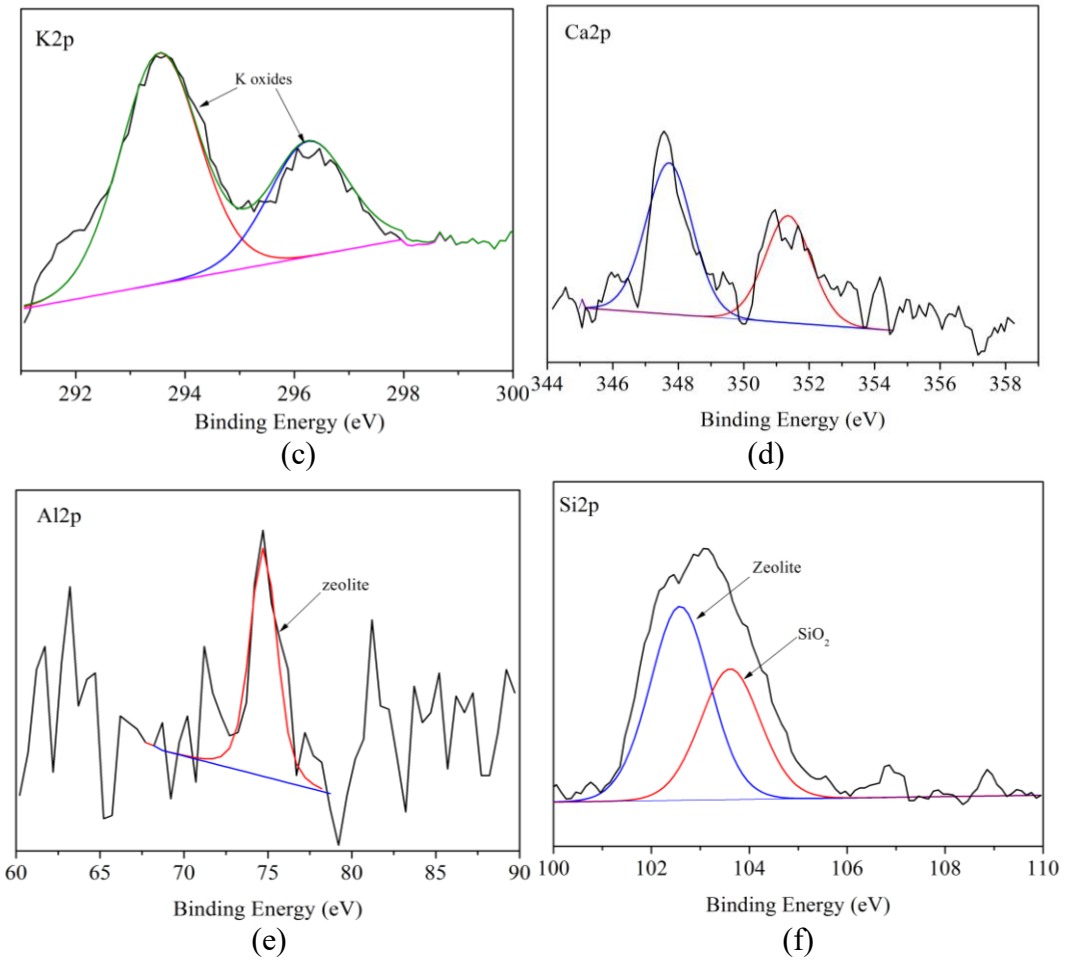
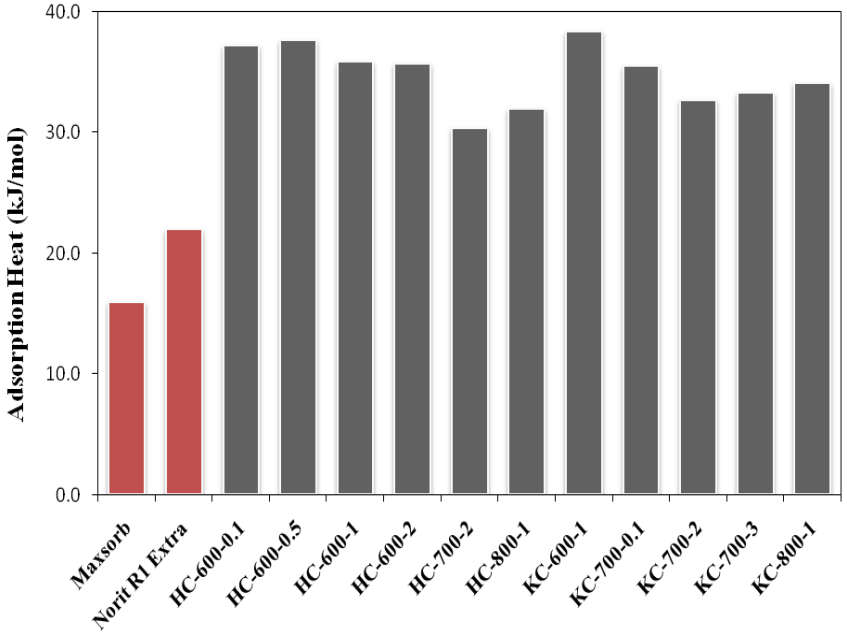


Figure 4.11 (a) SEM-EDX element mapping showing the spatial distribution of potassium in HC-600-2; (b)-(f) XPS spectra of the major heteroatoms identified in HC-600-2

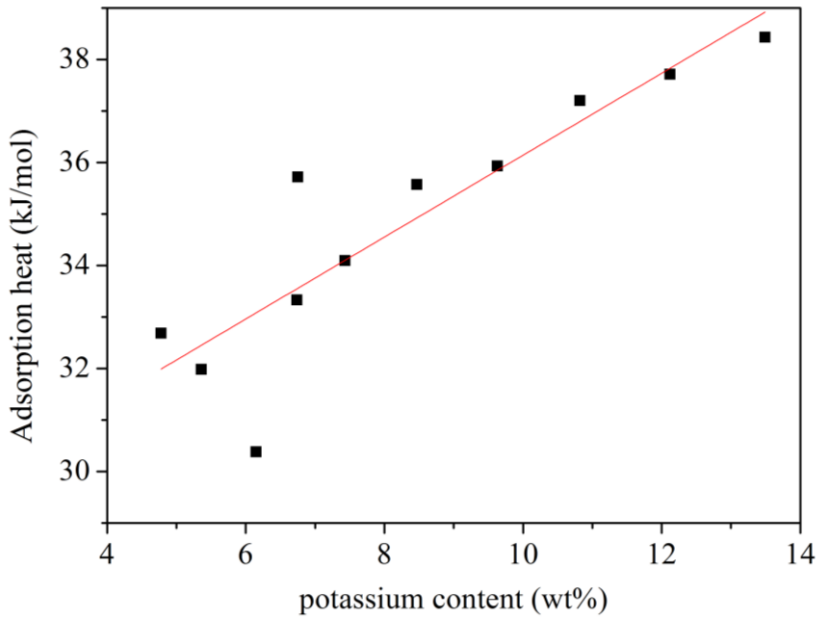
4.3.6 Heat of CO_2 adsorption of RH carbons

The heat or enthalpy of adsorption is an important parameter to indicate the surface affinity of an adsorbent toward CO_2 and hence reflect the strength of their interaction. Ideally, a suitable adsorbent for CO_2 capture should have a moderate heat of adsorption to facilitate high CO_2 uptakes at low CO_2 partial pressures and/or reasonable flue gas temperatures without energy-intensive flue gas deep cooling. This is because too high a heat of adsorption can lead to increased energy requirement for CO_2 desorption or sorbent regeneration whilst if the heat of adsorption of a sorbent is too low (e.g. those of typical commercial carbons (Himeno et al., 2005; Sethia et al., 2015; Zhang et al., 2013)), the sorbent will give rise to unacceptably low CO_2 uptakes at typical flue gas temperatures and CO_2 partial pressures. Fig. 4.12 shows the heat of CO_2 adsorption measured by TG-DSC

at 25 °C and a CO_2 partial pressure of 0.15 bar in N_2 for a selection of RH carbon samples. The heat or enthalpy of adsorption is an important parameter to indicate the surface of an adsorbent toward CO_2 and hence reflect the strength of their interaction. The heat of adsorption for the RH carbons ranged from 32 to 38.4 kJ/mol and showed a decrease with increasing activation temperature and the ratio of KOH or K_2CO_3 to RH (Fig. 4.12a), which corresponds well to the increased porosity development and hence the increased role of surface textural properties in adsorption. Though the measured adsorption heat by TG-DSC for the RH carbon represents the average heat of adsorption rather than the isosteric heat of adsorption used in prior studies, which is a function of surface coverage and usually calculated from using adsorption isotherms, they are still considerably higher than those reported for zeolite (Rege et al., 2000) and most MOFs (Sumida et al., 2011) and virtually any other carbon materials (Himeno et al., 2005; Zhang et al., 2013; Sethia et al., 2015) (e.g. Maxsorb and Norit R1 Extra (red bar), 17-25 kJ/mol (Himeno et al., 2005)), being indicative of the strong interaction of the adsorbed CO_2 phase with the surface. The observed strong linear increase of adsorption heat with increase in the content of intercalated potassium (Fig. 4.12b) confirms the significance of potassium intercalation in modifying the carbon surface chemistry via the formation of highly polarising extra-framework $K^{+\delta}$ ions or zwitterion-like structures. As shown in Fig. 4.12a and Table 2, the fact that the least activated samples prepared under the mildest activation conditions (e.g. HC-600-0.1, HC-600-0.5 and KC-600-1) was found to have the highest heat of adsorption further reflects the strong surface inhomogeneity of the potassium-intercalated RH carbons with incorporated zeolitic entities as revealed in Fig. 4.11. Further, compared to previous findings, the large y-intercept of ca. 28 kJ/mol derived from the linear relationship (Fig. 4.12b), presumably attributable to the non-electrostatic interactions, also suggests that the micropore filling/capillary condensation in the RH carbons could be significantly enhanced or the micropores filled to a higher degree due to the extended effect of strong surface electrostatic forcing.



(a)



(b)

Figure 4.12 (a) Specific heat of CO_2 adsorption measured by TG-DSC (flue gases: 15% CO_2 + 85% N_2; adsorption temperature: 25°C); (b) the relationship between K content and adsorption heat.

4.4 Conclusions

Novel activated carbons with exceedingly high ultra-microporosity and strongly modified surface chemistry in favour of CO_2 adsorption were prepared from the abundant agricultural waste of rich husk, using a facile approach that essentially integrated the carbonisation and simultaneous activation into a single one-step

process. The synthesized bio-carbons have showed exceedingly high levels of ultra-microporosity, owing to the unique templating role of the natural silicon species contained within the RH molecular framework structures. A combination of high ultra-microporosity and unique surface chemistries led to remarkable CO_2 uptake capacities of up to 5.91 mmol/g at 0 °C and 1.0 bar and 2.0 mmol/g at 25 °C and a CO_2 partial pressure of 0.15 bar, which represent one of the highest CO_2 uptakes ever reported for designer carbon and MOF materials. Taken with the exceptionally high heat of adsorption, the unusually prominent role of surface chemistry in CO_2 adsorption, which was responsible for up to 50% of total CO_2 uptake, were highly indicative of the significantly enhanced formation of extra-framework potassium ions leading to the extraordinary surface affinity to CO_2 observed for the RH carbons. Characterisations by XPS and EDX elemental have demonstrated the extensive uniform spatial distribution of the intercalated potassium at microscopic scales and the existence of various types of zeolitic aluminosilicate entities incorporated into the RH carbon frameworks, which essentially transformed the carbons into potassium-intercalated zeolite-carbon composite materials.

Chapter 5 Mechanochemical method to boost the CO_2 adsorption capacity and selectivity of bio-carbons

5.1 Introduction

In former chapter, rice husk, a typical low density biomass, was used as precursor to prepare efficient CO_2 adsorbents, the highest uptake of sample HC-600-2 was 2 mmol/g. This was the highest adsorption capacity of bio-carbons or nitrogen free carbons and competes well with polymer derived carbons. However, only sample HC-600-2 could reach such a high uptake. The adsorption capacity of other samples was lower than 1.5 mmol/g. Similarly, as reported in many papers, the highest adsorption of activated carbon derived from biomass to date is about 1.3-1.5 mmol/g, much lower than polymer derived carbons. Hence, increasing the adsorption capacity at low partial pressure is the key area of improvement. In this section, a mechanical tabletting pretreatment approach as well as nitrogen-rich additives was employed to modify the pore structure and surface chemistry of the biomass in order to boost the adsorption capacity.

5.2 Experimental procedure

Dried rice husk was pre-oxidized at 200 °C for 6 hours in 50 ml/min of air flow. The oxidized sample was mixed with 30 ml of KOH solution at a pre-set AC/KOH mass ratio for 24 h impregnation. For nitrogen doping experiments, additives like polyethylenimine (PEI) or polyisocyanurate (PIR) about 10 wt% of the sample was also added into the KOH solution. These samples were then dried at 105 °C and grinded into powder for pellet pressing. A 13 mm diameter evaluable pellet die with 10 tons of maximum load were employed to compress the samples into 1.5 mm thick pellets. The activation process was carried out in horizontal tube furnace with heating rate of 5 °C/min up to 700 °C in 1 L/min N_2 gas flow. This was kept under these conditions for 1 h. After it was cooled down to room temperature, the sample

was washed with distilled water until the pH became neutral. Activated samples were then labelled in the Rx_y form, where the x indicates the load used and the y represents the additives used. Sample R was the carbon prepared without compaction.

5.3 Results and discussion

5.3.1 Textual properties

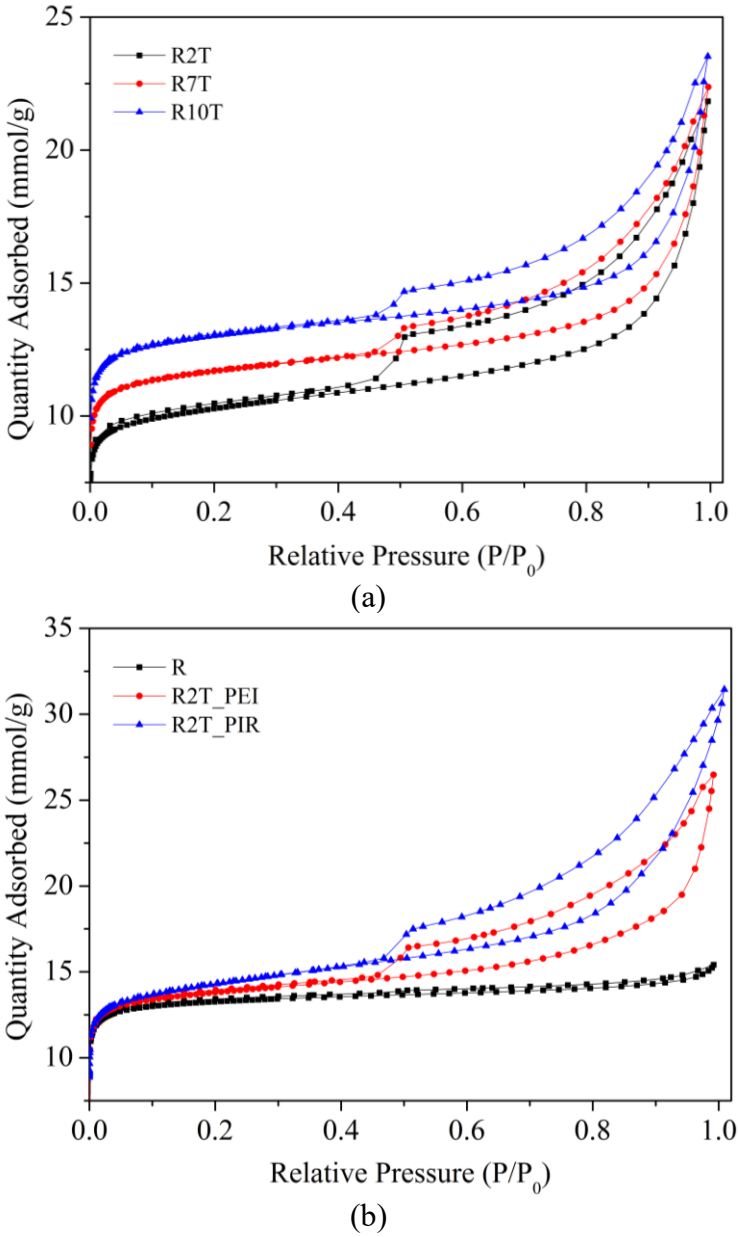


Figure 5.1 N_2 adsorption isotherms obtained at -196 °C: (a) sample prepared with different compaction load; (b)samples with additives and sample without compaction.

The nitrogen isotherms of the samples prepared under different conditions at 700 °C are shown in Figure 5.1. The R samples display a type I sorption isotherm with well-defined plateaus, indicating the microporous nature of the porous carbons. When compaction was employed, hysteresis at high relative pressures ($p/p_0 > 0.4$) started to emerge, which is indicative of the presence of mesopores. The isotherms of compacted samples showed type H3 isotherm and so, the mesopores in the sample were slit-like pores formed by aggregation of plate-like particles (Sing, 1985), which was the direct proof of the compaction's effect on porosity development. With the increase of compaction load from 2 tons to 10 tons, the nitrogen adsorption capacity of samples continues to rise, indicating the pore volume and surface area are also increasing. The detailed textural properties of all samples are listed in Table 5.1 and pore size distributions are shown in Figure 5.2.

It can be seen from Table 5.1 that pre-compaction is beneficial to the development of porosity. The BET surface area and micropore volume increased from 976 m^2/g and 0.343 cm^3/g to 1162 m^2/g and 0.403 cm^3/g with the increasing load from 0 tons to 10 tons. In comparison, additives are more effective in order to develop pores, the surface area and micropore volume of sample R2T_PEI and P2T_PIR were 1190 m^2/g, 0.422 cm^3/g and 1218 m^2/g, 0.408 cm^3/g respectively at 2 tons loading, which was even higher than that of R10T without additives. Meanwhile, compared to the microporosity domain structure of sample R, pre-compaction benefits the development of micro-mesoporous structure, a large amount of mesopores (accounting for about 50% of the total pore volume) were created and the total pore volume could reach up to 1cm^3/g. The pore volume of pores smaller than a certain diameter were calculated based on the cumulative pore volume curve.

The PSDs of all samples illustrated in Figure 5.2 showed that pre-compaction without additives using different load did not change the microporous structure, with the pore width mainly centered at 0.36 and 0.55 nm. However, with additives, the pore diameters changed to 0.36 nm and 1nm for R2T_PEI and only one peak centered at 0.36 nm and continuously distributed pores between 0.5 nm and 2 nm was observed for sample R2T_PIR. As for the mesoporous distribution, most

samples possess a continuous distribution while R2T_PIR obtained relative high peak centered at 10 nm.

Table 5.1 Specific surface areas, pore structures of prepared samples

Sample	S_{BET} (m^2/g)	V_{total} (cm^3/g)	V_{micro} (cm^3/g)	$V_{micro<0.42nm}$ (cm^3/g)	$V_{micro<0.7nm}$ (cm^3/g)
R	976	0.395	0.343	0.095	0.264
R2T	901	0.630	0.306	0.140	0.249
R7T	1037	0.645	0.358	0.140	0.310
R10T	1162	0.685	0.403	0.139	0.332
R2T _PEI	1190	0.777	0.422	0.175	0.175
R2T _PIR	1218	0.976	0.408	0.158	0.248

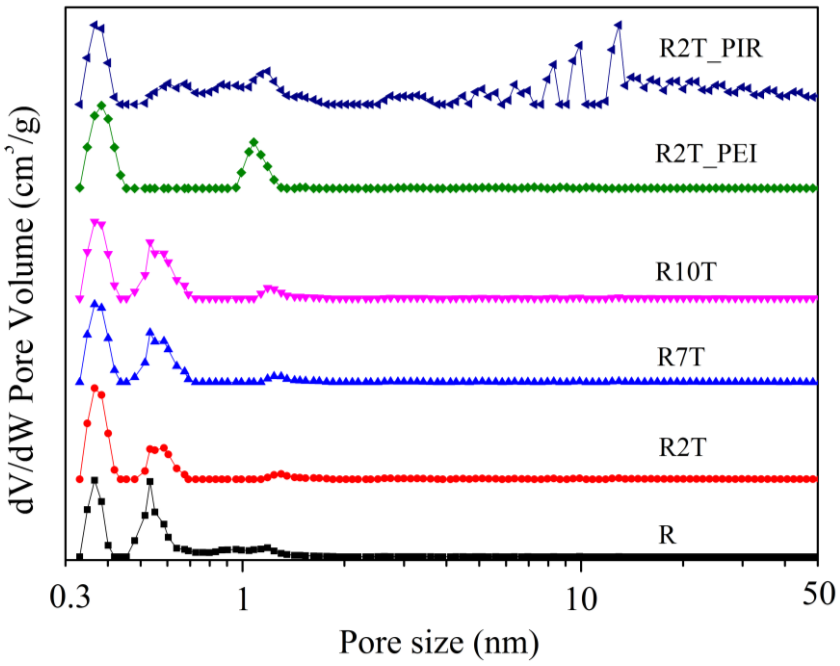
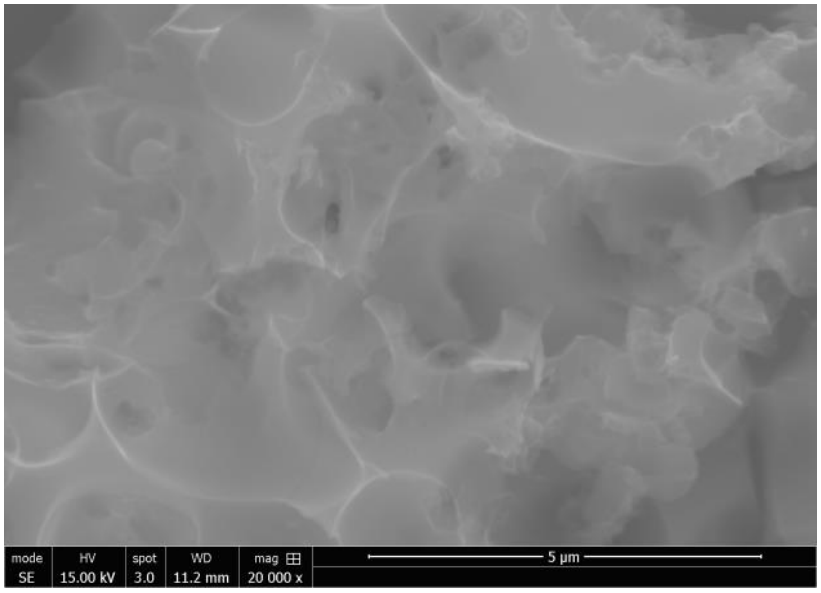
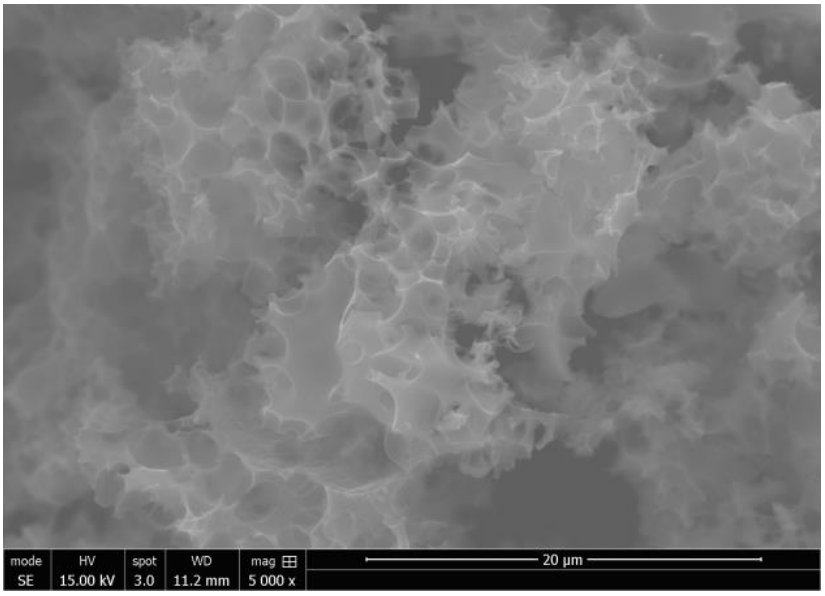


Figure 5.2 PSDs of all prepared samples by NLDFT method

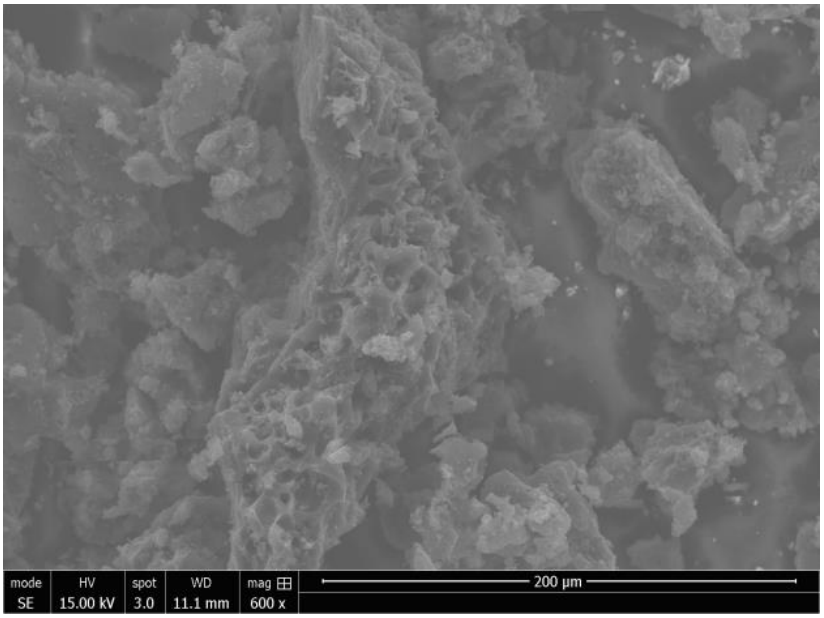


(a)

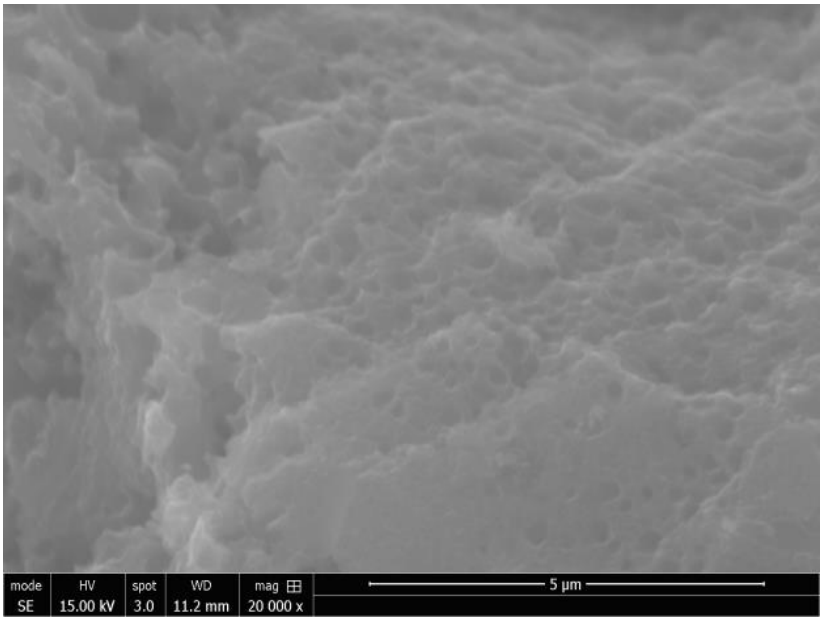


(b)

Figure 5.3 SEM images of selected samples: (a) (b) sample R; (c) (d) sample R2T (continued)



(c)



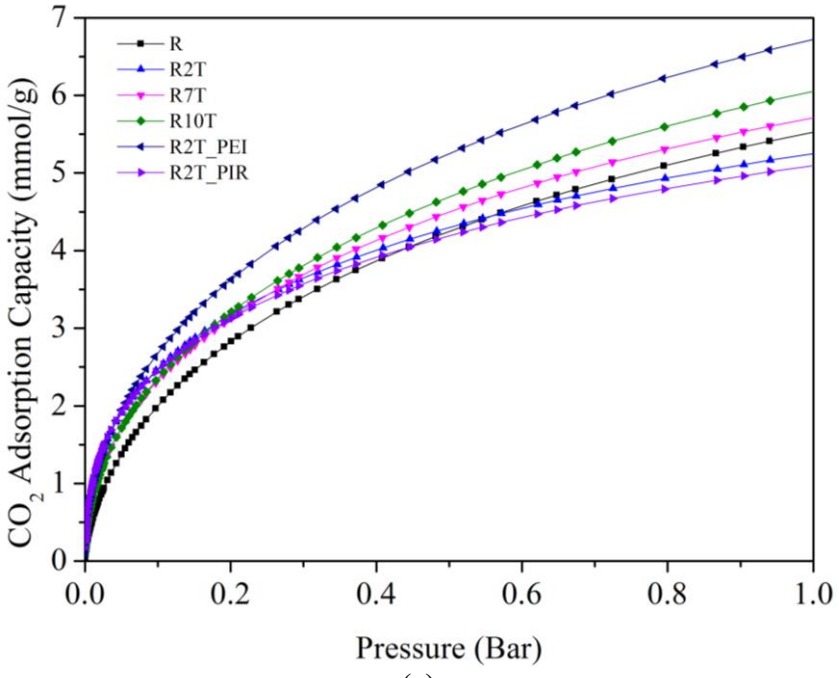
(d)

Figure 5.3 SEM images of selected samples: (a) (b) sample R; (c) (d) sample R2T

As shown in Figure 5.3a-b, the resulting sample R exhibits irregular morphology with sharp edges and large cavities. However, the morphology of the samples change dramatically with the introduction of pre-compaction. The compacted sample showed a layer by layer structure with many cavities on the surface.

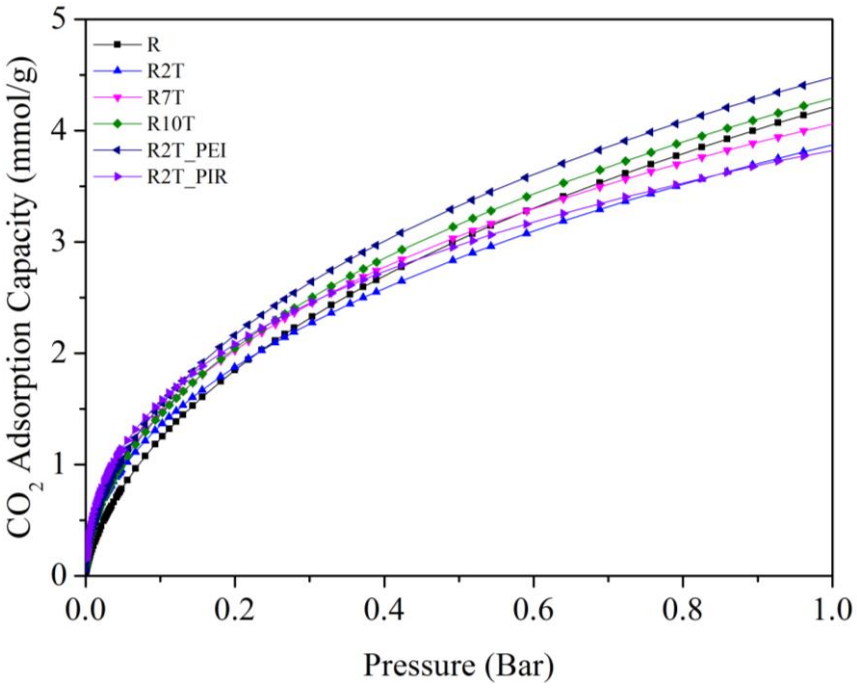
5.3.2 CO_2 adsorption performance

The CO_2 isotherms of samples were investigated at 0 °C and 25 °C up to 1 bar (Figure 5.4). Clearly, the CO_2 adsorption capacity was affected by the pre-compaction and additives. At the given activation temperature of 700 °C, the CO_2 uptake increased sharply from 5.28 and 3.88 mmol/g to 6.10 and 4.30 mmol/g at 0 and 25 °C at 1bar as the pre-compaction load increased from 2 tons to 10 tons. Interestingly, the adding of 10 wt% PEI was more effective, the uptake of sample P2T_PEI could reach 6.80 and 4.50 mmol/g at 0 and 25 °C respectively at 1 bar, which was the highest among all samples. In comparison, the uptake of the samples without pre-compaction was about 5.50 and 4.20 mmol/g that was much lower than samples R10T and R2T_PEI. It can be found that the adsorption capacity generally followed the rank of micropore volume (see Table 5.1).

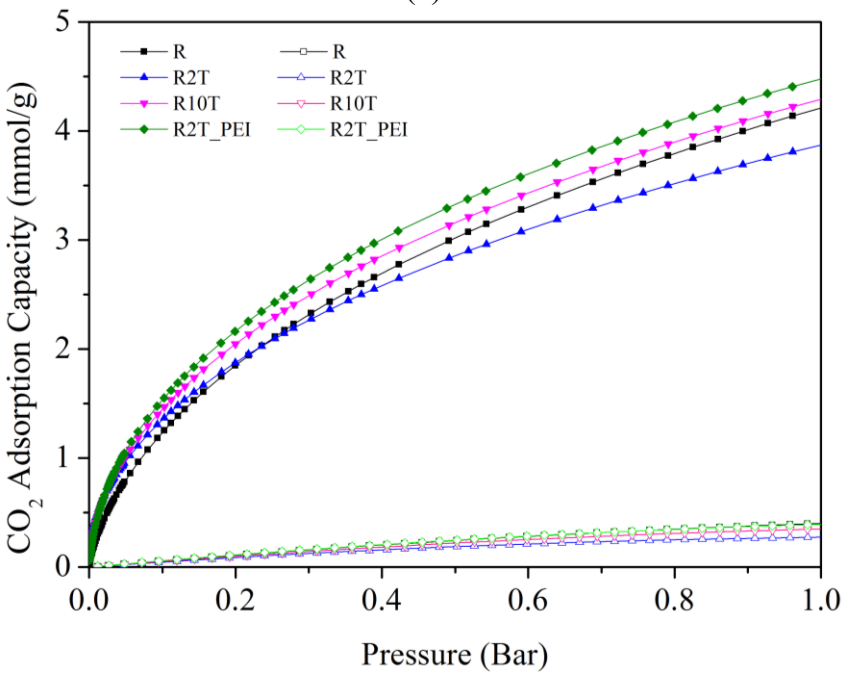


(a)

Figure 5.4 CO_2 adsorption profiles: (a) CO_2 adsorption at 0 °C; (b) CO_2 adsorption at 25 °C; (c) CO_2 and N_2 isotherms of selected samples at 25 °C (continued)



(b)



(c)

Figure 5.4 CO_2 adsorption profiles: (a) CO_2 adsorption at 0 °C; (b) CO_2 adsorption at 25 °C; (c) CO_2 and N_2 isotherms of selected samples at 25 °C

Table 5.2 Selectivity of samples at 25 °C

Sample	CO_2 uptake (mmol/g) 298K, 0.15bar	CO_2/N_2 (ISAT) 15%CO_2/85%N_2	Initial slope ratios
R	1.55	24	56
R2T	1.68	36	170
R10T	1.80	32	121
R2T_PEI	1.90	30	115

However, the trend was different at low CO_2 partial pressure (0.15bar) which corresponds to flue gas conditions. It was noteworthy that all samples with pre-compaction obtained a higher CO_2 adsorption capacity (1.68-1.90 mmol/g) than the sample without compaction, which was only 1.55 mmol/g at 0.15 bar and 25 °C. The CO_2 adsorption capacity of sample R2T_PEI could reach 1.90 mmol/g, which was higher than many 'designer' carbons and MOFs and was amongst the highest uptake ever reported (see Table 2.6). It can be seen that pre-compaction indeed improved the CO_2 adsorption performance of samples derived from the same precursor and preparation method especially at low partial pressure. But how pre-compaction works is not clear, the improvement at 0.15 bar and 25 °C is not directly correlated to micropore volume or ultra-micropore volume. For instance, sample R2T_PEI possessed the lowest ultra-micropore volume while the uptake was the highest among all samples. As was reported, the CO_2 adsorption on carbon materials can be depicted by a micropore filling mechanism rather than monolayer adsorption (Zhang et al., 2013; Ashourirad et al., 2016). Meanwhile, the adsorption potential increased with the decreasing pore size (Everett, et al., 1976), which means there was a specific pore size which meets the minimum force needed to keep CO_2 molecule in the pores under different conditions. So, the effect of pore size on CO_2 adsorption at 0.15 bar and 25 °C was investigated, the CO_2 adsorption capacity was found to be almost linear with the volume of micropores smaller than 0.42 nm (see Figure 5.5), which was consistent with the results reported in former chapter. It is obvious that the pre-compaction and additives could effectively increase the volume of micropore smaller than 0.42 nm from this work, which increased from 0.095 to 0.140 cm^3/g with pre-compaction only (2 tons to 10 tons) and to 0.175 cm^3/g when PEI was added to the samples.

This could be a potential method to boost the CO_2 uptake especially at low partial pressure of different precursors. However, ultra-micropore could not solely explain the high CO_2 uptake of samples in this work. Sample R_2T, R_7T and R_10T have similar volume of pores smaller than 0.42 nm while the CO_2 uptake at 0.15bar was different, which means the surface chemistry might also contribute to the CO_2 uptake. As was reported in the former chapter, potassium will intercalate into the carbon lattice in the form of surface potassium groups during KOH activation and remain in carbon lattice after water washing. Those have been proved to have significant contribution to CO_2 adsorption capacity at low partial pressure. It seems that pre-compaction changed the morphology of samples and kept more potassium intercalated in carbon lattice. In addition, sample R2T_PEI and R2T_PIR also possess nitrogen functionalities on carbon surface, which was 2 wt% and 0.5 wt% respectively. However, despite the discrepancy of nitrogen content, both samples have a similar adsorption capacity. Therefore, it is difficult to determine the direct contribution of nitrogen on CO_2 capture, which is consistent with papers reported by other research groups (Sun et al., 2013; Sevilla et al., 2013a; Zhang et al., 2013; Kumar et al. 2015). Actually, ultra-microporosity of materials played a key role.

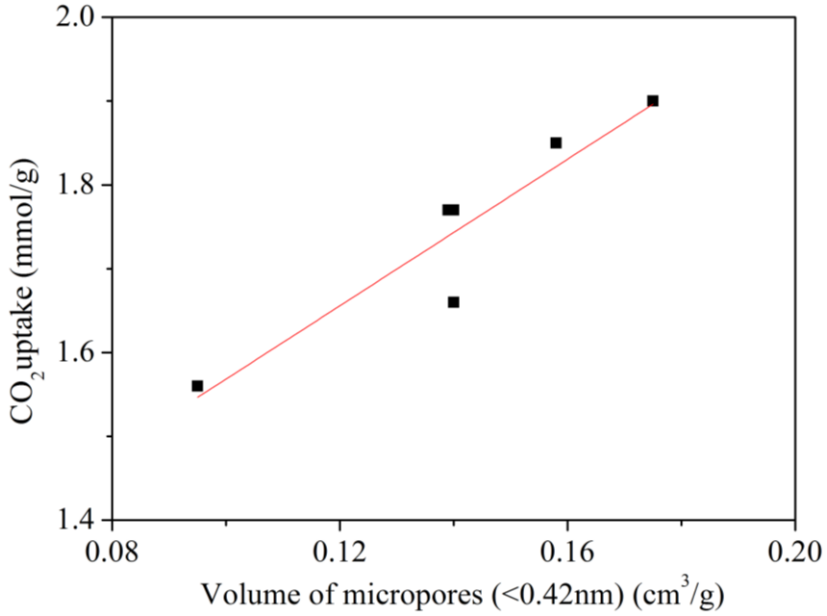


Figure 5.5 Relationship between CO_2 uptake at 0.15 bar and 25 °C and ultra-micropore volume of all samples prepared in this chapter

In order to study the surface affinity to CO_2 molecules, the isosteric heat of adsorption (Q_{st}) was calculated by using the Clausius–Clapeyron Equation.

Considering the heterogeneity of the surface caused by potassium intercalation, the dual-site Langmuir model was chosen to fit the CO_2 adsorption isotherms at 0 and 25 °C (Koresh et al., 1983; Mason et al., 2011). The plots of the Q_{st} value as a function of CO_2 adsorption capacity for selected samples are shown in Figure 5.6. The initial Q_{st} of the samples with pre-compaction at a CO_2 uptake level of 0.01 mmol/g range between 33-47 kJ/mol that is much higher than that of sample R (28 kJ/mol). The higher Q_{st} value means a stronger interaction between CO_2 molecules and the carbon surface. This means the treatment by pre-compaction enhanced the interaction force between the carbon and the CO_2 molecules. In comparison, the initial Q_{st} of the sample R2T (47 kJ/mol) was much higher than most carbon materials with similar or even higher ultra-micropore volumes, and/or with nitrogen functionalities such as nitrogen-free carbon PAF-1-450 (27.8kJ/g) (Ben et al., 2012), or a polymer derived carbon BIDC-0.5-700 (35.8 kJ/mol) with 17.6 wt% N (Ashourirad et al., 2016), indicating that the significant improvement of the initial Q_{st} mainly comes from the unique surface chemistry. As for nitrogen-free samples, potassium intercalation is the only surface heteroatom groups on carbon surface, which means the potassium intercalation is responsible for the high initial Q_{st}. However, nitrogen containing groups are not the key factor, which determine the initial Q_{st}, as the initial Q_{st} of P2T_PEI and P2T_PIR is lower than that of P2T.

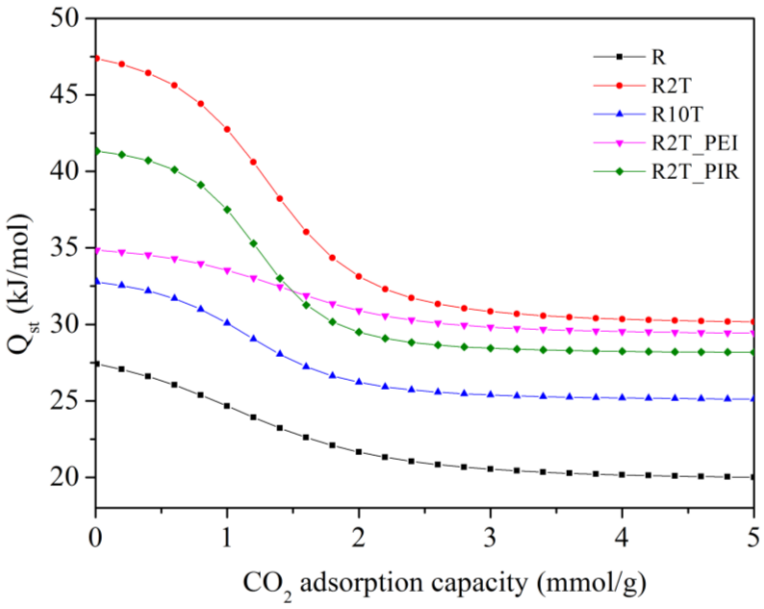
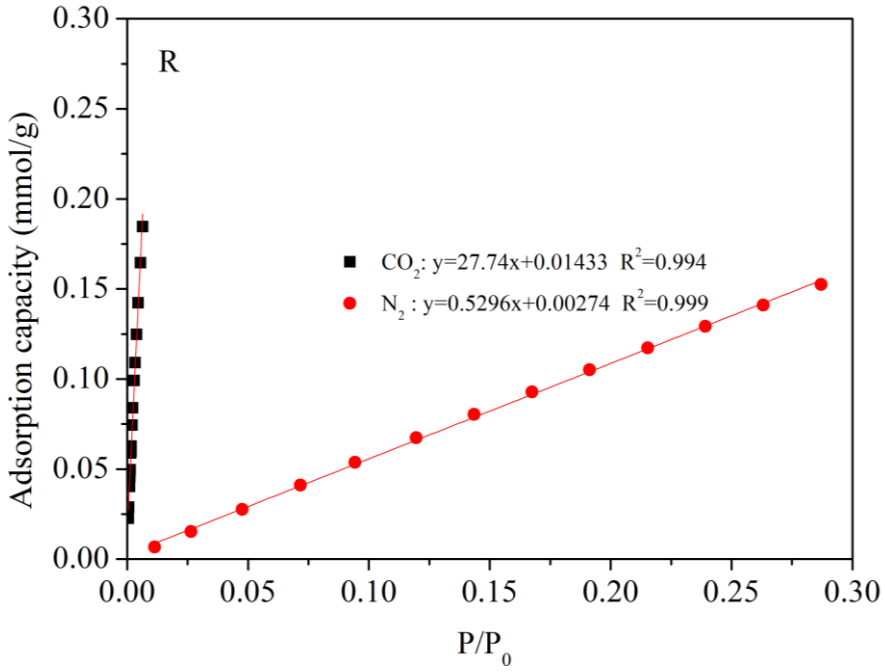
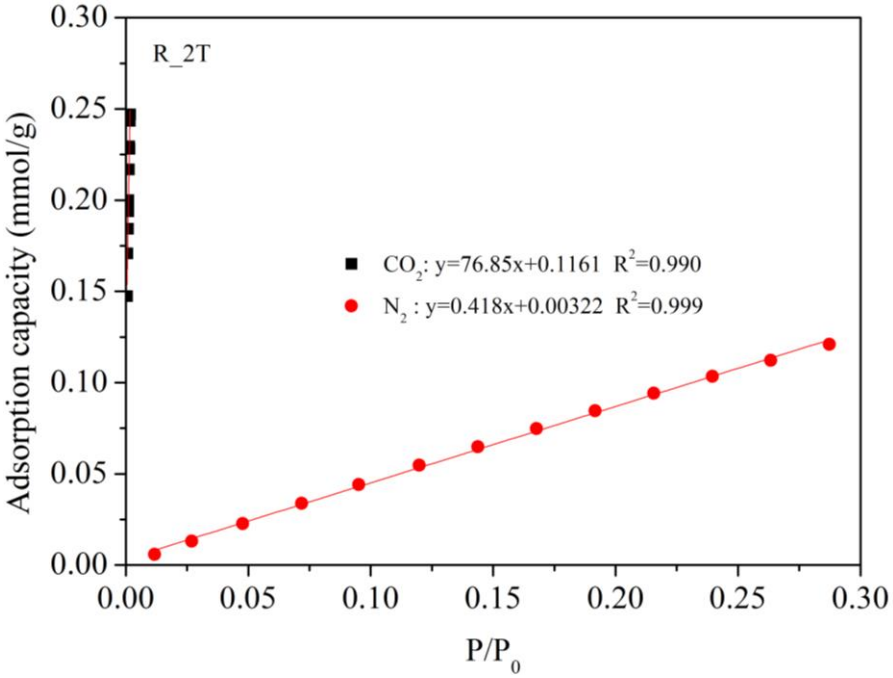


Figure 5.6 Isosteric heat of CO_2 adsorption on different samples calculated from the adsorption isotherms at 0 and 25 °C

In addition to the adsorption capacity, selectivity was also an important criterion to help to identify the potential of prepared carbons for industrial applications. The ideal adsorption solution theory (IAST) (Lu et al., 2011; Babarao et al., 2009; Zhao et al., 2012) and Henry's Law through the initial slopes of CO_2 and N_2 adsorption isotherms (IS) (Hao et al., 2011; Chandra et al., 2012) were employed to calculate the selectivity of the samples (see Table 5.2 and Figure 5.7). It can be found that the tableted samples exhibit high IS selectivity (105-170) which is twice or even three times that of sample without compaction (56). This was higher than that of most carbon materials reported. For instance, well-designed mesoporous carbon materials reported by Lee et al could reach very high selectivity (100 at 298K) while the uptake was only 0.8 mmol/g at 1bar and rationally designed hierarchical N-doped carbons exhibit high selectivity and uptake 124 and 1.72 mmol/g respectively. In comparison, abundant agriculture waste rice husk derived carbons R2T (1.68 mmol/g, 170), R10T (1.80 mmol/g, 121) and R2T_PEI (1.90 mmol/h, 115) achieved equivalent or even higher performance than the "designer" carbons, proving compaction could be an effective way to prepare high performance CO_2 adsorbents. Such high IS selectivity indicates a strong surface affinity to CO_2 molecule compared to N_2 at very low CO_2 coverage. In addition, the ideal adsorption solution theory (IAST) selectivity (assuming a 0.15/0.85 mixture of CO_2/N_2 at 1 bar) showed a similar trend to IS selectivity (see Table 5.2). The discrepancy between the Henry's law and IAST values can be attributed to the adsorption site heterogeneity.

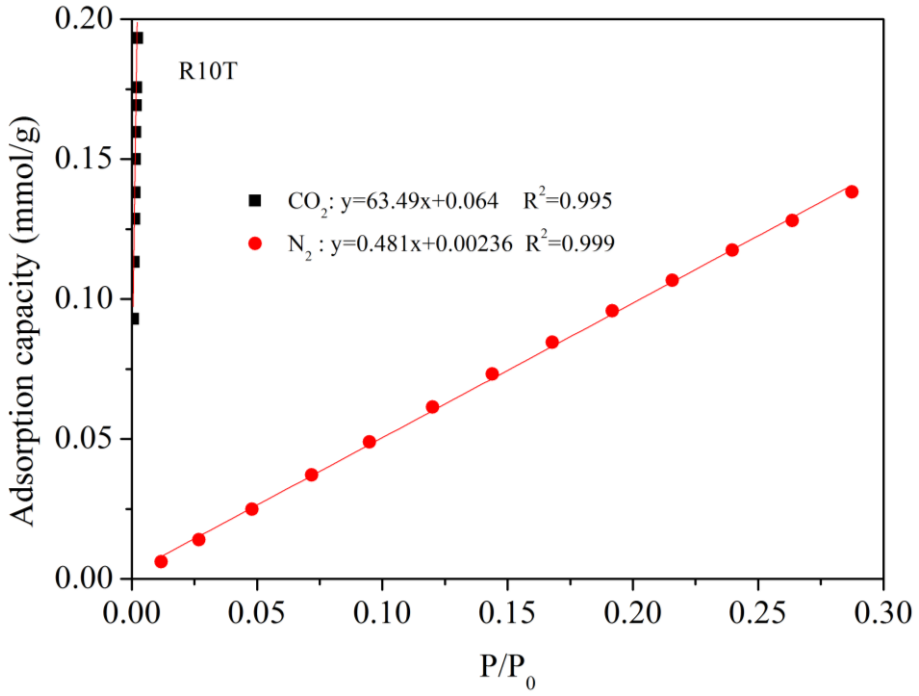


(a)

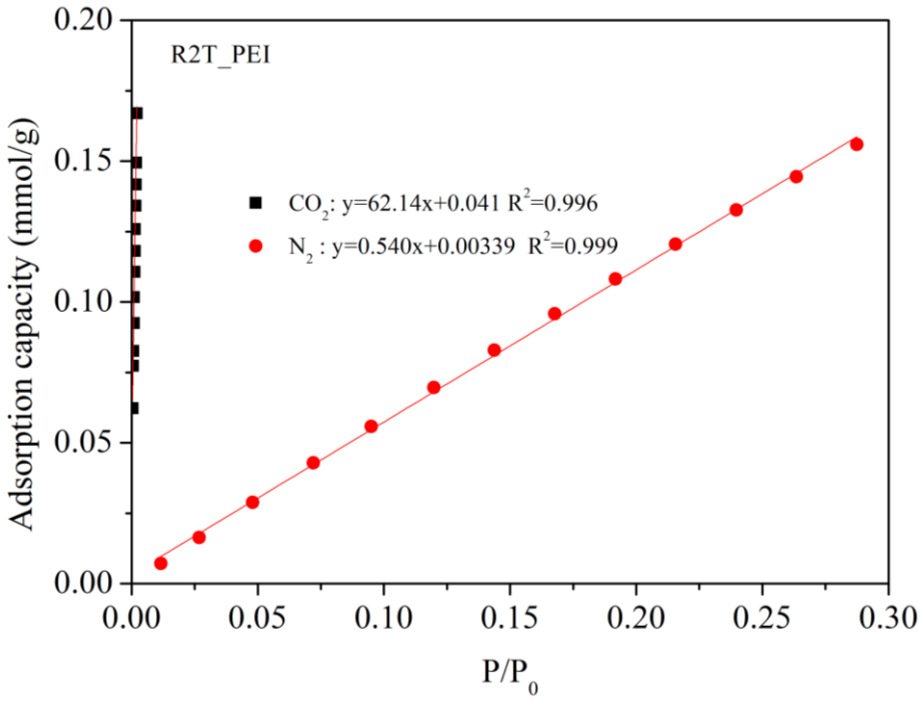


(b)

Figure 5.7 CO_2/N_2 adsorption selectivity at 298 K based initial slope method: (a) sample without compaction (b) sample R2T; (c) Sample R10T; (d) sample R2T_PEI (continued)



(c)



(d)

Figure 5.7 CO_2/N_2 adsorption selectivity at 298 K based initial slope method: (a) sample without compaction (b) sample R2T; (c) Sample R10T; (d) sample R2T_PEI

5.4 Conclusions

Activated carbons derived from tableted rice husk with high ultra-microporosity and modified surface chemistry which favours CO_2 adsorption were prepared in this chapter. Compared to samples without pre-treatment, the synthesized carbons from pressed rice husk exhibited much higher ultra-microporosity especially in pores smaller than 0.42 nm and in a large amount of mesopores. With the increase of press load, both the surface area and micropore volume increased. In comparison, the introduction of N-rich additives like PEI and PIR not only increased the micropore volume and surface area but also changed the pore size distribution of the synthesized carbons which favored CO_2 adsorption. The high ultra-microporosity and unique surface chemistry of the samples with pre-treatment led to exceedingly high CO_2 uptake up to 6.80 and 4.50 mmol/g at 0 and 25 °C at 1 bar respectively and 1.90 mmol/g at 25 °C at a CO_2 partial pressure of 0.15 bar. This was much higher than samples without compaction and was one of the highest uptake values ever reported for a designer carbon or MOF. In addition to high adsorption capacity, the compacted samples showed a high IS CO_2/N_2 selectivity up to 170 at 25 °C as well as high isosteric heat of adsorption, which is attributed to the prominent role of surface chemistry especially extra-framework potassium ions leading to the increased surface affinity to CO_2.

Chapter 6 Ultra-microporous carbon foams for exceptional CO_2 adsorption and separation from flue gas

6.1 Introduction

In addition to biomass, polymers have also been widely used as the precursors to prepare activated carbon due to their rich and controllable surface functional groups and adjustable porosity. In particular, nitrogen rich precursors with favorable surface chemistry, nitrogen functionalities is increasingly gaining attention. Many precursors like acrylonitrile, benzimidazole, polypyrrole, polyurethane and biomass like bean dreg have been widely studied. It has been displayed by some papers that the introduction of N containing groups into carbon materials increases the basicity and delocalization of charge on carbon surface, which can enhance selective CO_2 adsorption (Shen et al., 2013; Sivadas et al., 2016; Xing et al., 2012; Wang et al., 2011) as well as the heat of adsorption (Sánchez-Sánchez et al., 2014; Sevilla et al., 2011; Fan et al., 2013; Xing et al., 2012). In this chapter, we reported for the first time the use of nitrogen-rich polyisocyanurate (PIR) as a single source precursor to prepare highly porous and potassium, nitrogen co-doped carbon molecular sieves that exhibited record high CO_2 uptake at low partial pressure and high selectivity values among porous carbons via a one-step KOH activation protocol. The effect of heteroatoms and pore structure on CO_2 adsorption at low partial pressure (0.10 bar and 0.15 bar) was studied.

6.2 Experiments

The PIR foam was firstly oxidised under flowing compressed air (50 ml/min) in a horizontal tube furnace. The temperature was increased from ambient to 260 °C at a heating rate of 0.5 °C/min and was kept there for 6 hours after which it was cooled to room temperature. The oxidised foam was then mixed with 15 ml of KOH solution with a certain amount of KOH for 24 hours before it was dried overnight

in an oven at 60 °C. The dried samples were then put into the horizontal tube furnace and were heated up in nitrogen atmosphere from ambient to the set temperature (600-700 °C) at a heating rate of 5.0 °C/min and kept there for 1h. The samples were collected after it had cooled to ambient temperature and washed until a neutral filtrate was obtained. The washed samples were then dried overnight in an oven at 80 °C. For the convenience of subsequent discussion, the carbons activated by KOH under different conditions are labelled as FCxy, where x and y represent activation temperature and mass ratio between KOH and sample respectively.

6.3 Results and Discussion

6.3.1 Textual properties

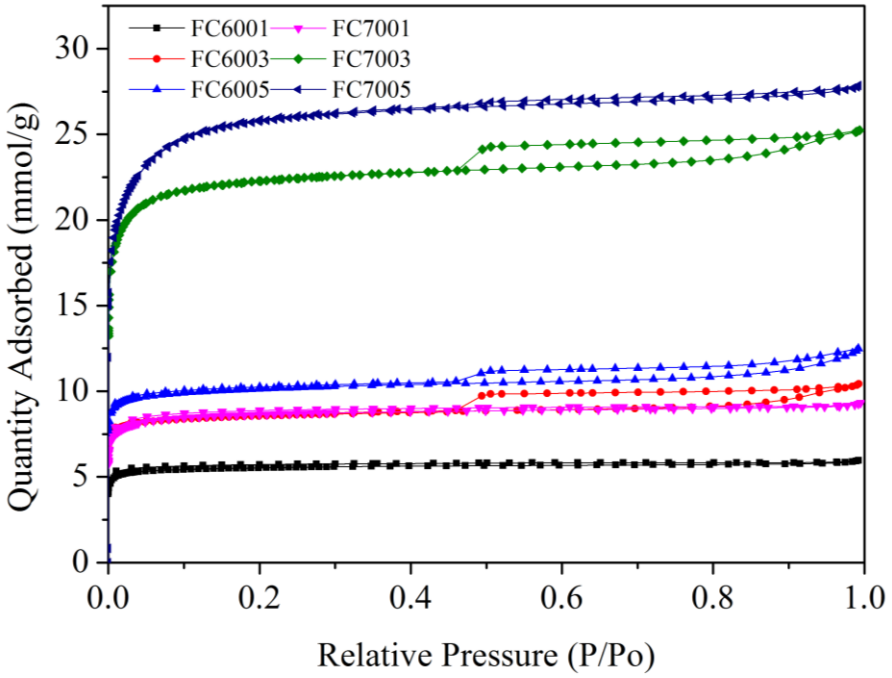


Figure 6.1 N_2 isotherms at -196 °C of carbon foam samples prepared at different KOH to foam weight ratio and temperatures

The nitrogen isotherms of the carbon samples prepared under relatively mild activation with KOH/FC mass ratio from 1 to 5 at 600 and 700 °C are shown in Figure 6.1. It can be seen that all the isotherms possess a sharp uptake at relative pressure typically <0.1 followed by horizontal plateaus at high relative pressures, indicating that the micropores are dominant in all samples. However, when the

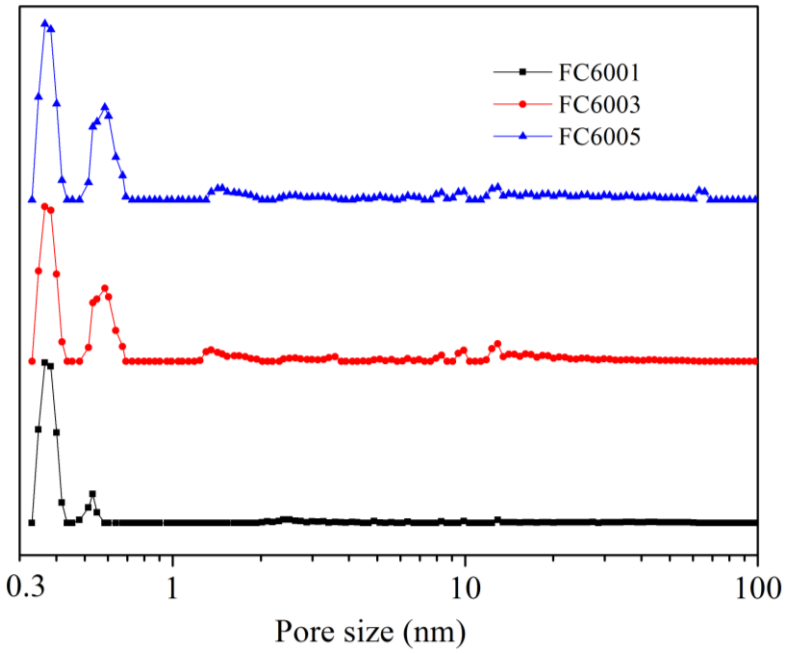
KOH/FC mass ratio was higher than 1 at different temperatures, hysteresis at high relative pressures at $p/p_0 > 0.4$ started to emerge, which is indication of the presence of mesopores. Meanwhile, it can be found that the isotherms of sample FC6003, FC6005 and FC7003 showed type H4 isotherm, indicating the mesopores in the samples were narrow slit-like pores (Sing, 1985).

Table 6.1 Specific surface areas, pore structure parameters of polymer based activated carbons

Sample	S_{BET} (m^2/g)	V_{total} (cm^3/g)	V_{micro} (cm^3/g)	$V_{micro<0.7nm}$ (cm^3/g)	XPS (wt%)		
					O	N	K
FC6001	502	0.194	0.182	0.182	13.61	4.68	4.98
FC6003	770	0.334	0.273	0.256	16.20	4.29	5.82
FC6005	911	0.395	0.324	0.304	13.32	4.14	5.61
FC7001	773	0.298	0.282	0.255	12.87	1.77	6.45
FC7003	1992	0.794	0.713	0.435	12.55	1.01	5.03
FC7005	2207	0.876	0.829	0.336	9.14	1.43	4.23

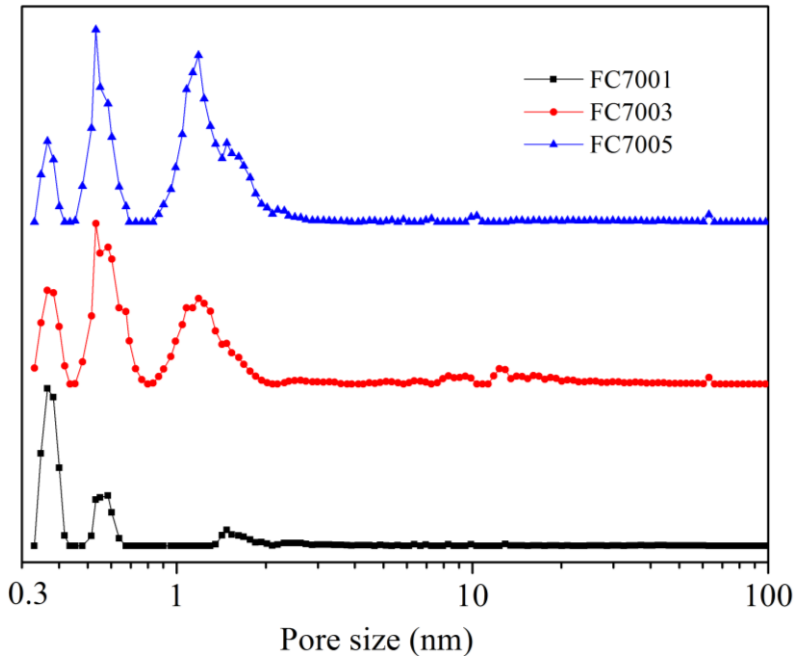
The textural parameters of these porous carbons are listed in Table 6.1. The pore size distribution of FC samples and cumulative pore volume obtained by applying NLDFT method on their nitrogen isotherms at -196 °C and CO_2 isotherms at 0 °C are shown in Figure 3. It can be seen that the total pore volume and BET surface area increased from 0.194 to 0.878 cm^3/g and 502 to 2207 m^2/g, respectively when KOH/FC mass ratio increased from 1 to 5 and the activation temperature from 600 to 700 ℃. It is clear that all FC carbons are extremely microporous, with microporosity accounting for 80~95% of the total porosity. Most importantly, as shown in Figure 6.2 and Table 6.1, the micropores of samples prepared at 600 ℃ or low KOH/FC ratio at 700 ℃ such as FC7001 consist mostly of ultra-micropores with pore diameters centered on 0.36 and 0.55 nm, which account for over 77% of the total pore volume with the ultra-micropore volume reaching up to 0.304 cm^3/g. Note that sample FC6001 possesses an ultra-micropore volume of 0.182 cm^3/g, which constitutes a remarkable 100% of micropore volume and 94% of the total pore volume, with almost all the pores centered at around 0.4 nm. This sample can

be considered as a high quality ultra-microporous carbon molecular sieve with a pore size around 0.4nm. Such ordered microporous structure could only be found in zeolites and MOFs built from using a single small ligand (Shekhah et al., 2014; Wilson et al., 1982). However, with an increase in KOH/FC mass ratio at 700 °C, pores with diameter centered on 1.2 nm emerged and quickly escalated, which could reach 60% of the total micropore volume for sample FC7005. The cumulative pore volume curve of the samples activated at 700 °C reveals that the pores centered at 0.4 nm continuously decreased while those centered at 0.55 and 1.1 nm increased in intensity with the KOH/FC mass ratio, indicating the change of microporosity at 700 °C was caused by pore widening effect. In addition, it can be found that the rest of pores in FC carbons are continuously distributed mesopores. Although mesopores or macrospores have marginal contribution to adsorption capacity, they are still play an important role on the enhancement of the CO_2 adsorption rate (Balsamo et al 2013, Wahby et al 2010).

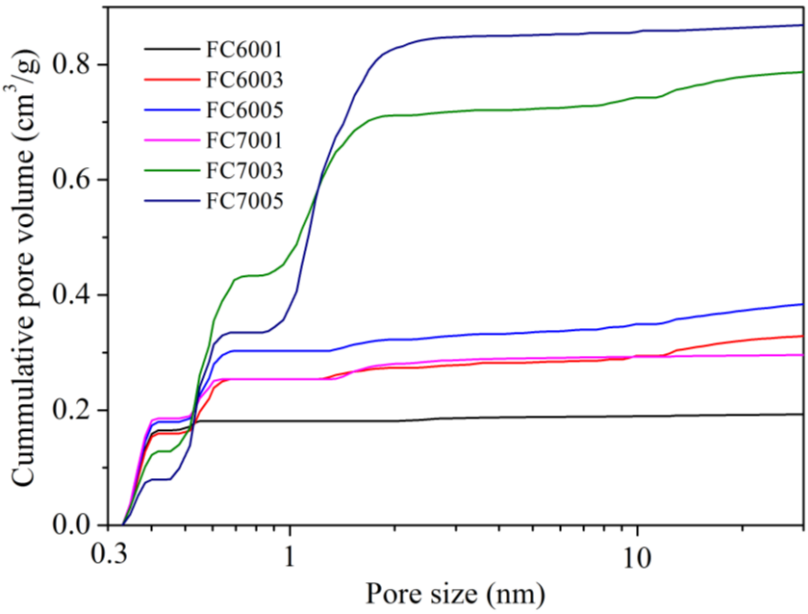


(a)

Figure 6.2 NLDFT pore size distributions for FC samples: (a) PSDs of samples prepared at 600 °C; (b) PSDs of samples prepared at 700 °C (c) cumulative pore volume vs pore size of all samples (continued)



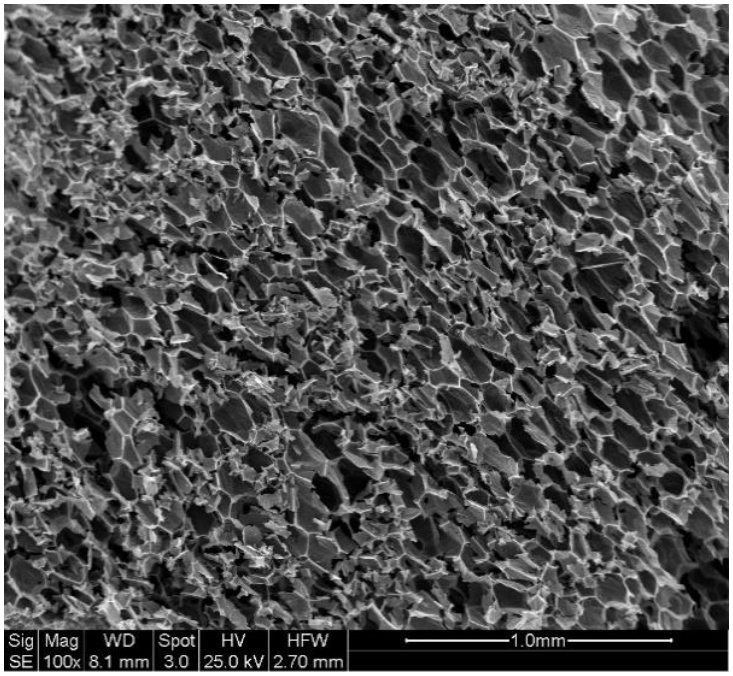
(b)



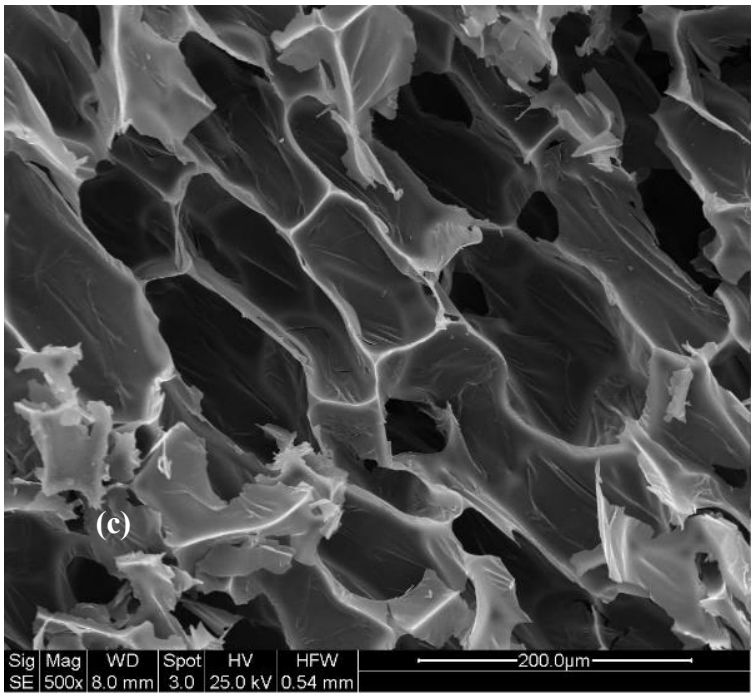
(c)

Figure 6.2 NLDFT pore size distributions for FC samples: (a) PSDs of samples prepared at 600 °C; (b) PSDs of samples prepared at 700 °C (c) cumulative pore volume vs pore size of all samples (continued)

Figure 6.3 illustrates the SEM images of sample FC7001 and FC7003. It can be seen that the samples have honeycomb-like structure, there are many cell-like units existing. With the increase in KOH/AC ratio, the carbon sample shows a much more developed porous structure, being consistent with the results shown in Table 6.1.

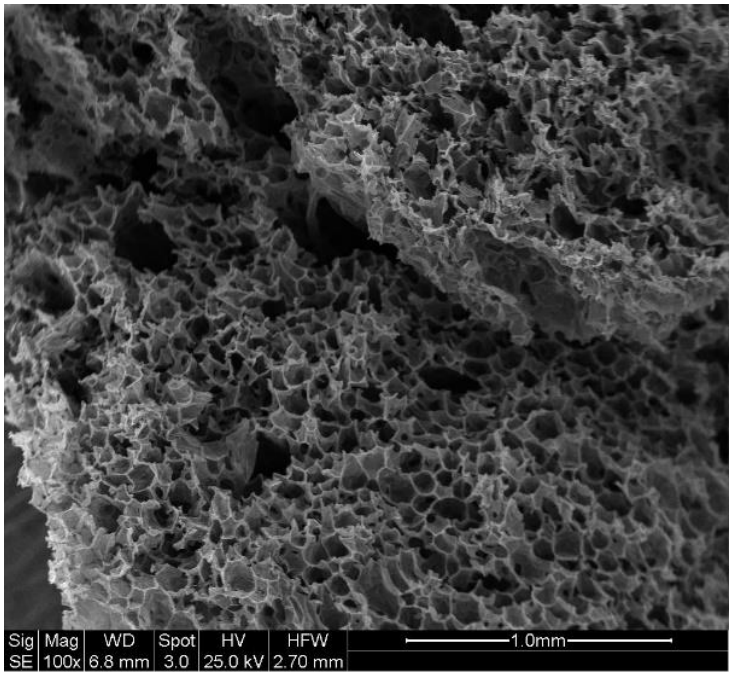


(a)

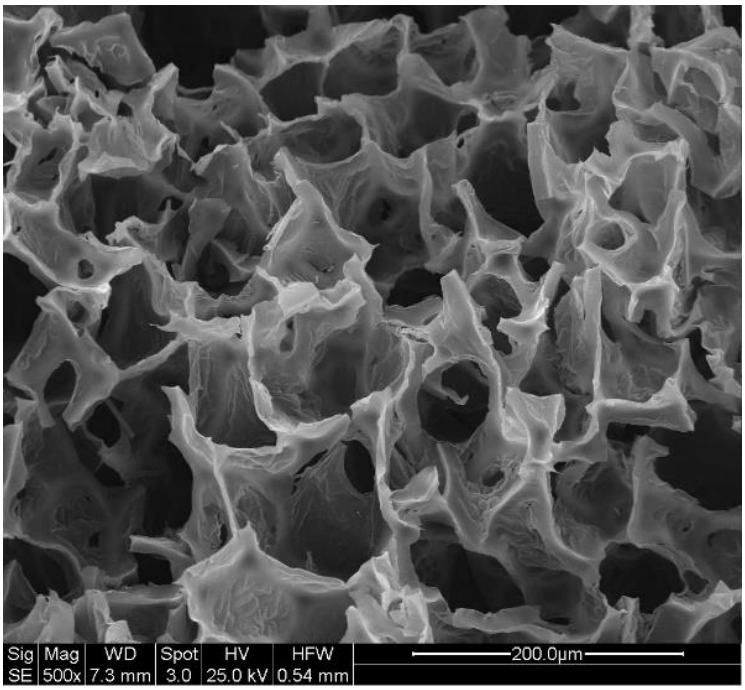


(b)

Figure 6.3 SEM Images of FC7001 (a, b) and of FC7003 (c, d) (continued)



(c)



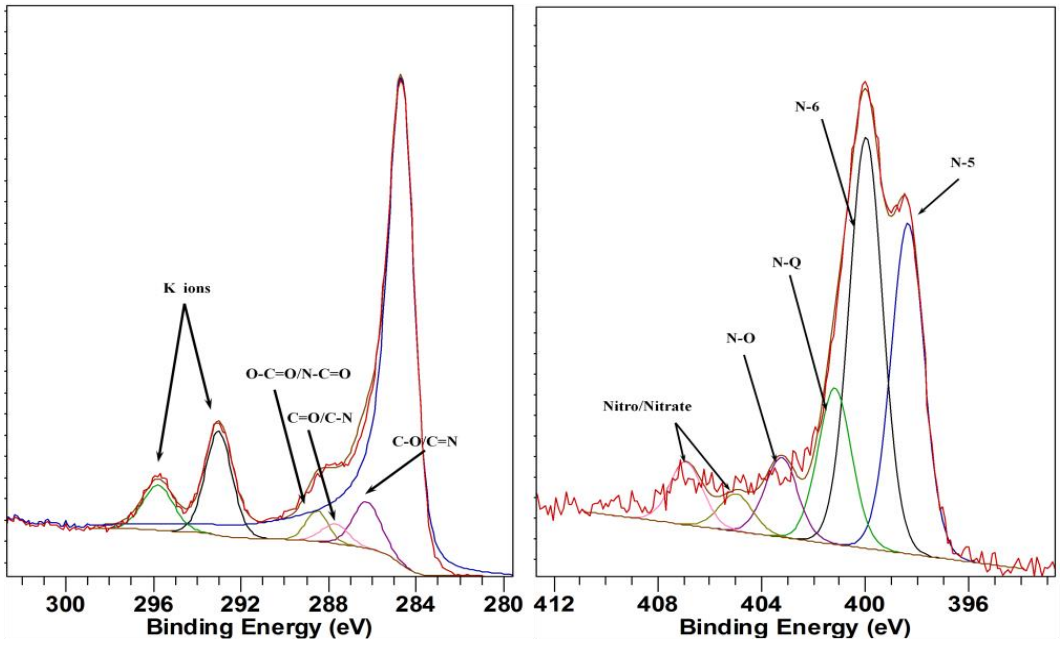
(d)

Figure 6.3 SEM Images of FC7001 (a, c) and of FC7003 (b, d)

6.3.2 Chemical components of the prepared samples

The X-ray photoelectron spectroscopy (XPS) was employed to investigate the surface functional groups of FC based samples prepared under different conditions. The XPS survey spectra presented four distinct peaks that were related to carbon,

potassium, nitrogen and oxygen respectively. The corresponding nitrogen, carbon and potassium containing functional forms of chosen sample FC6001 are shown in Figure 6.4 a-b. The C1s peaks are dominated by C-C bond in the form of diamond or graphite at 284.8 ev. The peaks also show the presence of a small amount of C-O/C=N (286.2ev), C-N/C=O (287.8ev) and O-C=O/N-C=O (289.0ev) (Gu et al., 2013; Liu et al., 2014), which can be attributed to the existence of O and N functional groups. The N1s signal could be deconvoluted into 6 components. The corresponding binding energies of 398.4, 400.1, 401.2 and 403.2ev were ascribed to pyridine-type nitrogen (N-6), pyridonic (N-5), quaternary (N-Q) and N-oxides of pyridinic N-6 (N-O) respectively (Sevilla et al., 2013; Gu et al., 2013; Sethia et al., 2015; Sevilla et al., 2011). In addition, it should also be noticed that there were two kinds of peaks at high binding energy between 405.5 ev and 407 ev existing in all samples, which indicates that the nitrogen is in the form of $-NO_2$ (405.5ev) and $-NO_3$ (407.0ev), likely due to the oxidizing condition (Beard et al., 1990; Zheng et al., 1997; Adenier et al., 2005).



(a) (b)

Figure 6.4 (a) C1s and (b) N1s and spectra for FC6001; (c) the amount of nitrogen containing groups in samples; (d) relative proportion of different nitrogen containing groups in samples (continued)

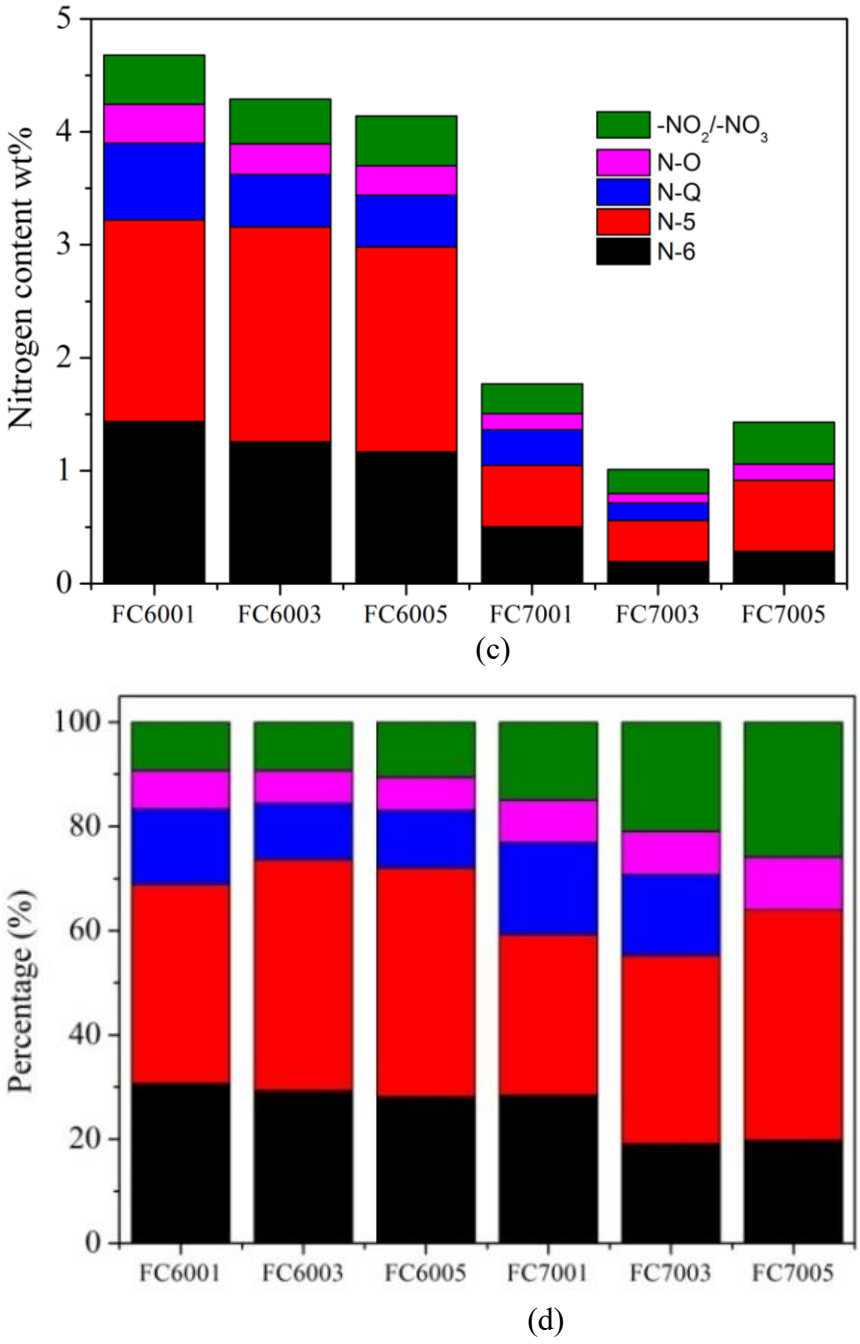
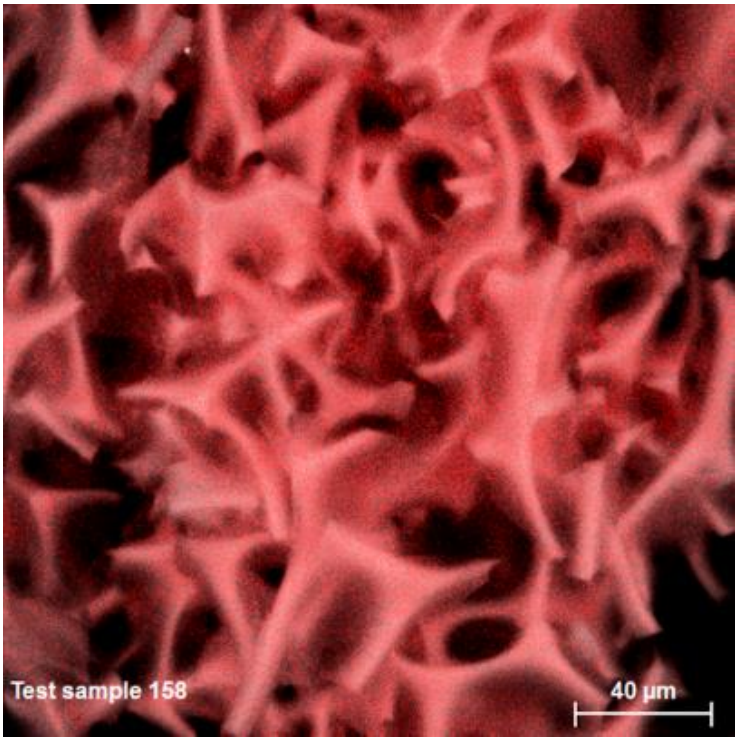


Figure 6.4 (a) C1s and (b) N1s and spectra for FC6001; (c) the amount of nitrogen containing groups in samples; (d) relative proportion of different nitrogen containing groups in samples

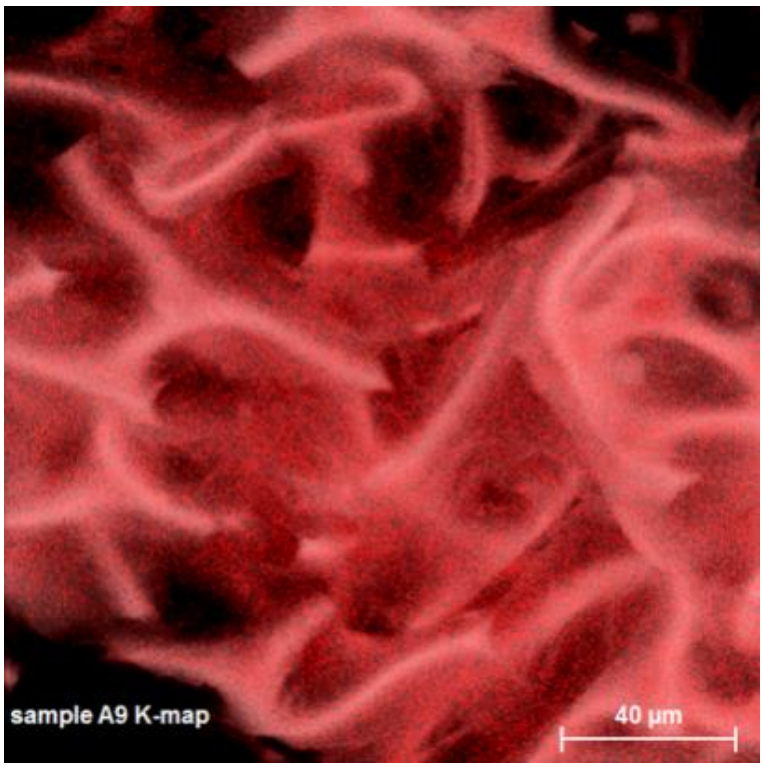
The different N-containing groups were quantitatively characterized by XPS and the results are illustrated in Table 6.1 and Figure 6.4. It can be found that the nitrogen content decreases with the activation temperature and the KOH/FC mass ratio. At 600°C, the nitrogen content decreased noticeably when the mass ratio of KOH/FC was raised from 1 to 5 °C with the change in nitrogen content smaller than 1 wt% (absolute). However, when the activation temperature was increased from

600 °C to 700 °C, the nitrogen content of the samples with the same KOH/FC mass ratio decreased dramatically, from about 4 wt% to below 2 wt%, indicating the poor thermal stability of nitrogen groups (Sevilla et al., 2011) and about 50% of nitrogen groups on the surface decomposed as a result of the temperature increase°C. The results on the analysis of the detailed nitrogen containing groups (Figure 6.4c) reveal the main components after activation are N-5 and N-6. With an increase in the activation temperature, the relative percentages of N-Q and N-O increased, which is in agreement with the finding from Gu et al. (2013), whereas the relative content of N-6 decreased. Figure 5d clearly shows that the relative content of oxidized nitrogen groups increased with an increase in the activation temperature or the KOH/FC mass ratio, which means that more and more nitrogen containing groups were converted into oxidized nitrogen species. The relative weight percentage of nitrogen in oxidized nitrogen groups could reach 30% of the total nitrogen for the sample prepared with KOH/FC mass ratio of 5:1 and activation temperature of 700 °C.

In addition to nitrogen, the peak of potassium was also observed in all samples. Figure 6.4a also shows the K2p spectra of sample FC6001. The K2p spectrum consists of two peaks at binding energies of 293.2 eV and 296.0 eV and their intensity ratio is 2:1, therefore, they are the spin-orbit-split doublet ($K2p_{3/2}$ and $K2p_{1/2}$) of the surface potassium oxides rather than carbonate species (Moulder et al., 1992; Li et al., 2001), which usually have their $K2p_{3/2}$ peak at 292.2 eV (Shchukarev et al., 2004). The surface oxides were formed during activation via the reaction between KOH and carbon materials, remaining in the lattice after water washing. Meanwhile, SEM-EDX element mappings obtained for the sample FC6003 and FC7001 shown in Figure 6.5 revealed the extensive uniform spatial distribution of the intercalated potassium species at microscopic scales.



(a)



(b)

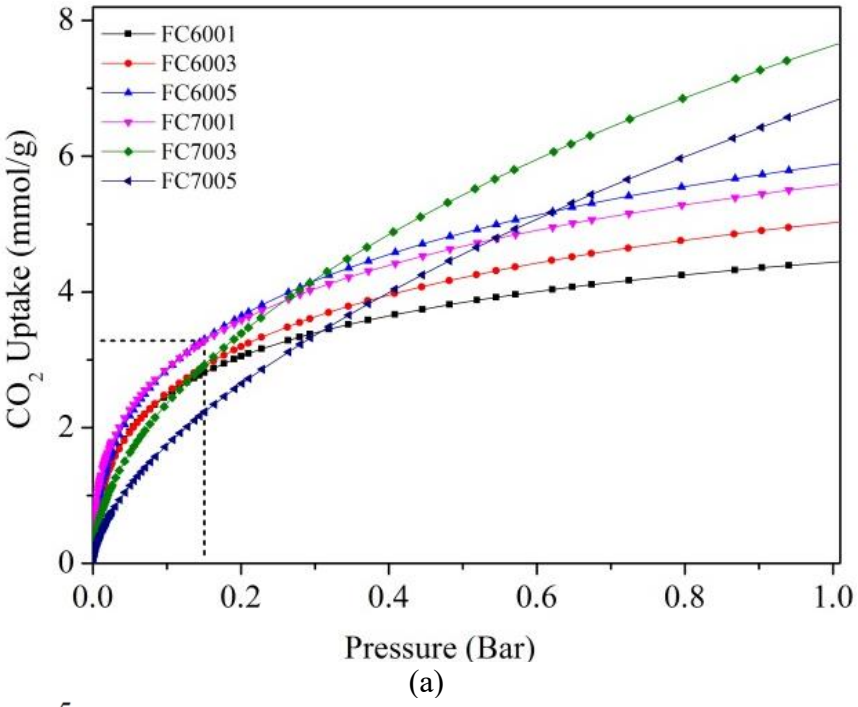
Figure 6.5 K-maps of samples: (a) FC6003 and (b) FC7001

6.3.3 CO_2 capture at low partial pressure

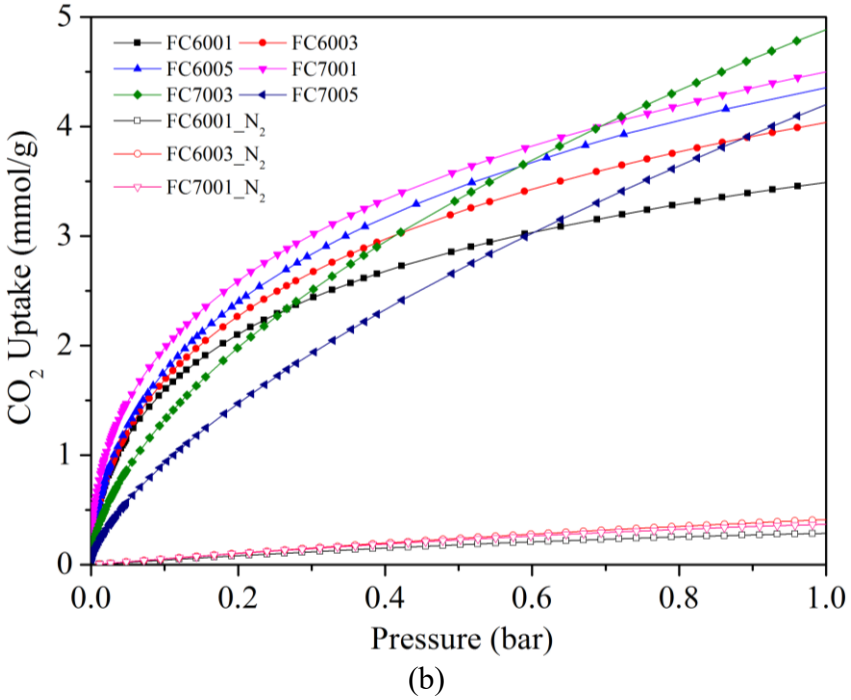
Figure 6.6 illustrated CO_2 adsorption isotherms at 0 ºC and 25 ºC and N_2 isotherms of selected samples at 25 °C. The adsorption capacities of the selected samples at 0.1 bar and 0.15 bar representing the realistic partial pressure of CO_2 in flue gases are presented in Table 6.2. It can be seen that FC7003 achieves a remarkable value of 7.65 mmol/g at 0 °C and 4.90 mmol/g at 25 °C. The heteroatom content of FC7003 was not outstanding when compared with other samples while the ultra-micropore volume was the highest amongst all samples. The uptake of samples at 1 bar generally followed the ranking of ultra-micropore volume, which was consistent with the findings of previous studies that pores smaller than 0.8 nm were preferred at 1 bar to achieve a high uptake (Zhang et al., 2013a; Presser et al., 2011). However, at low CO_2 partial pressures, the trend of CO_2 adsorption capacity was different. Sample FC7001 showed unprecedentedly high uptakes of 1.97 mmol/g (0.10 bar) and 2.30 mmol/g (0.15 bar) at 25 °C. To the best of our knowledge, these represent the highest for porous carbons that have been reported so far and are even higher than many MOFs and zeolites under similar conditions (Samanta et al., 2011; Sumida et al., 2011; Zhang et al., 2014a). The uptake of FC7001 at 0.10 bar was even higher than the uptakes of most of the carbon materials reported at 0.15 bar and 25 °C (Table 2.6). Meanwhile, it can be found that the samples that were activated at 600 °C performed well at low partial pressures, the adsorption capacity at 0.10 bar/0.15 bar increased with the KOH/FC mass ratiomass ratio. Sample FC6005 achieved an uptake of 1.77 mmol/g at 0.10 bar and 2.10 mmol/g at 0.15 bar, which was slightly lower than that of FC7001. However, when the activation temperature reached 700 °C, the adsorption capacity dramatically decreased from 2.30 mmol/g to 1.34 mmol/g at 0.15 bar and 25 °C when the KOH/FC mass ratio was increased from 1:1 to 5:1.

The CO_2 uptake performance of the FC samples especially at low CO_2 partial pressures cannot be fully explained by use of the general textural properties listed in Table 6.1. For instance, sample FC7003, which has the largest ultra-micropore volume at 0.435 cm^3/g, obtained the highest CO_2 uptake amongst all samples at 1 bar 0 °C and 25 °C while the uptake was only 1.68 mmol/g at 0.15 bar and 25 °C,

which is significantly lower than the record high uptake of 2.30 mmol/g obtained with sample FC7001 that has a relatively low ultra-micropore volume of 0.255 cm^3/g. Even sample FC6001 that had the smallest ultra-micropore volume had achieved the adsorption capacity of 1.89 mmol/g. This indicates that the existence of unique PSDs is of special relevance to the CO_2 uptake at low partial pressures.



(a)



(b)

Figure 6.6 CO_2 isotherms of all samples: (a) CO_2 isotherms at 0 °C;(b) CO_2 and N_2 isotherms of selected samples at 25 °C

Table 6.2 CO_2 adsorption capacity and selectivity of selected samples at low CO_2 partial pressure

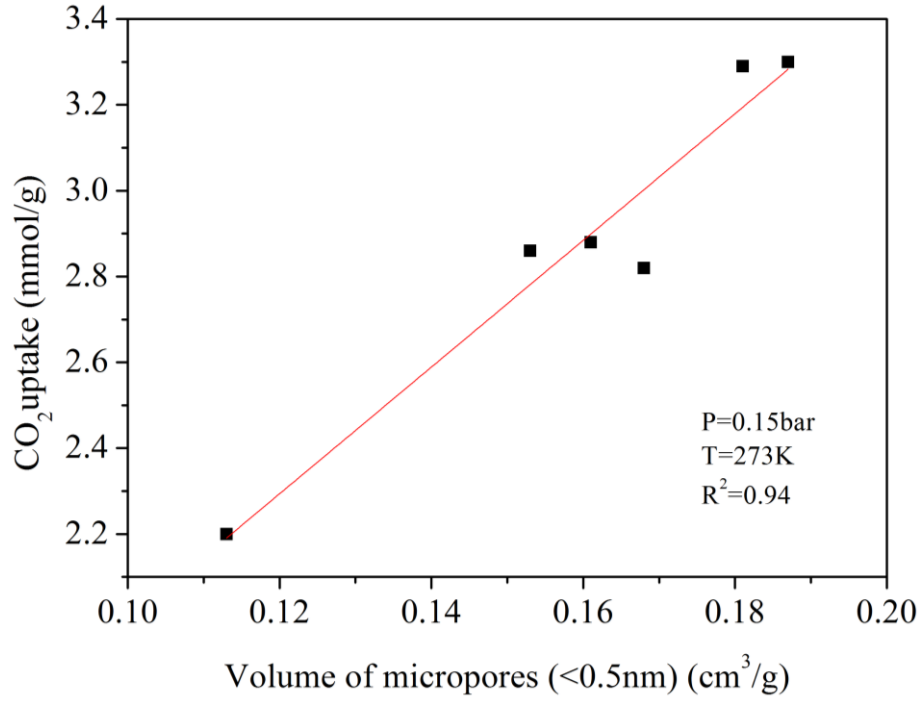
Sample	CO_2 uptake at 25ºC (mmol/g)		Selectivity CO_2/ N_2 (ISAT)		Initial slope ratios
	0.10 bar	0.15 bar	10/90	15/85	
FC6001	1.60	1.89	57	44	200
FC6003	1.69	2.02	43	34	152
FC7001	1.97	2.30	51	39	169

6.3.3.1 The role of textual and surface chemical properties on CO_2 adsorption

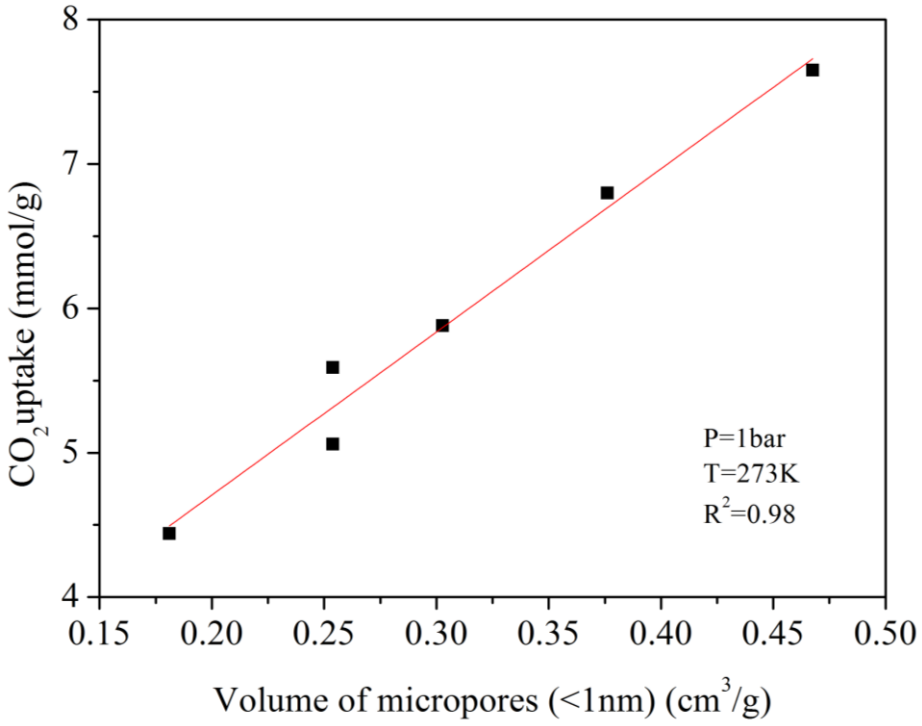
The correlations between CO_2 adsorption capacity at 0.15 bar and 1 bar for FC carbons and the volume of pores smaller than a specific pore size were illustrated in Figure 6.7. It can be observed that CO_2 uptakes at 1 bar and 0 °C was almost linear with the volume of micropores smaller than 1 nm, with a high correlation coefficient (R^2) of 0.98. This unique pore size decreased to 0.5 nm as the particle pressure decreased to 0.15 bar (R^2=0.94). Similar linear relationships were also obtained at 25 °C: CO_2 uptakes at 0.15 bar and 1 bar gave the best correlation with the volume of micropores smaller than 0.44 nm (R^2=0.96) and 0.60 nm (R^2=0.98) respectively. It is well known that the ultra-micropores strengthen the adsorption potential due to the superposition of the stronger Van der Waals force produced by the adjacent walls of ultra-micropores while the adsorption potential is inversely proportional to pore radius and decreases with the pore width (Everett, et al., 1976). Adsorption at a higher temperature or lower CO_2 partial pressure, needs a stronger interaction force and hence the unique pore size becomes much smaller in order to provide a sufficient force to keep the CO_2 molecules in the pores (Wickramaratne et al., 2013a; Zhang et al., 2013; Presser et al., 2011; Ashourirad et al., 2016; Sevilla et al., 2013).

As reported by previous studies, some carbon materials had similar or even higher ultra-microporosity but their uptakes were only about 1.3-1.5 mmol/g at 0.15 bar and 25 °C (Sevilla et al., 2011a; Yang et al., 2015; Wei et al., 2012). Although ultra-

microporosity played a key role in CO_2 adsorption, it cannot solely rationalize the extraordinary CO_2 uptakes of the FC carbons observed with this study, especially at low partial pressures which reached 1.97 mmol/g at 0.10 bar and 25 °C and 2.30 mmol/g at 0.15 bar and 25 °C. The existence of surface heteroatom groups might have contributed to the adsorption, especially at low partial pressures. The existence of the surface heteroatom-containing groups changed the electrostatics of the surface which could enhance the affinity to CO_2. The effects of the sample nitrogen and potassium contents on the adsorption content are shown in Figure 8. Apparently, there is no direct relationship between the CO_2 adsorption capacity and the nitrogen content or different nitrogen containing groups ($R^2 = 0.30$). This indicates that the nitrogen content is not a critical factor to enhance the CO_2 uptake for FC samples, and this agrees with the experimental results reported by Zhang et al. (2013) and the simulation results of Kumar et al. (2015) in that N-doping can only marginally improve the single component adsorption of CO_2. In addition to the nitrogen containing groups, there is potassium in the form of surface potassium oxides groups evenly distributed on the surface, which has been proved by the XPS and EDX results. As can been seen from Figure 6.7f, there was almost linear relationship between the CO_2 uptake at 25 °C and 0.15 bar and the potassium content on the surface, indicating the significant improvement of CO_2 adsorption is at least partly attributed to the potassium ions exposed on the surface that acted like extra-framework cations in MOFs and zeolites (Pirngruber et al., 2010; Pulido et al., 2009; Valenzano et al., 2010). Detailed study on the role of potassium on CO_2 capture had been investigated with our previous studies (Liu et al., 2015).

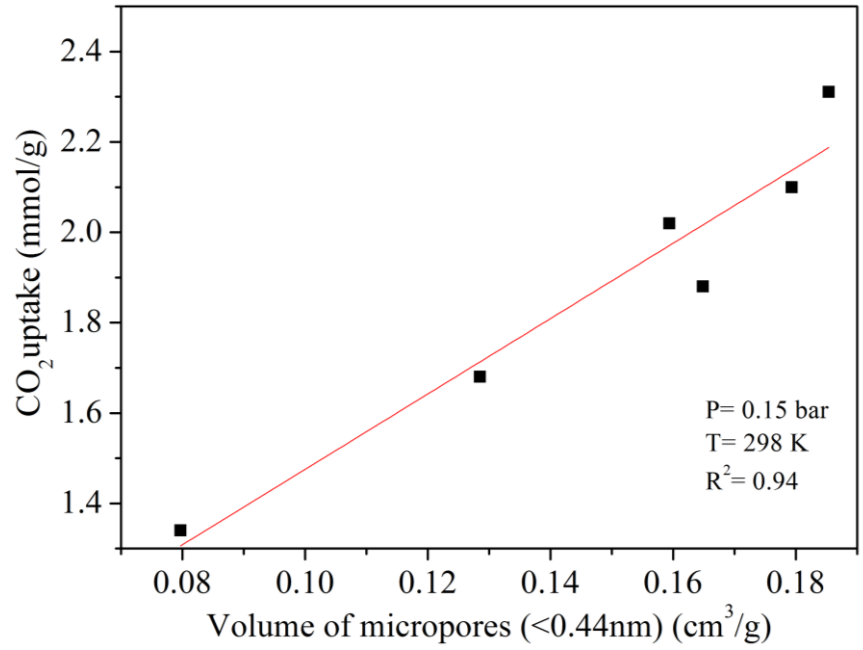


(a)

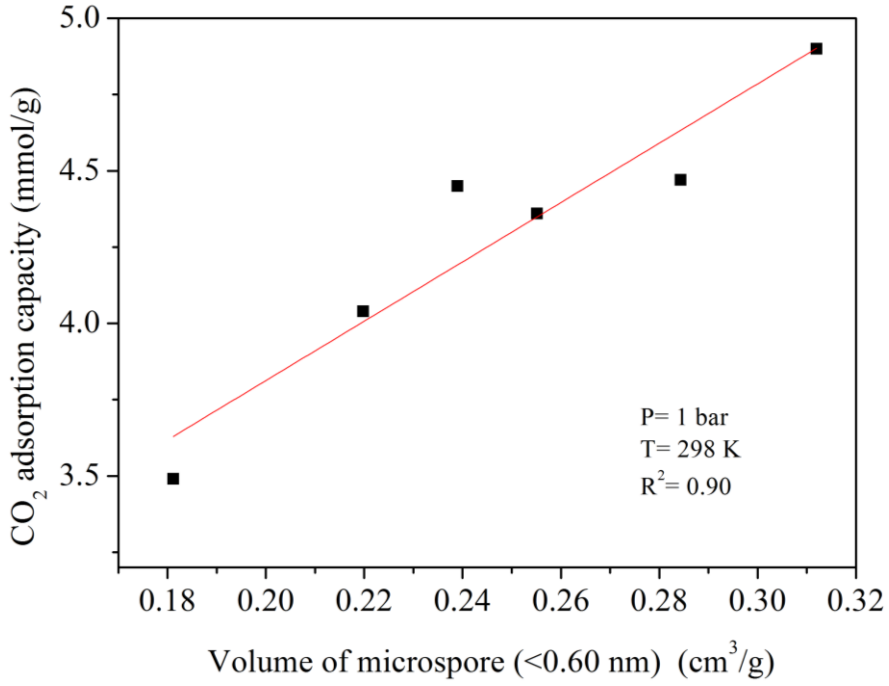


(b)

Figure 6.7 The relationship between CO_2 adsorption capacity at 25 °C and 0.15 bar and different parameters: (a)-(d) micropore volume of pores smaller than certain pore size and heteroatom content (e) nitrogen content; (f) potassium content (continued)

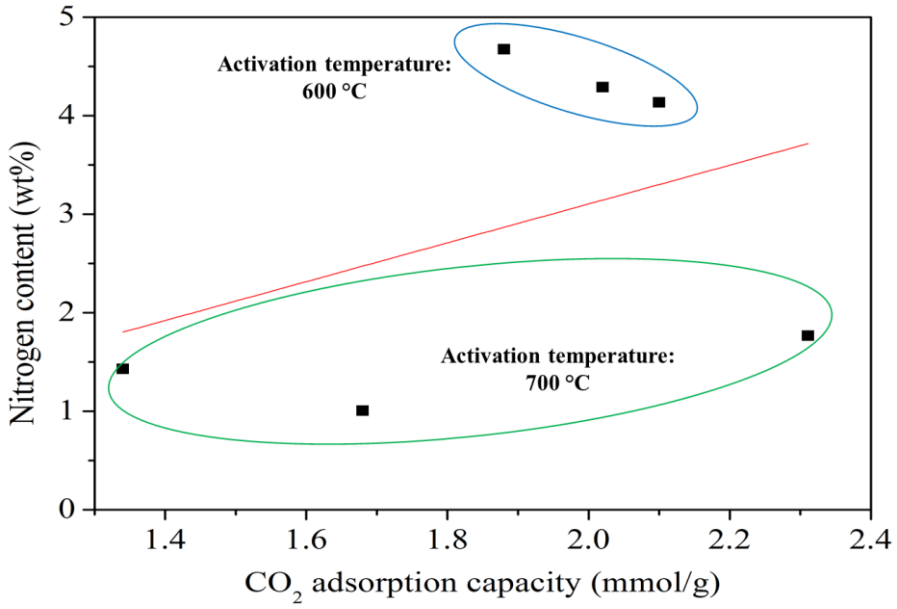


(c)

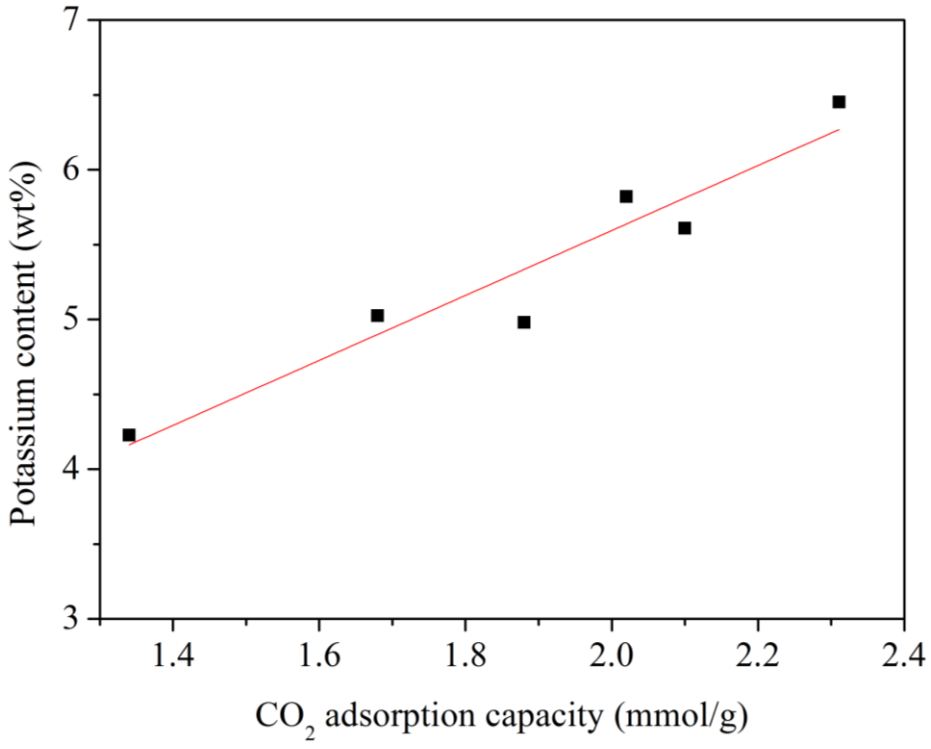


(d)

Figure 6.7 The relationship between CO_2 adsorption capacity at 25 °C and 0.15 bar and different parameters: (a)-(d) micropore volume of pores smaller than certain pore size and heteroatom content (e) nitrogen content; (f) potassium content (continued)



(e)



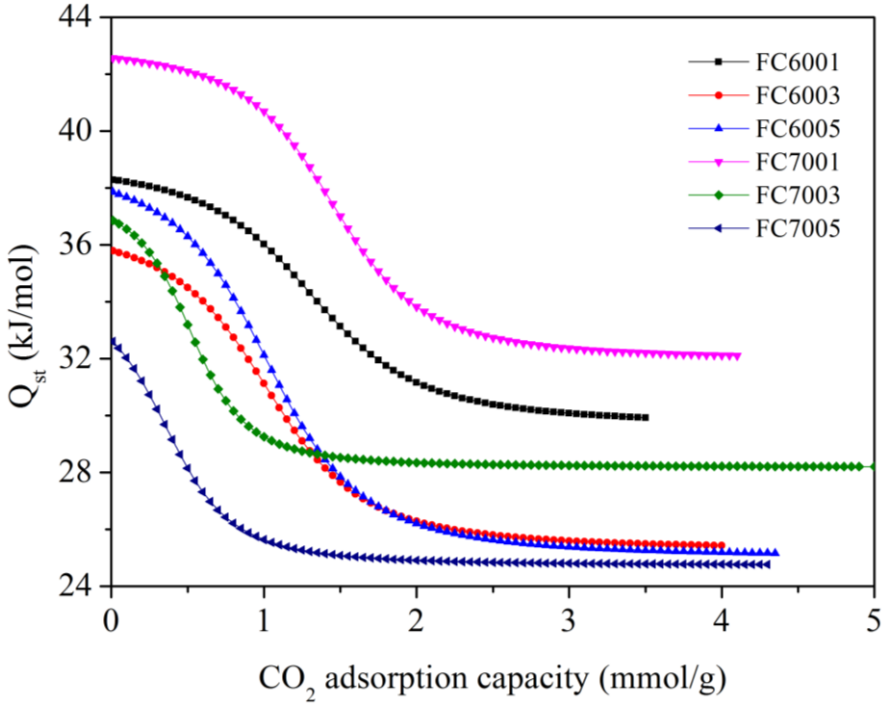
(f)

Figure 6.7 The relationship between CO_2 adsorption capacity at 25 °C and 0.15 bar and different parameters: (a)-(d) micropore volume of pores smaller than certain pore size and heteroatom content (e) nitrogen content; (f) potassium content

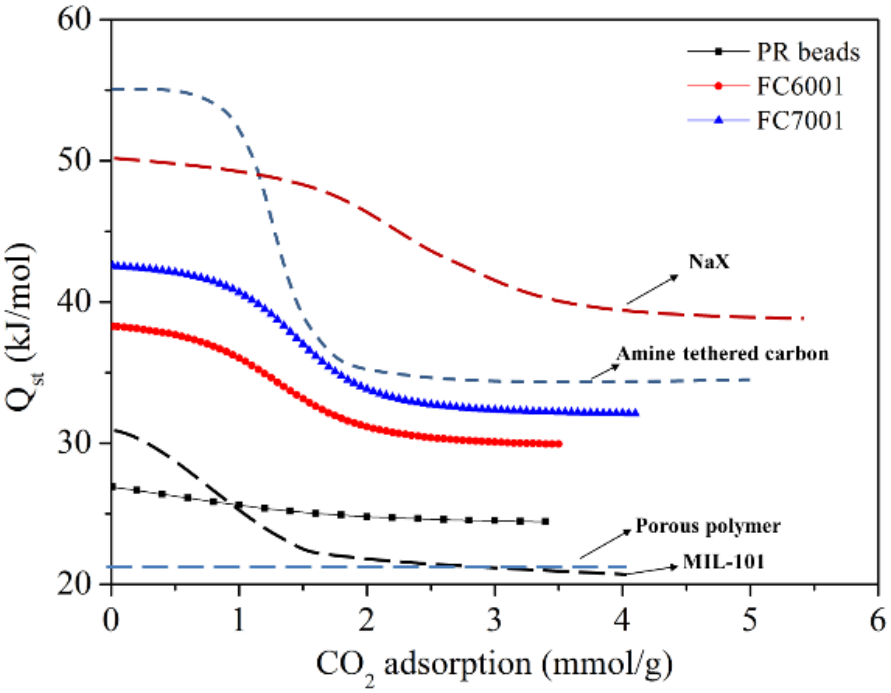
In order to better understand the interaction strength between CO_2 and the carbon surface, the isosteric heats (Q_{st}) of CO_2 adsorption on FC carbons were calculated

from the CO_2 adsorption isotherms measured at 0 and 25 °C via the Clausius-Clapeyron equation. In this work, considering the heterogeneity of surface caused by surface potassium intercalation, the dual-site Langmuir equation was used to fit the adsorption isotherms of FC carbons. The plots of Q_{st} values as a function of CO_2 adsorption capacity for all FC carbons are presented in Figure 6.8a. The initial Q_{st} values for the carbons at a CO_2 uptake level of 0.01 mmol/g vary within the range of 32-43 kJ/mol, which are higher than those of most activated carbon adsorbents, porous polymers and even some MOFs such as MIL-101 (Xiang et al., 2012) and the amine/carbon(Lu et al., 2012) samples shown in Figure 6.8b. Sample FC7001 has the highest Q_{st} values, which range from 43 to 36 kJ/mol at CO_2 loading of 0.01-2.1 mmol/g (uptakes at 0.15bar), indicating the existence of strong interaction force between CO_2 and the adsorbent. The reported initial Q_{st} values of porous carbon materials without surface modification are generally smaller than 30 kJ/mol such as phenolic resin (PR) beads (26 kJ/mol) (Liu et al., 2015), porous polymer (20 kJ/mol) (Lu et al., 2012) and PAF-1-450 (27.8 kJ/mol) (Ben et al., 2012). As shown in Figure 6.9, the initial Q_{st} values increase with the potassium content on the surface while there is no clear relationship between the nitrogen content and the initial Q_{st}.

Similar to the Q_{st} curves of the various samples from the references in Figure 6.8b, the Q_{st} curves of our FC samples especially FC7001 and FC6001 over the whole range of CO_2 adsorption capacity can also be generally divided into three stages: being kept at a high Q_{st} value at CO_2 loading up to 1 mmol/g, gradually decreasing and then becoming constant. These trends are similar to those of NaX (Bae et al., 2013), amine tethered carbon (Lu et al., 2012) and MIL-101 (Xiang et al., 2012) that had extra framework ions or $–NH_2$ amine groups on the surface, indicating the existence of strong surface affinity that was quite similar to the extra framework ions in zeolites/MOFs or amine groups with strong basicity on carbon.



(a)



(b)

Figure 6.8 (a) Isosteric heat of CO_2 adsorption on FC samples calculated from the adsorption isotherms at 0 and 25 °C; (b) isosteric heat of CO_2 adsorption on different porous materials from references: amine tethered carbon & porous carbon (Lu et al., 2012); NaX (Bae et al., 2013); MIL-101 (Xiang et al., 2012).

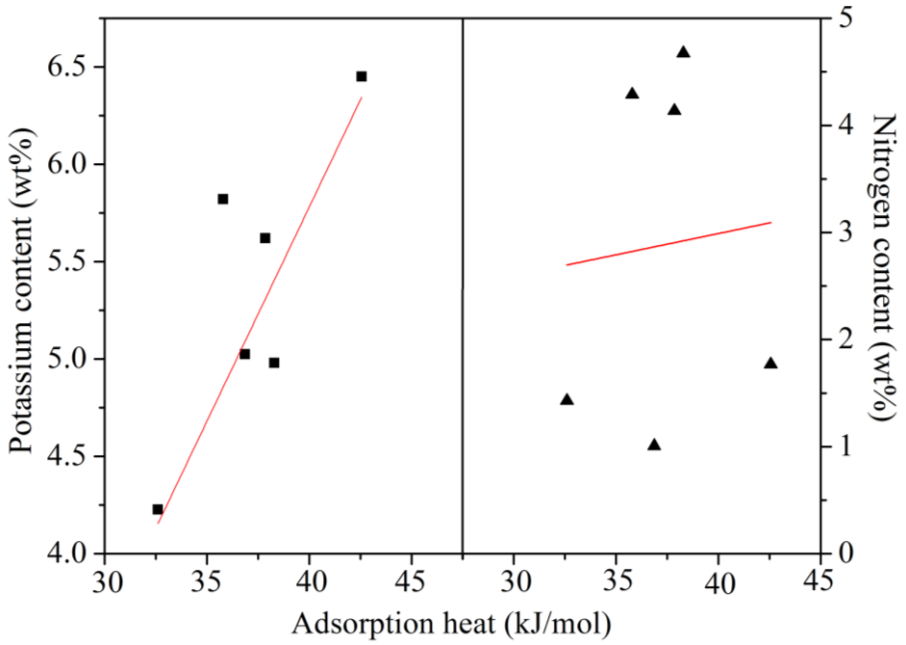


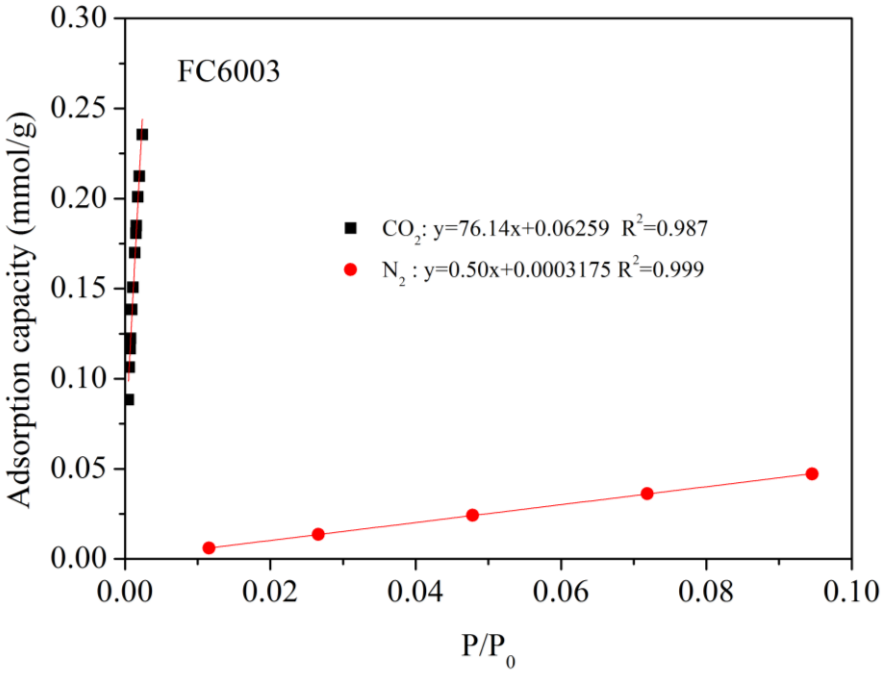
Figure 6.9 the relationship between initial Q_{st} and potassium and nitrogen content

6.3.3.2 Selectivity and stability

To be a good candidate of sorbent for CO_2 capture from flue gases, the sorbent must have high selectivity and stability. The selectivity of selected FC samples was calculated by means of the initial slope method (Hao et al., 2011; Chandra et al., 2012) and the ideal adsorption solution theory (IAST) method (Lu et al., 2011; Babarao et al., 2009; Zhao et al., 2012) and the results are listed in Table 6.2. Based on the initial slope method, the CO_2/N_2 selectivity of FC 6001, FC6003 and FC7001 was found to be 200, 152, 169 at 298K, respectively (Figure 6.10). These selectivity values are higher than all kinds of porous carbons reported, indicating the existence of strong affinity to CO_2 on surface. The IAST selectivity of CO_2/N_2 in 10/90 and 15/85 mixture gases was also calculated. Sample FC6001 had the highest selectivity of 57 and 44 for 10/90 and 15/85 mixture gases at the total pressure of 1 bar respectively, followed by FC 7001 and FC6003, showing the same trend observed with the initial slop method. The difference in the value of selectivity between two methods can be attributed to the adsorption site heterogeneity.

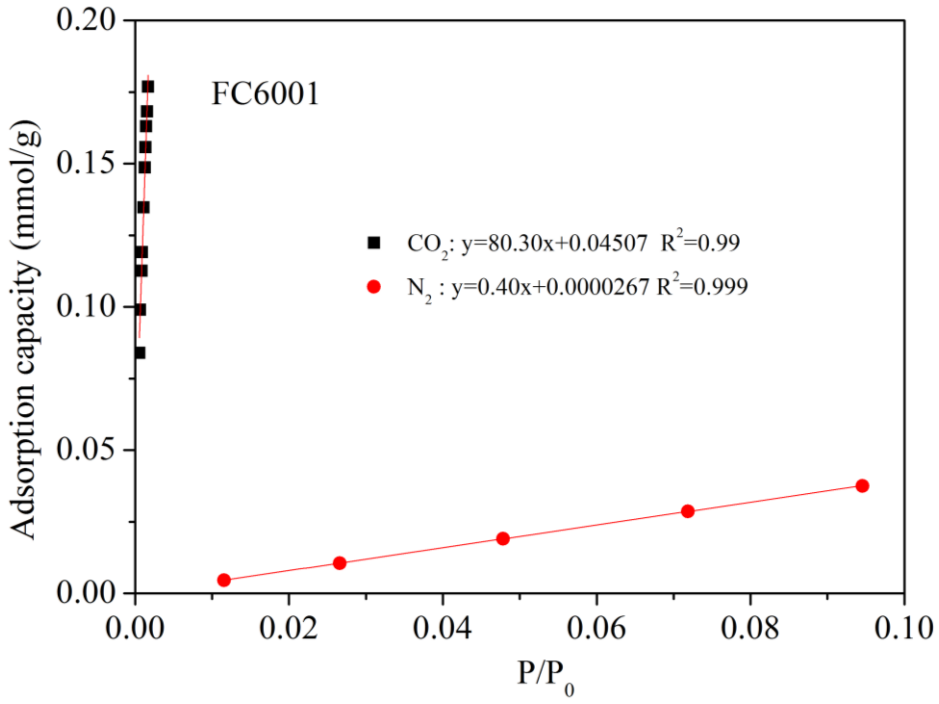
As reported by some previous researchers, the heteroatom containing groups especially N-rich groups were considered as the key contributor to high CO_2

selectivity but the existence of small ultra-micropores was counterproductive due to the adsorption of nitrogen (Patel et al., 2013; Ashourirad et al., 2016). However, in this work, we found that the pore structure or the fraction of ultra-micropores rather than heteroatom containing groups on surface determined the selectivity of samples. There was no clear relationship between the potassium content/nitrogen content and the selectivity but a strong linear relationship (R^2>0.94) between the fraction of micropore volume (<0.50 nm) and selectivity is found as shown in Figure 6.10. Within the ultra-micropores smaller than 0.5 nm, the interaction force between CO_2 and pores were significant enhanced while only marginally contributed to nitrogen adsorption that had larger dynamic diameter (To et al., 2016). For sample FC6001, most of the pores were smaller than 0.5 nm and hence it had the highest selectivity.

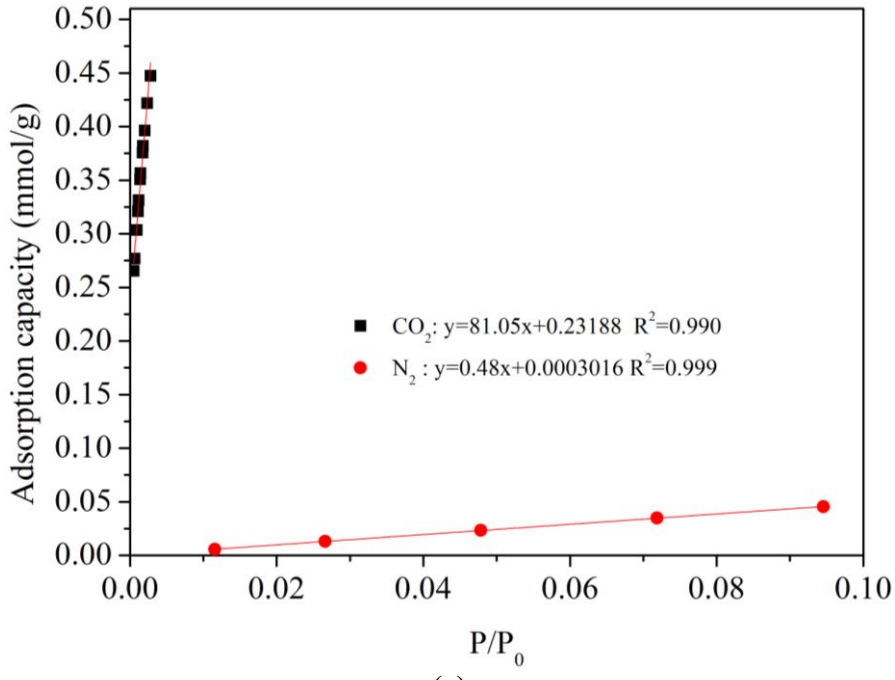


(a)

Figure 6.10 CO_2/N_2 adsorption selectivity at 298 K based on initial slope method: (a) FC6003; (b)FC6001; (c) FC7001; (d) the relationship between CO_2/N_2 selectivity calculated by IS method and fraction of ultra-micropore volume (<0.5 nm), potassium content and nitrogen content (continued)

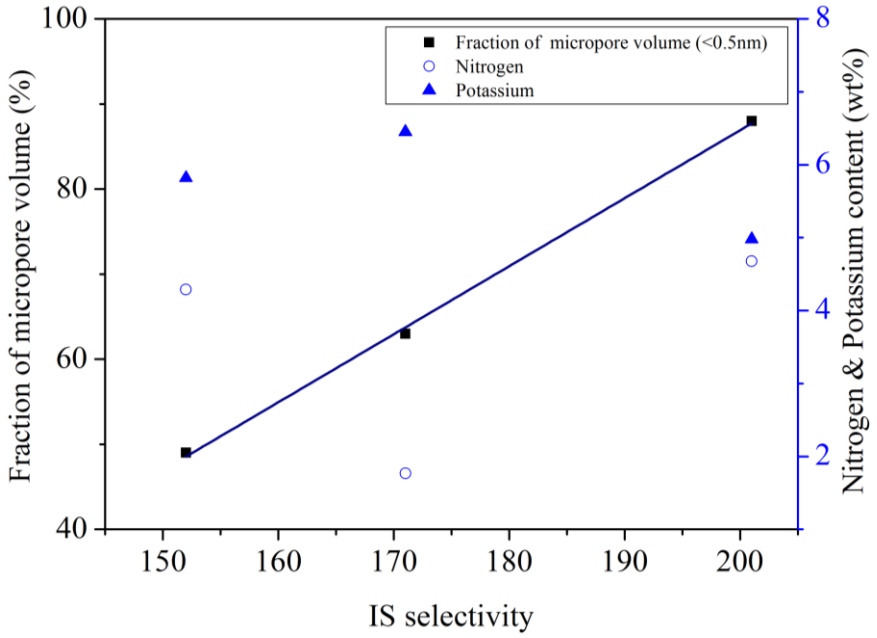


(b)



(c)

Figure 6.10 CO_2/N_2 adsorption selectivity at 298 K based on initial slope method: (a) FC6003; (b)FC6001; (c) FC7001; (d) the relationship between CO2/N2 selectivity calculated by IS method and fraction of ultra-micropore volume (<0.5 nm), potassium content and nitrogen content (continued)



(d)

Figure 6.10 CO_2/N_2 adsorption selectivity at 298 K based on initial slope method: (a) FC6003; (b)FC6001; (c) FC7001; (d) the relationship between CO_2/N_2 selectivity calculated by IS method and fraction of ultra-micropore volume (<0.5 nm), potassium content and nitrogen content

In addition to high selectivity, the FC samples of this study have showed fast adsorption kinetics and good stability during cyclic tests (Figure 6.11), indicating their great potential for practical applications. CO_2 adsorption tests with all FC samples and the multicycle (up to 50 cycles) of adsorption-desorption tests with the selected samples (FC6001 and FC7001) were conducted with TGA under the simulated flue-gas conditions (15% CO_2/85% N_2, 25 °C). As it can be seen from Figure 11a, CO_2 was quickly adsorbed by both samples and reached the equilibrium capacity within 10min. In addition, the adsorption capacity had already exceeded 90% of the equilibrium capacity in the first 3min and the activation temperature or the potassium content in samples had little effect on the adsorption kinetics. Figure 6.11b shows the results of the multi-cycle tests of the best two samples FC6005 and FC7001. The adsorption was conducted in 15% CO_2/85% N_2 at 25 °C while desorption was conducted in pure nitrogen at 120 °C. It can be found that both samples were quite stable, especially sample FC6005, with adsorption capacity remaining almost constant during the 50 cycles.

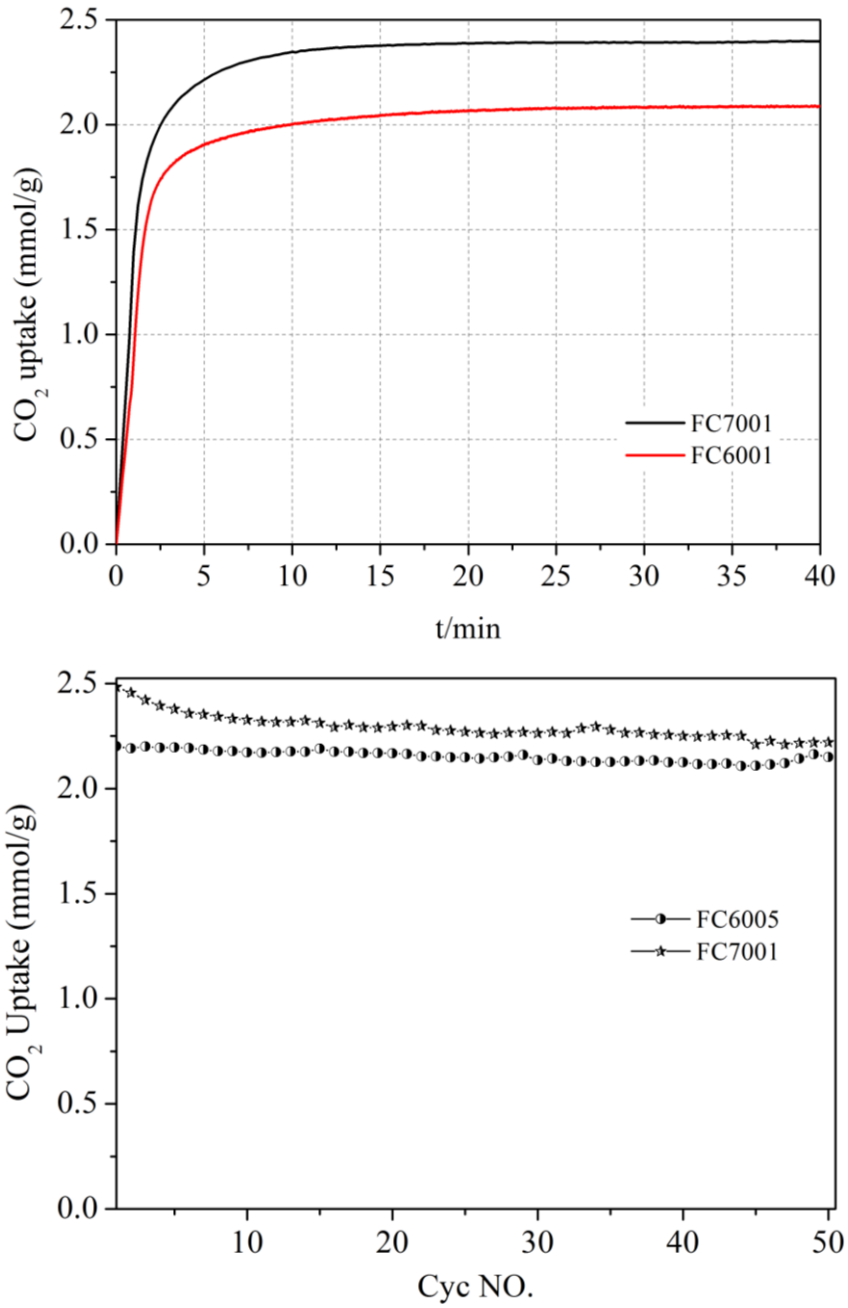


Figure 6.11 CO_2 adsorption curve and cyclic performance of selected samples (flue gases: 15% CO_2 + 85% N_2; adsorption temperature: 25°C; desorption temperature: 120°C)

6.4 Conclusions

In conclusion, we have demonstrated a novel ultra-microporous carbon foam successfully prepared by a facile, reproducible one-step carbonization and KOH

activation of polyisocyanurate. The synthesized FC carbons showed exceedingly high level of ultra-microporosity and unique surface chemistry for CO_2 adsorption. The resulting ultra-microporous carbon samples achieved a record high CO_2 uptake at 25 °C and 0.15 bar and record-high CO_2/N_2 selectivity compared with those of porous carbon materials reported so far and most MOFs. Ultra-microporosity and potassium intercalation play key roles in CO_2 adsorption at low partial pressures while no direct relationship between nitrogen containing groups and CO_2 adsorption capacity can be observed. In addition, the introduction of surface potassium containing groups has enhanced the surface affinity to CO_2, resulting in a high isosteric heat of adsorption of FC carbons while the pore structure or the fraction of ultra-micropore volume (<0.50 nm) rather than surface chemistry has a significant effect on CO_2/N_2 selectivity at 25 °C.

Chapter 7 Ultra-microporous K doped carbons with exceedingly high adsorption capacity at flue gas conditions

7.1 Introduction

The temperature of flue gas from a coal-fired power plant is about 40-50 °C, it is impractical to further cool the flue gas to room temperature. So, the performance of carbons at 40-50 °C and 0.15 bar is crucial when determining their potential for industrial applications. As reported in former chapter, the polyisocyanurate derived carbons have record high CO_2 adsorption capacity at 25 °C and 0.15bar. Therefore, in this chapter, the adsorption performance of polyisocyanurate derived carbons at 40-50 °C were studied. Meanwhile, as shown in Chapter 5, pre-compaction was beneficial to increase their adsorption capacity and CO_2/N_2 selectivity at low partial pressure, so pre-compaction was also used to prepare polyisocyanurate derived carbons.

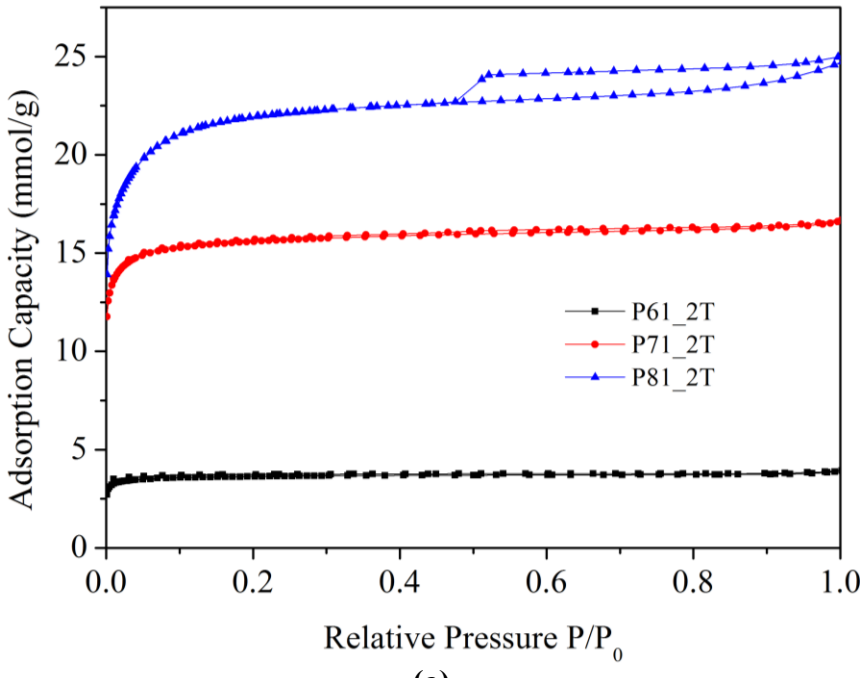
7.2 Experimental Procedure

Polyisocyanurate was pre-oxidized in horizontal tube furnace at 260 °C for 6 hours in 50 ml/min air flow. The sample obtained after oxidation was then mixed with 20 ml KOH solution (KOH/polyisocyanurate weight ratio was equal to 1) and left overnight, then all samples were dried in an oven at 105 °C. After that, the dried samples were compressed into pellets with a diameter of 13 mm under different loads, 2 tons, 5 tons and 10 tons, respectively. The pellet was then heated in a horizontal tube furnace from ambient to a pre-selected temperature at a rate of 5 °C/min under the protection of N_2 flow and maintained at the selected temperature for an hour. The activated samples were then washed with DI water until the pH value became about 7. The samples were labelled in the form of Pxyz, where x, y, and z represent the activation temperature, the KOH/AC mass ratio and load.

All CO_2 adsorption test were carried out on a thermo gravimetric analyzer (TGA, Q500, TA instruments). The CO_2 adsorption capacity as a function of temperature was tested as follows: the sample was first degassed at 150 ºC for 30 min in N_2 before cooling down to 25 °C, and then the simulated flue gas (15%/85% CO_2/N_2) was introduced into the sample chamber with a flow of 100 ml/min. The sample was slowly heated up to 120 °C with a heating rate of 0.5 °C/min. CO_2 adsorption kinetics at 40 °C was measured by the same degas and adsorption procedure. Once the adsorption reached equilibrium at the selected temperature, the sample was heated up to 150 °C for 10 min in N_2 for desorption. Up to 50 adsorption-desorption cycles were performed to test the stability and cyclability of the sample. A TG-DSC instrument (Setaram SENSYS evo) was used to measure the adsorption heat.

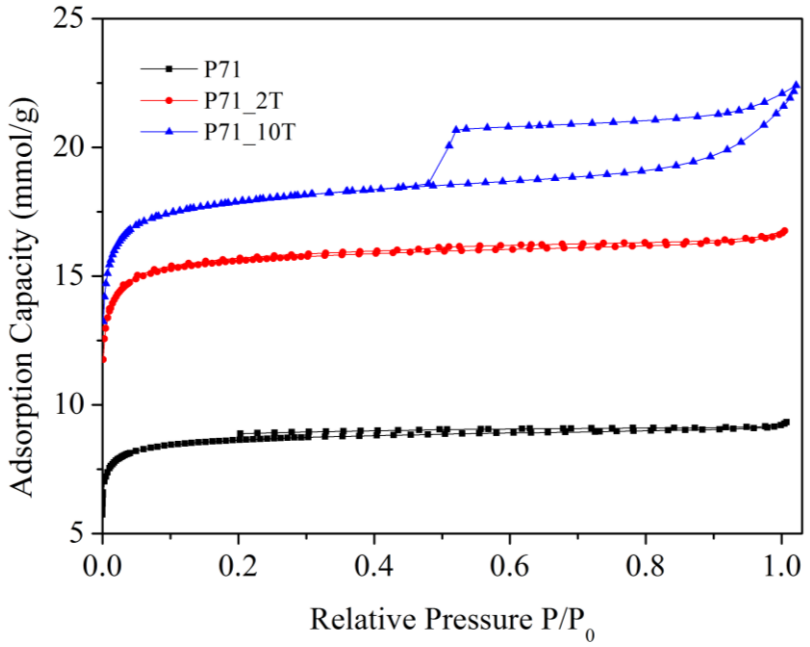
7.3 Results and discussions

7.3.1 Textual properties



(a)

Figure 7.1 N_2 adsorption isotherms obtained at -196 °C: (a) samples prepared with 2 tons compaction load at different temperatures; (b) samples prepared with different compaction load at 700 °C (continued)



(b)

Figure 7.1 N_2 adsorption isotherms obtained at -196 °C: (a) samples prepared with 2 tons compaction load at different temperatures; (b) samples prepared with different compaction load at 700 °C

The nitrogen isotherms of all samples analysed at 77 K are shown in Figure 7.1. It can be seen that the samples prepared at 600-700 °C with a compaction load 2-5 ton, present type I isotherm behaviour, with significant nitrogen adsorption capacity at relative pressure P/P0<0.1, indicating a micropores domain nature. However, when the temperature is increased to 800 °C or the compaction load is 10 tons, an obvious hysteresis loop at a relative pressure P/P0>0.4 appears, indicating the presence of mesopores. Meanwhile, it can be found that the isotherms of sample P71_10T and P81_2T showed type H4 isotherm, indicating the mesopores in the samples were narrow slit-like pores (Sing, 1985).

The textural structure parameters of all samples including BET surface area, total pore volume, micropore volume and narrow micropore volume that can be calculated by the combination of N_2 isotherm and CO_2 isotherms at 0 °C are summarized in Table 7.1. It can be observed that the pressed samples prepared at 600-800 °C have a surface area ranging from 328 to 1906 m^2/g and total pore volume ranging from 0.124 to 0.797 cm^3/g. With the increase of activation temperature, the surface area, total pore volume and micropore volume increased, indicating an enhanced activation effect. At a given temperature 700 °C, it can be

found that compaction is beneficial to porosity development, surface area, pore volume and micropore volume, as they all increased as the compaction load increased from 0 tons to 10 tons. Clearly, the carbon samples prepared by KOH activation are microporous, with the microporosity accounting for 80-100% of total pore volume. The samples, as shown in Figure 7.2, were found to consist of micropores with pore size centered at 0.38 nm, 0.53 nm and 1.2 nm. With the increase of activation temperature and compaction pressure, the ultra-micropore volume increased from 0.254 to 0.407cm^3/g, while the ultra-micropore volume as a fraction of micropore volume decreased, which is attributed to the formation of increasingly larger micropores with broader size distribution. Mesoporosity emerged at a temperature of 800 °C and a compaction load 10 tons. In comparison, sample P61_2T had a low surface area only 328m^2/g, but 100% of the total pores are ultra-micropores and centered at 0.38 nm, which mean this sample could be considered as a high quality ultra-microporous molecular sieve.

Table 7.1 Specific surface areas and pore structures of polymer derived carbons

Sample	S_{BET} (m^2/g)	V_{total} (cm^3/g)	V_{micro} (cm^3/g)	$V_{micro<0.7nm}$ (cm^3/g)	XPS	
					N (wt%)	K (wt%)
P61_2T	328	0.124	0.124	0.124	3.10	4.08
P71	773	0.298	0.282	0.255	12.87	1.77
P71_2T	1407	0.535	0.511	0.378	1.36	4.01
P71_5T	1392	0.540	0.498	0.372	0.6	4.42
P71_10T	1606	0.715	0.572	0.407	1	2.18
P81_2T	1906	0.797	0.702	0.342	0.35	10.09
P81_5T	1514	0.622	0.557	0.297	0.23	9.06

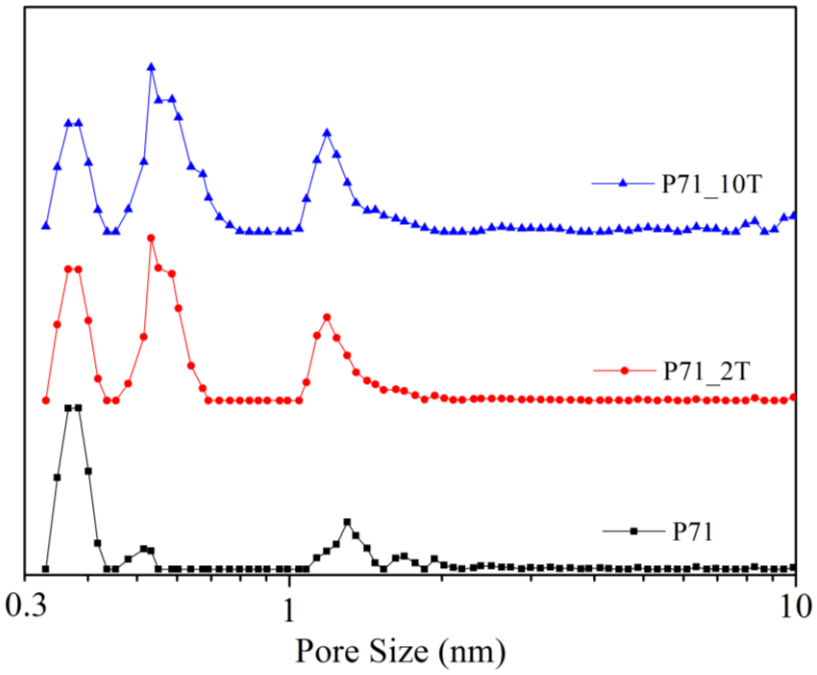
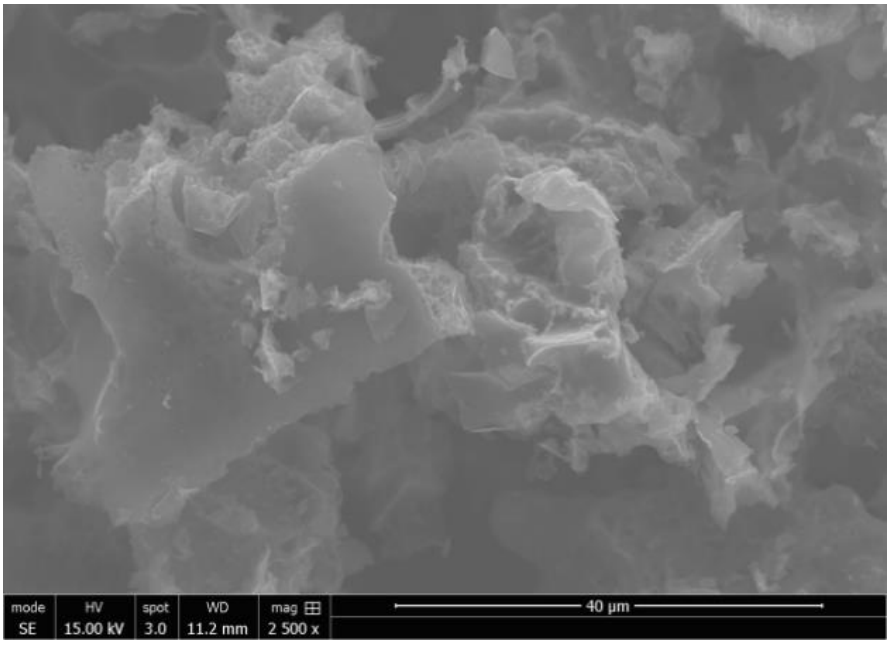
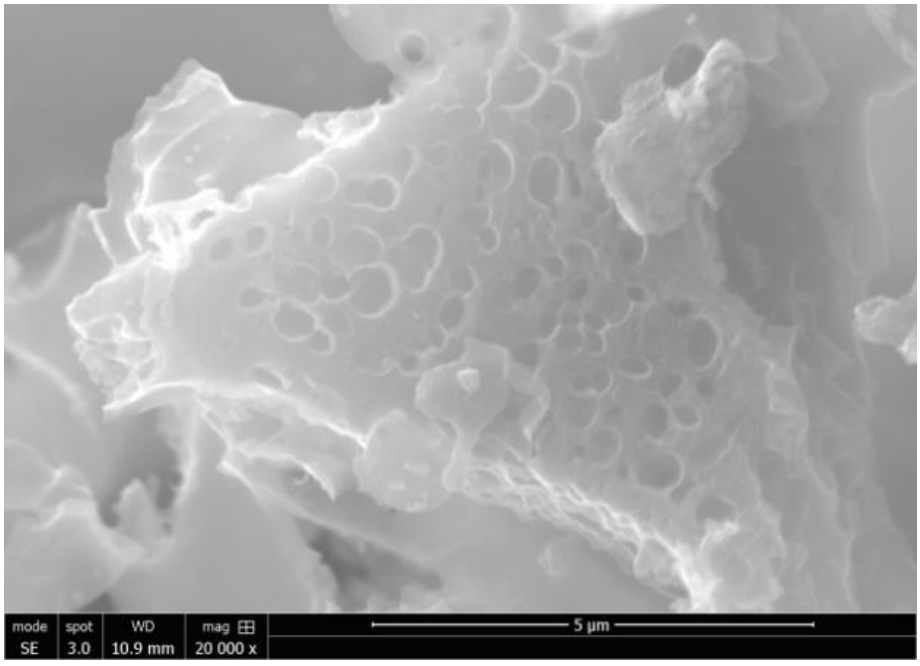


Figure 7.2 NLDFT pore size distributions for the samples prepared at 700 °C with different compaction loads

The morphology of prepared samples was analysed by scanning electron microscopy (SEM). Before analysis, the sample with a regular shape after activation was cracked into a powder. As shown in Figure 7.3 a-b, the granular particles had cheese-like pore structures with plenty of macropores. The transmission electron microscopy images of sample P71_2T mainly shows the disordered slit-shaped micropores randomly distributed in the structures (see Figure 7.4). The worm-like interlocked micropores is attributed to the stacking of curved graphene layers. So, activated samples with pre-compaction showed a kind of macro-micropore hierarchical structure, which is beneficial for CO_2 diffusion and adsorption.

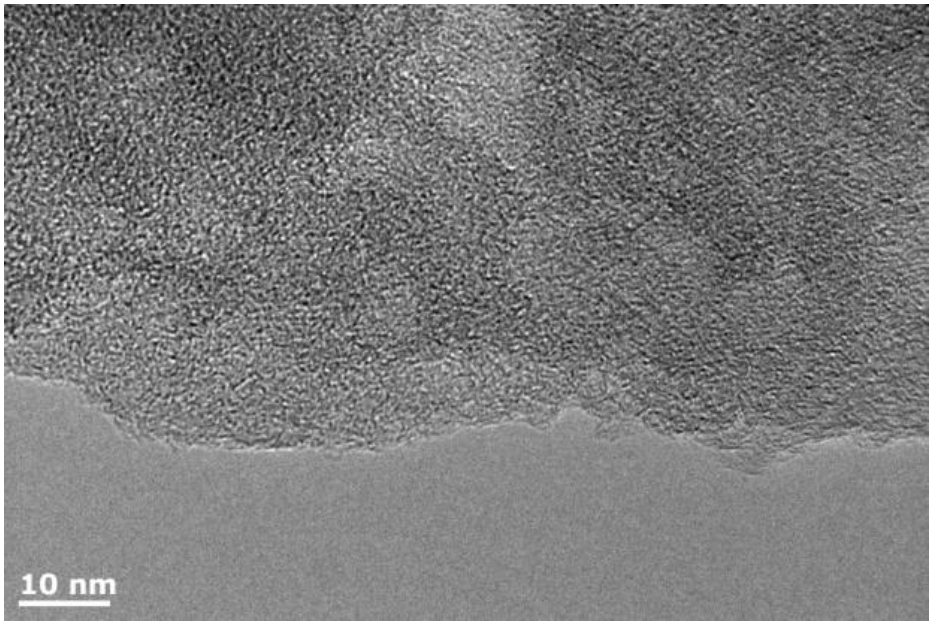


(a)

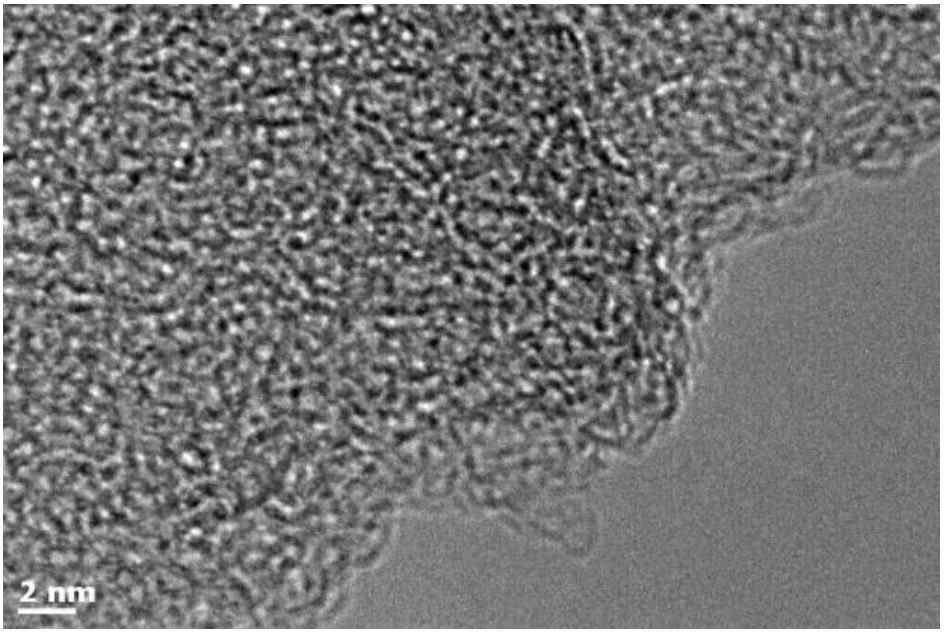


(b)

Figure 7.3 SEM images of sample P71_2T (a)-(b)



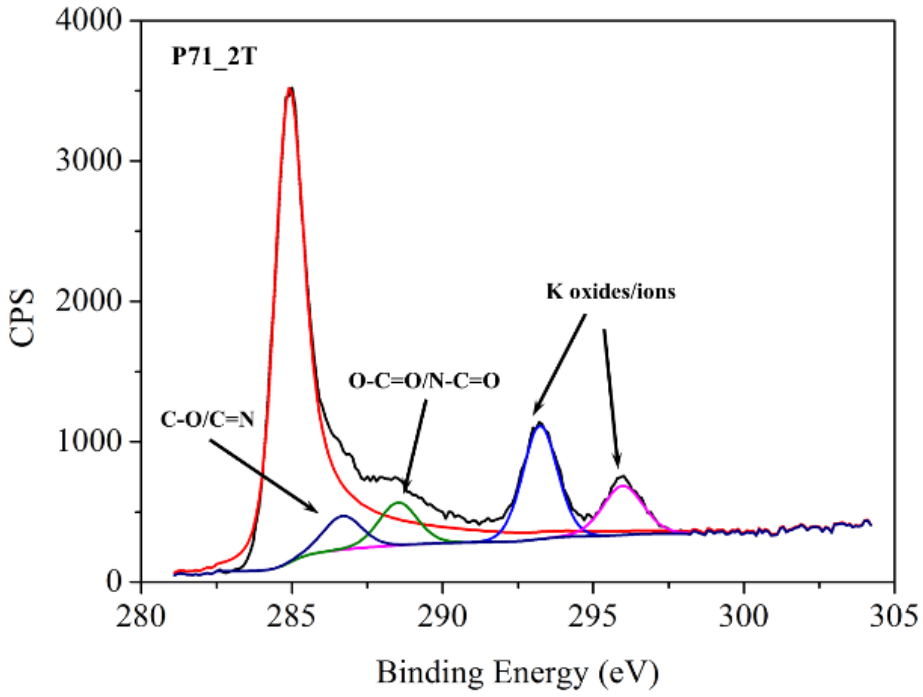
(a)



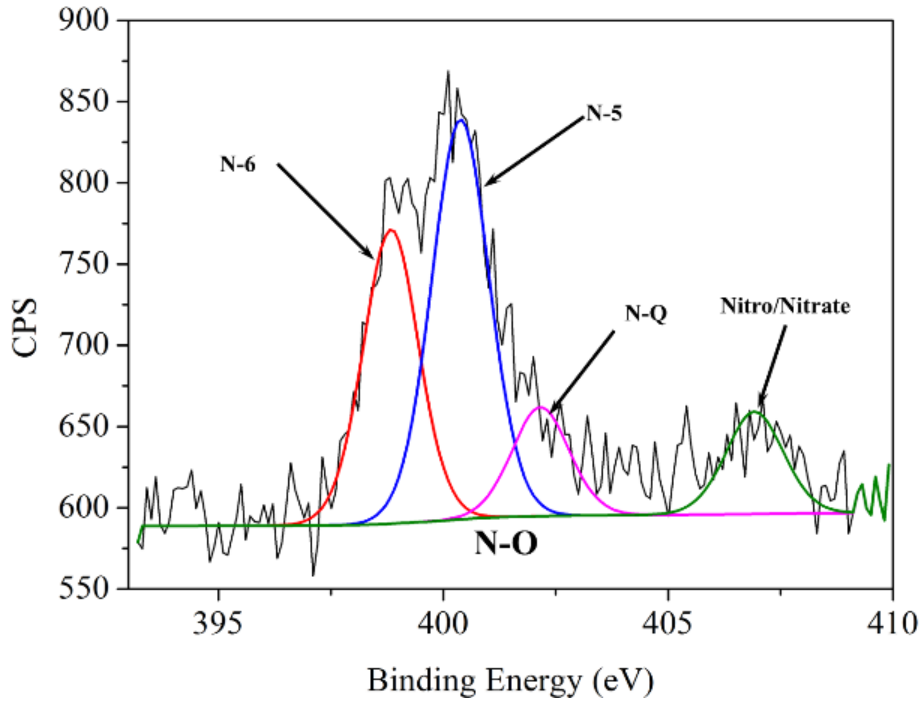
(a)

Figure 7.4 TEM images of sample P71_2T (a)-(b)

7.3.2 Chemical properties



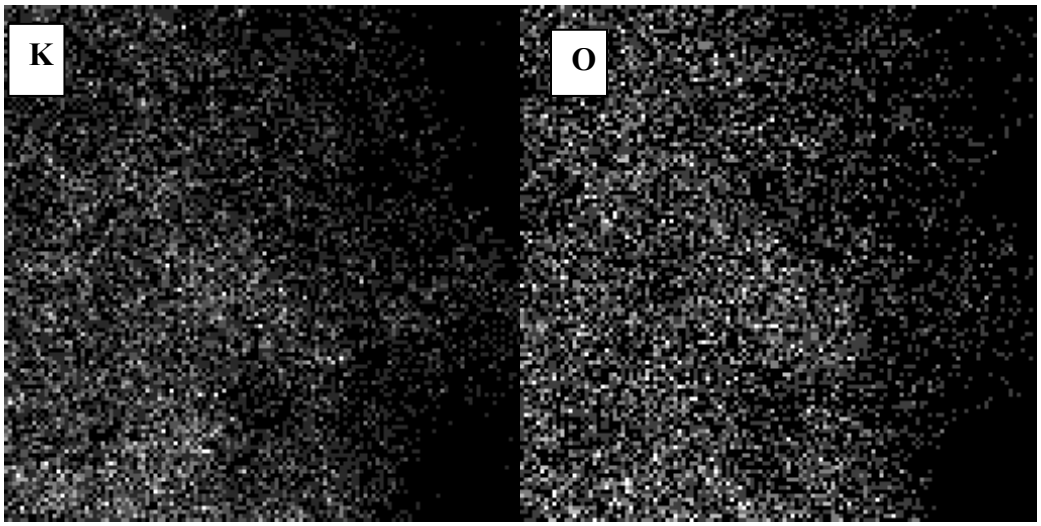
(a)



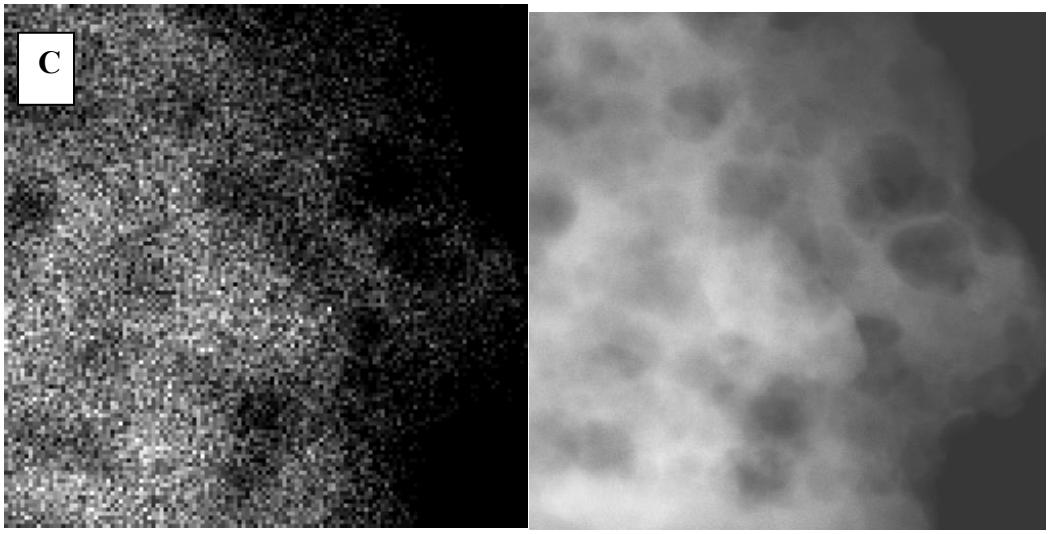
(b)

Figure 7.5 XPS spectra of prepared samples (a) C1s of sample P71_2T (b) N1s of sample P61_2T

XPS was used to characterize the elemental composition of the samples. As shown in Figure 7.5, the C1s peak was centered at 284.8 eV with a tail at high binding energy, which is attributed to heteroatoms like nitrogen and oxygen. There were small amount of C-O/C=N (286.2ev) and O-C=O/N-C=O (289.0ev) (Gu et al., 2013; Liu et al., 2014) existing in sample. The high resolution N1s could be deconvoluted into four components: pyridinic N, pyrrolic N, graphitic N and Nitrate resulting from the oxidizing condition (Beard et al., 1990; Zheng et al., 1997; Adenier et al., 2005). It can be found from Table 7.1 that the nitrogen content sharply decreased from 3 wt% to 0.23 wt% with the increase of activation temperature from 600 to 800 °C, which means most of the nitrogen containing groups have poor thermal stability (Sevilla et al., 2011). In addition to nitrogen, the peak of potassium was also observed in all samples. The K2p spectrum in Figure 7.5b consists of two peaks at BEs of 293.2 eV and 296.0 eV and their intensity ratio is exactly 2:1, so they are the spin-orbit-split doublet ($K2p_{3/2}$ and $K2p_{1/2}$) of the surface potassium oxides rather than carbonate species (Moulder et al., 1992; Li et al., 2001), which usually have their $K2p_{3/2}$ peak at 292.2 eV (Shchukarev et al., 2004). These kinds of surface potassium oxides are generated by the reaction between KOH and carbon during the activation process and was probably in the form of C-O-K. The elemental mapping results (see Figure 7.6) showed that potassium is distributed evenly along with the oxygen atoms.



(a) **(b)**

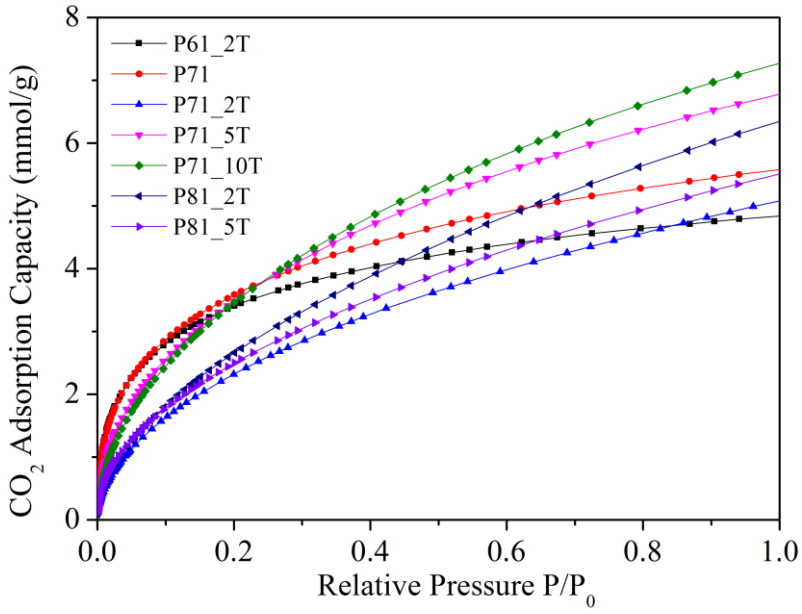


(c) (d)

Figure 7.6 Elemental mapping of sample P71_2T: (a) potassium; (b) oxygen; (c) carbon; (d) mapping area

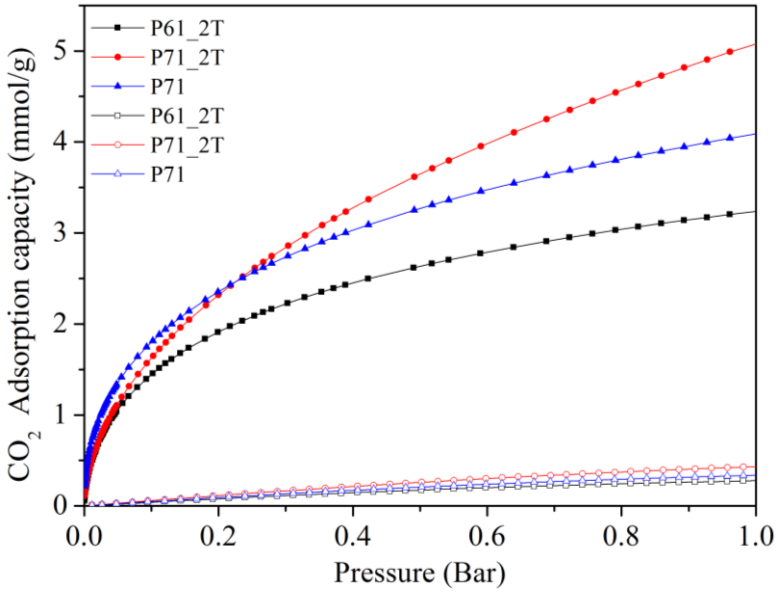
7.3.3 CO_2 adsorption performance

7.3.3.1 CO_2 adsorption at low temperature



(a)

Figure 7.7 CO_2 adsorption profiles: (a) adsorption isotherms at 0 °C; (b) adsorption isotherms at 25 °C (continued)



(b)

Figure 7.7 CO_2 adsorption profiles: (a) adsorption isotherms at 0 °C; (b) adsorption isotherms at 25°C

The CO_2 adsorption isotherms of all samples at 0 °C and CO_2 and N_2 isotherms of selected samples at 25 °C are displayed in Figure 7.7. Clearly, it can be found that the CO_2 uptake of the samples was affected by the activation temperature and compaction load. At the given load 2 tons, increasing the temperature from 600 to 700 °C, the CO_2 adsorption capacity sharply increased from 4.82 mmol/g to 7.24mmol/g at 0 °C and 1 bar, while the capacity decreased to 6.32 mmol/g at 800 °C. The change of capacities with temperature seems closely related to the volume of the ultra-micropores. Although sample P81_2T got the highest micropore volume 0.702 cm^3/g, the ultra-micropore volume is lower than that of P71_2T. The results of the samples activated at 700 °C under different compaction load showed that tableting benefits the CO_2 adsorption. The uptake at 1 bar increased from 5.57 mmol/g (without compaction) to 7.28 mmol/g (10 tons load), consistent with the trend observed for the ultra-micropore volume. Similarly, at 25 °C, compared to P61_2T and P71, sample P71_2T showed a higher CO_2 adsorption capacity of 5.10 mmol/g at 1 bar and 298 K, which was also one of the highest uptakes of CO_2 reported for activated carbon materials. However, at low CO_2 partial pressure, the trend of CO_2 adsorption capacity was different from 1 bar. Similarly, samples

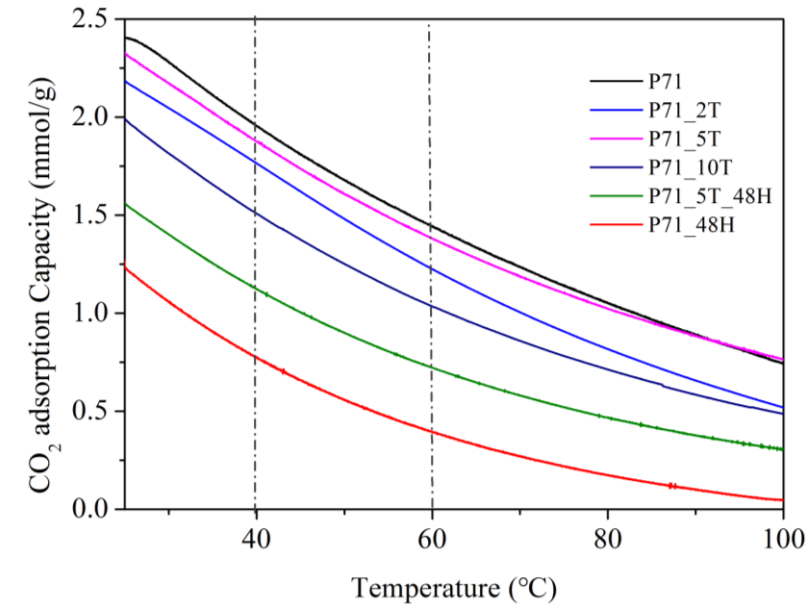
activated at 600-700 °C achieved a quite substantial uptake 3-3.27 mmol/g at 0.15 bar and 0 °C.

Considering practical applications, both high capacity and selectivity are required. In this study, Henry's Law through the initial slopes of CO_2 and N_2 adsorption isotherms (Hao et al., 2011; Chandra et al., 2012) at 25 °C was employed. It can be seen from Table 7.2 that all samples displayed quite impressive Henry's Law selectivity, sample P61_2T could reach 199, the highest value reported for carbon materials, indicating a strong affinity to CO_2 molecule. Compared to other carbon materials reported, with even higher ultra-micropore volumes, their Henry's Law selectivity was much lower than samples in this work. At the beginning of adsorption, CO_2 will be preferentially adsorbed by the sites with a strong adsorption potential. The strong adsorption potential is attributed to their unique surface chemistry and is much higher than any Van der Waals force. It is known that adsorption on carbon materials is very sensitive to temperature, and the capacity of which sharply decreases as temperature increases. The existence of such surface chemistry might be helpful to maintain the carbon materials with high capacity at flue gas temperatures (40-50 °C).

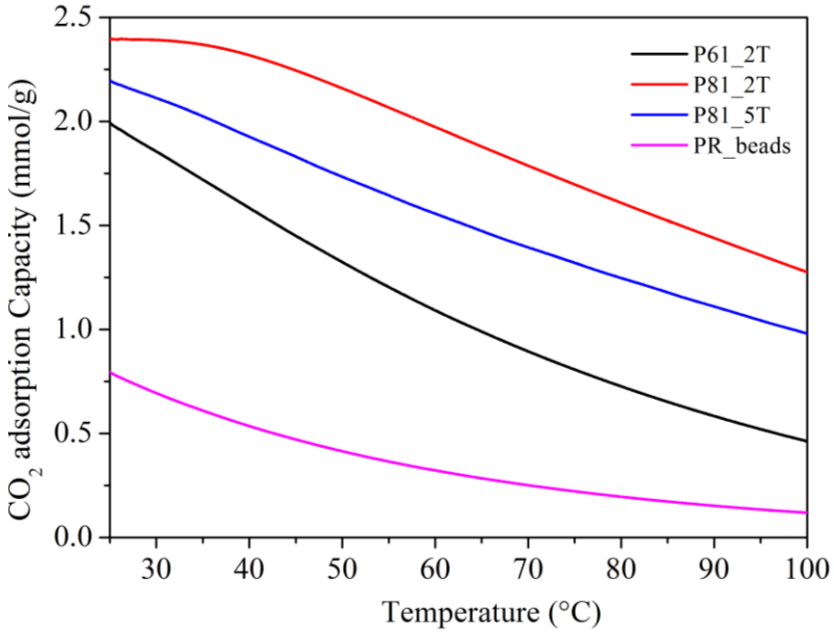
Table 7.2 CO_2/N_2 selectivity of selected samples at 25 °C calculated with the IS method

	Initial slope ratios
P61_2T	199
P71_2T	114
P71	184

7.3.3.2 CO_2 adsorption at flue gas temperature



(a)

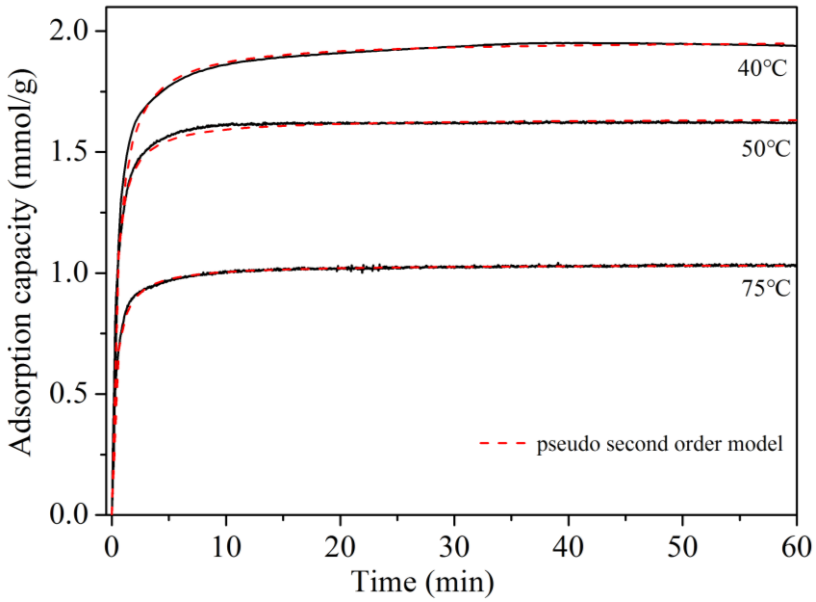


(b)

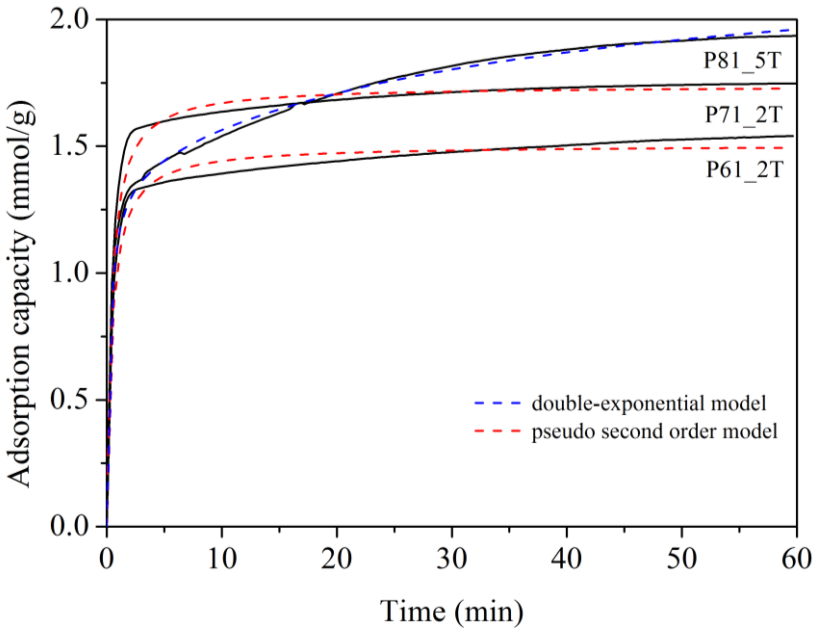
Figure 7.8 CO_2 adsorption profiles: the change of CO_2 adsorption capacity with the increase of temperature in simulated flue gas condition (15% CO_2 + 85% N_2): (a) samples prepared with different compaction load at 700 °C and selected samples (P71 and P71_5T) for further 48 h washing using soxhlet extraction; (b) samples prepared at 600 and 800 °C and carbon beads

In order to analyse the CO_2 capacity of samples under simulated flue gas conditions (15% CO_2 + 85% N_2) with temperature starting from 25 °C, temperature designed

adsorption tests with low a heating rate were carried out by TGA. Figure 7.8 displays the CO_2 adsorption curves of all samples. It can be found that all prepared carbons achieved a maximum CO_2 adsorption capacity at 25 °C and decreased gradually with increasing temperature. The uptake of samples at different temperatures was obtained from the adsorption curves. Typically, the uptake at 25 °C and 0.15 bar was between 2.00-2.40 mmol/g, at 40 °C it was in the range of 1.50-2.20 mmol/g, while at 50 °C the carbons adsorbed between 1.25 and 2.10 mmol/g. It is clear that the both pre-compaction and activation temperature affected the adsorption capacities greatly. At a given pre-compaction load, 2 tons, the adsorption capacity of samples increased with the increasing activation temperature, which is consistent with the significant increase in pore volume and surface area. Similar results were observed as the compaction pressure increased to 5 tons. However, at the given activation temperature, sample P71 and P81_2T presented the highest adsorption capacities at different temperature at 0.15 bar of CO_2, indicating low compaction pressure is beneficial for CO_2 capture at low partial pressure. Of all the samples, samples P81_2T exhibited highest CO_2 uptake under flue gas conditions, reaching about 2.20 mmol/g at 40 °C and about 2.05 mmol/g at 50 °C. Compared to the other materials listed in Table 2.7, the exceedingly high CO_2 adsorption capacities of P carbons under flue gas conditions represent the highest capacities ever reported for any carbon materials, and is even higher than the capacities of most carbons obtained at 0.15 bar and 25 °C. Even in comparison with other classes of materials like MOFs and zeolites, their performance ranks amongst the best, the uptake at 50 °C is higher than one of the best zeolite material zeolite 13X (Lee et al., 2002).

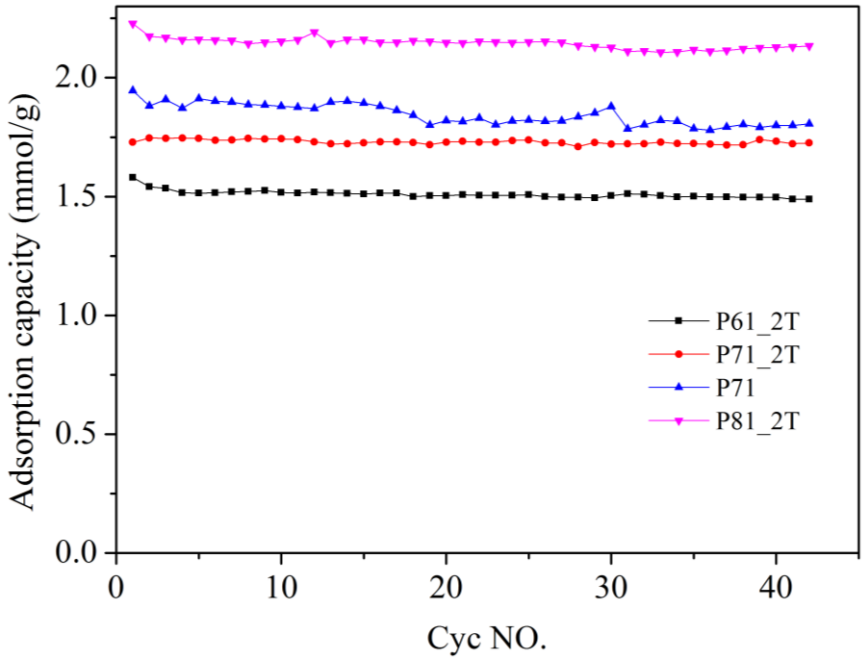


(a)



(b)

Figure 7.9 Adsorption curves of CO_2: (a) kinetics curves and fitting results of sample P71 at different temperatures; (b) kinetics curves and fitting results of different samples at 40 ℃; (c) cyclic performance of selected samples at different adsorption temperatures (flue gases: 15% CO_2 + 85% N_2; adsorption temperature: 40 ℃; desorption temperature: 120 ℃). (continued)



(c)

Figure 7.9 Adsorption curves of CO_2: (a) kinetics curves and fitting results of sample P71 at different temperatures; (b) kinetics curves and fitting results of different samples at 40 °C; (c) cyclic performance of selected samples at different adsorption temperatures (flue gases: 15% CO_2 + 85% N_2; adsorption temperature: 40 °C; desorption temperature: 120 °C).

The adsorption characteristics for the selected samples, obtained from TGA at different temperatures at 0.15 bar CO_2 (N_2 balance), was shown in Figure 7.9. It can be found that most of the samples exhibit fast adsorption kinetics in simulated flue gas at 40 °C and 90% of the equilibrium capacity was achieved in less than 5 minutes. The adsorption capacity of sample P71 declined with increased temperature to 75 °C, indicating that the CO_2 adsorption-desorption is a reversible process, where the decrease of adsorption capacity with increasing temperature is attributed to simultaneous desorption. In contrast, sample P81_5T was differed from the other samples exibiting a two-step process: the first step showed a sharp increase in the weight within the first 10 min, followed by a second, much slower process that slowly increased to a maximum value 1.93 mmol/g. To get deeper insight into the adsorption process of adsorbents, the pseudo second order model was adopted to describe the kinetics of CO_2 adsorption on carbon. It can be seen from Table 7.3 that the pseudo-second order kinetics model fitted well with the adsorption kinetics data of the selected samples at different temperatures, with high

R^2 values. The reaction rate coefficient k that quantifies the rate of a chemical reaction reveals the diffusion of CO_2 molecules. The data in Table 7.3 exhibited that the samples prepared by pre-compaction obtained a higher reaction rate coefficient k than the sample without pre-compaction, with P61_2T possessing the highest reaction rate coefficient k among the selected samples. This means the diffusion of the CO_2 molecules is quicker in sample with pre-compaction. Similarly, the reaction rate coefficient of sample P71 increased sharply with temperature, indicating the faster diffusion of CO_2 molecules with increasing temperature. In addition, sample P81_5T could not be fitted with a Pseudo second order model, the two-step process observed for P81_5T is similar to the adsorption process of PEI silica, indicating the existence of two kinds of controlling mechanism, which can be described by the double-exponential model that has been utilized by many studies (Kondo et al., 2012):

$$M_t/M_e = A_s\,(1\text{-}exp\,(-k_s\,t)) + A_d\,(1\text{-}exp\,(-k_d\,t)) \qquad (7.1)$$

Where M_t and M_e represent the adsorption capacity at time t and equilibrium adsorption capacity respectively. A_s and A_d are defined as the relative contribution of the surface and diffusion barriers respectively, controlling the overall adsorption process, $A_s + A_d = 1$. k_s and k_d are the corresponding surface and diffusion rate constants respectively. The double-exponential model fitted well with the experimental result of P81_5T (R^2>0.99). The surface rate constant (k_s =2.73) is much higher than the diffusion rate constant (k_d =0.058) due to the surface adsorption and surface adsorption is predominant (A_s=0.64) during adsorption. In addition to adsorption kinetics, the cyclic test of selected samples was also carried out, as shown in Figure 7.7c. All samples exhibited good, stable, and revisable performance at 0.15 bar and 40 °C and remained almost unchanged after 40 cycles.

Table 7.3 Pseudo second order kinetics model parameters of CO_2 adsorption for the selected samples

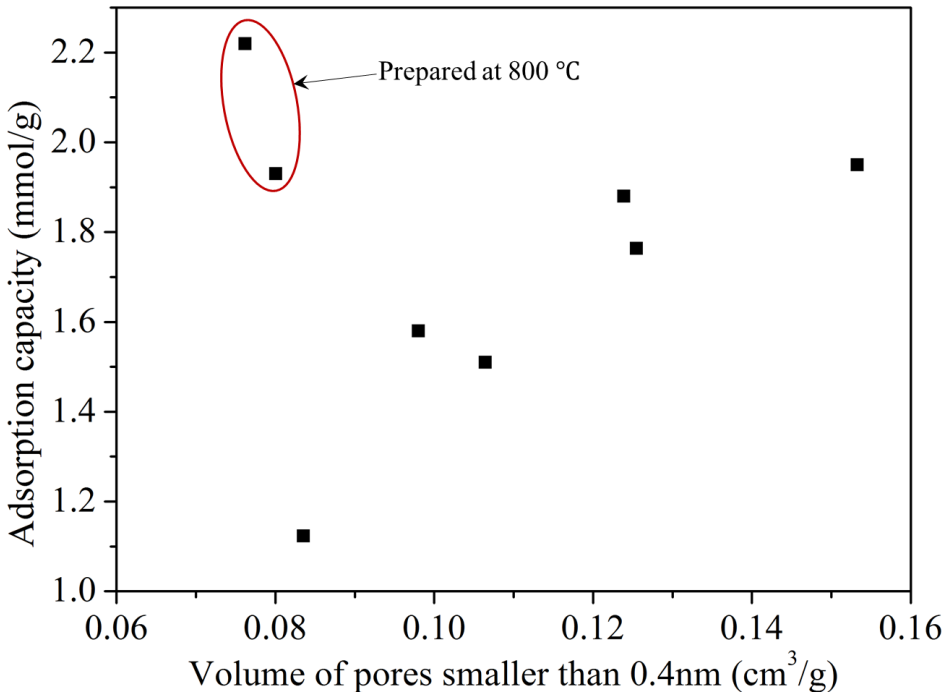
Sample		k	q_e	R^2
P61_2T	40 °C	1.52	1.51	0.96
P71_2T	40 °C	1.39	1.74	0.97
	40 °C	1.01	1.96	0.99
P71	50 °C	2.07	1.64	0.98
	70 °C	3.06	1.04	0.99

7.3.3.3 Role of surface chemistry and pore structure

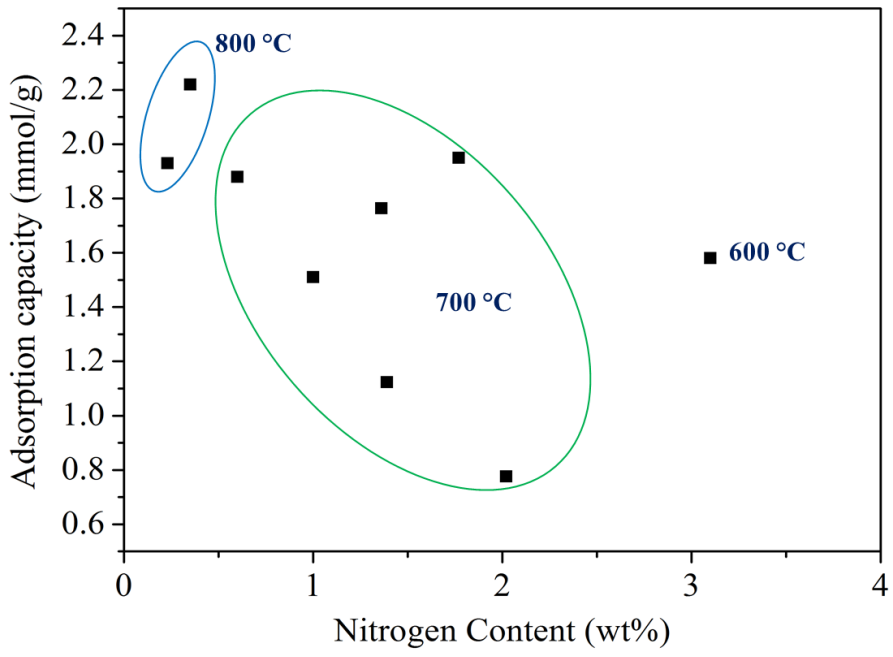
It is clear that the textural properties listed in Table 7.1 showed no direct relationship with CO_2 adsorption performance of P carbons prepared in different conditions at 40 °C and 0.15 bar. For example, sample P71_10T had the highest micropore volume and ultra-micopore volume while the CO_2 uptake at 0.15 bar is the lowest among all samples. In comparison, samples P61_2T (1.56 mmol/g) and sample R71 (1.95 mmol/g) possess much lower micropore volume and ultra-micorpore volume. Additionally, microporous phenolic resin beads prepared by steam activation with a micropore volume of 0.43 cm^3/g was also tested, its uptake at 40 °C and 0.15 bar was only 0.5 mmol/g. These results indicate that the existence of a unique pore size distribution and surface chemistry have special relevance to CO_2 adsorption at 40 °C and 0.15 bar. As reported in some papers, narrow micropores can effectively enhance the interaction force between pore wall and CO_2 molecules due to higher degree of Van der Waals force produced by the adjacent pore walls. Pores smaller than 0.5 nm is preferred to achieve high CO_2 adsorption capacity at low partial pressures (0.10-0.15 bar) and high temperatures. More specifically, Ashourirad et al. (2016) found that the uptake of benzimidazole derived carbon (BIDC) at 0.15 bar and 50 -75 °C had the best correlation with pores volume, with diameter smaller than 0.4 nm. Similar to BIDC, the effect of pore size on CO_2 uptake at 0.15 bar and 40 °C was investigated. It can be observed that the CO_2 adsorption capacity at 40 °C and 0.15 bar of samples prepared at 600-700 °C, is directly proportional to the

volume of pores smaller than 0.40 nm. However, samples prepared at 800 °C did not follow this trend, although they have a very low volume of ultra-micropores smaller than 0.4 nm (0.090 and 0.091 cm^3/g), while their adsorption capacities were the highest among all samples. Therefore, pore structure cannot solely rationalize the enhanced CO_2 uptake of the P carbons and surface chemistry also played an important role in high temperature CO_2 adsorption.

As nitrogen-rich precursor were used, the prepared samples have two kinds of surface containing groups: nitrogen containing groups and surface potassium groups. Apparently, there is no direct relationship between the CO_2 adsorption capacity and the nitrogen content or the nature of nitrogen containing groups (see Figure 7.10b). This is confirmed as there is a low coefficient of determination, indicating that nitrogen containing groups are not directly responsible for the high adsorption capacity, which was consistent with experimental and simulation results reported by other papers. In this work, it seems that nitrogen containing groups showed marginal contribution or even hindered the adsorption of CO_2, where the adsorption capacity decreased with increasing nitrogen content, indicating the key role of other surface properties. As shown in Figure 7.10c, the CO_2 uptake of the samples increased with the increasing potassium content. Sample P81_2T and P81_5T possessed the highest surface potassium content, so their uptake was higher than the other samples, despite their lack of pores smaller than 0.4 nm and lowest nitrogen content. The potassium exposed on surface on surface of the samples acts like the extra framework in the same manner seen in MOFs and zeolites, increasing the delocalization of charge and the polarity of surface. Therefore, the surface affinity to CO_2 molecules is increased. In order to further investigate the efficacy of potassium, samples P71 and P71_5T were continuously washed in hot water using a Soxhlet extractor for 48h. There was little change in the porosity, while the potassium content of P71 and P71_5T dropped from 6.45 wt% and 4.42 wt% to around 2 wt% respectively, but the adsorption capacity sharply decreased to 1.10 (P71_5T_48H) and 0.75 mmol/g (P71_48H) (see Figure 7.8).

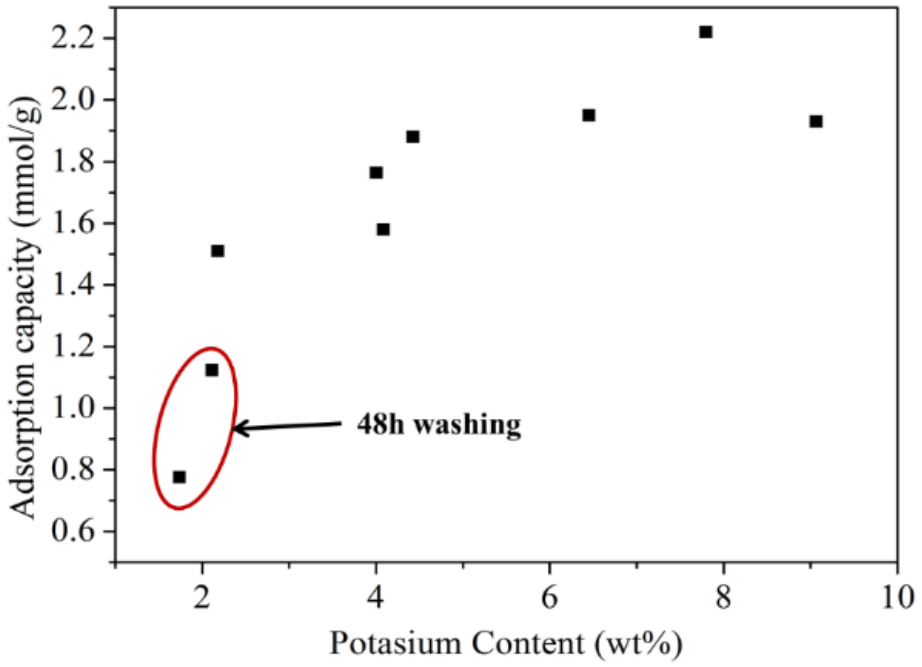


(a)



(b)

Figure 7.10 Relationship between CO_2 uptake and different factors: (a) the volume of pores smaller than 0.4nm; (b) nitrogen content; (c) potassium (continued)

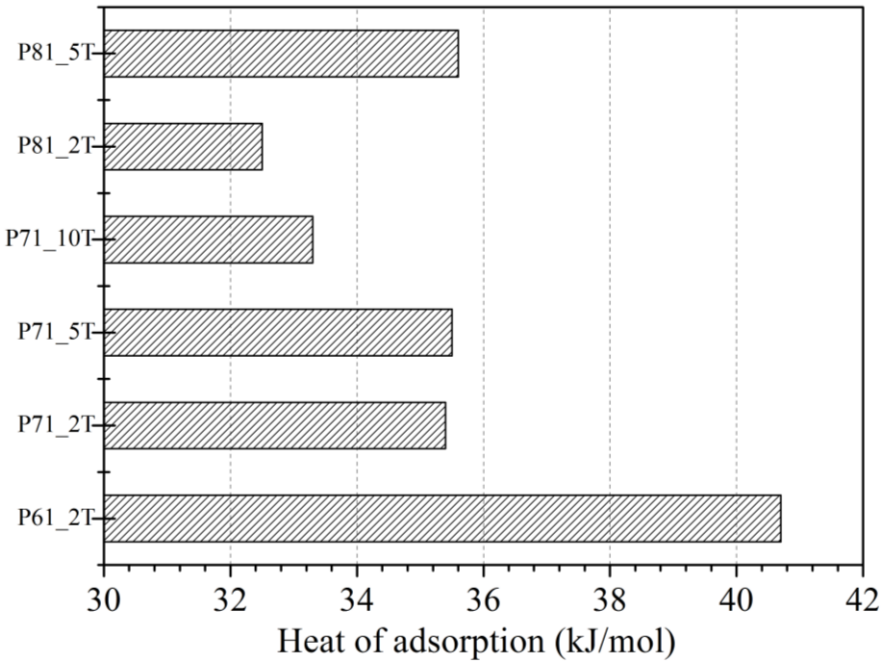


(c)

Figure 7.10 Relationship between CO_2 uptake and different factors: (a) the volume of pores smaller than 0.4nm; (b) nitrogen content; (c) potassium

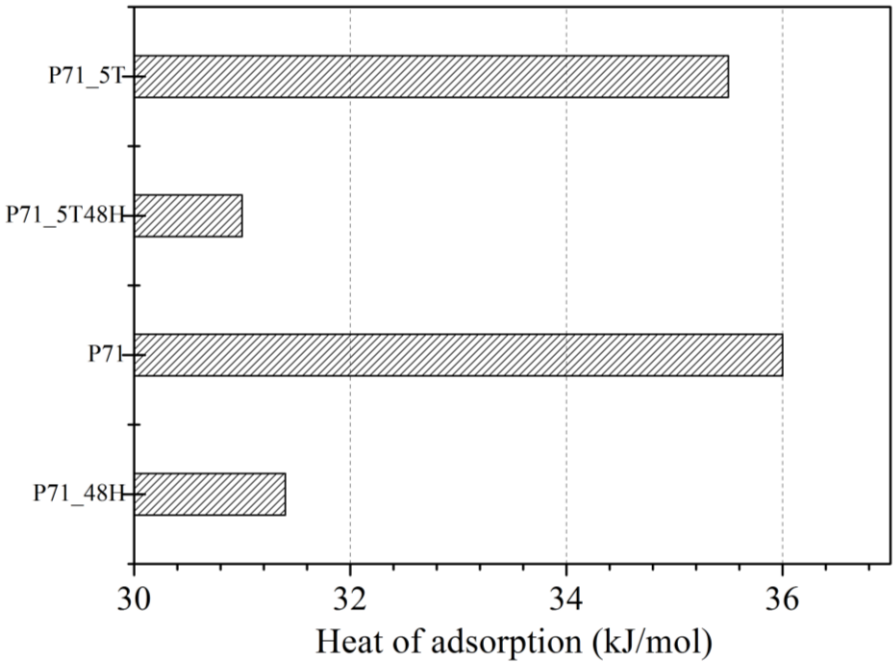
The enthalpy of adsorption is a crucial parameter to understand the interaction strength between CO_2 and carbon surface. In this paper, the heat of adsorption of all samples was tested by TG-DSC under simulated flue gas condition (40 °C and 15% CO_2 /85% N_2). It can be found from Figure 7.11 the heat of adsorption for the prepared samples ranged from 32.5 kJ/mol to 40.7 kJ/mol and showed a decrease with the increase of activation temperature, which corresponds well to the development of porosity and increased role of textural properties in adsorption. Similar trend was observed for samples with different pre-compaction load. In comparison, the heat of adsorption of the prepared samples were higher than any other carbon materials and even some zeolites and MOFs. Although both pore size and surface chemistry affected the heat of adsorption, the high value of 40.7 kJ/mol for P61_2T was higher than dopant free carbons with high ultra-micropore volume like phenolic resin (PR) beads (26 kJ/mol) (Liu et al., 2015) and commercial activated carbon (20 kJ/mol), indicating the existing strong interaction between CO_2 and carbon surface, which mainly attribute to the exposed potassium ions on the surface. However, potassium content is not direct proportion to heat of the adsorption, it can be found from Table 2 that the potassium content of P81_5T were

the highest but the heat of adsorption was around 36 kJ/mol that was much lower than P61_2T. The reason might be that P81_5T got much high pore volume and wide pore size distribution while P81_2T only have ultrafine pores and smallest pore volume and so the potassium density (potassium content divided total pore volume) in P61_2T is higher than that in P81_5T. The relationship between potassium density and heat of adsorption in Figure 9 showed that the heat of adsorption increased with the increasing potassium density. Meanwhile, the heat of adsorption of samples with further 48hrs water washing was also measured and a decrease was observed. The heat of adsorption of sample P71 and P71_5T decreased from around 36 kJ/mol to about 31 kJ/mol. Hence, it can be concluded that at low partial pressure and high temperature, exposed potassium on surface can effectively enhance the surface affinity while the improvement of overall affinity or heat of adsorption mainly depended on potassium density.

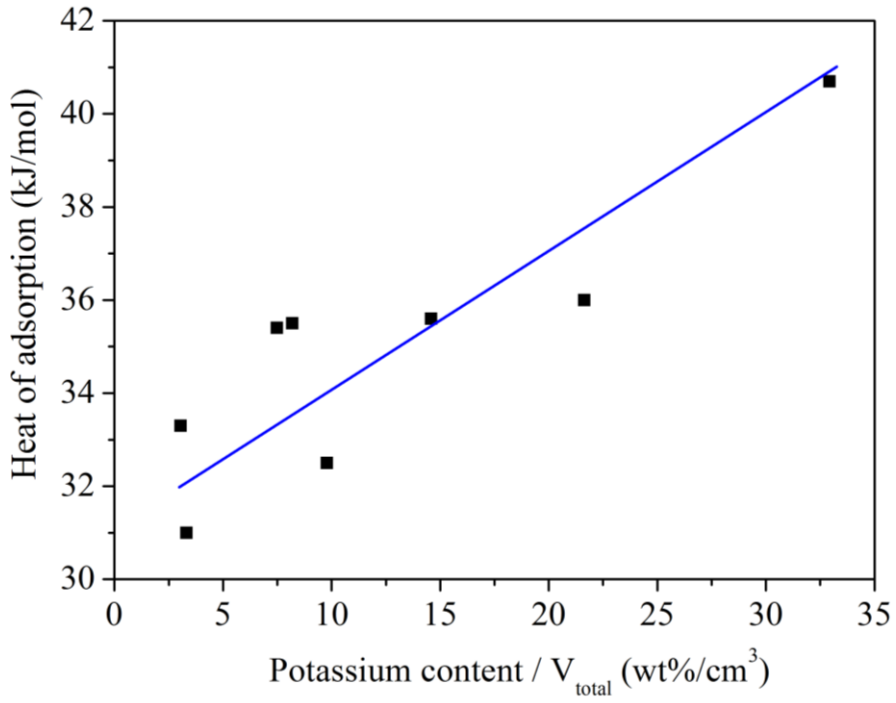


(a)

Figure 7.11 Heat of adsorption of P samples: (a)-(b) heat of adsorption of all samples; (c) the relationship between heat of adsorption and potassium and pore structures (continued)



(b)



(c)

Figure 7.11 Heat of adsorption of P samples: (a)-(b) heat of adsorption of all samples; (c) the relationship between heat of adsorption and potassium and pore structures

7.4 Conclusions

In conclusion, N, K co-doped ultra-micorporous carbons were prepared by chemical activation of compacted polyisocyanurate with KOH. The mechanical compaction method could effectively develop textural properties especially ultra-microporosity. It should highlight that the unique combination of ultra-microporosity and surface chemistry in prepared carbons enabled the record-high CO_2 uptake at flue gas condition (40-50 °C and 0.15 bar CO_2), which was higher than any carbon materials from a sophisticated and cost-prohibitive methodology, zeolites and MOFs. This carbon exhibited fast adsorption kinetics and excellent stability and regenerability under simulated flue gas condition. Taken with the high heat of adsorption, the dominant role of surface chemistry in CO_2 adsorption, were highly indicative of the significantly enhanced formation of extra-framework potassium ions leading to the extraordinary surface affinity to CO_2 observed for the prepared carbons.

Chapter 8 Conclusions and future work

8.1 General discussion

In this PhD project, two kinds of materials, rice husk (typical biomass) and PIR foam (nitrogen-rich polymer) have been used to prepare carbons using a facile methodology that effectively integrated carbonization, activation and potassium intercalation into a one-step process. As discussed in chapter 4 to 7, the samples prepared by this one-step method showed excellent CO_2 adsorption capacity. But it should be noticed that the optimized condition (activation temperature and KOH/carbon ratio) to prepare CO_2 adsorbent differed from the precursor or pretreatment method selected. In other words, the precursor's chemistry and internal structure played an important role in designing suitable CO_2 adsorbents especially for post combustion (low partial pressure and high temperature). In this section, the role of precursor's chemistry and pretreatment methods in porosity development and CO_2 adsorption will be discussed.

8.1.1 Textural properties of samples from different precursors and pretreatment method

The textural properties and CO_2 adsorption capacities of selected samples from different precursors and pretreatment method were listed in Table 8.1. It can be found that polymer and biomass precursors show differences in KOH chemical activation under the same condition. In comparison, biomass samples were more susceptible to KOH attack, the final biomass derived carbon had higher surface area, total pore volume and volume of ultra-micropores especially at high activation temperature or KOH/carbon mass ratio. For example, under the chemical conditions of activation temperature 600 °C and KOH/mass ratio=3:1, rice husk derived activated carbon had a surface area of 1303 m^2/g and total volume 0.52 cm^3/g. For PIR derived carbon, the surface area and total pore volume were 770 m^2/g and 0.33 cm^3/g, respectively. It had to say that the composition of precursor significantly affected the development of porosity. In this project, raw rice husk was directly mixed with KOH and activated at designed condition. The volatilization of volatile

compounds in rice husk created excess pore structure and defects that was beneficial for KOH activation. Meanwhile, compared to PIR polymer, high amount of molecular level silicon existed in rice husk inner structure, which reacted with KOH to form soluble potassium silicate and was then removed by water washing process. As shown in Chapter 4, there was almost linear relationship between silicon content removed and micropore volume especially ultra-micropore volume. This is unique advantage of rice husk. Additionally, as for the same precursor, the pretreatment methods also had significant contributions to the porosity development, there were obvious differences between samples prepared with/without pre-compaction. As shown in Table 8.1, sample HC-700-1 and R10T were prepared under same activation condition (KOH/rice husk=1:1, activation temperature 700 ℃) while the surface area and total pore volume increased from 976 m^2/g and 0.39 cm^3/g to 1162 m^2/g and 0.69 cm^3/g, respectively. Similar trend was observed for PIR derived carbons. The reason might be that the pre-compaction changed the initial inner structure of raw materials, lots of interparticle channels or slits were created during compaction process, which will become pores or help to create more pores.

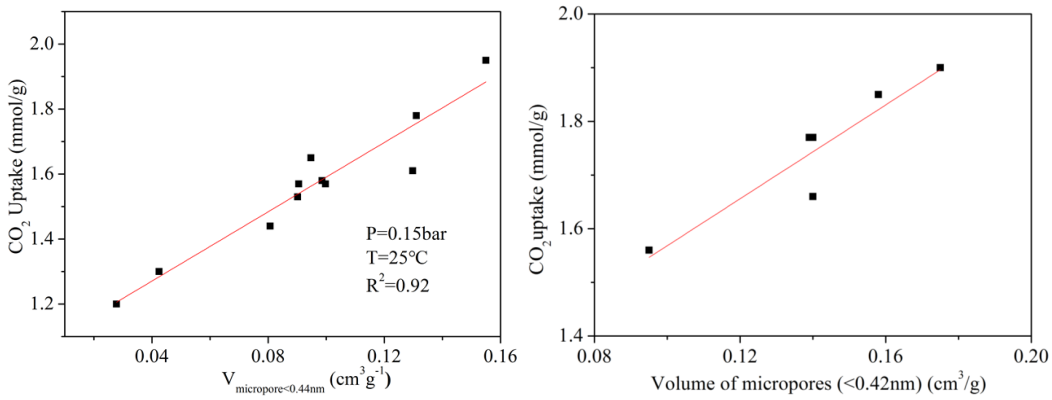
Table 8.1 Textural properties and CO_2 adsorption capacities of selected samples derived from rice husk and polymer

Sample	S_{BET} (m^2/g)	V_{total} (cm^3/g)	V_{micro} (cm^3/g)	$V_{micro<0.7nm}$ (cm^3/g)	CO_2 adsorption capacity 25 ℃ (mmol/g)	
					0.15bar	1bar
HC-600-1	536	0.24	0.19	0.16	1.58	3.02
HC-600-3	1303	0.52	0.47	0.34	1.50	4.02
HC-700-1	976	0.39	0.33	0.26	1.80	--
R10T	1162	0.69	0.40	0.33	1.80	4.30
FC6001	502	0.19	0.18	0.18	1.89	3.49
FC6003	770	0.33	0.27	0.26	2.02	4.04
FC7001	773	0.30	0.28	0.26	2.30	4.42
P71_2T	1407	0.54	0.51	0.38	2.10	5.10

8.1.2 CO_2 adsorption performance

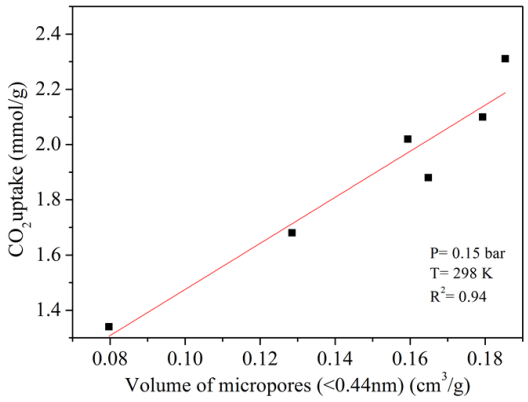
CO_2 adsorption capacities of selected samples at 25 °C and different partial pressure were also listed in Table 8.1. The CO_2 adsorption capacities at 1 bar were generally following the change of ultra-micropore volume. Sample P71_2T with the highest ultra-micropore volume overall possessed the highest adsorption capacity 5.10 mmol/g. The micropore volume of sample HC-600-1 and FC6001 as well as adsorption capacities were the lowest. It was also found that polymer derived carbons had higher adsorption capacity than rice husk derived carbons with similar or even slightly higher ultra-micropore volume. But when the partial pressure decreased to 0.15bar, the trend of CO_2 adsorption capacity was different from that of 1 bar. The adsorption capacity of sample FC7001 was much higher than all samples including samples with much higher ultra-micropore volume like HC-600-3, R10T, P71_2T. It means that the adsorption performance of carbon samples could not be solely rationalized by one single parameter but was codetermined by several parameters. In this project, the role of porous structure and surface chemistry were investigated.

8.1.2.1 the effect of porosity on CO_2 adsorption



(a) (b)

Figure 8.1 Relationship between CO_2 uptake and ultra-micropore volume of carbons at 25 °C, 0.15 bar CO_2: (a) rice husk derived samples without pre-compaction (b) rice husk derived samples with pre-compaction (c) PIR derived carbons without compaction (continued)



(c)

Figure 8.1 Relationship between CO_2 uptake and ultra-micropore volume of carbons at 25 °C, 0.15 bar CO_2: (a) rice husk derived samples without pre-compaction (b) rice husk derived samples with pre-compaction (c) PIR derived carbons without compaction

As physical adsorbent, porous structure or porosity of activated carbons played the main role in CO_2 adsorption. So how to tune the porous structure of carbon materials to increase the CO_2 adsorption capacity is the key to their future practical application. Actually, the CO_2 adsorption on activated carbon was determined by the interaction force between CO_2 molecule and carbon surface, which originated from the superposition of weak Van der Waals force generated by the two adjacent pore walls. It is well known that the Van der Waals force is inversely proportional to pore radius and decreases with the pore width (Everett, et al., 1976). Therefore, a critical pore size exists that can exactly keep the CO_2 molecule in the pores at a known condition (temperature and CO_2 partial pressure), if the pore slightly expands, the CO_2 molecule will escape form the pore. The critical pore size can be a good indicator to help to design carbons.

The critical pore size for post combustion carbon capture were investigated in this thesis. Figure 8.1 illustrated the relationship between CO_2 uptake and ultra-micropore volume at 25 °C, 0.15 bar CO_2 for samples derived from different precursors and pretreatment method. It can be found that even though the samples were prepared by using different precursors or pretreatment methods, it came to the same conclusion that the critical pore size at 0.15 bar CO_2 and 25 °C was about 0.42-0.44 nm. The correlation coefficient sharply decreased as the increase of pore size. In other words, pores smaller than 0.44 nm are preferable place for CO_2

adsorption at 25 °C, 0.15 bar. In addition, Chapter 4 and Chapter 6 also reported the critical pore size at temperature 0 °C, 25 °C and pressure 0.15bar, 1 bar, when adsorption temperature decreased or CO_2 partial pressure increased, the critical pore size increased. So, it means that we can design the adsorbents with specific pore size distribution to meet the requirement of different conditions. Carbons with ultra-micropore (<0.44nm) dominated structure are suitable adsorbents for CO_2 capture and separation from flue gas. Our results indicated that ultra-micropore (<0.44 nm) domain structure can be achieved by the mild KOH activation process such as sample HC-600-2, FC7001, FC6001. It should be highlighted that sample FC6001 possessed pure ultra-micropores (smaller than 0.4 nm), which can be considered as the CO_2 molecular sieve.

Our results also indicated that the pore volume of final carbons increased and the pore was widened (small pores shifted to big pores) with the increase of activation temperature and KOH/carbon mass ratio. In Figure 6.2b, the pores centered at 0.4 nm continuously decreased while those centered at 0.55 and 1.1 nm increased in intensity with the KOH/FC mass ratio. Those carbons might be suitable for pre-combustion (high CO_2 partial pressure) carbon capture. Those results provided a useful strategy to design adsorbents for CO_2 adsorption under different conditions.

8.1.2.2 the effect of surface modification on CO_2 adsorption

In addition to the control of pore size, surface modification by incorporating heteroatom groups into the carbon framework was another method to increase the interaction force between CO_2 and carbon surface. CO_2 is a kind of acidic gase and at the same time, it has a very large electrical quadrupole moment, which is over three times higher than that of another main component in flue gas N_2 ($-1.43\pm0.06 \times 10^{-39}$ Cm^2 *vs* $-4.65\pm0.08\times10^{-40}Cm^2$) (Raab et al., 1998), implying that CO_2 molecules can be preferentially polarized in an electrostatic field. Because of this, the introduction of N containing groups into carbon materials has been widely studied as these groups increase the basicity and charge delocalization of the carbon surface which could enhance selective CO_2 adsorption (Shen et al., 2013; Sivadas et al., 2016; Xing et al., 2012; Wang et al., 2011). But till now, the role of nitrogen in CO_2 adsorption is still unclear, there are two diametrically opposed views. Some

of the research believed that nitrogen functionalities could increase the CO_2 uptake and heat of adsorption (Sánchez-Sánchez et al., 2014; Sevilla et al., 2011; Fan et al., 2013; Xing et al., 2012). However, some papers presented that there was no clear relationship between CO_2 adsorption capacity and nitrogen containing groups (Adeniran et al. 2016; Sun et al., 2013; Sevilla et al., 2013). As shown in Table 2.6, the carbons from nitrogen-rich precursors generally had higher CO_2 adsorption capacity than nitrogen-free adsorption capacity, but the adsorption capacity was not related to the nitrogen content.

In this project, two kinds of materials, rice husk (nitrogen-free) and PIR materials (nitrogen-rich) were selected as the precursors. Chapter 6 and 7 reported the results of PIR material derived carbons, the results showed that there was no clearly linear relationship between CO_2 adsorption capacity and total nitrogen content or the content of different nitrogen containing group. Meanwhile, the adsorption capacity of sample HC-600-2 from rice husk (nitrogen-free) was about 2 mmol/g, which was higher than most of the carbon materials including nitrogen-doping sorbents. So, it seems that nitrogen containing groups did not play a key role in enhancing CO_2 adsorption.

We found that potassium intercalation, which can easily be achieved via an innovative chemical activation protocol, can be used as a facile but more powerful technique to greatly enhance the surface CO_2 affinity of carbon materials. The role of potassium on the surface was like the extra framework cations existing in zeolites and MOFs. Our results showed that the CO_2 adsorption capacity at 0.15bar and 25 °C increased with the potassium content. And for the first time, the relative contribution of microporosity and surface chemistry on CO_2 adsorption were delineated unambiguously. It was found that up to 50% of the total CO_2 uptake is attributable to the unique surface chemistry. Meanwhile, potassium intercalation indeed increased the surface affinity of carbon to CO_2, the heat of adsorption was closely related to the potassium density on carbon surface. Compared to other carbons preparation and/or surface modification methodologies, alkali intercalation can potentially serve as a versatile and more effective approach for remarkably

enhancing CO_2 capture performance of carbon-based adsorbents from biomass or polymer.

Usually, modification of the surface chemistry of carbon materials for CO_2 adsorption is achieved by doping heteroatoms onto carbon, the heteroatom is linked to carbon framework by covalent bond. However, the so called 'change of surface chemistry by potassium intercalation or zeolitic structure' in this thesis was not qualified for this category. There was no strong covalent bond existing between potassium/zeolitic structure and carbon. It was modification of adsorbent rather than surface modification of carbons, which was mostly like the relationship between support and catalyst. Although the support was not involved in the catalytic reaction, but the properties of support significantly affected the performance of catalyst. In the same way, the inner structure and chemical composition of carbons had significant effect on potassium intercalation or zeolitic modification and their performance, as shown in Chapter 4 to 7, samples prepared under different conditions showed different degree of potassium intercalation. In other words, the modified samples can be defined as a kind of nano composite materials.

All in all, the study of porous structure and surface modification on CO_2 adsorption in this thesis provided useful data and analysis for the design of new class of carbon based adsorbents in the future.

8.2 Conclusions

This project aimed to develop carbon-based adsorbents using abundant and easily accessible materials for post-combustion CO_2 capture. The specific conclusions from this work are as follows:

1) For rice husk derived carbons, the textural characterization demonstrates that these synthesized bio-carbons exhibit exceedingly high ultra-microporosity accounting for up to 95% of total porosity mainly as a result of the naturally occurring silicon compounds within the RH molecular framework structures. The best performing RH carbon has showed exceptionally high and fully reversible CO_2 uptake capacities of 5.91 mmol/g at 0 °C and 1.0 bar and 2.0 mmol/g at 25 °C and

a CO_2 partial pressure of 0.15 bar. It has been found that up to 50% of the total CO_2 uptake is attributable to the unique surface chemistry of the RH carbons, which appears to be dominated by the enhanced formation of extra-framework potassium cations owing to the exceedingly high levels of ultra-microporosity and the presence of zeolitic structures incorporated within the carbon matrices. Characterisations by EDX element mapping, XPS and the heat of adsorption measurements confirm the existence of a range of zeolitic entities, which essentially transforms the RH carbons into a kind of zeolite-carbon nanocomposite materials with strong surface affinity to CO_2.

2) In addition to sample HC-6002 (2 mmol/g at 25°C), the adsorption capacity of other samples prepared under different conditions was very low. In order to improve the adsorption performance of samples activated at 700 °C, a tableting method was employed. The results showed that the synthesized carbons from the rice husk under pressed different pressure exhibited much higher ultra-microporosity, especially in pores smaller than 0.42 nm, along with a large amount of mesopores. With the increase in press load, both the surface area and micropore volume increased. High ultra-microporosity and the unique surface chemistry of samples with pre-treatment led to exceedingly high CO_2 uptake, up to 6.80 and 4.50 mmol/g at 0 and 25 °C and 1 bar respectively, and 1.90 mmol/g at 25 °C and a CO_2 partial pressure of 0.15 bar, which was much higher than the samples without compaction. Meanwhile, the compacted samples showed recorded high IS CO_2/N_2 selectivity up to 170 at 25 °C as well as a high isosteric heat of adsorption.

3) As for the PIR foam precursors, the synthesized carbon foam has shown an exceedingly high level of ultra-microporosity and unique surface chemistry for CO_2 adsorption. The resulting ultra-microporous carbon foam achieved a record high CO_2 uptake at 25 °C and 0.15 bar, as well as record high CO_2/N_2 selectivity among other reported porous carbon materials and most MOFs. Systematic studies of these materilas showed that ultra-microporosity and potassium intercalation played key roles in the CO_2 adsorption at low partial pressure. In addition, the introduction of surface potassium containing groups enhanced the surface affinity to CO_2, resulting in a high isosteric heat of adsorption of carbon foams. The results also showed that

the pore structure or the fraction of ultra-micropore volume (<0.5 nm) rather than the surface chemistry had a significant effect on CO_2/N_2 selectivity at 25 °C.

4) The adsorption performance of PIR foam derived carbons at flue gas conditions (40-50 °C and 0.15 bar) were also examined. It should highlight that the unique combination of ultra-microporosity and surface chemistry in prepared carbons enabled the record high CO_2 uptake at flue gas conditions (up to 2 mmol/g at 40°C and 0.15 bar), which was higher than any carbon materials from a sophisticated and cost-prohibitive methodology, such as zeolites and MOFs. This carbon also exhibited fast adsorption kinetics and excellent stability and regenerability under simulated flue gas conditions. Taken with the high heat of adsorption and therefore the dominant role of surface chemistry in CO_2 adsorption, were highly indicative of the significantly enhanced formation of extra framework potassium ions leading to the extraordinary surface affinity to CO_2 observed for the prepared carbons.

Chapter 9 Future work

9.1 The role of potassium intercalated in carbon

In this project, a novel potassium intercalated carbon adsorbent for post combustion CO_2 capture was proposed and studied. It was proven that the exposed potassium on surface indeed improved the surface affinity to CO_2 molecules, increasing the adsorption capacity of carbons especially at low partial pressure. The distribution of potassium ions on carbon surface was identified by EDX and XPS and the relationship between potassium ions and adsorption capacity, adsorption heat and selectivity were also investigated. Even though those experimental results verified the efficacy of potassium ions, there was no data directly showing the change of surface due to the introduction of potassium. The potassium ions on surface acted like the extra framework, similar to those in MOFs or zeolites. It changed the distribution of electrostatics fields and the charge of surface. For future work, the surface potential or electrostatics field analysis using Kelvin probe force microscopy (KPFM) or Electrostatic force microscopy (EFM) will be helpful to understand the mechanism.

In addition to experiments, molecular simulation by using quantum chemistry software like Gaussian and Material Studio (MS) is also needed. Gaussian can be used to analyze the binding energy between CO_2 and potassium containing groups while MS can be used to simulate the whole isotherm at different temperatures.

9.2 Study on CO_2/N_2 selectivity

CO_2/N_2 selectivity is also an important parameter for future industrial applications. In this project, the effect of surface chemistry and porosity on IAST CO_2/N_2 selectivity of at 0.15/0.85 CO_2/N_2 gas mixture was also investigated. The preliminary results indicated that the surface chemistry has no direct relationship with selectivity, while there was an almost linear relationship between the fraction of micropore volume in pores <0.5 nm, and selectivity. However, only several

samples were studied in this project. In the future, a detailed study should be carried out on:

1) the effect of the surface chemistry of N containing groups and potassium containing groups on CO_2/N_2 selectivity

2) the effect of the pore structure on selective CO_2 capture on carbon

9.3 The effect of moisture

Flue gas from a typical coal-fired power plant also contains a certain amount of moisture, which will affect the performance of adsorbents. Both MOFs and zeolites show low tolerance to moisture, which were the main drawback for their application. As for activated carbon, the structure of activated carbon was stable in humid conditions, but moisture will still be co-adsorbed during the CO_2 capture process. Some papers reported that the existence of moisture could marginally affect the adsorption capacity of carbons. However, the desorption of co-adsorbed moisture during CO_2 desorption process is a big concern, which might increase the requirement of regeneration energy. There was no paper which reported this. So, more work concerning the effect of moisture should be carried out:
1) The adsorption kinetics of moisture and the effect of moisture on the regeneration process of carbon, which was important data for processing design of large-scale applications.
2) Design of activated carbons with hydrophobic surface *via* surface modification to reduce the adsorption capacity of moisture.

9.4 Others

Carbon preparation In this work, the activated carbon based CO_2 adsorbents were prepared based on fixed activation time 1 h based on references (Liu et al., 2015; Lozano-Castello et al., 2001; Zhang et al., 2013; Tseng & Tseng, 2005). Actually, activation time was also an important parameter for the development of porous structure. The increase of activation time increased the reaction time between KOH and carbons and so, the pore volume and surface area increased (Zhang et al., 2013). However, the volume and surface area of the micropores decreased dramatically if

the activation time was too long, which was attributed to the collapse and widening of pores and the decrease of porosity (Tsai et al., 1998). So the study of the effect of activation time on porous structure development and CO_2 adsorption should be carried out in the future.

CO_2 capture In this project, a mixture of CO_2/N_2 gas rather than real flue gas was used. For future work, the effect of impurities in flue gas on CO_2 adsorption should also be investigated. Furthermore, fixed bed or fluidized bed tests should be done in order to obtain valuable data for industrial applications.

References

ADENIER, A., CABET-DELIRY, E., CHAUSSÉ, A., GRIVEAU, S., MERCIER, F., PINSON, J. & VAUTRIN-UL, C., 2005. Grafting of nitrophenyl groups on carbon and metallic surfaces without electrochemical induction. *Chemistry of Materials*, *17*(3), 491-501.

ADDOUN, A., DENTZER, J., & EHRBURGER, P. 2002. Porosity of carbons obtained by chemical activation: effect of the nature of the alkaline carbonates. *Carbon*, 40(7), 1140-1143.

ADENIRAN, B., MASIKA, E. & MOKAYA, R., 2014. A family of microporous carbons prepared via a simple metal salt carbonization route with high selectivity for exceptional gravimetric and volumetric post-combustion CO_2 capture. *Journal of Materials Chemistry A*, *2*(35), 14696-14710.

ADENIRAN, B. & MOKAYA, R., 2016. Is N-doping in porous carbons beneficial for CO2 storage? Experimental demonstration of the relative effects of pore size and N-doping. *Chemistry of Materials*, *28*(3), 994-1001.

AHMADPOUR, A., & DO, D. D. 1997. The preparation of activated carbon from macadamia nutshell by chemical activation. *Carbon*, 35(12), 1723-1732.

AKHTAR, F., LIU, Q., HEDIN, N., & BERGSTRÖM, L. 2012. Strong and binder free structured zeolite sorbents with very high CO_2-over-N_2 selectivities and high capacities to adsorb CO_2 rapidly. *Energy & Environmental Science*, 5(6), 7664-7673.

ALABADI, A., RAZZAQUE, S., YANG, Y., CHEN, S. & TAN, B., 2015. Highly porous activated carbon materials from carbonized biomass with high CO_2 capturing capacity. *Chemical Engineering Journal*, *281*, 606-612.

ALCAÑIZ-MONGE, J., LILLO-RÓDENAS, M. Á., BUENO-LÓPEZ, A., & ILLÁN-GÓMEZ, M. J. 2007. The influence of iron chloride addition to the precursor pitch on the formation of activated carbon fibers. *Microporous and mesoporous materials*, 100(1), 202-209.

ANSON, A., JAGIELLO, J., PARRA, J. B., SANJUAN, M. L., BENITO, A. M., MASER, W. K., & MARTÍNEZ, M. T. 2004. Porosity, surface area, surface energy, and hydrogen adsorption in nanostructured carbons. *The Journal of Physical Chemistry B*, 108(40), 15820-15826.

APREA, P., CAPUTO, D., GARGIULO, N., IUCOLANO, F. & PEPE, F., 2010. Modeling carbon dioxide adsorption on microporous substrates: Comparison between Cu-BTC metal-organic framework and 13X zeolitic molecular sieve. *Journal of Chemical & Engineering Data*, *55*(9), 3655-3661.

ASHOURIRAD, B., SEKIZKARDES, A.K., ALTARAWNEH, S. & EL-KADERI, H.M., 2015. Exceptional gas adsorption properties by nitrogen-doped porous carbons derived from benzimidazole-linked polymers. *Chemistry of Materials*, *27*(4), 1349-1358.

ASHOURIRAD, B., ARAB, P., ISLAMOGLU, T., CYCHOSZ, K.A., THOMMES, M. & EL-KADERI, H.M., 2016. A cost-effective synthesis of heteroatom-doped porous carbons as efficient CO_2 sorbents. *Journal of Materials Chemistry A*, *4*(38), 14693-14702.

BABARAO, R., & JIANG, J. 2009. Unprecedentedly high selective adsorption of gas mixtures in rho zeolite-like metal-organic framework: a molecular simulation study. *Journal of the American Chemical Society*, 131(32), 11417-11425.

BAE, Y.S., SNURR, R.Q. 2011. Development and evaluation of porous materials for carbon dioxide separation and capture. *Angewandte Chemie International Edition*, 50(49), 11586-11596.

BAE, T.H., HUDSON, M.R., MASON, J.A., QUEEN, W.L., DUTTON, J.J., SUMIDA, K., MICKLASH, K.J., KAYE, S.S., BROWN, C.M. & LONG, J.R., 2013. Evaluation of cation-exchanged zeolite adsorbents for post-combustion carbon dioxide capture. *Energy & Environmental Science*, *6*(1), 128-138.

BAE, W., KIM, J., & CHUNG, J. 2014. Production of granular activated carbon from food-processing wastes (walnut shells and jujube seeds) and its adsorptive properties. *Journal of the Air & Waste Management Association*,*64*(8), 879-886.

BAE, Y. S., LIU, J., WILMER, C. E., SUN, H., DICKEY, A. N., KIM, M. B., ... & SNURR, R. Q. 2014a. The effect of pyridine modification of Ni–DOBDC on CO_2 capture under humid conditions. *Chemical Communications*, 50(25), 3296-3298.

BALSAMO, M., SILVESTRE-ALBERO, A., SILVESTRE-ALBERO, J., ERTO, A., RODRIGUEZ-REINOSO, F., & LANCIA, A. 2014. Assessment of CO_2 adsorption capacity on activated carbons by a combination of batch and dynamic tests. *Langmuir*, 30(20), 5840-5848.

BALSAMO, M., RODRÍGUEZ-REINOSO, F., MONTAGNARO, F., LANCIA, A., & ERTO, A. 2013. Highlighting the role of activated carbon particle size on CO_2 capture from model flue gas. *Industrial & Engineering Chemistry Research*, 52(34), 12183-12191.

BANSAL, R. C., & GOYAL, M. 2005. *Activated carbon adsorption*. CRC press.

BARR, T.L., 1983. An XPS study of Si as it occurs in adsorbents, catalysts, and thin films. *Applications of Surface Science*, *15*(1-4), 1-35.

BASTA, A. H., FIERRO, V., EL-SAIED, H., & CELZARD, A. 2009. 2-Steps KOH activation of rice straw: an efficient method for preparing high-performance activated carbons. *Bioresource technology*, 100(17), 3941-3947.

BEARD, B.C., 1990. Cellulose nitrate as a binding energy reference in N (1s) XPS studies of nitrogen-containing organic molecules. *Applied surface science*, *45*(3), 221-227.

BEN, T., LI, Y., ZHU, L., ZHANG, D., CAO, D., XIANG, Z., YAO, X. & QIU, S., 2012. Selective adsorption of carbon dioxide by carbonized porous aromatic framework (PAF). *Energy & Environmental Science*, *5*(8), 8370-8376.

BOLLINI, P., BRUNELLI, N.A., DIDAS, S.A. & JONES, C.W., 2012. Dynamics of CO_2 adsorption on amine adsorbents. 2. Insights into adsorbent design. *Industrial & Engineering Chemistry Research*, *51*(46), 15153-15162.

BOUCHELTA, C., MEDJRAM, M.S., BERTRAND, O. AND BELLAT, J.P., 2008. Preparation and characterization of activated carbon from date stones by physical activation with steam. *Journal of Analytical and Applied Pyrolysis*, *82*(1), pp.70-77.

BRANDANI, F. & RUTHVEN, D.M., 2004. The effect of water on the adsorption of CO_2 and C3H8 on type X zeolites. *Industrial & engineering chemistry research*, *43*(26), pp.8339-8344.

BRITT, D., FURUKAWA, H., WANG, B., GLOVER, T.G. & YAGHI, O.M., 2009. Highly efficient separation of carbon dioxide by a metal-organic framework replete with open metal sites. *Proceedings of the National Academy of Sciences*, *106*(49), 20637-20640.

BROWN, D.R. & GROSZEK, A.J., 2000. Heats of adsorption of ammonia on a zeolite catalyst and an acid-activated clay catalyst determined by flow adsorption microcalorimetry. *Langmuir*, *16*(9),.4207-4212.

BRUNAUER, S., EMMETT, P.H. & TELLER, E., 1938. Adsorption of gases in multimolecular layers. *J. Am. Chem. Soc*, *60*(2), 309-319.

BRUNAUER, S., DEMING, L.S., DEMING, W.E. & TELLER, E., 1940. On a theory of the van der Waals adsorption of gases. *Journal of the American Chemical society*, *62*(7), 1723-1732.

BURDYNY, T. & STRUCHTRUP, H., 2010. Hybrid membrane/cryogenic separation of oxygen from air for use in the oxy-fuel process. *Energy*, 35(5), 1884-1897.

CAI, J., QI, J., YANG, C., & ZHAO, X. 2014. Poly (vinylidene chloride)-Based Carbon with Ultrahigh Microporosity and Outstanding Performance for CH_4 and H_2 Storage and CO_2 Capture. *ACS applied materials & interfaces*, 6(5), 3703-3711.

CARDOSO, B., MESTRE, A. S., CARVALHO, A. P., & PIRES, J. 2008. Activated carbon derived from cork powder waste by KOH activation: preparation, characterization, and VOCs adsorption. *Industrial & Engineering Chemistry Research*, 47(16), 5841-5846.

CARRASCO-MALDONADO, F., SPÖRL, R., FLEIGER, K., HOENIG, V., MAIER, J. & SCHEFFKNECHT, G., 2016. Oxy-fuel combustion technology for cement production–State of the art research and technology development. *International Journal of Greenhouse Gas Control*, 45, 189-199.

CATURLA, F., MOLINA-SABIO, M., & RODRIGUEZ-REINOSO, F. 1991. Preparation of activated carbon by chemical activation with ZnCl 2. *Carbon*, 29(7), 999-1007.

CHANDRA, V., YU, S.U., KIM, S.H., YOON, Y.S., KIM, D.Y., KWON, A.H., MEYYAPPAN, M. & KIM, K.S., 2012. Highly selective CO_2 capture on N-doped carbon produced by chemical activation of polypyrrole functionalized graphene sheets. *Chemical communications*, *48*(5), 735-737.

CHEN, Y., ZHU, Y., WANG, Z., LI, Y., WANG, L., DING, L., GAO, X., MA, Y. & GUO, Y., 2011. Application studies of activated carbon derived from rice husks produced by chemical-thermal process-A review. *Advances in colloid and interface science*, *163*(1), 39-52.

CHEN, C., KIM, J., & AHN, W. S. 2012. Efficient carbon dioxide capture over a nitrogen-rich carbon having a hierarchical micro-mesopore structure. *Fuel*, 95, 360-364.

CHEN, L., YONG, S.Z. & GHONIEM, A.F., 2012a. Oxy-fuel combustion of pulverized coal: characterization, fundamentals, stabilization and CFD modeling. *Progress in Energy and Combustion Science*, *38*(2), 156-214.

CHESTER, A.W. & DEROUANE, E.G., 2009. *Zeolite characterization and catalysis*. Springer Science & Business Media.

CHOI, M., & RYOO, R. 2007. Mesoporous carbons with KOH activated framework and their hydrogen adsorption. *J. Mater. Chem.*, 17(39), 4204-4209.

CHOI, S., WATANABE, T., BAE, T.H., SHOLL, D.S. & JONES, C.W., 2012. Modification of the Mg/DOBDC MOF with amines to enhance CO2 adsorption from ultradilute gases. *The journal of physical chemistry letters*, *3*(9), 1136-1141.

CHUI, S.S.Y., LO, S.M.F., CHARMANT, J.P., ORPEN, A.G. &WILLIAMS, I.D., 1999. A chemically functionalizable nanoporous material $[Cu_3(TMA)_2(H2O)_3]_n$. *Science*, *283*(5405), 1148-1150.

Climate change 2014: synthesis Report. Intergovernmental panel on climate change IPCC: Geneva, Switzerland, 2014.

CORIANI, S., HALKIER, A., RIZZO, A. & RUUD, K., 2000. On the molecular electric quadrupole moment and the electric-field-gradient-induced birefringence of CO_2 and CS_2. *Chemical Physics Letters*, *326*(3), 269-276.

COROMINA, H.M., WALSH, D.A. & MOKAYA, R., 2016. Biomass-derived activated carbon with simultaneously enhanced CO_2 uptake for both pre and post

combustion capture applications. *Journal of Materials Chemistry A*, *4*(1), pp.280-289.

D'ALESSANDRO, D.M., SMIT, B. & LONG, J.R., 2010. Carbon dioxide capture: prospects for new materials. *Angewandte Chemie International Edition*, *49*(35), 6058-6082.

DARMSTADT, H., & ROY, C. 2003. Surface spectroscopic study of basic sites on carbon blacks. *Carbon*, 41(13), 2662-2665.

DAUD, W.M.A.W. AND ALI, W.S.W. 2004. Comparison on pore development of activated carbon produced from palm shell and coconut shell. *Bioresource Technology*, 93(1), 63-69.

DE SOUZA, L. K., WICKRAMARATNE, N. P., ELLO, A. S., COSTA, M. J., DA COSTA, C. E., & JARONIEC, M. 2013. Enhancement of CO_2 adsorption on phenolic resin-based mesoporous carbons by KOH activation. *Carbon*, 65, 334-340.

DINCĂ, M., HAN, W. S., LIU, Y., DAILLY, A., BROWN, C. M., & LONG, J. R. 2007. Observation of Cu^{2+}–H_2 interactions in a Fully Desolvated Sodalite-Type Metal–Organic Framework. *Angewandte Chemie International Edition*, 46(9), 1419-1422.

DRAGE, T. C., ARENILLAS, A., SMITH, K. M., PEVIDA, C., PIIPPO, S., & SNAPE, C. E. 2007. Preparation of carbon dioxide adsorbents from the chemical activation of urea–formaldehyde and melamine–formaldehyde resins. *Fuel*, 86(1), 22-31.

Dreisbach, F., Staudt, R. & Keller, J.U., 1999. High pressure adsorption data of methane, nitrogen, carbon dioxide and their binary and ternary mixtures on activated carbon. *Adsorption*, *5*(3), 215-227.

DUTCHER, B., FAN, M. & RUSSELL, A.G., 2015. Amine-Based CO2 Capture Technology Development from the Beginning of 2013- A Review. *ACS applied materials & interfaces*, *7*(4), 2137-2148.

DZIURA, A., MARSZEWSKI, M., CHOMA, J., DE SOUZA, L. K., OSUCHOWSKI, Ł., & JARONIEC, M. 2014. Saran-derived carbons for CO_2 and benzene sorption at ambient conditions. *Industrial & Engineering Chemistry Research*.

EL-HENDAWY, A. N. A. 2009. An insight into the KOH activation mechanism through the production of microporous activated carbon for the removal of Pb^{2+} cations. *Applied Surface Science*, 255(6), 3723-3730.

EL-KADERI, H.M., HUNT, J.R., MENDOZA-CORTÉS, J.L., CÔTÉ, A.P., TAYLOR, R.E., O'KEEFFE, M. & YAGHI, O.M. 2007. Designed synthesis of 3D covalent organic frameworks. *Science*, *316*(5822), 268-272.

EL-SAYED, Y., & BANDOSZ, T. J. 2004. Adsorption of valeric acid from aqueous solution onto activated carbons: role of surface basic sites. *Journal of colloid and interface science*, 273(1), 64-72.

Everett, D.H. & Stone, F.S. eds., 1958. *The structure and properties of porous materials* (Vol. 10). Butterworths.

EVERETT, D. H., & POWL, J. C. 1976. Adsorption in slit-like and cylindrical micropores in the henry's law region. A model for the microporosity of carbons. *Journal of the Chemical Society, Faraday Transactions 1: Physical Chemistry in Condensed Phases*, 72, 619-636.

FAN, X., ZHANG, L., ZHANG, G., SHU, Z., & SHI, J. 2013. Chitosan derived nitrogen-doped microporous carbons for high performance CO 2 capture. *Carbon*, 61, 423-430.

FREITAS, J.C., SCHETTINO, M.A., CUNHA, A.G., EMMERICH, F.G., BLOISE, A.C., DE AZEVEDO, E.R. & BONAGAMBA, T.J., 2007. NMR investigation on the occurrence of Na species in porous carbons prepared by NaOH activation. *Carbon*, *45*(5), 1097-1104.

FOO, K.Y. & HAMEED, B.H., 2012. Mesoporous activated carbon from wood sawdust by K_2CO_3 activation using microwave heating. *Bioresource technology*, *111*, 425-432.

FOX, D. A., & WHITE, A. H. 1931. Effect of sodium carbonate upon gasification of carbon and production of producer gas. *Industrial & Engineering Chemistry*, 23(3), 259-266.

FREITAS, J. C., SCHETTINO, M. A., EMMERICH, F. G., WONG, A., & SMITH, M. E. 2007. A multiple-field 23 Na NMR study of sodium species in porous carbons. *Solid state nuclear magnetic resonance*, 32(4), 109-117.

FU, H., YANG, L., WAN, Y., XU, Z., & ZHU, D. 2011. Adsorption of pharmaceuticals to microporous activated carbon treated with potassium hydroxide, carbon dioxide, and steam. *Journal of environmental quality*, 40(6), 1886-1894.

FUJIKI, J. & YOGO, K., 2016. The increased CO_2 adsorption performance of chitosan-derived activated carbons with nitrogen-doping. *Chemical Communications*, *52*(1), 186-189.

FURUKAWA, H., KO, N., GO, Y.B., ARATANI, N., CHOI, S.B., CHOI, E., YAZAYDIN, A.Ö., SNURR, R.Q., O'KEEFFE, M., KIM, J. & YAGHI, O.M., 2010. Ultrahigh porosity in metal-organic frameworks. *Science*, *329*(5990), 424-428.

GADIPELLI, S., PATEL, H.A. & GUO, Z., 2015. An Ultrahigh Pore Volume Drives Up the Amine Stability and Cyclic CO_2 Capacity of a Solid-Amine@ Carbon Sorbent. *Advanced Materials*, *27*(33), 4903-4909.

GADIPELLI, S. & GUO, Z.X., 2015. Tuning of ZIF-Derived Carbon with High Activity, Nitrogen Functionality, and Yield–A Case for Superior CO_2 Capture. *ChemSusChem*, *8*(12), 2123-2132.

GAO, Y., LI, L., JIN, Y., WANG, Y., YUAN, C., WEI, Y., CHEN, G., GE, J. & LU, H., 2015. Porous carbon made from rice husk as electrode material for electrochemical double layer capacitor. *Applied Energy*, *153*, 41-47.

GERGOVA, K., PETROV, N. & ESER, S. 1994. Adsorption properties and microstructure of activated carbons produced from agricultural by-products by steam pyrolysis. Carbon, 32(4), 693-702.

GOETTMANN, F., FISCHER, A., ANTONIETTI, M., & THOMAS, A. 2006. Chemical Synthesis of Mesoporous Carbon Nitrides Using Hard Templates and Their Use as a Metal-Free Catalyst for Friedel–Crafts Reaction of Benzene.*Angewandte Chemie International Edition*, 45(27), 4467-4471.

GÓMEZ-SERRANO, V., PIRIZ-ALMEIDA, F., DURÁN-VALLE, C. J., & PASTOR-VILLEGAS, J. 1999. Formation of oxygen structures by air activation. A study by FT-IR spectroscopy. *Carbon*, 37(10), 1517-1528.

GORKA, J., ZAWISLAK, A., CHOMA, J., & JARONIEC, M. 2008. KOH activation of mesoporous carbons obtained by soft-templating. *Carbon,* 46(8), 1159-1161.

GREGG, S.J. & SING, K.S., 1983. Adsorption, surface area, and porosity.Academic Press.

GU, J.M., KIM, W.S., HWANG, Y.K. & HUH, S., 2013. Template-free synthesis of N-doped porous carbons and their gas sorption properties. *Carbon*, *56*, 208-217.

GUPTA, R., SLIMANE, R. B., BLAND, A. E., & WRIGHT, I. 2008. Progress in carbon dioxide separation and capture: a review. *Journal of Environmental Sciences*, 1, 14-27.

HAO, G. P., LI, W. C., QIAN, D., WANG, G. H., ZHANG, W. P., ZHANG, T., ... & LU, A. H. 2011. Structurally designed synthesis of mechanically stable poly (benzoxazine-co-resol)-based porous carbon monoliths and their application as high-performance CO_2 capture sorbents. *Journal of the American Chemical Society,* 133(29), 11378-11388.

HAO, G. P., LI, W. C., QIAN, D., & LU, A. H. 2010. Rapid Synthesis of Nitrogen-Doped Porous Carbon Monolith for CO_2 Capture. *Advanced Materials*, 22(7), 853-857.

HAYASHI, J. I., KAZEHAYA, A., MUROYAMA, K., & WATKINSON, A. P. 2000. Preparation of activated carbon from lignin by chemical activation. *Carbon*,38(13), 1873-1878.

HAYASHI, J. I., HORIKAWA, T., TAKEDA, I., MUROYAMA, K., & NASIR ANI, F. 2002. Preparing activated carbon from various nutshells by chemical activation with K_2CO_3. Carbon, 40(13), 2381-2386.

HIMENO, S., KOMATSU, T. AND FUJITA, S., 2005. High-pressure adsorption equilibria of methane and carbon dioxide on several activated carbons. *Journal of Chemical and Engineering Data*, *50*(2), pp.369-376.

HEYDARI-GORJI, A., BELMABKHOUT, Y. & SAYARI, A., 2011. Polyethylenimine-impregnated mesoporous silica: effect of amine loading and surface alkyl chains on CO_2 adsorption. *Langmuir*, *27*(20), 12411-12416.

HONG, S.M., JANG, E., DYSART, A.D., POL, V.G. & LEE, K.B., 2016. CO_2 Capture in the Sustainable Wheat-Derived Activated Microporous Carbon Compartments. *Scientific Reports*, *6*.

HSU, L. Y., & TENG, H. 2000. Influence of different chemical reagents on the preparation of activated carbons from bituminous coal. *Fuel Processing Technology*, 64(1), 155-166.

HU, X., RADOSZ, M., CYCHOSZ, K. A., & THOMMES, M. 2011. CO_2-filling capacity and selectivity of carbon nanopores: synthesis, texture, and pore-size distribution from quenched-solid density functional theory (QSDFT). *Environmental science & technology*, 45(16), 7068-7074.

HU, Z., & VANSANT, E. F. 1995. Carbon molecular sieves produced from walnut shell. *Carbon*, 33(5), 561-567.

HULICOVA, D., YAMASHITA, J., SONEDA, Y., HATORI, H., & KODAMA, M. 2005. Supercapacitors prepared from melamine-based carbon. *Chemistry of materials*, 17(5), 1241-1247.

IBARRA, J., MOLINER, R., & PALACIOS, J. 1991. Catalytic effects of zinc chloride in the pyrolysis of Spanish high sulphur coals. *Fuel*, 70(6), 727-732.

Ioannidou, O. & Zabaniotou, A., 2007. Agricultural residues as precursors for activated carbon production-a review. *Renewable and Sustainable Energy Reviews*, *11*(9), 1966-2005.

JAGTOYEN, M. & DERBYSHIRE, F. 1998. Activated carbons from yellow poplar and white oak by H_3PO_4 activation. Carbon, 36(7-8), 1085-1097.

JANG, D. I., & PARK, S. J. 2012. Influence of nickel oxide on carbon dioxide adsorption behaviors of activated carbons. *Fuel*, 102, 439-444.

JANSEN, D., GAZZANI, M., MANZOLINI, G., VAN DIJK, E. AND CARBO, M., 2015. Pre-combustion CO_2 capture. *International Journal of Greenhouse Gas Control*, *40*, pp.167-187.

JEON, J.W., SHARMA, R., MEDURI, P., AREY, B.W., SCHAEF, H.T., LUTKENHAUS, J.L., LEMMON, J.P., THALLAPALLY, P.K., NANDASIRI, M.I., MCGRAIL, B.P. & NUNE, S.K., 2014. In situ one-step synthesis of hierarchical nitrogen-doped porous carbon for high-performance supercapacitors. *ACS applied materials & interfaces*, *6*(10), 7214-7222.

JI, Y., LI, T., ZHU, L., WANG, X., & LIN, Q. 2007. Preparation of activated carbons by microwave heating KOH activation. *Applied Surface Science*, 254(2), 506-512.

JIN, J., TANAKA, S., EGASHIRA, Y., & NISHIYAMA, N. 2010. KOH activation of ordered mesoporous carbons prepared by a soft-templating method and their enhanced electrochemical properties. *Carbon,* 48(7), 1985-1989.

KALDERIS, D., BETHANIS, S., PARASKEVA, P. & DIAMADOPOULOS, E., 2008. Production of activated carbon from bagasse and rice husk by a single-stage chemical activation method at low retention times. *Bioresource technology*, *99*(15), 6809-6816.

KAN, Y., YUE, Q., KONG, J., GAO, B. & LI, Q., 2015. The application of activated carbon produced from waste printed circuit boards (PCBs) by H_3PO_4 and steam activation for the removal of malachite green. *Chemical Engineering Journal*, *260*, 541-549.

KIM, B. J., CHO, K. S., & PARK, S. J. 2010. Copper oxide-decorated porous carbons for carbon dioxide adsorption behaviors. *Journal of colloid and interface science*, 342(2), 575-578.

KIM, S.M., LEE, J.D., LEE, H.J., LEE, E.K. AND KIM, Y., 2011. Gas hydrate formation method to capture the carbon dioxide for pre-combustion process in IGCC plant. *International journal of hydrogen energy*, 36(1), 1115-1121.

KONDO, A., KOJIMA, N., KAJIRO, H., NOGUCHI, H., HATTORI, Y., OKINO, F., MAEDA, K., OHBA, T., KANEKO, K. & KANOH, H., 2012. Gas Adsorption Mechanism and Kinetics of an Elastic Layer-Structured Metal–Organic Framework. *The Journal of Physical Chemistry C*, *116*(6), 4157-4162.

KONDURU, N., LINDNER, P.& ASSAF-ANID, N.M., 2007. Curbing the greenhouse effect by carbon dioxide adsorption with zeolite 13X. *AIChE journal*, *53*(12), 3137-3143.

KORESH, J. & SOFFER, A., 1983. Application of the two-site Langmuir isotherm to microporous adsorbents. *Journal of Colloid and Interface Science*, *92*(2), 517-524.

KOU, J. & SUN, L.B., 2016. Fabrication of nitrogen-doped porous carbons for highly efficient CO_2 capture: rational choice of a polymer precursor. *Journal of Materials Chemistry A*, *4*(44), 17299-17307.

KUMAR, K.V., PREUSS, K., LU, L., GUO, Z.X. & TITIRICI, M.M., 2015. Effect of Nitrogen Doping on the CO_2 Adsorption Behavior in Nanoporous Carbon

Structures: A Molecular Simulation Study. *The Journal of Physical Chemistry C*, *119*(39), 22310-22321.

KUMAR, P., KIM, K.H., KWON, E.E. & SZULEJKO, J.E., 2016. Metal–organic frameworks for the control and management of air quality: advances and future direction. *Journal of Materials Chemistry A*, *4*(2), 345-361.

LANNING, F.C., 1963. Silicon in rice. *Journal of agricultural and food chemistry*, *11*, 435-437.

LÁSZLÓ, K., TOMBÁCZ, E., & JOSEPOVITS, K. 2001. Effect of activation on the surface chemistry of carbons from polymer precursors. *Carbon*, 39(8), 1217-1228.

LASZLO, K., & SZŰCS, A. 2001a. Surface characterization of polyethyleneterephthalate (PET) based activated carbon and the effect of pH on its adsorption capacity from aqueous phenol and 2, 3, 4-trichlorophenol solutions. *Carbon*, 39(13), 1945-1953.

LEE, J.H., LEE, H.J., LIM, S.Y., KIM, B.G. & CHOI, J.W., 2015. Combined CO2-philicity and Ordered Mesoporosity for Highly Selective CO_2 Capture at High Temperatures. *Journal of the American Chemical Society*, *137*(22), 7210-7216.

LEE, J. S., KIM, J. H., KIM, J. T., SUH, J. K., LEE, J. M., & LEE, C. H., 2002. Adsorption equilibria of CO2 on zeolite 13X and zeolite X/activated carbon composite. *Journal of Chemical & Engineering Data*, *47*(5), 1237-1242.

LEE, S. Y., & PARK, S. J. 2013. Determination of the optimal pore size for improved CO_2 adsorption in activated carbon fibers. *Journal of colloid and interface science*, *389*(1), 230-235.

LEUNG, D.Y., CARAMANNA, G. AND MAROTO-VALER, M.M., 2014. An overview of current status of carbon dioxide capture and storage technologies. *Renewable and Sustainable Energy Reviews*, *39*, 426-443.

LEZANSKA, M., PIETRZYK, P., & SOJKA, Z. 2009. Investigations into the structure of nitrogen-containing CMK-3 and OCM-0.75 carbon replicas and the nature of surface functional groups by spectroscopic and sorption techniques. *The Journal of Physical Chemistry C*, 114(2), 1208-1216.

LI, S., KANG, E.T., NEOH, K.G., MA, Z.H., TAN, K.L. & HUANG, W., 2001. In situ XPS studies of thermally deposited potassium on poly (p-phenylene vinylene) and its ring-substituted derivatives. *Applied surface science*, *181*(3), 201-210.

LI, G., XIAO, P., WEBLEY, P., ZHANG, J., SINGH, R. & MARSHALL, M., 2008. Capture of CO2 from high humidity flue gas by vacuum swing adsorption with zeolite 13X. *Adsorption*, *14*(2-3), 415-422.

LI, M., LI, W., & LIU, S. 2011. Hydrothermal synthesis, characterization, and KOH activation of carbon spheres from glucose. *Carbohydrate research*, 346(8), 999-1004.

LI, Q., YANG, J., FENG, D., WU, Z., WU, Q., PARK, S. S., ... & ZHAO, D. 2010. Facile synthesis of porous carbon nitride spheres with hierarchical three-dimensional mesostructures for CO_2 capture. *Nano Research*, 3(9), 632-642.

LI, W., BOLLINI, P., DIDAS, S.A., CHOI, S., DRESE, J.H. & JONES, C.W. 2010a. Structural changes of silica mesocellular foam supported amine-functionalized CO_2 adsorbents upon exposure to steam. *ACS applied materials & interfaces*, *2*(11), 3363-3372.

LI, J., LU, R., DOU, B., MA, C., HU, Q., LIANG, Y., WU, F., QIAO, S. & HAO, Z. 2012. Porous graphitized carbon for adsorptive removal of benzene and the electrothermal regeneration. *Environmental science & technology*, *46*(22), 12648-12654.

LI, Z., XU, Z., TAN, X., WANG, H., HOLT, C. M., STEPHENSON, T., ... & MITLIN, D. 2013. Mesoporous nitrogen-rich carbons derived from protein for ultra-high capacity battery anodes and supercapacitors. *Energy & Environmental Science*, 6(3), 871-878.

LIANG, T., CHEN, C., LI, X. & ZHANG, J. 2016. Popcorn-Derived Porous Carbon for Energy Storage and CO_2 Capture. *Langmuir*, *32*(32), 8042-8049.

LILLO-RÓDENAS, M. A., LOZANO-CASTELLÓ, D., CAZORLA-AMORÓS, D., & LINARES-SOLANO, A. 2001. Preparation of activated carbons from Spanish anthracite: II. Activation by NaOH. *Carbon*, *39*(5), 751-759.

LILLO-RÓDENAS, M. A., CAZORLA-AMORÓS, D., & LINARES-SOLANO, A. 2003. Understanding chemical reactions between carbons and NaOH and KOH: an insight into the chemical activation mechanism. *Carbon*, 41(2), 267-275.

LILLO-RÓDENAS, M. A., JUAN-JUAN, J., CAZORLA-AMORÓS, D., & LINARES-SOLANO, A. 2004. About reactions occurring during chemical activation with hydroxides. *Carbon*, 42(7), 1371-1375.

LILLO-RÓDENAS, M. A., MARCO-LOZAR, J. P., CAZORLA-AMORÓS, D., & LINARES-SOLANO, A. 2007. Activated carbons prepared by pyrolysis of mixtures of carbon precursor/alkaline hydroxide. *Journal of analytical and applied pyrolysis*, 80(1), 166-174.

LINARES-SOLANO, A. 2001. Preparation of activated carbons from Spanish anthracite: I. Activation by KOH. *Carbon*, 39(5), 741-749.LIU, L., DENG, Q. F., HOU, X. X., & YUAN, Z. Y. 2012. User-friendly synthesis of nitrogen-containing polymer and microporous carbon spheres for efficient CO_2 capture. *Journal of Materials Chemistry*, 22(31), 15540-15548.

LIPPENS, B.C. & DE BOER, J.H., 1965. Studies on pore systems in catalysts: V. The t method. *Journal of Catalysis*, *4*(3), 319-323.

LIU, J., WANG, Y., BENIN, A.I., JAKUBCZAK, P., WILLIS, R.R. & LEVAN, M.D., 2010. CO_2/H_2O adsorption equilibrium and rates on metal-organic frameworks: HKUST-1 and Ni/DOBDC. *Langmuir*, *26*(17), 14301-14307.

LIU, L., DENG, Q.F., HOU, X.X. & YUAN, Z.Y., 2012. User-friendly synthesis of nitrogen-containing polymer and microporous carbon spheres for efficient CO_2 capture. *Journal of Materials Chemistry*, *22*(31), 15540-15548.

LIU, Z., DU, Z., SONG, H., WANG, C., SUBHAN, F., XING, W. & YAN, Z., 2014. The fabrication of porous N-doped carbon from widely available urea formaldehyde resin for carbon dioxide adsorption. *Journal of colloid and interface science*, *416*, 124-132.

LIU, J., SUN, N., SUN, C., LIU, H., SNAPE, C., LI, K., WEI, W. & SUN, Y., 2015. Spherical potassium intercalated activated carbon beads for pulverised fuel CO_2 post-combustion capture. *Carbon*, *94*, 243-255.

LIU, X., SUN, Y., LIU, J., SUN, C., LIU, H., XUE, Q., SMITH, E. AND SNAPE, C. 2017. Potassium and zeolitic structure modified ultra-microporous adsorbent materials from a renewable feedstock with favorable surface chemistry for CO_2 capture. ACS Applied Materials & Interfaces, 9(32), 26826-26839.

LOTA, G., CENTENO, T. A., FRACKOWIAK, E., & STOECKLI, F. 2008. Improvement of the structural and chemical properties of a commercial activated carbon for its application in electrochemical capacitors. *Electrochimica Acta*, 53(5), 2210-2216.

LOWELL, S., SHIELDS, J.E., THOMAS, M.A. & THOMMES, M., 2012. *Characterization of porous solids and powders: surface area, pore size and density* (Vol. 16). Springer Science & Business Media.

LOZANO-CASTELLO, D., LILLO-RODENAS, M. A., CAZORLA-AMORÓS, D., & LINARES-SOLANO, A. (2001). Preparation of activated carbons from Spanish anthracite: I. Activation by KOH. *Carbon*, 39(5), 741-749.

LU, A. H., & ZHENG, J. T. 2002. Microstructures of PAN-ACF modified by catalytic benzene deposition. *Carbon*, 40(8), 1353-1361.

LU, A., KIEFER, A., SCHMIDT, W., & SCHÜTH, F. 2004. Synthesis of polyacrylonitrile-based ordered mesoporous carbon with tunable pore structures. *Chemistry of materials*, 16(1), 100-103.

LU, W., YUAN, D., SCULLEY, J., ZHAO, D., KRISHNA, R., & ZHOU, H. C. 2011. Sulfonate-grafted porous polymer networks for preferential CO_2 adsorption at low pressure. *Journal of the American Chemical Society*, 133(45), 18126-18129.

LU, W., SCULLEY, J.P., YUAN, D., KRISHNA, R., WEI, Z. & ZHOU, H.C., 2012. Polyamine-Tethered Porous Polymer Networks for Carbon Dioxide Capture from Flue Gas. *Angewandte Chemie International Edition*, *51*(30), 7480-7484.

LUDWINOWICZ, J. & JARONIEC, M., 2015. Potassium salt-assisted synthesis of highly microporous carbon spheres for CO_2 adsorption. *Carbon*, *82*, pp.297-303.

LV, Y., GAN, L., LIU, M., XIONG, W., XU, Z., ZHU, D., & WRIGHT, D. S. 2012. A self-template synthesis of hierarchical porous carbon foams based on banana peel for supercapacitor electrodes. *Journal of Power Sources*, 209, 152-157.

MA, X., CAO, M. & HU, C., 2013. Bifunctional HNO_3 catalytic synthesis of N-doped porous carbons for CO_2 capture. *Journal of Materials Chemistry A*, *1*(3), 913-918.

MA, X., LI, Y., CAO, M. & HU, C., 2014. A novel activating strategy to achieve highly porous carbon monoliths for CO_2 capture. *Journal of Materials Chemistry A*, *2*(13), pp.4819-4826.

MACDOWELL, N., FLORIN, N., BUCHARD, A., HALLETT, J., GALINDO, A., JACKSON, G., ADJIMAN, C.S., WILLIAMS, C.K., SHAH, N. & FENNELL, P., 2010. An overview of CO_2 capture technologies. *Energy & Environmental Science*, *3*(11), 1645-1669.

MAJCHRZAK-KUCĘBA, I., & NOWAK, W. 2005. A thermogravimetric study of the adsorption of CO_2on zeolites synthesized from fly ash. *Thermochimica acta*, 437(1), 67-74.

MASEL, R.I., 1996. *Principles of adsorption and reaction on solid surfaces* (Vol. 3). John Wiley & Sons.

MASON, J.A., SUMIDA, K., HERM, Z.R., KRISHNA, R. & LONG, J.R., 2011. Evaluating metal–organic frameworks for post-combustion carbon dioxide capture via temperature swing adsorption. *Energy & Environmental Science*, *4*(8), 3030-3040.

MARSH, H., YAN, D. S., O'GRADY, T. M., & WENNERBERG, A. 1984. Formation of active carbons from cokes using potassium hydroxide. *Carbon*, 22(6), 603-611.

MARTIN-CALVO, A., PARRA, J.B., ANIA, C.O. & CALERO, S., 2014. Insights on the anomalous adsorption of carbon dioxide in LTA zeolites. *The Journal of Physical Chemistry C*, *118*(44), 25460-25467.

MCKEE, D. W. 1983. Mechanisms of the alkali metal catalysed gasification of carbon. *Fuel*, *62*(2), 170-175.

MCDONALD, T. M., LEE, W. R., MASON, J. A., WIERS, B. M., HONG, C. S., & LONG, J. R. 2012. Capture of carbon dioxide from air and flue gas in the

alkylamine-appended metal–organic framework mmen-Mg_2(dobpdc). *Journal of the American Chemical Society*, 134(16), 7056-7065.

MENG, L., & PARK, S. 2012. Investigation of narrow pore size distribution on carbon dioxide capture of nanoporous carbons. *Bull Korean Chem Soc*, 33, 3749-3754.

MENG, L.Y., MENG, W., CHEN, T. & JIN, L.Y., 2014. CO_2 Adsorption capacity of activated N-doping porous carbons prepared from graphite nanofibers/polypyrrole. *Journal of Applied Polymer Science*, *131*(15).

MESQUITA, J. P., & SAPAG, K. 2009. Preparation of activated carbons from coffee husks utilizing $FeCl_3$ and $ZnCl_2$ as activating agents. *Journal of Hazardous Materials*, 165(1), 87-94.

MILLER, M.L. & LINTON, R.W., 1985. X-ray photoelectron spectroscopy of thermally treated silica (SiO_2) surfaces. *Analytical Chemistry*, *57*(12), 2314-2319.

MISHRA, A. K., & RAMAPRABHU, S. 2011. Carbon dioxide adsorption in graphene sheets. *AIP Advances*, 1(3), 032152.

MORENO-CASTILLA, C., LOPEZ-RAMON, M. V., & CARRASCO-MARIN, F. 2000. Changes in surface chemistry of activated carbons by wet oxidation.*Carbon*, 38(14), 1995-2001.

MONDAL, M.K., BALSORA, H.K., & VARSHNEY, P., 2012. Progress and trends in CO_2 capture/separation technologies: a review. *Energy*, 46(1), 431-441.

MORRIS, R.E. & WHEATLEY, P.S., 2008. Gas storage in nanoporous materials. *Angewandte Chemie International Edition*, *47*(27), 4966-4981.

MOULDER, J.F., STICKLE, W.F., SOBOL, P.E. & BOMBEN, K.D., 1992. *Handbook of X-ray Photoelectron Spectroscopy*; Perkin-Elmer: Eden Prairie, MN.

NANDI, S., DE LUNA, P., DAFF, T.D., ROTHER, J., LIU, M., BUCHANAN, W., HAWARI, A.I., WOO, T.K. & VAIDHYANATHAN, R., 2015. A single-ligand ultra-microporous MOF for precombustion CO_2 capture and hydrogen purification. *Science advances*, *1*(11), e1500421.

OKADA, K., YAMAMOTO, N., KAMESHIMA, Y., & YASUMORI, A. 2003. Porous properties of activated carbons from waste newspaper prepared by chemical and physical activation. *Journal of colloid and interface science*, 262(1), 179-193.

OLAJIRE, A.A., 2010. CO_2 capture and separation technologies for end-of-pipe applications–a review. *Energy*, 35(6), 2610-2628.

OLIVEIRA, L. C., PEREIRA, E., GUIMARAES, I. R., VALLONE, A., PEREIRA, M., OTAKE, Y., & JENKINS, R. G. 1993. Characterization of oxygen-containing surface complexes created on a microporous carbon by air and nitric acid treatment. *Carbon*, 31(1), 109-121.

OLIVIER, J.G., JANSSENS-MAENHOUT, G., MUNTEAN, M., PETERS, J.A., 2016. Trends in global CO_2 emissions 2016 report.

OTOWA, T., TANIBATA, R., & ITOH, M. 1993. Production and adsorption characteristics of MAXSORB: high-surface-area active carbon. *Gas separation & purification*, 7(4), 241-245.

PARAKNOWITSCH, J.P. & THOMAS, A. 2013. Doping carbons beyond nitrogen: an overview of advanced heteroatom doped carbons with boron, sulphur and phosphorus for energy applications. *Energy & Environmental Science*, *6*(10), 2839-2855.

PARK, S. J., & JUNG, W. Y. 2002. Effect of KOH activation on the formation of oxygen structure in activated carbons synthesized from polymeric precursor. *Journal of colloid and interface science*, 250(1), 93-98.

PATEL, H.A., JE, S.H., PARK, J., CHEN, D.P., JUNG, Y., YAVUZ, C.T. & COSKUN, A., 2013. Unprecedented high-temperature CO_2 selectivity in N_2-phobic nanoporous covalent organic polymers. *Nature communications*, *4*, 1357.

PARSHETTI, G.K., CHOWDHURY, S. & BALASUBRAMANIAN, R., 2015. Biomass derived low-cost microporous adsorbents for efficient CO_2 capture. *Fuel*, *148*, 246-254.

PELS, J. R., KAPTEIJN, F., MOULIJN, J. A., ZHU, Q., & THOMAS, K. M. 1995. Evolution of nitrogen functionalities in carbonaceous materials during pyrolysis. *Carbon*, 33(11), 1641-1653.

PETROLEUM, B., 2014. *BP energy outlook 2035*. BP stats, Jan.

PEVIDA, C., PLAZA, M. G., ARIAS, B., FERMOSO, J., RUBIERA, F., & PIS, J. J. 2008. Surface modification of activated carbons for CO_2 capture. *Applied Surface Science*, 254(22), 7165-7172.

PEVIDA, C., DRAGE, T.C. AND SNAPE, C.E., 2008. Silica-templated melamine–formaldehyde resin derived adsorbents for CO_2 capture. *Carbon*, *46*(11), 1464-1474.

PIRNGRUBER, G.D., RAYBAUD, P., BELMABKHOUT, Y., ČEJKA, J. & ZUKAL, A., 2010. The role of the extra-framework cations in the adsorption of CO_2 on faujasite Y. *Physical Chemistry Chemical Physics*, *12*(41), 13534-13546.

PLAZA, M. G., THURECHT, K. J., PEVIDA, C., RUBIERA, F., PIS, J. J., SNAPE, C. E., & DRAGE, T. C. 2013. Influence of oxidation upon the CO_2 capture performance of a phenolic-resin-derived carbon. *Fuel Processing Technology*, 110, 53-60.

PLAZA, M. G., PEVIDA, C., ARIAS, B., FERMOSO, J., RUBIERA, F., & PIS, J. J. (2009). A comparison of two methods for producing CO_2 capture adsorbents. *Energy Procedia*, 1(1), 1107-1113.

PLAZA, M.G., RUBIERA, F., PIS, J.J. & PEVIDA, C., 2010. Ammoxidation of carbon materials for CO_2 capture. *Applied Surface Science*, *256*(22), 6843-6849.

PLAZA, M.G., GONZÁLEZ, A.S., PIS, J.J., RUBIERA, F. & PEVIDA, C., 2014. Production of microporous biochars by single-step oxidation: Effect of activation conditions on CO_2 capture. *Applied Energy*, *114*, 551-562.

PRESSER, V., MCDONOUGH, J., YEON, S. H., & GOGOTSI, Y. 2011. Effect of pore size on carbon dioxide sorption by carbide derived carbon. *Energy & Environmental Science*, 4(8), 3059-3066.

PULIDO, A., NACHTIGALL, P., ZUKAL, A., DOMÍNGUEZ, I. & ČEJKA, J., 2009. Adsorption of CO_2 on sodium-exchanged ferrierites: the bridged CO_2 complexes formed between two extra framework cations. *The Journal of Physical Chemistry C*, *113*(7), pp.2928-2935.

PURI, B. R., & WALKER JR, P. L. 1970. Chemistry and physics of carbon. *Vol. 6Marcel Dekker, New York*, 191.

QIU, H., LV, L., PAN, B.C., ZHANG, Q.J., ZHANG, W.M. & ZHANG, Q.X., 2009. Critical review in adsorption kinetic models. *Journal of Zhejiang University-Science A*, *10*(5), 716-724.

RAAB, C.G.D.I.R., 1998. Measurement of the electric quadrupole moments of CO2, CO, N2, Cl2 and BF3. *Molecular Physics*, *93*(1), 49-56.

RAHMAN, F.A., AZIZ, M.M.A., SAIDUR, R., BAKAR, W.A.W.A., HAININ, M.R., PUTRAJAYA, R. & HASSAN, N.A., 2017. Pollution to solution: Capture and sequestration of carbon dioxide (CO_2) and its utilization as a renewable energy source for a sustainable future. *Renewable and Sustainable Energy Reviews*, 71, 112-126.

RAYMUNDO-PINERO, E., AZAIS, P., CACCIAGUERRA, T., CAZORLA-AMORÓS, D., LINARES-SOLANO, A., & BÉGUIN, F. 2005. KOH and NaOH activation mechanisms of multiwalled carbon nanotubes with different structural organisation. *Carbon*, 43(4), 786-795.

REED, A.R. AND WILLIAMS, P.T. 2004. Thermal processing of biomass natural fibre wastes by pyrolysis. *International Journal of Energy Research*, 28(2), 131-145.

REGE, S.U., YANG, R.T. & BUZANOWSKI, M.A., 2000. Sorbents for air prepurification in air separation. *Chemical Engineering Science*, *55*(21), 4827-4838.

RODRIGUEZ-REINOSO, F., & MOLINA-SABIO, M. 1992. Activated carbons from lignocellulosic materials by chemical and/or physical activation: an overview. *Carbon*, 30(7), 1111-1118.

RODRIGUEZ-RAMOS, I., & RODRIGUEZ-REINOSO, F. 1988. The adsorption of N 2 and CO 2 on PAN carbons. *Carbon*, 26(6), 905-906.

ROMANOS, J., BECKNER, M., RASH, T., FIRLEJ, L., KUCHTA, B., YU, P., ... & PFEIFER, P. 2012. Nanospace engineering of KOH activated carbon. *Nanotechnology*, 23(1), 015401.

RUFFORD, T. E., ZHU, J., & HULICOVA-JURCAKOVA, D. (Eds.). 2014. *Green Carbon Materials: Advances and Applications*. CRC Press.

ROCHELLE, G.T., 2009. Amine scrubbing for CO2 capture. *Science*, 325(5948), 1652-1654.

SAIDUR, R., ABDELAZIZ, E. A., DEMIRBAS, A., HOSSAIN, M. S., & MEKHILEF, S. 2011. A review on biomass as a fuel for boilers. *Renewable and sustainable energy reviews*, 15(5), 2262-2289.

SAMANTA, A., ZHAO, A., SHIMIZU, G.K., SARKAR, P. & GUPTA, R., 2011. Post-combustion CO2 capture using solid sorbents: a review. *Industrial & Engineering Chemistry Research*, *51*(4), 1438-1463.

SÁNCHEZ-SÁNCHEZ, A., SUÁREZ-GARCÍA, F., MARTÍNEZ-ALONSO, A., & TASCÓN, J. M. 2014. Influence of porous texture and surface chemistry on the CO2 adsorption capacity of porous carbons: acidic and basic site interactions. *ACS applied materials & interfaces*, 6(23), 21237-21247.

SANZ-PÉREZ, E.S., ARENCIBIA, A., SANZ, R. & CALLEJA, G., 2016. New developments on carbon dioxide capture using amine-impregnated silicas. *Adsorption*, *22*(4-6), 609-619.

SAYARI, A. BELMABKHOUT, Y., 2010. Stabilization of amine-containing CO_2 adsorbents: dramatic effect of water vapor. *Journal of the American Chemical Society*, *132*(18), 6312-6314.

SCHOEDEL, A., JI, Z. AND YAGHI, O.M., 2016. The role of metal–organic frameworks in a carbon-neutral energy cycle. *Nature Energy*, 1, 16034.

SEBBAHI, S., AHMIDO, A., KIFANI-SAHBAN, F., EL HAJJAJI, S. & ZOULALIAN, A., 2014. Preoxidation and Activation of the Lignin Char: Carbonization and Oxidation Procedures. *Journal of Engineering*, *2014*.

SETHIA, G. & SAYARI, A., 2015. Comprehensive study of ultra-microporous nitrogen-doped activated carbon for CO_2 capture. *Carbon*, *93*, 68-80.

SEVILLA, M., & FUERTES, A. B. 2011a. Sustainable porous carbons with a superior performance for CO 2 capture. *Energy & Environmental Science*, 4(5), 1765-1771.

SEVILLA, M., PARRA, J.B. & FUERTES, A.B., 2013. Assessment of the role of micropore size and N-doping in CO_2 capture by porous carbons. *ACS applied materials & interfaces*, 5(13), 6360-6368.

SEVILLA, M., VALLE-VIGÓN, P., & FUERTES, A. B. 2011. N-Doped Polypyrrole-Based Porous Carbons for CO_2 Capture. *Advanced Functional Materials*, 21(14), 2781-2787.

SEVILLA, M., & FUERTES, A. B. 2012. CO_2 adsorption by activated templated carbons. *Journal of colloid and interface science*, 366(1), 147-154.

SHAFEEYAN, M. S., DAUD, W. M. A. W., HOUSHMAND, A., & SHAMIRI, A. 2010. A review on surface modification of activated carbon for carbon dioxide adsorption. *Journal of analytical and applied pyrolysis*, 89(2), 143-151.

SHAO, X., FENG, Z., XUE, R., MA, C., WANG, W., PENG, X., & CAO, D. 2011. Adsorption of CO_2, CH_4, CO_2/N_2 and CO_2/CH_4 in novel activated carbon beads: preparation, measurements and simulation. *AIChE Journal*, 57(11), 3042-3051.

SHCHUKAREV, A. & KOROLKOV, D., 2004. XPS study of group IA carbonates. *Open Chemistry*, *2*(2), 347-362.

SHEKHAH, O., BELMABKHOUT, Y., CHEN, Z., GUILLERM, V., CAIRNS, A., ADIL, K. & EDDAOUDI, M., 2014. Made-to-order metal-organic frameworks for trace carbon dioxide removal and air capture. *Nature communications*, *5*.

SHEN, W., LI, Z., & LIU, Y. 2008. Surface chemical functional groups modification of porous carbon. *Recent Patents on Chemical Engineering*, 1(1), 27-40.

SHEN, Z., & XUE, R. 2003. Preparation of activated mesocarbon microbeads with high mesopore content. *Fuel processing technology*, 84(1), 95-103.

SHEN, W. & FAN, W., 2013. Nitrogen-containing porous carbons: synthesis and application. *Journal of Materials Chemistry A*, *1*(4), 999-1013.

SHRESTHA, S., & MUSTAIN, W. E. 2010. Properties of nitrogen-functionalized ordered mesoporous carbon prepared using polypyrrole precursor. *Journal of The Electrochemical Society*, 157(11), B1665-B1672.

SMITH, D.M., HUA, D.W. & EARL, W.L., 1994. Characterization of Porous Solids. *MRS Bulletin*, *19*(04), 44-48.

SING, K.S.W., 1982. Reporting physisorption data for gas/solid systems with special reference to the determination of surface area and porosity (Provisional). Pure and applied chemistry, 54(11), 2201-2218.

SING, K. S. 1985. Reporting physisorption data for gas/solid systems with special reference to the determination of surface area and porosity (Recommendations 1984). *Pure and applied chemistry*, 57(4), 603-619.

SIVADAS, D.L., VIJAYAN, S., RAJEEV, R., NINAN, K.N. & PRABHAKARAN, K., 2016. Nitrogen-enriched microporous carbon derived from sucrose and urea with superior CO_2 capture performance. *Carbon*, *109*, 7-18.

SNOEYINK, V. L., & WEBER, W. J. 1967. The surface chemistry of active carbon; a discussion of structure and surface functional groups. *Environmental Science & Technology*, 1(3), 228-234.

STANGER, R., WALL, T., SPOERL, R., PANERU, M., GRATHWOHL, S., WEIDMANN, M., SCHEFFKNECHT, G., MCDONALD, D., MYÖHÄNEN, K., RITVANEN, J. & RAHIALA, S., 2015. Oxyfuel combustion for CO_2 capture in power plants. *International Journal of Greenhouse Gas Control*, 40, 55-125.

SOMY, A., MEHRNIA, M. R., AMREI, H. D., GHANIZADEH, A., & SAFARI, M. 2009. Adsorption of carbon dioxide using impregnated activated carbon promoted by Zinc. *International Journal of Greenhouse Gas Control*, 3(3), 249-254.

SONG, X., ZHANG, Y., & CHANG, C. 2012. Novel method for preparing activated carbons with high specific surface area from rice husk. *Industrial & Engineering Chemistry Research*, 51(46), 15075-15081.

SONG, J., SHEN, W., WANG, J. & FAN, W., 2014. Superior carbon-based CO_2 adsorbents prepared from poplar anthers. *Carbon*, *69*, 255-263.

SPIGARELLI, B.P. AND KAWATRA, S.K., 2013. Opportunities and challenges in carbon dioxide capture. *Journal of CO_2 Utilization*, 1, 69-87.

STIPP, S.L. & HOCHELLA, M.F., 1991. Structure and bonding environments at the calcite surface as observed with X-ray photoelectron spectroscopy (XPS) and low energy electron diffraction (LEED). *Geochimica et Cosmochimica Acta*, *55*(6), 1723-1736.

SUMIDA, K., ROGOW, D.L., MASON, J.A., MCDONALD, T.M., BLOCH, E.D., HERM, Z.R., BAE, T.H. &LONG, J.R., 2011. Carbon dioxide capture in metal–organic frameworks. *Chemical reviews*, 112(2), 724-781.

SUN, L., WANG, C., ZHOU, Y., ZHAO, Q., ZHANG, X., & QIU, J. 2014. Activated nitrogen-doped carbons from polyvinyl chloride for high-performance electrochemical capacitors. *Journal of Solid State Electrochemistry*, 18(1), 49-58.

SUN, N., SUN, C., LIU, H., LIU, J., STEVENS, L., DRAGE, T., ... & SUN, Y. 2013. Synthesis, characterization and evaluation of activated spherical carbon materials for CO_2 capture. *Fuel*, 113, 854-862.

SUN, N., SUN, C., LIU, J., LIU, H., SNAPE, C.E., LI, K., WEI, W. & SUN, Y. 2015. Surface-modified spherical activated carbon materials for pre-combustion carbon dioxide capture. *RSC Advances*, 5(42), 33681-33690.

TENG, H., YEH, T.S. & HSU, L.Y., 1998. Preparation of activated carbon from bituminous coal with phosphoric acid activation. *Carbon*, *36*(9), 1387-1395.

TENG, H., & WANG, S. C. 2000. Influence of oxidation on the preparation of porous carbons from phenol-formaldehyde resins with KOH activation. *Industrial & engineering chemistry research*, 39(3), 673-678.

TENG, H., WANG, S. C. 2000a. Preparation of porous carbons from phenol–formaldehyde resins with chemical and physical activation. *Carbon*, 38(6), 817-824.

THEO, W.L., LIM, J.S., HASHIM, H., MUSTAFFA, A.A. & HO, W.S., 2016. Review of pre-combustion capture and ionic liquid in carbon capture and storage. *Applied Energy*, 183, 1633-1663.

TIAN, X., SU, F., & ZHAO, X. S. 2008. Sulfonated polypyrrole nanospheres as a solid acid catalyst. *Green Chemistry*, 10(9), 951-956.

TO, J.W., HE, J., MEI, J., HAGHPANAH, R., CHEN, Z., KUROSAWA, T., CHEN, S., BAE, W.G., PAN, L., TOK, J.B.H. & WILCOX, J., 2016. Hierarchical N-doped carbon as CO_2 adsorbent with high CO_2 selectivity from rationally designed polypyrrole precursor. *Journal of the American Chemical Society*, *138*(3), 1001-1009.

TOFTEGAARD, M.B., BRIX, J., JENSEN, P.A., GLARBORG, P. AND JENSEN, A.D., 2010. Oxy-fuel combustion of solid fuels. *Progress in energy and combustion science*, *36*(5), pp.581-625.

TRAVIS, W., GADIPELLI, S. GUO, Z., 2015. Superior CO_2 adsorption from waste coffee ground derived carbons. *RSC Advances*, *5*(37), 29558-29562.

TSAI, W. T., CHANG, C. Y., & LEE, S. L. 1998. A low cost adsorbent from agricultural waste corn cob by zinc chloride activation. *Bioresource Technology*, 64(3), 211-217.

TSENG, R. L., & TSENG, S. K. 2005. Pore structure and adsorption performance of the KOH-activated carbons prepared from corncob. *Journal of Colloid and Interface Science*, 287(2), 428-437.

TSENG, R. L. 2007. Physical and chemical properties and adsorption type of activated carbon prepared from plum kernels by NaOH activation. *Journal of hazardous materials*, 147(3), 1020-1027.

UKÁYU, S., HOÁKIM, S., SEOBÁYOON, Y., YOUNGÁKIM, D., & HYUNÁKWON, A. 2012. Highly selective CO2 capture on N-doped carbon produced by chemical activation of polypyrrole functionalized graphene sheets. *Chemical communications*, 48(5), 735-737.

VALENZANO, L., CIVALLERI, B., CHAVAN, S., PALOMINO, G.T., AREÁN, C.O. & BORDIGA, S., 2010. Computational and Experimental Studies on the

Adsorption of CO, N_2, and CO_2 on Mg-MOF-74. *The Journal of Physical Chemistry C*, *114*(25), 11185-11191.

VAN DER ZWAAN, B., & GERLAGH, R. 2009. Economics of geological CO_2 storage and leakage. *Climatic change*, 93(3-4), 285-309.

VAN DER HEIDE, P., 2011. *X-ray photoelectron spectroscopy: an introduction to principles and practices*. John Wiley & Sons.

VARGAS, D. P., GIRALDO, L., & MORENO-PIRAJÁN, J. C. 2012. CO_2 adsorption on activated carbon honeycomb-monoliths: A comparison of Langmuir and Toth models. *International journal of molecular sciences*, 13(7), 8388-8397.

WAHBY, A., SILVESTRE-ALBERO, J., SEPÚLVEDA-ESCRIBANO, A., & RODRÍGUEZ-REINOSO, F. 2012. CO_2 adsorption on carbon molecular sieves. *Microporous and Mesoporous Materials*, 164, 280-287.

WAHBY, A., RAMOS-FERNÁNDEZ, J. M., MARTÍNEZ-ESCANDELL, M., SEPÚLVEDA-ESCRIBANO, A., SILVESTRE-ALBERO, J., & RODRÍGUEZ-REINOSO, F. 2010. High-Surface-Area carbon molecular sieves for selective CO_2 adsorption. *ChemSusChem*, 3(8), 974-981.

WALL, T.F., 2007. Combustion processes for carbon capture. *Proceedings of the combustion institute*, 31(1), 31-47.

WAN, L., WANG, J., FENG, C., SUN, Y. & LI, K., 2015. Synthesis of polybenzoxazine based nitrogen-rich porous carbons for carbon dioxide capture. *Nanoscale*, *7*(15), 6534-6544.

WANG, H., GAO, Q., & HU, J. 2009. High hydrogen storage capacity of porous carbons prepared by using activated carbon. *Journal of the American Chemical Society*, 131(20), 7016-7022.

WANG, Q., LUO, J., ZHONG, Z. & BORGNA, A., 2011. CO_2 capture by solid adsorbents and their applications: current status and new trends. *Energy & Environmental Science*, *4*(1), 42-55.

WANG, L. & YANG, R.T., 2011. Significantly increased CO_2 adsorption performance of nanostructured templated carbon by tuning surface area and nitrogen doping. *The Journal of Physical Chemistry C*, *116*(1), 1099-1106.

WANG, W., MARTIN, J.C., FAN, X., HAN, A., LUO, Z. AND SUN, L. 2012. Silica nanoparticles and frameworks from rice husk biomass. *ACS applied materials & interfaces*, 4(2), 977-981.

WANG, J., HUANG, L., YANG, R., ZHANG, Z., WU, J., GAO, Y., WANG, Q., O'HARE, D. & ZHONG, Z., 2014. Recent advances in solid sorbents for CO_2 capture and new development trends. *Energy & Environmental Science*, *7*(11), 3478-3518.

WANG, J., & KASKEL, S. 2012. KOH activation of carbon-based materials for energy storage. *Journal of Materials Chemistry*, 22(45), 23710-23725.

WANG, W., MARTIN, J.C., FAN, X., HAN, A., LUO, Z. & SUN, L., 2012a. Silica nanoparticles and frameworks from rice husk biomass. *ACS applied materials & interfaces*, *4*(2), 977-981.

WANG, Y., SU, F., WOOD, C. D., LEE, J. Y., & ZHAO, X. S. 2008. Preparation and characterization of carbon nanospheres as anode materials in lithium-ion secondary batteries. *Industrial & Engineering Chemistry Research*, 47(7), 2294-2300.

WEI, H., DENG, S., HU, B., CHEN, Z., WANG, B., HUANG, J., & YU, G. 2012. Granular Bamboo-Derived Activated Carbon for High CO_2 Adsorption: The Dominant Role of Narrow Micropores. *ChemSusChem*, 5(12), 2354-2360.

WEI, J., ZHOU, D., SUN, Z., DENG, Y., XIA, Y. & ZHAO, D., 2013. A controllable synthesis of rich nitrogen-doped ordered mesoporous carbon for CO_2 capture and supercapacitors. *Advanced Functional Materials*, *23*(18), 2322-2328.

WENNERBERG, A. N., & O'GRADY, T. M. 1978. *U.S. Patent No. 4,082,694*. Washington, DC: U.S. Patent and Trademark Office.

WICKRAMARATNE, N. P., & JARONIEC, M. 2013a. Importance of small micropores in CO_2 capture by phenolic resin-based activated carbon spheres. *Journal of Materials Chemistry A*, 1(1), 112-116.

WICKRAMARATNE, N. P., & JARONIEC, M. 2013b. Activated carbon spheres for CO_2 adsorption. *ACS applied materials & interfaces*, 5(5), 1849-1855.

WICKRAMARATNE, N. P., XU, J., WANG, M., ZHU, L., DAI, L., & JARONIEC, M. 2014. Nitrogen enriched porous carbon spheres: Attractive materials for supercapacitor electrodes and CO_2 adsorption. *Chemistry of Materials*,26(9), 2820-2828.

WILSON, S.T., LOK, B.M., MESSINA, C.A., CANNAN, T.R. & FLANIGEN, E.M., 1982. Aluminophosphate molecular sieves: a new class of microporous crystalline inorganic solids. *Intrazeolite Chemistry*, 79-106

World Energy Outlook Special Report 2015: Energy and Climate Change. International Energy Agency (IEA), 2015.

WU, F. C., TSENG, R. L., & JUANG, R. S. 2005. Comparisons of porous and adsorption properties of carbons activated by steam and KOH. *Journal of colloid and interface science*, 283(1), 49-56.

WU, M., ZHA, Q., QIU, J., GUO, Y., SHANG, H., & YUAN, A. 2004. Preparation and characterization of porous carbons from PAN-based preoxidized cloth by KOH activation. *Carbon*, 42(1), 205-210.

XIA, Y., MOKAYA, R., WALKER, G.S. AND ZHU, Y., 2011. Superior CO_2 Adsorption Capacity on N-doped, High-Surface-Area, Microporous Carbons Templated from Zeolite. *Advanced Energy Materials*, *1*(4), 678-683.

XIANG, S., HE, Y., ZHANG, Z., WU, H., ZHOU, W., KRISHNA, R. & CHEN, B., 2012. Microporous metal-organic framework with potential for carbon dioxide capture at ambient conditions. *Nature communications*, *3*, 954.

XING, W., LIU, C., ZHOU, Z., ZHANG, L., ZHOU, J., ZHUO, S., ... & QIAO, S. Z. 2012. Superior CO_2 uptake of N-doped activated carbon through hydrogen-bonding interaction. *Energy & Environmental Science*, 5(6), 7323-7327.

XING, W., LIU, C., ZHOU, Z., ZHOU, J., WANG, G., ZHUO, S., ... & YAN, Z. 2014. Oxygen-containing functional group-facilitated CO_2 capture by carbide-derived carbons. *Nanoscale research letters*, 9(1), 1-8.

XU, R., PANG, W., YU, J., HUO, Q. & CHEN, J., 2009. *Chemistry of zeolites and related porous materials: synthesis and structure*. John Wiley & Sons.

YAHYA, M.A., AL-QODAH, Z. & NGAH, C.Z., 2015. Agricultural bio-waste materials as potential sustainable precursors used for activated carbon production: a review. *Renewable and Sustainable Energy Reviews*, *46*, 218-235.

YAMASHITA, Y., & OUCHI, K. 1982. Influence of alkali on the carbonization process—II: Carbonization of various coals and asphalt with NaOH. *Carbon*,20(1), 47-53.

YAMASHITA, Y., & OUCHI, K. 1982. Influence of alkali on the carbonization process—II: Carbonization of various coals and asphalt with NaOH. *Carbon*,20(1), 47-53.

YANG, S., HU, H. & CHEN, G., 2002. Preparation of carbon adsorbents with high surface area and a model for calculating surface area. *Carbon*, *40*(3), 277-284.

YANG, H., XU, Z., FAN, M., GUPTA, R., SLIMANE, R.B., BLAND, A.E. & WRIGHT, I., 2008. Progress in carbon dioxide separation and capture: A review. *Journal of environmental sciences*, 20(1), 14-27.

YANG, M., GUO, L., HU, G., HU, X., XU, L., CHEN, J., DAI, W. & FAN, M., 2015. Highly cost-effective nitrogen-doped porous coconut shell-based CO_2 sorbent synthesized by combining ammoxidation with KOH activation. *Environmental science & technology*, *49*(11), pp.7063-7070.

YEON, J.S., LEE, W.R., KIM, N.W., JO, H., LEE, H., SONG, J.H., LIM, K.S., KANG, D.W., SEO, J.G., MOON, D. & WIERS, B., 2015. Homodiamine-functionalized metal–organic frameworks with a MOF-74-type extended structure for superior selectivity of CO_2 over N_2. *Journal of Materials Chemistry A*, *3*(37), 19177-19185.

YELETSKY, P. M., YAKOVLEV, V. A., MEL'GUNOV, M. S., PARMON, V. N., 2015. Synthesis of mesoporous carbons by leaching out natural silica templates of rice husk. *Micropor. Mesopor. Mat.*, *121*, 34-40.

YIN, G., LIU, Z., LIU, Q., & WU, W. 2013. The role of different properties of activated carbon in CO_2 adsorption. *Chemical Engineering Journal*, 230, 133-140.

ZHANG, L., XU, C. C., & CHAMPAGNE, P. 2010. Overview of recent advances in thermo-chemical conversion of biomass. *Energy Conversion and Management*, *51*(5), 969-982.

ZHANG, Z., ZHOU, J., XING, W., XUE, Q., YAN, Z., ZHUO, S., & QIAO, S. Z. 2013. Critical role of small micropores in high CO_2 uptake. *Physical Chemistry Chemical Physics*, 15(7), 2523-2529.

ZHANG, Z., YAO, Z.Z., XIANG, S. & CHEN, B. 2014a. Perspective of microporous metal–organic frameworks for CO_2 capture and separation. *Energy & Environmental Science*, *7*(9), 2868-2899.

ZHANG, Y., SONG, X.L., HUANG, S.T., GENG, B.Y., CHANG, C.H. & SUNG, I.Y., 2014. Adsorption of nitrate ions onto activated carbon prepared from rice husk by NaOH activation. *Desalination and Water Treatment*, *52*(25-27), 4935-4941.

ZHANG, X., WU, J., YANG, H., SHAO, J., WANG, X., CHEN, Y., ZHANG, S. & CHEN, H., 2016. Preparation of nitrogen-doped microporous modified biochar by high temperature CO_2–NH_3 treatment for CO_2 adsorption: effects of temperature. *RSC Advances*, *6*(100), 98157-98166.

ZHANG, C., SONG, W., MA, Q., XIE, L., ZHANG, X. & GUO, H., 2016a. Enhancement of CO_2 Capture on Biomass-Based Carbon from Black Locust by KOH Activation and Ammonia Modification. *Energy & Fuels*, *30*(5), 4181-4190.

ZHAO, L., BACSIK, Z., HEDIN, N., WEI, W., SUN, Y., ANTONIETTI, M., & TITIRICI, M. M. 2010. Carbon dioxide capture on amine-rich carbonaceous materials derived from Glucose. *ChemSusChem*, 3(7), 840-845.

ZHAO, Y., LIU, X., YAO, K. X., ZHAO, L., & HAN, Y. 2012. Superior capture of CO_2 achieved by introducing extra-framework cations into N-doped microporous carbon. *Chemistry of Materials*, 24(24), 4725-4734.

ZHAO, Y., DING, H. & ZHONG, Q., 2013. Synthesis and characterization of MOF-aminated graphite oxide composites for CO_2 capture. *Applied Surface Science*, *284*, 138-144.

ZHENG, W.T., XING, K.Z., HELLGREN, N., LÖGDLUND, M., JOHANSSON, Å., GELIVS, U., SALANECK, W.R. & SUNDGREN, J.E., 1997. Nitrogen 1s electron binding energy assignment in carbon nitride thin films with different structures. *Journal of electron spectroscopy and related phenomena*, *87*(1), 45-49.

ZHENG, X., HUANG, Y., DUAN, J., WANG, C., WEN, L., ZHAO, J. & LI, D., 2014. A microporous Zn (II)–MOF with open metal sites: structure and selective adsorption properties. *Dalton Transactions*, *43*(22), 8311-8317.

ZHOU, J., LI, Z., XING, W., ZHU, T., SHEN, H. AND ZHUO, S., 2015. N-doped microporous carbons derived from direct carbonization of K^+ exchanged meta-aminophenol–formaldehyde resin for superior CO_2 sorption. *Chemical Communications*, *51*(22), 4591-4594.

ZHOU, J., LI, Z., XING, W., SHEN, H., BI, X., ZHU, T., QIU, Z. & ZHUO, S., 2016. A New Approach to Tuning Carbon Ultramicropore Size at Sub-Angstrom Level for Maximizing Specific Capacitance and CO_2 Uptake. *Advanced Functional Materials*, *26*(44), pp.7955-7964.

ZHU, H., YIN, J., WANG, X., WANG, H., & YANG, X. 2013. Microorganism-derived heteroatom-doped carbon materials for oxygen reduction and supercapacitors. *Advanced Functional Materials*, 23(10), 1305-1312.